Experimental studies of the structure, stability and thermochemistry of amphiboles in the systems Na_2O-MgO-Al_2O_3-SiO_2-H_2O and Na_2O-CaO-MgO-SiO_2-H_2O

Alison Ruth Pawley

PhD

University of Edinburgh

1989

ABSTRACT

A number of experimental studies of amphiboles in the systems Na_2O-MgO-Al_2O_3-SiO_2-H_2O (NMASH) and Na_2O-CaO-MgO-SiO_2-H_2O (NCMSH) have been undertaken. These build on foundations provided by recent work, making use of modern experimental and analytical techniques. The results have implications for the compositions of amphiboles crystallising in natural metamorphic rocks, and for the thermodynamic behaviour of amphiboles.

Natural and synthetic high pressure glaucophanic amphiboles frequently exhibit solid solution towards nyböite ($Na_3Mg_3Al_3Si_7O_{22}(OH)_2$). Experiments in the system NMASH on compositions on the nyböite-glaucophane join and on nyböite + $7SiO_2$, at 8-32 kbar/600-900°C, demonstrate that end-member nyböite is not stable. The highest nyböite content (~70 mol%) is in a quaternary nyböite - glaucophane - magnesio-katophorite - eckermannite (Ny-Gl-Mk-Ek) solid solution, synthesised from the silica-undersaturated nyböite bulk composition. It is stable up to >32 kbar at 600-900°C, and breaks down below ~14-15.5 kbar/600-800°C through the reaction amphibole + sheet silicate = albite + nepheline + sodium phlogopite. Amphiboles synthesised from silica-saturated bulk compositions are less nyböite-rich, and are ternary Ny-Gl-Mk solid solutions. They are stable up to >30 kbar and break down below ~14-22 kbar/600-900°C through the reaction amphibole + quartz = albite + talc. The presence or absence of quartz determines whether the amphibole is ternary or quaternary, in agreement with natural data, and implying that Ernst's (1963) "glaucophane" polymorphs GII and GIII are, respectively, quaternary Ny-Gl-Mk-Ek and ternary Ny-Gl-Mk solid solutions.

Thermochemical data, essential for deriving activity-compositions relations, have been obtained for the "pseudo-binary" solid solution $tremolite_{92}$magnesio-$cummingtonite_8$ - richterite ($Ca_{1.84}Mg_{5.16}Si_8O_{22}(OH)_2$ - $Na_2CaMg_5Si_8O_{22}(OH)_2$) ($Tr_{92}Mc_8$-$Ri_{100}$). Eight compositions on the join have been synthesised at 2-6 kbar/850°C. Characterisation by electron microprobe analysis, hydrogen extraction and high resolution transmission electron microscopy demonstrate close-to-ideal compositions and micro-structure. Cell parameters vary smoothly with composition, with ΔV_{mix} approximately linear. Infrared and Raman spectroscopy reveal only minor vacancies on the A-site in Ri_{100}, and few changes in vibrational frequencies along the solid solution, indicating minimal excess entropy of mixing. Enthalpies of solution, measured at 976 K, vary from 361.83 ± 4.76 kJ mol^{-1} for $Tr_{92}Mc_8$ to 441.07 ± 9.84 kJ mol^{-1} for Ri_{100}, the latter obtained by drop-solution calorimetry as Ri_{100} undergoes a disordering transformation of uncertain nature during thermal equilibration in the

calorimeter. The deviation from ideality is consistent with a regular solution model. W_H (67.56 ± 8.12 kJ mol^{-1}) is offset by high configurational entropy of mixing to stabilise intermediate members of the solid solution at the temperature of synthesis. This requires significant short range order in richterite-rich compositions, in which A-site positional order-disorder is important. Short range order and a full A-site in richterite account for its increased P-T stability over tremolite.

Tremolite is an important metamorphic amphibole whose dehydration reaction has been shown to be divariant such that phase equilibrium-derived thermodynamic data may be in error. Its enthalpy of formation ($\Delta H°_f$) obtained by high-temperature solution calorimetry using a pure natural sample is compared with the value obtained by combining a further (8 kbar) bracket on the reaction Tr = 2 Di + 1.5 En + β-Qz + H_2O with brackets already obtained by Welch (1987) at 250-2000 bars. $\Delta H°_f$ (calorimetric) = -12323.89 ± 8.93 'kJ mol^{-1}, while $\Delta H°_f$ (phase equilibrium) = -12300.47 ± 14.81 kJ mol^{-1} and S° = 551.6 ± 9.8 J K^{-1} mol^{-1}. No explanation can be given for the discrepancy between the two values of $\Delta H°_f$.

$\Delta H°_f$ of sodium phlogopite ($NaMg_3AlSi_3O_{10}(OH)_2$), obtained by high-temperature solution calorimetry, is -6155.04 ± 9.35 kJ mol^{-1}. Disagreement with existing data has implications for the use of thermodynamic datasets in calculations of stability relations of other complex minerals such as amphiboles.

An F-OH exchange enthalpy, $\Delta H_{F\text{-}OH}$ = 9.88 ± 8.92 kJ mol^{-1}, has been derived from calorimetric data for synthetic sodium phlogopite and fluor-sodium phlogopite. Comparison with existing data suggests that $\Delta H_{F\text{-}OH}$ is largely dependent on M(1) and M(3) site-occupancy.

These studies demonstrate that although there are many problems associated with experiments on amphiboles, careful characterisation in future studies should allow much useful information and data to be extracted.

ACKNOWLEDGEMENTS

There are many people I would like to thank for their invaluable help and advice to me over the last three years.

Beginning with my week at East Kilbride, I thank Tony Fallick and Gawen Jenkin for their instruction and assistance in the technique of hydrogen extraction.

At Cambridge I thank Michael Carpenter for teaching me how to operate the transmission electron microscope, and Ian Marshall for keeping it running; and Anne Graeme-Barber for her help with XRD and unit cell refinements.

Over at Arizona State University, I thank Paul McMillan and Juang-Ling Sheu for their help with the IR and Raman spectroscopy, and especially Paul for being so enthusiastic that I decided to go back for more.

At Princeton University, I thank Alex Navrotsky for her advice on calorimetry, and Chuck for keeping me supplied with platinum. I am particularly grateful to Sue Circone for looking after me when I first arrived, showing me how to use the calorimeter, and running two of my samples after I came home, when she already had plenty of her own yet to do.

Back here at the Grant Institute, I thank Cliff Ford and Gordon Biggar for tuition in experimental methods; Bob Brown and Bill Tullis for technical assistance, particularly Bob for making all those salt-cells; Geoff Angel for assistance with XRD; and Dodie James for running XRF samples. I especially thank Pete Hill, Stuart Kearns and John Craven for their help and encouragement during my many sessions on the electron microprobe.

Down in the extension, I thank Steve Elphick for providing endless advice on experimental techniques, and livening up tea-times.

To Mark Welch, office-mate for nearly two years and maker of most of those cups of tea, I especially thank for all his help, from teaching me the techniques of experimental petrology, to preparing this gel and polishing that probe slide for me; for making useful suggestions for experiments, and for his continued support and interest in my work.

To Colin Graham, my supervisor, I owe a special thank-you for conveying to me and sustaining within me an interest in amphiboles through an infectious enthusiasm and optimism.

Financial support for this work was provided by the Natural Environment Research Council of Great Britain, and is gratefully acknowledged.

Finally, I thank my parents for their constant love and support, for always being around, and Mum in the last few weeks for proof-reading this thesis, which I dedicate to them.

CONTENTS

CHAPTER 1

INTRODUCTION

CONTENTS

1.1. INTRODUCTION

Amphiboles are a diverse group of minerals: their complex structure not only offers mineralogic interest, but also allows for considerable compositional variation, making them potentially very useful indicators of conditions of crystallisation of the wide variety of rock-types in which they occur, provided their stabilities and thermodynamic properties can be determined. It is therefore not surprising that many experimental studies of amphiboles have been undertaken over the last thirty years, ranging from x-ray structure refinements to phase equilibrium experiments, heat capacity measurements to spectroscopic investigations, and yielding a vast amount of data.

The end-member compositions most suitable for experimentation are rare in nature, and therefore experimental studies have generally had to make use of synthetic phases. However the complexity of the amphibole structure and composition have led to innumerable difficulties in synthesis and consequently in conducting successful experiments. Until recently any errors in derived data were generally ignored, partly because their possible extent was not fully realised, and partly because the means of characterisation necessary to reveal them were not available. A number of recent studies have drawn attention to these problems and gone some way towards either overcoming them or revealing their full extent. These form the foundation for the experimental studies described in this thesis.

The following is therefore a brief review of relevant aspects of recent experimental studies on amphiboles, beginning with a short summary of the general amphibole structure, as it is the complexity and flexibility of this which allow for numerous variations in both micro-structure and composition and hence create most of the problems with experimental studies.

1.2. PREVIOUS EXPERIMENTAL STUDIES OF AMPHIBOLES

1.2.(i). Amphibole structure

A thorough discussion of the structure and other aspects of the crystal chemistry of the amphiboles is given by Hawthorne (1981).

The standard amphibole formula is

$$A_{0-1}B_2C_5T_8O_{22}(OH,F,Cl)_2$$

where A = Na, K

B = Na, Li, Ca, Mn, Fe^{2+}, Mg

C = Mg, Fe^{2+}, Mn, Al, Fe^{3+}, Ti

T = Si, Al

The structure consists of double chains of TO_4 tetrahedra extending infinitely along z (Fig. 1.1). The C cations occupy M(1), M(2) and M(3) sites and form an octahedral strip sandwiched by the apical oxygens of two facing tetrahedral strips, while the B cations, in 6-8 fold coordinated M(4) sites, cross-link these 'I-beams' in a three-dimensional array. The large cavity between the back-to-back double chains, the A-site, is surrounded by 12 bridging oxygens, providing additional linkages between double chains. The occupancy of this site varies from 0-1, and it will accept only large cations such as Na or K. The monovalent anion O(3) is coordinated by the M(1) and M(3) sites in a pseudo-trigonal array.

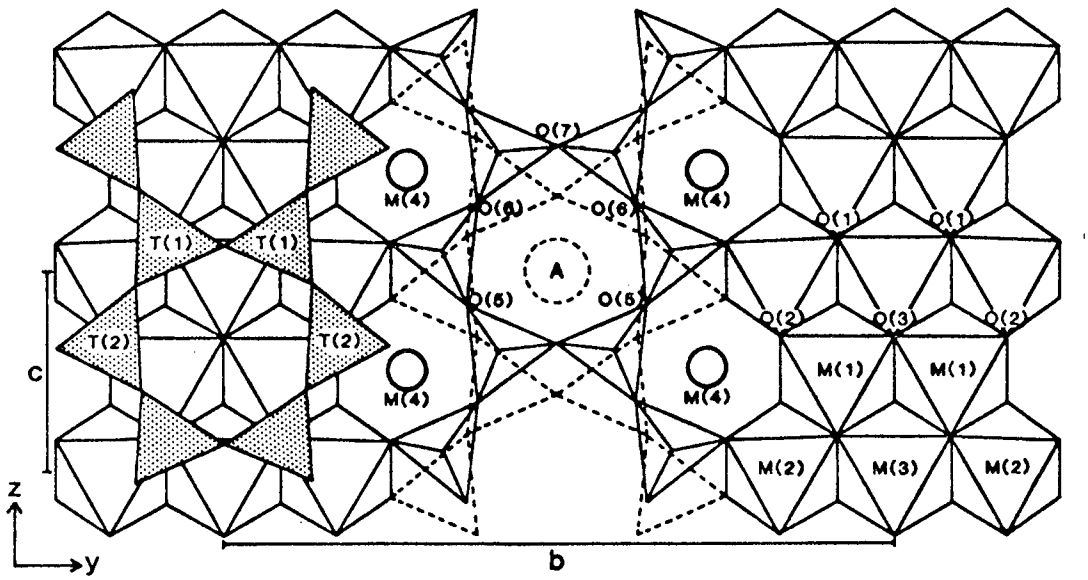

Fig. 1.1. (100) projection of the C2/m amphibole structure.

1.2.(ii). Chain multiplicity faults

Thompson (1981) has drawn attention to the important relationship between amphiboles, pyroxenes and sheet silicates, all members of the continuous polysomatic series of "biopyriboles", such that amphiboles can be regarded as consisting of alternating slabs of pyroxene and sheet silicate. Members of the series may also be described in terms of the multiplicity, m, of the tetrahedral sub-chains linked to form a multiple chain. For a pyroxene, m = 1, for a sheet silicate, m = ∞ and for an amphibole, m = 2. Because amphiboles are simply an intermediate member of the continuous biopyribole series, faults within its structure, due to the introduction of extra pyroxene or sheet silicate slabs, are a common occurrence. Fig 1.2 illustrates the effect on the amphibole structure of incorporating an additional pyroxene slab,

resulting in a chain of multiplicity m = 3, known as a chain multiplicity fault (CMF) (Czank & Liebau, 1980).

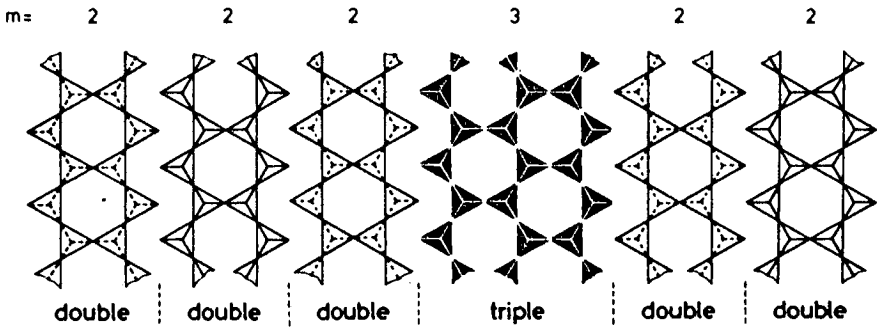

Fig. 1.2. Schematic (100) projection of a triple-chain multiplicity fault inserted into a sequence of ideal amphibole double chains. From Maresch & Czank (1983).

1.2.(iii). High resolution transmission electron microscopy (HRTEM)

As CMFs can only be recognised in HRTEM images, their possible presence in synthetic phases has until recently been generally neglected, though they may well affect thermodynamic behaviour and hence experimentally-derived data. Recently, Maresch & Czank (1983, 1988) used HRTEM for a detailed characterisation of CMFs in synthetic amphiboles of the solid solution series $(Mn^{2+},Mg)_7Si_8O_{22}(OH)_2$. A number of their observations are relevant to other studies, including those described in this thesis. For example they observed that CMF density decreased with increasing synthesis temperature and with increasing silica-activity, but was apparently not dependent on experimental run duration. Furthermore, reaction pathway was an important factor in controlling CMF density, which they suggested was the reason that alkali-rich compositions tended to be less susceptible to CMFs than Fe-Mg-Mn amphiboles. Their most relevant observation concerning CMFs was probably that a synthetic amphibole (a tirodite) contained a higher density than its natural counterpart, and therefore while the effect of CMFs on thermodynamic properties remains uncertain, it was considered that detailed characterisation of synthetic amphiboles in these studies was both necessary to ascertain their structural similarity to natural compositions, and valuable to compare with HRTEM images of other synthetic amphiboles and perhaps provide new information regarding CMF formation. The application of HRTEM (primarily in the characterisation of synthetic tremolite-richterite amphiboles) is described in Chapter 4.

1.2.(iv). Non-stoichiometry – tremolite case study

The ideal amphibole structure, described above, is very flexible, allowing it to accommodate a wide variety of cations through a range of substitutions, the extent of which will depend on such factors as bulk chemistry, pressure, temperature and f_{O_2}. Therefore in experimental studies it must be expected that deviations from desired stoichiometry are likely to occur and will lead to erroneous experimentally-derived data if neglected. Tremolite is a good example of an amphibole for which there exist numerous experimental data on synthetic samples assumed to be stoichiometric but in fact not so (see Chapter 5, Table 5.2). Only recently has it been demonstrated (Jenkins, 1987) that end-member tremolite cannot be synthesised at high temperatures, as above ~500°C it begins to break down divariantly through the reaction Tr = Tr_{ss} + Di + Qz + H_2O (see Chapter 5, Section 5.1.(i) and Fig. 5.1). Tremolite is an important natural amphibole composition for which accurate phase diagram determinations would be useful, but errors introduced into calculated stability relations by compositional uncertainties are significant. Therefore it is essential that detailed compositional analysis by electron microprobe (EMP) is undertaken of all amphiboles before they are used in any experiments. Experiments such as those of Jenkins, in which the same amphibole was synthesised from a number of different starting compositions, are useful to indicate the reason for non-stoichiometry, which in the case of tremolite was due to instability rather than sluggish reaction kinetics, as had previously been thought.

1.2.(v). Kinetics

In some instances it may be kinetics which are responsible for a synthetic amphibole being off-composition. For example the structural and chemical complexity of amphiboles compared to pyroxenes and sheet silicates leads to a greater kinetic barrier to their nucleation. Sheet silicate and pyroxene grow rapidly and must then react to form amphibole, for which at low temperatures the activation energy may be too great, and thus the sheet silicate and pyroxene will persist metastably, while in short runs at higher temperatures, complete equilibration may not be achieved. Grinding and re-running are often necessary to ensure complete reaction.

1.2.(vi). Contamination

In early experimental studies on amphiboles, compositions were seldom analysed as grain sizes were too small for routine electron microprobe analysis (EMPA). Modern probes with back-scattered electron imaging have improved the

situation, but crystals are frequently so small that the x-ray excitation volume does not lie wholly within a single grain, and therefore contamination by neighbouring grains or epoxy is common. Fig. 1.3 illustrates the effects of contamination of an amphibole, TA, by a single phase, X, the composition of which is coplanar with ternary amphibole space A-B-C. Contaminated analyses such as EMP 1 and EMP 2 are in fact legitimate amphibole compositions, and only EMP 3 would be discarded if contamination was not suspected. EMP 1 and EMP 2 may indeed be closer to the ideal amphibole composition than is TA. Therefore when fine-grained samples are being analysed by EMPA, it is necessary both to make full use of the back-scattered electron imaging facility to select the most suitable area for analysis, and to use any knowledge of possible contaminants to infer likely contamination trends and recognise these in the final analyses.

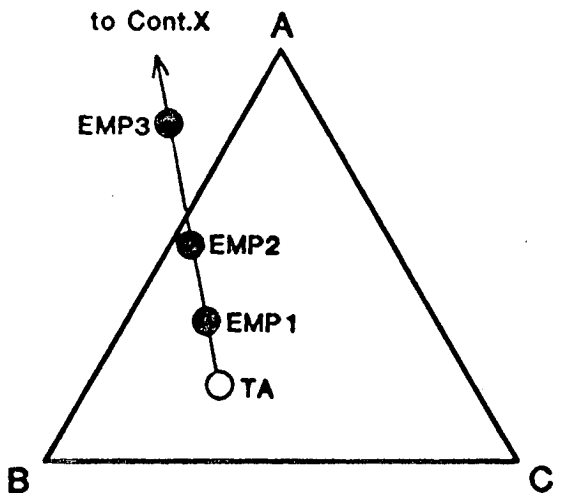

Fig. 1.3. Hypothetical three-component ternary amphibole diagram illustrating the effects of contamination of microprobe analyses of a 'true' amphibole composition (TA). From Graham et al. (1989).

1.2.(vii). H_2O-content

Another common assumption in experimental studies on synthetic amphiboles is that the H_2O-content of the amphibole, which cannot be determined by EMPA, is ideal. The possibility of an excess has long been recognised (eg. Leake, 1968), and in one case the proton-bearing coupled substitution proposed to explain it has been shown to have a considerable effect on amphibole stability ($Na_2Mg_6Si_8O_{22}(OH)_2$ + $NaHMg_{-1}$ = $Na_3Mg_5Si_8O_{21}(OH)_3$: Witte, 1975). Thermo-gravimetric analysis or vacuum heating (undertaken for the tremolite-richterite amphiboles, Chapter 4) are recommended to determine the H_2O-content of synthetic amphiboles, though

vibrational spectroscopy may reveal (among other information - see below) the presence of OH-groups in the structure other than on the O(3) sites.

1.2.(viii). Spectroscopy

Previous experimental studies on synthetic amphiboles, in assuming that they can be used as analogues of natural compositions, have also generally assumed that their crystal chemistry is analogous, ie. that the same ions occupy the same structural sites in synthetic and natural samples. But whereas cation order is common in natural samples, synthetic ones are often highly disordered (eg. synthetic pargasite - Raudsepp et al., 1987), and again such disorder may have a considerable effect on derived thermodynamic data, particularly entropies. Furthermore, positional disorder of the A-site cation, first observed by Hawthorne & Grundy (1972) and recently modelled by Docka et al. (1987), may be important in both synthetic and natural samples. Both of these order-disorder phenomena have been investigated in single crystal x-ray structure refinements. Unfortunately the size of crystal required for these studies is generally prohibitively large for synthetic phases, whose state of order has therefore had to be assumed in past studies. However recent developments in spectroscopic techniques (both vibrational – infrared and Raman – and nuclear magnetic resonance spectroscopy) have considerably improved their suitability for the study of geologic materials. The more such techniques are used in the future, the more quantitative and less empirical the results that will be obtained from them. Therefore vibrational spectroscopy was considered to be both necessary for the characterisation of amphiboles in this study (tremolite-richterite amphiboles – Chapter 4), and a good foundation for future studies.

1.2.(ix). Calorimetry

Another technique which recent developments have made suitable for amphibole studies is calorimetry. Its application to experiments on non-hydrous phases is well-established, but previously considerable uncertainty existed regarding the behaviour of H_2O in the calorimeter flux, ie. whether or not it vaporised and escaped before it could dissolve. However recent studies (Kiseleva & Ogorodova, 1984; Clemens et al., 1987) have demonstrated that it does dissolve and that therefore the enthalpy of solution of hydrous phases can be measured. Here is an alternative method to phase equilibrium experiments for deriving thermodynamic data, which may be used where no reliable phase equilibrium data exist (eg. sodium phlogopite - Chapter 5) or where the phase of interest is unstable on its own composition at its limiting reactions (eg. tremolite - Chapter 5).

1.2.(x). Vector notation

With the realisation that non-stoichiometry is a common property of synthetic amphiboles, the need arises for a simple yet efficient means of describing the numerous compositions which may be produced in attempted synthesis experiments. The elegant vector notation of Thompson (1981) is used throughout this thesis, in which chemical variation is described in terms of "exchange vectors" in composition space. An important end-member is selected as the origin, or "additive component", and other compositions are related to this by the addition of fractions of one or more exchange vectors. For example, taking tremolite ($Ca_2Mg_5Si_8O_{22}(OH)_2$) as the additive component, richterite ($Na_2CaMg_5Si_8O_{22}(OH)_2$) is then equal to tremolite plus the exchange vector $Na^{A}Na^{M(4)}\square^{A}_{-1}Ca^{M(4)}_{-1}$ (Na_2Ca_{-1}, $\square$ = vacancy):

$$Ca_2Mg_5Si_8O_{22}(OH)_2 + Na_2Ca_{-1} = Na_2CaMg_5Si_8O_{22}(OH)_2$$

and

$$tremolite_{50}richterite_{50} = Ca_2Mg_5Si_8O_{22}(OH)_2 + 0.5\ Na_2Ca_{-1}$$

The advantage of this descriptive method is that the number of exchange vectors needed to describe the majority of synthetic and natural amphibole compositions is small. For example Fig. 1.4, taken from Welch (1987), shows how a large number of amphibole compositions, plotted on a vector cage, are related to tremolite by just three exchange vectors.

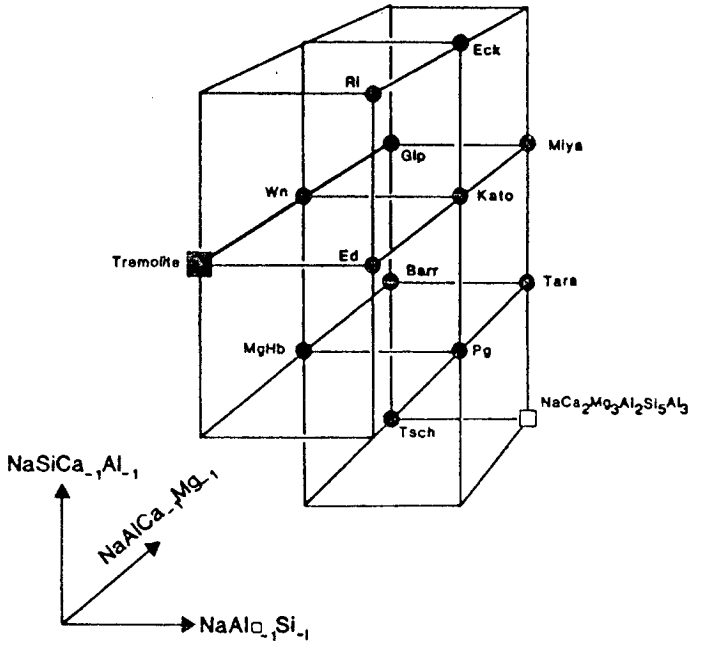

Fig. 1.4. Thompson vector cage of clino-amphiboles in the system Na_2O-CaO-MgO-Al_2O_3-SiO_2-H_2O (NCMASH). Barr = barroisite, Eck = eckermannite, Ed = edenite, Gl = glaucophane, Kato = katophorite, MgHb = magnesio-hornblende, Miya = nyböite, Pg = pargasite, Ri = richterite, Tara = taramite, Tsch = tschermakite, Wn = winchite. From Welch (1987).

The above review highlights many of the problems associated with experimental studies on amphiboles, but also indicates how, thanks to recent advances in experimental and analytical techniques, some of these may be overcome. The studies described in this thesis, building on the foundations provided by these recent studies, are outlined below.

1.3. OBJECTIVES OF THESE STUDIES

(1) To synthesise nyböite ($Na_3Mg_3Al_3Si_7O_{22}(OH)_2$), and derive its enthalpy of formation ($\Delta H°_f$ [nyböite]) from phase equilibrium experiments; then, by addition of the enthalpy of the 'edenite' exchange $NaAlSi_{-1}$, to extrapolate $\Delta H°_f$ [nyböite] to yield $\Delta H°_f$ [glaucophane]. Glaucophane ($Na_2Mg_3Al_2Si_8O_{22}(OH)_2$) cannot be synthesised but is an important component of high pressure amphibole solid solutions.

This study was undertaken primarily because recent experiments on the synthesis and stability of fluor-glaucophane in the system Na_2O-MgO-Al_2O_3-SiO_2-F_2 (Welch, 1987, 1989) suggested that while fluor-glaucophane cannot be synthesised, nyböite might be amenable to synthesis at low pressure. The study would not have been possible without the electron microprobe with back-scattered electron imaging facility in the Geology Department at Edinburgh University, as though nyböite could not be synthesised at any pressure, the compositions of fine-grained amphiboles were able to be analysed and their variation with pressure and temperature documented. This was achieved both for silica-undersaturated bulk compositions applicable to theoretical end-member nyböite phase relations, and silica-saturated compositions, more relevant to natural glaucophane-bearing assemblages, which almost always also contain quartz. The results in the former case have implications for the compositions of sodic amphiboles in silica-undersaturated rocks, while those in the latter case are in agreement with existing observations on, and have additional important implications for, the compositions of natural glaucophanic amphiboles coexisting with quartz..

(2) To synthesise the tremolite-richterite solid solution ($Ca_2Mg_5Si_8O_{22}(OH)_2$ - $Na_2CaMg_5Si_8O_{22}(OH)_2$), defined by the A-site filling substitution $Na^{A}Na^{M(4)}$-$\square^{A}{}_{-1}Ca^{M(4)}{}_{-1}$, and derive activity-composition relationships by high temperature solution calorimetry. A-site filling substitutions are common in natural amphiboles (eg. the 'edenite' substitution in calcic and sodic amphiboles), while previous studies (eg. Graham & Navrotsky, 1986, on synthetic F-tremolite - F-edenite amphiboles) have suggested that they are important for stabilising the solid solutions. This study was therefore undertaken to determine the energetics of the A-site filling substitution, as well as the nature and extent of A-site order-disorder, site-splitting and interactions

with other sites, and to confirm the importance of the A-site in stabilising the solid solution. Solution calorimetry could be used because, as mentioned in Section 1.2.(ix), its reliability for the measurement of enthalpies of solution of hydrous minerals has recently been demonstrated (eg. Clemens et al., 1987). But without the availability of some techniques which had formerly seldom been used in amphibole studies, eg. Raman spectroscopy, the detailed characterisation necessary for the interpretation of the calorimetric results could not have been achieved. Synthesis problems in fact prevented the tremolite-richterite solid solution from being studied, but the "pseudo-binary" solid solution which was eventually synthesised is similar enough to the true binary that its thermodynamic properties may be considered to apply equally to both solid solutions.

(3) To determine $\Delta H°_f$ of a sample of natural tremolite by solution calorimetry. $\Delta H°_f$ [tremolite] was obtained using the same sample in recent phase equilibrium experiments (Welch, 1987) on the reaction

$$Tr = 2\,Di + 1.5\,En + Qz + H_2O$$

but, as suggested by discrepancies in existing data and the fact that the above reaction is probably divariant (Section 1.2.(iv)), there may be an error in this data. $\Delta H°_f$ obtained by calorimetry would provide an independent check on $\Delta H°_f$ (phase equilibrium), and would confirm the suitability of solution calorimetry for the determination of $\Delta H°_f$ data. Use of this technique was again made possible by the recent calorimetric work on other hydrous minerals (eg. Clemens et al., 1987). It was also decided to further constrain the phase equilibrium data by obtaining another bracket on the above reaction at higher pressure.

(4) To apply the same calorimetric technique to the determination of $\Delta H°_f$ of synthetic sodium phlogopite ($NaMg_3AlSi_3O_{10}(OH)_2$), for which $\Delta H°_f$ is poorly constrained by phase equilibrium data.

(5) To derive an F-OH exchange enthalpy from the enthalpies of solution of the same synthetic sodium phlogopite and synthetic fluor-sodium phlogopite ($NaMg_3AlSi_3O_{10}F_2$). While hydrous minerals are now known to be suitable for calorimetric study, sometimes synthesis of hydroxy-amphiboles is not possible and their fluorine-analogues, usually more amenable to synthesis, must be studied instead. Comparison with F-OH exchange enthalpies already obtained for other minerals (tremolite, pargasite, phlogopite) should indicate if the enthalpy of the F-OH exchange depends only on the local atomic environment, in which case a value obtained here would find useful applications in future amphibole studies.

The above may appear to be a somewhat unconnected set of objectives for these studies, but as will become apparent, conclusions drawn from one study are relevant to others, and together have implications for natural amphibole-bearing mineral assemblages and thermodynamic datasets, as well as for the usefulness and hence the future of experimental studies on amphiboles.

CHAPTER 2

EXPERIMENTAL TECHNIQUES

CONTENTS

2.1. HIGH-PRESSURE APPARATUS

The synthesis and phase equilibrium experiments conducted in the studies described in this thesis required the use of all three types of pressure vessel available in the Experimental Petrology unit at Edinburgh University:

(i). Piston-cylinder apparatus, for experiments at $14 < P \leq 32$ kbar;

(ii). Internally-heated vessels, for experiments at $2 \leq P < 9$ kbar;

(iii). Cold-seal vessels, for experiments at 2 kbar ($T \leq 850°C$).

2.1.(i). Piston-cylinder apparatus

Design

The piston-cylinder apparatus is of Boyd & England (1960) design (Fig. 2.1). The sample is contained at the centre of the apparatus in the furnace assembly, two different diameters of which may be used, depending on the pressure required for the experiment. A 1/2" diameter assembly is used in all high-pressure experiments (> ~22 kbar), while at lower pressures a 3/4" diameter assembly, capable of containing larger samples, may be used instead. Talc-pyrex or talc-boron nitride (BN) were used as pressure media in 1/2" diameter furnace assembly cells in these studies, whilst all 3/4" diameter assemblies used salt (NaCl) as a pressure medium.

1/2" talc-pyrex and talc-BN furnace assemblies (Fig. 2.2)

The sample, typically ~10 mg of powder, is contained in a welded platinum (Pt) capsule, 2 mm diameter and ~ 4 mm long (compressed from ~ 6 mm in a pin-press). This is supported within the graphite furnace by alumina pieces. Lead foil around the talc sleeve is coated with MoS_2 grease to reduce friction against the bore wall. Above the furnace is a stainless-steel power lead insulated by a soft-fired pyrophyllite sleeve. The purpose of the silver-steel cone is to prevent extrusion of the stainless-steel through the thermocouple hole, and shearing of the thermocouple, during the run.

Talc is used as a pressure medium because of its low shear strength and good insulating properties. At $T > 750°C$ pyrex also has these properties, but at lower temperatures the friction is found to increase significantly and BN is used instead.

3/4" salt-cell (Fig 2.3)

Two samples may be run together in the salt-cell, and being symmetrically disposed about its axis will experience identical P-T conditions. They are contained in welded 2 mm diameter, 10 mm long Pt capsules within holes drilled in a cylinder of

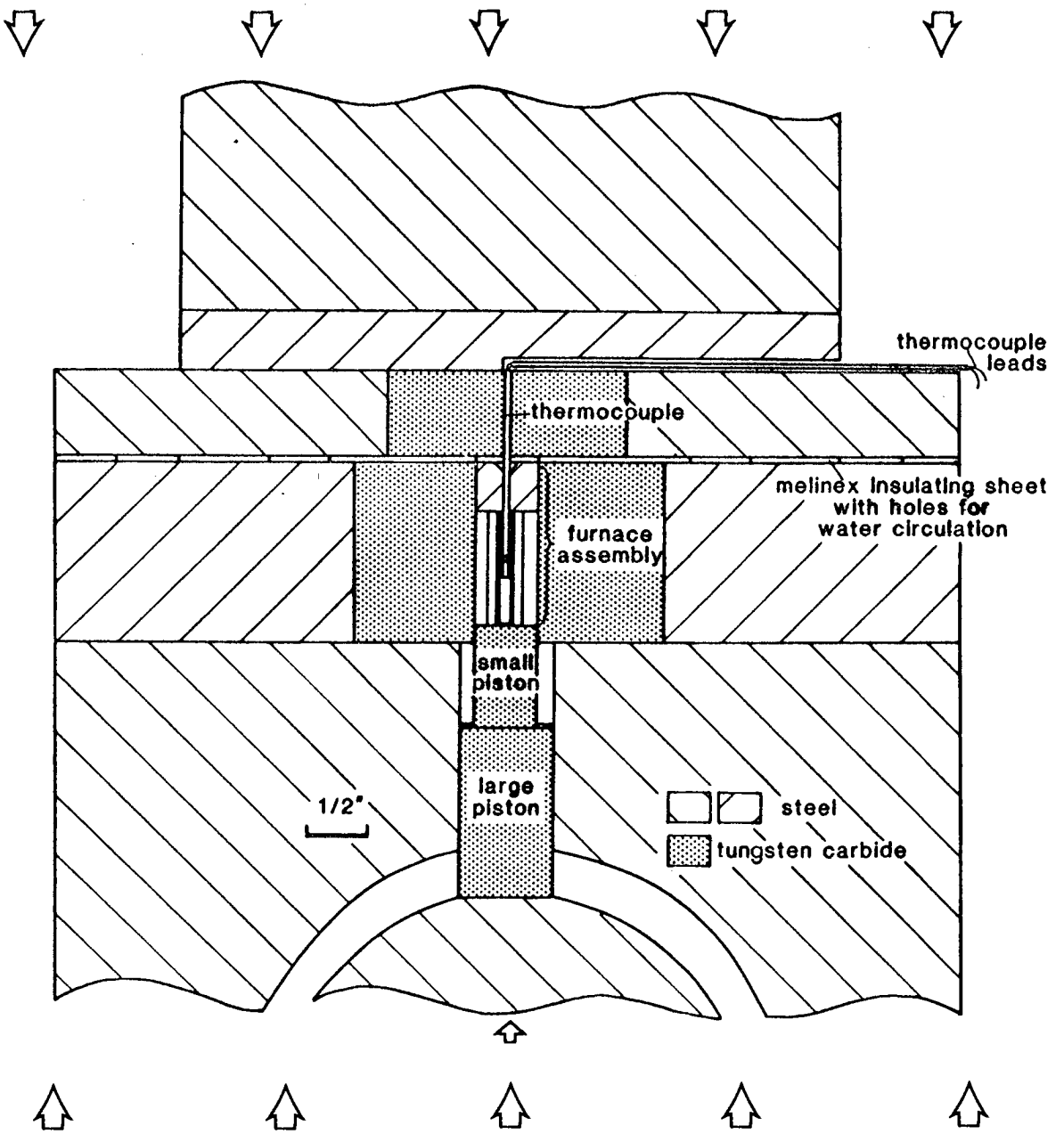

Fig. 2.1. Schematic section through the piston-cylinder apparatus, showing direction of force exerted by large ram (large arrows) and small ram (small arrow). A half-inch diameter furnace assembly is shown.

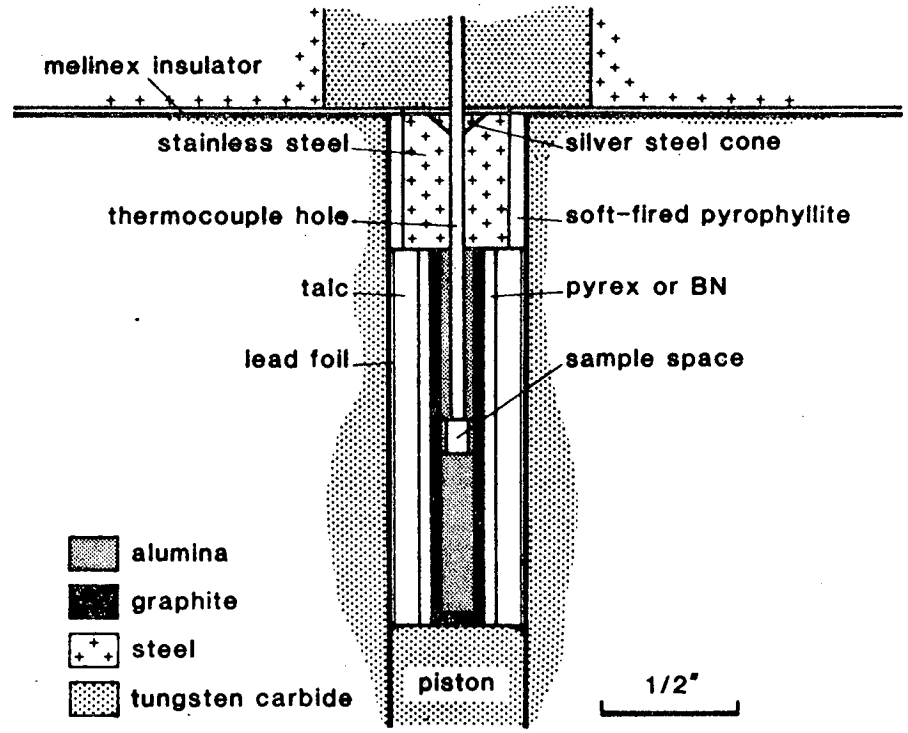

Fig. 2.2. Section through talc-pyrex/talc-BN furnace assembly used in piston-cylinder apparatus.

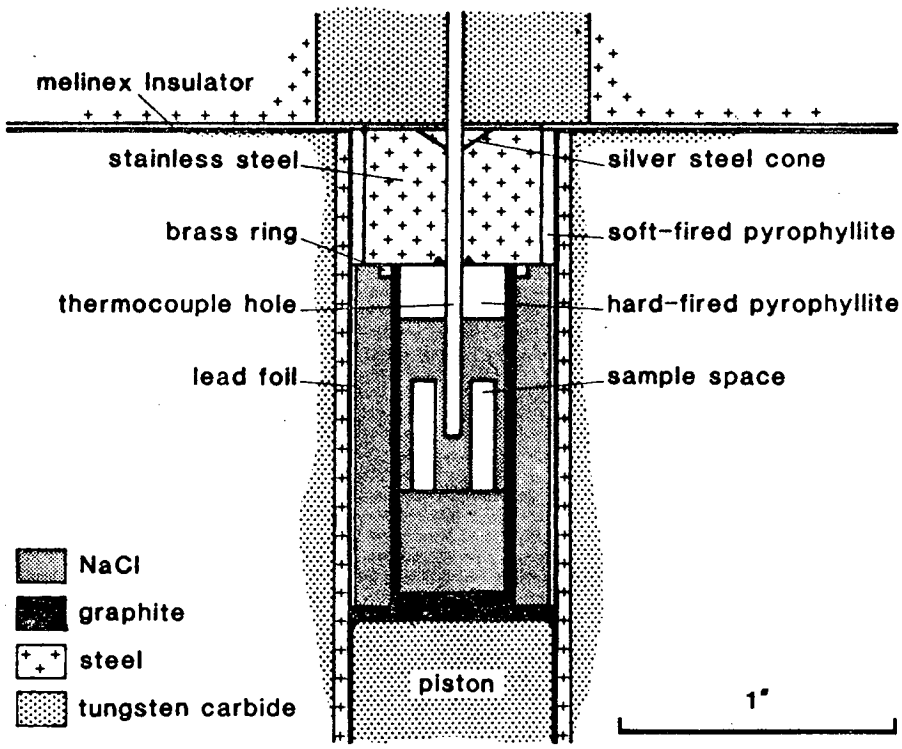

Fig. 2.3. Section through salt-cell used in piston-cylinder apparatus.

pressed salt. A hole for the thermocouple is also drilled in this piece, with its end half-way down the length of the sample holes. The hard-fired pyrophyllite and circular notch on the base of the steel piece are designed to grip the thermocouple to prevent extrusion and breaking on the run-up to pressure and temperature. The brass ring increases the area of contact between power lead and furnace.

Temperature measurement

Temperature was recorded in the 1/2" cells using a Pt/Pt13Rh thermocouple and in the salt-cell using a chromel-alumel thermocouple. Though there are no direct measurements of the effects of pressure on thermocouple e.m.f., they are thought to be very small (Boyd & England, 1960). The precision of temperature measurements is taken to be ± 10°C (Welch, 1987).

In the talc-pyrex/talc-BN cells the thermocouple tip is always in contact with, and frequently embeds itself into, the sample. When pressurised the sample is only ~3 mm long, and therefore axial temperature gradients within it and differences from measured temperature are negligible. Such is not necessarily the case for the salt-cell, however, for two reasons. Firstly, being off-axis, the samples may be affected by a radial temperature gradient; and secondly they are more likely to experience an axial gradient because of their greater length (~ 8 mm after compression). A temperature calibration was not conducted for this study as no quantitative phase equilibrium experiments were undertaken in the piston-cylinder apparatus.

Pressure measurement and calibration

(a). Talc-pyrex/Talc-BN cells

Pressures were measured using an oil-filled Heise gauge. Friction within the cell leads to recorded pressures higher than actual pressures. To ensure consistency of pressure-correction, and minimum friction, all experiments were run "piston-out" (Johannes et al., 1971), that is they were pressurised to an over-pressure of ~5 kbar and the excess bled off manually. The talc-pyrex/talc-BN cells were calibrated at 600-1000°C (pyrex used at T >750°C) by M.D.Welch and C.M.Graham, by bracketing the reactions:

(i) high-albite = jadeite + α-quartz

(ii) α-quartz = coesite

and comparing with published calibrated data. For reaction (i), a 1:1:1 molar mix of synthetic high-albite and jadeite and natural α-quartz was used. Comparison of the results with the data of Holland (1980) (Fig. 2.4(b)) shows pressure differences of

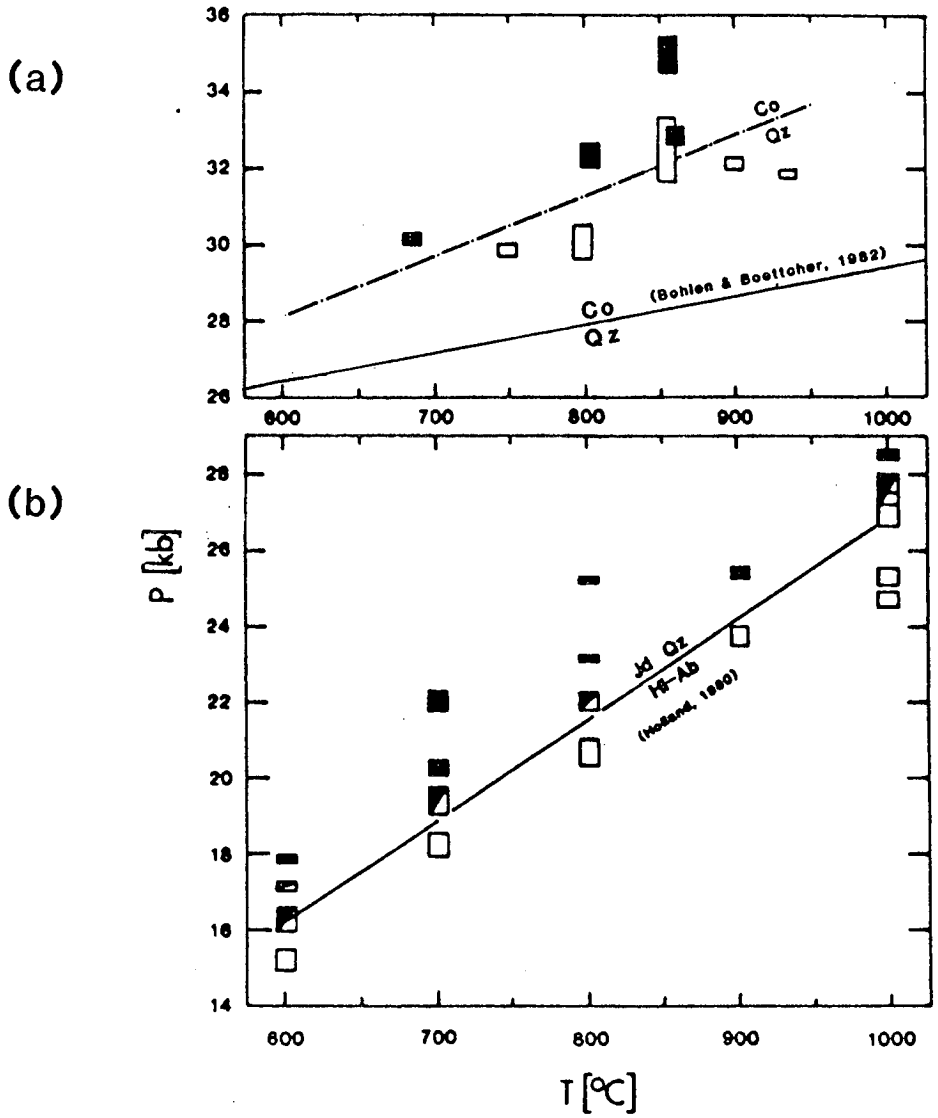

Fig. 2.4. Experimental data used in the calibration of the 1/2" diameter talc-pyrex/talc-BN cells in the piston-cylinder apparatus.

(a) α-quartz = coesite (data from Welch, 1987, 1989).

(b) high-albite = jadeite + α-quartz (Welch & Graham, unpubl. data).

From Welch (1987).

<1 kbar. Reaction (ii) was bracketed in synthesis experiments in the system NMASF (Welch, 1987, 1989), and is shown in Fig. 2.4(a) along with the position as located by Bohlen & Boettcher (1982). The underpressures here are clearly greater than at lower pressure, and increase with temperature. Welch (1989) corrected his experimental data by assuming that the underpressure varied continuously between the conditions of the two reactions, and could be extrapolated to slightly higher and lower pressures, to include all of his data-points, and accordingly he contoured P-T space in the percentage correction required. The same correction map was used in this study, but extrapolation was required to even higher pressures, for which the calibration is therefore rather uncertain.

(b) Salt-cell

Previous studies using salt-cells (eg. Holland, 1980, and Bohlen & Boettcher, 1982, on reactions (i) and (ii) above) have demonstrated that recorded "piston-out" pressures correspond to true hydrostatic pressures within the cell, and therefore no pressure-correction is necessary. "Piston-out" conditions were present at the beginning of each run in this study, but were probably not maintained throughout the runs because of unavoidable diurnal pressure fluctuations associated with variations in laboratory temperature.

Experimental procedure

In all experiments, samples were pressurised to within 5 kbar of final run-pressure before heating. Two hydraulic rams apply the pressure, one exerting an end-load on the entire vessel (large arrows on Fig. 2.1), and the other pushing the piston into the bore containing the furnace assembly (small arrow on Fig. 2.1). For the talc-pyrex cell an overpressure of ~5 kbar was applied, and then the sample was heated slowly (over 10-15 minutes), during which time the pressure fell by ~5 kbar as the pyrex softened. The overpressure was then re-applied and bled off manually so that the piston was in a state of retreat during the run. For the talc-BN cell a small overpressure was applied, which increased slightly on heating and was bled off manually when the run-temperature was reached.

When a salt-cell was used, a pressure 3-4 kbar below the desired run-pressure was applied. Before heating, the apparatus was left to stand for several hours or overnight (during which time the pressure dropped by up to 1 kbar) to allow stresses to equilibrate and hence minimise the chances of thermocouple shear during heating. The temperature was then increased slowly (over at least 20 minutes), during which

time the pressure rose ~4-5 kbar as the salt expanded, resulting in a "piston-out" condition. Any excess pressure was bled off manually.

Comparison of the two cell-types

The known advantages of salt as a pressure-medium over talc/pyrex/BN are its lower friction, such that pressures closely approach true hydrostatic pressures, and the ease of sample recovery it affords, being soluble in water, and hence leaving capsules clean and uncontaminated. However before this study was started, salt-cells had not been used successfully in Edinburgh, though assemblies in use elsewhere have for some time comprised salt pieces to various extents. Previous attempts to use 1/2" salt-cells had failed because of the difficulty involved and precision required in making the small pieces. Therefore the first experiments in the glaucophane-nyböite study (Chapter 3), most of which were conducted at high pressure (> 22 kbar), used talc-pyrex or talc-BN cells. These are generally satisfactory for synthesis experiments, though in this study the underpressures experienced were not always consistent. However because of the small sample-size, and the inability to recover samples uncontaminated by adhering corundum from the recrystallised alumina sleeve, re-runs of material synthesised in talc-pyrex or talc-BN cells could not be attempted. Fortunately the pressure range of most interest in this study was low enough for experimentation using 3/4" assemblies, and the 3/4" salt-cell was therefore developed. A number of designs, using an assortment of salt and non-salt pieces and different thermocouple types, were tested before an assembly was found in which there was only a small chance of the thermocouple breaking during run-up to pressure and temperature; and in which there was minimal vertical displacement of the thermocouple tip away from the sample midpoints. Chromel-alumel thermocouples were found to be stronger than those made of Pt/Pt13Rh, but nevertheless the chances of breakages were still slightly higher than in the 1/2" cells. The other drawback of the salt-cell is, as already mentioned, the temperature uncertainty and high chances of thermal gradients within the samples, but the advantages described above considerably outweighed these disadvantages as far as this study was concerned.

2.1.(ii). Internally-heated pressure vessels

Design

The internally-heated pressure vessels are of the design described by Holloway (1971). They are capable of sustaining pressures of up to 10 kbar. Argon gas was used as the pressure medium.

Measurement of pressure and temperature

Pressures were read using Manganin gauges attached to each vessel. These were calibrated against the freezing point of mercury at 298 K by Dr C.E.Ford and found to be accurate to ± 20 bars. Temperatures were measured using two near-axial Pt/Pt13Rh thermocouples, ~1 cm different in length, one of which acted as a temperature-controller. A thermal gradient between thermocouples could usually be eliminated by raising or lowering one end of the pressure vessel from the horizontal position. Temperature was calibrated using the melting curve of NaCl and is accurate to ± 5°.

Operation

The large size of the furnace compared to that in the piston-cylinder apparatus allows up to at least six samples to be run simultaneously, the number depending on the capsule size being used and the type of experiment. For example, reconnaissance runs on the tremolite-richterite solid solution (Chapter 4) needed only small sample sizes, but samples of six different compositions were required to be run under the same conditions. Pt capsules ~1 cm long and 2 or 3 mm diameter were used in such experiments, and packed around the thermocouples using "Kao wool". Larger samples for bulk syntheses were contained in up to two Pt capsules ~2 cm long and 4 mm diameter.

Runs were brought up to pressure at room temperature. The layout of the pumping system is shown in Welch (1987). Heating was generally done isobarically over ~20 minutes with the valve of the vessel open. Pressures and temperatures were monitored daily, and vessels re-pumped if necessary. Quenching was also isobaric.

2.1.(iii). Externally-heated pressure vessels

Design

The externally-heated pressure vessels are vertical "Tuttle" cold-seal vessels. They were used for experiments at 2 kbar and up to 850°C. Argon gas was used as the pressure medium.

Measurement of pressure and temperature

Pressures were read from a factory-calibrated, dead-weight tested Heise gauge, and are accurate to ± 30 bars (Welch, 1987). Temperatures were controlled by an external Pt/Pt13Rh thermocouple between the pressure vessel and the furnace wall,

Fig. 2.5. Thermal profiles for externally-heated pressure vessel furnaces. Axial temperature variation was measured at nominal reference temperatures of 400, 600, 800 and 900°C, using a single sheathed Pt/Pt13Rh87 thermocouple inserted into the pressure vessel. From Welch (1987).

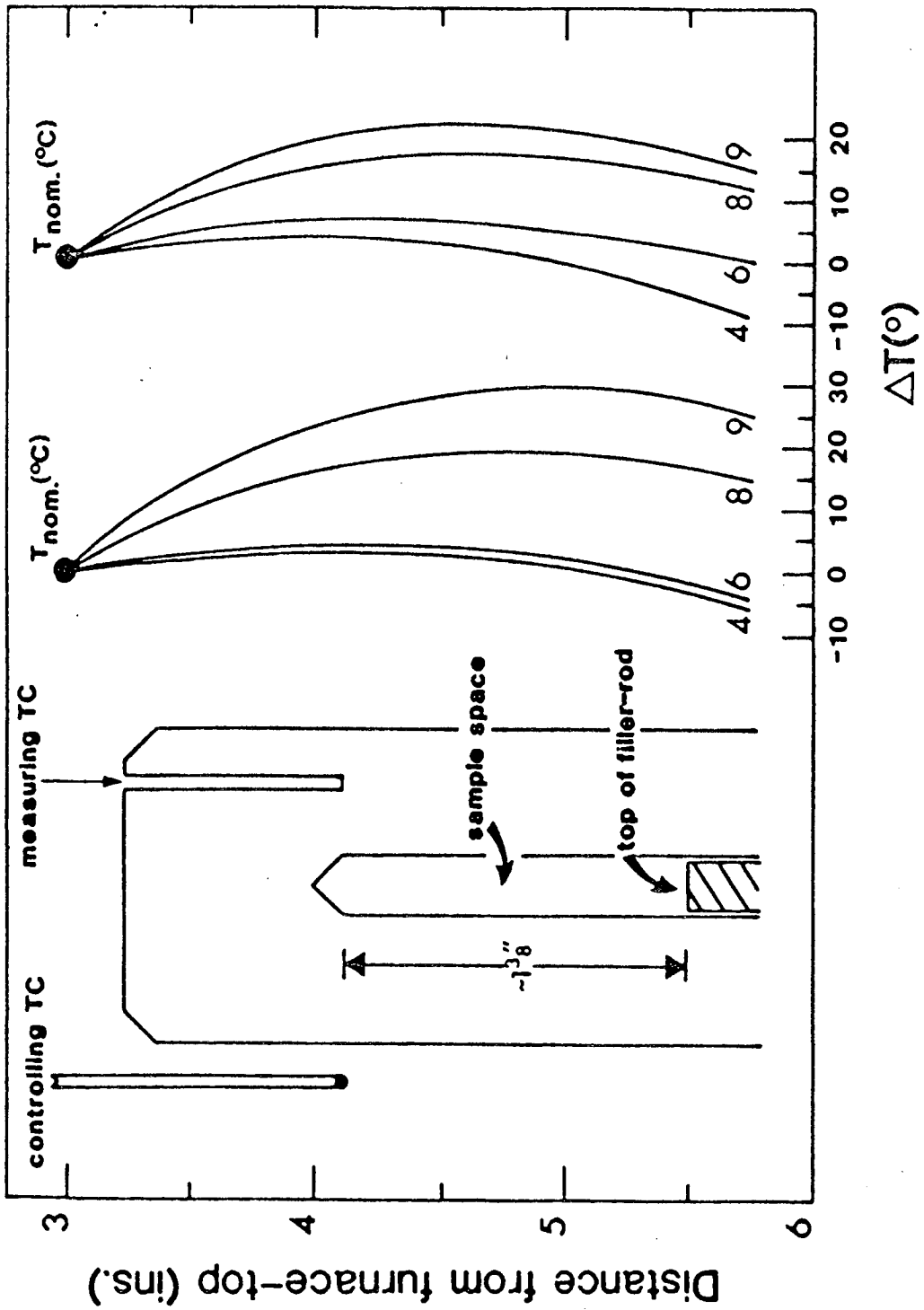

and measured with an internal thermocouple inserted in a hole in the top of the vessel, the tip of which was level with the controlling thermocouple and the top of the sample space (Fig. 2.5). Errors on quoted temperatures are ± 5°, comprising an accuracy in temperature measurement of ± 3° (Ford, 1972) and a typical fluctuation of ± 2° during an experiment.

Operation

Thermal profiles of several cold-seal furnaces, obtained by M.D.Welch, two of which are shown in Fig. 2.5, indicate that for a length of ~4 cm the sample space in most pressure vessels experiences only a small thermal gradient (<5°) at the typical temperatures used in these studies (around 800°C). Therefore several small samples may be run together, or a single 4 mm diameter capsule up to 4 cm long may be used for bulk synthesis in a single run.

Pumping and heating of the cold-seal vessels followed the same procedure as for the internally-heated vessels. Compressed air was used to cool the vessels during isobaric quenching.

2.2. ELECTRON MICROPROBE

The electron microprobe (EMP) used for all compositional analyses of synthetic samples presented in this thesis was a Cameca "Camebax" system with backscattered electron imaging facility, operated in wavelength-dispersive spectroscopy (WDS) mode. Samples were mounted in epoxy on glass slides, and polished to quarter-micron grade. Element standards used were periclase (for Mg), wollastonite (Ca, Si), corundum (Al) and jadeite (Na).

Analytical precision was calculated using the formula:

$$\text{precision } \sigma = \frac{100}{\sqrt{T_p}} \times \frac{1}{\sqrt{R_p} - \sqrt{R_b}} \%$$

where T_p = time on peak,

R_p = peak count rate,

R_b = background count rate.

Values of σ were typically in the range 0.5-2.0 %. Precision is not quoted on presented analyses as it was almost always less than the scatter from a single sample, implying compositional variation within the sample, or contamination to various degrees from epoxy or other phases. This is discussed more fully in the relevant chapters.

The amphiboles investigated in this thesis ideally contain 2.2-2.3 wt% H_2O. Oxide totals of EMP analyses should therefore be 97.7-97.8 wt%, and unless otherwise specified a ± 2 wt% discrepancy in observed oxide total was accepted. Sheet silicates contain about twice as much water as do amphiboles – eg. 4.5 wt% for sodium phlogopite and 5.0 wt% for talc – and hence oxide totals of 95.0-95.5 wt% are expected. Again a ± 2 wt% error was allowed.

EMP analyses were recalculated as amphibole formulae on the basis of 23 oxygens, and as sheet silicate formulae on the basis of 11 oxygens.

2.3. POWDER X-RAY DIFFRACTION

The instrument used for routine examination of experimental run products was a Phillips diffractometer with automatic counter and chart-recorder. Powdered samples were deposited from acetone as smears on glass slides. A scan-rate of 1-2°2θ min^{-1} was used over the range 6-50°2θ, and a chart speed of 1.2 m $hour^{-1}$. When measurement of peak heights was required for reaction direction determination, several scans were made, redepositing the powder between each scan to minimise any orientational effects.

The Guinier camera used for unit-cell refinements is described in Chapter 4.

2.4. HIGH TEMPERATURE CALORIMETRY

Mineral enthalpies of solution were measured for this thesis by the techniques of solution calorimetry and drop-solution calorimetry. The calorimeter used was a Calvet-type twin microcalorimeter (Navrotsky, 1977) at the Department of Geological and Geophysical Sciences, Princeton University, USA. Fig. 2.6 is a schematic diagram showing the principal features. The sample chambers, heated to a constant and uniform temperature (976 K), are surrounded by two thermopiles, connected in opposition.

2.4.(i). Solution calorimetry

This technique is used for samples which are stable at 700°C. The sample is held in a Pt holder made of a piece of perforated Pt foil. This is attached to the end of the glass manipulation rod and suspended over the lead borate ($2PbO.B_2O_3$) flux contained in a Pt crucible. The distance between the sample holder and the flux is known and kept constant for each experiment, so that the manipulation rod may be

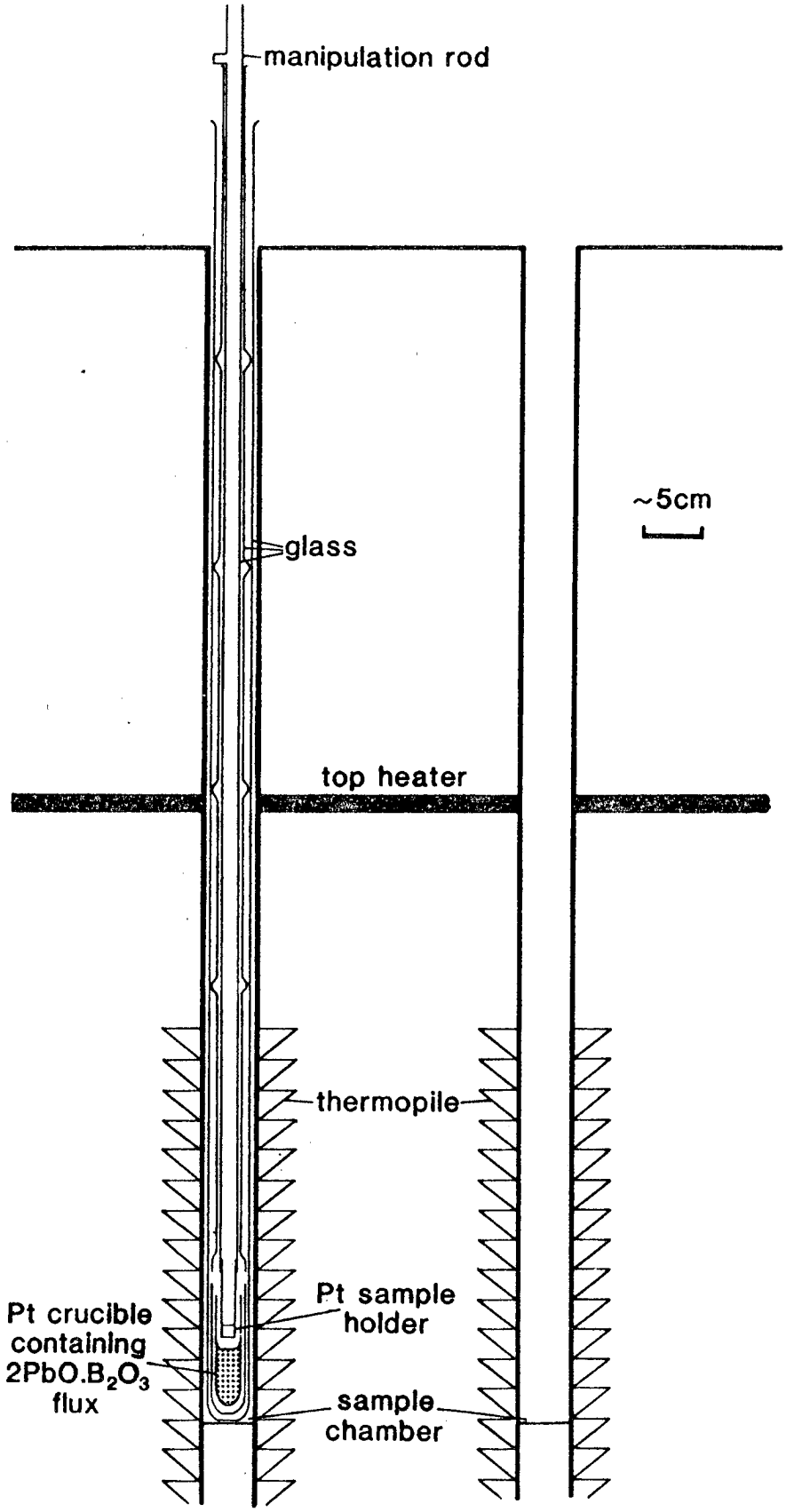

Fig. 2.6. Schematic section through calorimeter. The glass-ware and platinum pieces, shown as assembled for a solution experiment, are identical on both sides of the calorimeter.

lowered manually from the top to dip the sample holder into the flux by a predetermined amount. The holder fills with flux, in which the sample dissolves and drains out through the perforations when the manipulation rod is raised. The thermopile detects temperature changes resulting from the reaction or the movement of the manipulation rod.

For each solution experiment, dried sample is accurately weighed into both sample holders, the glass-ware assembled and lowered into the calorimeter, which is left overnight to come to thermal equilibrium. The signal from the thermopiles is then monitored over 10 minutes to ensure a stable baseline, and reaction is initiated by dipping the sample holder into the flux. The number of dips required to completely dissolve the sample depends on the kinetics of the solution reaction. The same dipping procedure is followed for every experiment. The reaction is assumed to be complete when the signal returns to baseline. It is recorded for another 10 minutes. The integrated e.m.f. for the reaction is then calculated as follows:

V_0 = average baseline e.m.f at start of reaction
= (integral counts after 10 minutes)/10

V_F = average baseline e.m.f at end of reaction
= (counts 10 minutes after end of reaction - counts at end of reaction)/10

$\bar{V}$ = average baseline e.m.f.
$= (V_F - V_0)/2$

t = length of reaction

NET_r = net counts
= counts at end of reaction - $t\,\bar{V}$ - $10\,V_0$

Because there is an enthalpy effect associated with the stirring procedure, this must be measured and the reaction enthalpy corrected for it. This is usually done immediately after the solution experiment by resetting the integral counter to zero, following exacly the same stirring procedure as before, and calculating the net stirring effect, NET_s, in the same way as NET_r.

To convert the integral counts for the dissolution reaction (NET_r - NET_s, μV.min) to enthalpy (joules) requires a conversion factor, which is obtained from calibration by the Pt-drop method. Sample holders are not attached to the manipulation rod, which being hollow allows pieces of Pt of known mass to be dropped from room temperature straight into the molten flux at 976 K. This is done several times on each side of the calorimeter, each time measuring NET_r as before. Here, NET_r is the integral e.m.f. associated with the known heat content of the Pt piece (H_{976}-$H_{room\ T}$). The derived conversion factor is usually averaged over 10 measurements on each side of the calorimeter.

Before doing any solution experiments it is necessary to check that the sample does not partially decompose while the calorimeter is equilibrating. This is usually done by suspending a sample over the flux in the calorimeter overnight, removing it and comparing its x-ray diffractogram with that of an untreated sample. A check of the mass will also indicate whether any of the sample has fallen through the perforations in the Pt foil. If the sample is unstable, its ΔH_{sol} may be measured by drop-solution calorimetry.

2.4.(ii). Drop-solution calorimetry

In this technique the sample is dropped straight into the molten flux from room temperature, as in the Pt-drop calibration experiments. For each experiment, dried sample is accurately weighed into a capsule made of fused lead borate of known mass. After monitoring a steady baseline for ten minutes, the capsule containing the sample is dropped down the manipulation rod into the flux. The lead borate melts and the sample dissolves. After the baseline has returned to zero and remained steady for 10 minutes, the integrated e.m.f. of the reaction is calculated as for a solution experiment, and converted to an enthalpy using the predetermined Pt-calibration factor.

Room temperature is maintained at a constant value throughout the experiments. The value of heat content plus enthalpy of fusion of lead borate is measured in similar experiments using empty capsules. The product of this value and the capsule mass is subtracted from the total drop-solution enthalpy to give the drop-solution enthalpy of the sample ($\Delta H_{drop\text{-}sol}$).

Now $\Delta H_{drop\text{-}sol} = \Delta H_{sol}$ + heat content (H_{976}-$H_{room\ T}$). The heat content is determined in dry-drop experiments, performed in the same manner as the drop-solution experiments, only with the sample contained in a Pt rather than a lead borate capsule, and with no flux in the calorimeter.

$\Rightarrow \Delta H_{sol} = \Delta H_{drop\text{-}sol}$ - heat content (after subtracting the Pt heat content).

2.4.(iii). Sample enthalpy of solution calculation

Table 2.1 and Fig. 2.7 comprise the actual printer output for a typical solution experiment (on a sample of natural tremolite) and measurement of stirring effect.

Table 2.1. Voltage (μV), integral (μV.min) and slope (μV.min/min) per minute for (a) a typical solution experiment, and (b) measurement of the stirring effect. Experiments began at t = 10 and ended at t = 46 minutes.

TREM-3L 20.77mg

Time	Voltage, uV	Integral "uV-min"	Slope (uV-min)/min
0	0.000	0.000	
1	-.001	.002	
2	-.004	.000	
3	-.002	-.000	
4	.007	-.001	
5	.003	.005	.0010
6	.003	.010	.0015
7	.007	.012	.0024
8	.009	.014	.0029
9	.002	.019	.0039
—10	.025	.034	.0058
11	1.802	.622	.1225
12	5.319	4.717	.9409
13	6.106	10.631	2.1233
14	5.694	16.538	3.3038
15	4.942	21.797	4.3526
16	4.235	26.321	5.1397
17	3.551	30.145	5.0055
18	2.961	33.340	4.5419
19	2.459	35.997	3.8918
20	2.037	38.181	3.2768
21	1.761	40.056	2.7471
22	1.477	41.657	2.3025
23	1.235	42.995	1.9311
24	1.023	44.104	1.6214
25	.850	45.022	1.3682
26	.685	45.777	1.1441
27	.554	46.386	.9459
28	.446	46.885	.7779
29	.368	47.288	.6369
30	.289	47.600	.5156
31	.224	47.848	.4143
32	.152	48.039	.3304
33	.118	48.179	.2589
34	.085	48.277	.1978
35	.055	48.342	.1484
36	.018	48.379	.1061
37	.008	48.398	.0719
38	-.004	48.401	.0443
39	-.012	48.390	.0226
40	-.022	48.368	.0052
41	-.048	48.332	.0003
42	-.054	48.288	-.0221
43	-.057	48.230	-.0330
44	-.058	48.180	-.0421
45	-.071	48.115	-.0505
—46	-.002	48.042	.0500
47	-.076	47.963	.0049
48	-.082	47.886	-.0700
49	-.077	47.803	-.0754
50	-.075	47.725	.0700
51	-.090	47.640	-.0004
52	-.000	47.556	.0014
53	-.091	47.471	-.0031
54	-.087	47.387	-.0033
55	-.001	47.304	-.0042
—56	-.100	47.210	-.0044
57	-.092	47.130	-.0053
58	-.099	47.038	-.0065
59	-.094	46.946	-.0081
60	-.104	46.845	-.0010

TREM-3L STIR

Time	Voltage, uV	Integral "uV-min"	Slope (uV-min)/min
0	0.000	0.000	
1	-.001	.001	
2	-.003	-.000	
3	.000	-.005	
4	-.006	-.009	
5	-.004	-.015	-.0030
6	-.009	-.020	-.0041
7	-.010	-.027	-.0054
8	-.013	-.042	-.0074
9	-.012	-.048	-.0078
—10	-.007	-.057	-.0084
11	-.081	-.116	-.0193
12	-.030	-.174	-.0294
13	-.066	-.228	-.0372
14	-.047	-.290	-.0484
15	-.067	-.354	-.0594
16	.011	-.369	-.0506
17	.041	-.341	-.0334
18	.076	-.280	-.0103
19	.071	-.211	.0157
20	.026	-.169	.0371
21	.061	-.119	.0500
22	.052	-.061	.0559
23	.072	.005	.0570
24	.069	.077	.0575
25	.072	.146	.0630
26	.065	.210	.0659
27	.067	.267	.0657
28	.048	.318	.0625
29	.049	.369	.0505
30	.046	.416	.0538
31	.038	.458	.0496
32	.025	.490	.0445
33	.015	.514	.0391
34	.015	.535	.0331
35	.014	.557	.0283
36	-.001	.570	.0223
37	.004	.575	.0170
38	.000	.579	.0131
39	-.003	.579	.0088
40	-.001	.574	.0034
41	-.000	.570	.0001
42	-.002	.566	-.0016
43	-.011	.562	.0034
44	.000	.553	-.0051
45	.009	.544	-.0059
—46	.007	.537	-.0007
47	-.017	.528	-.0077
48	-.012	.518	.0088
49	.016	.505	.0007
50	-.013	.493	-.0103
51	.010	.483	.0100
52	-.010	.472	-.0112
53	-.005	.461	-.0114
54	-.000	.453	-.0103
55	.005	.450	-.0006
—56	-.003	.451	.0064
57	.018	.458	-.0028
58	.019	.475	.0028
59	.033	.510	.0113
60	.031	.545	.0191

Fig. 2.7. Voltage (μV) and integral (μV.min) data of Table 2.1 plotted against time for (a) the solution experiment and (b) the stirring effect.

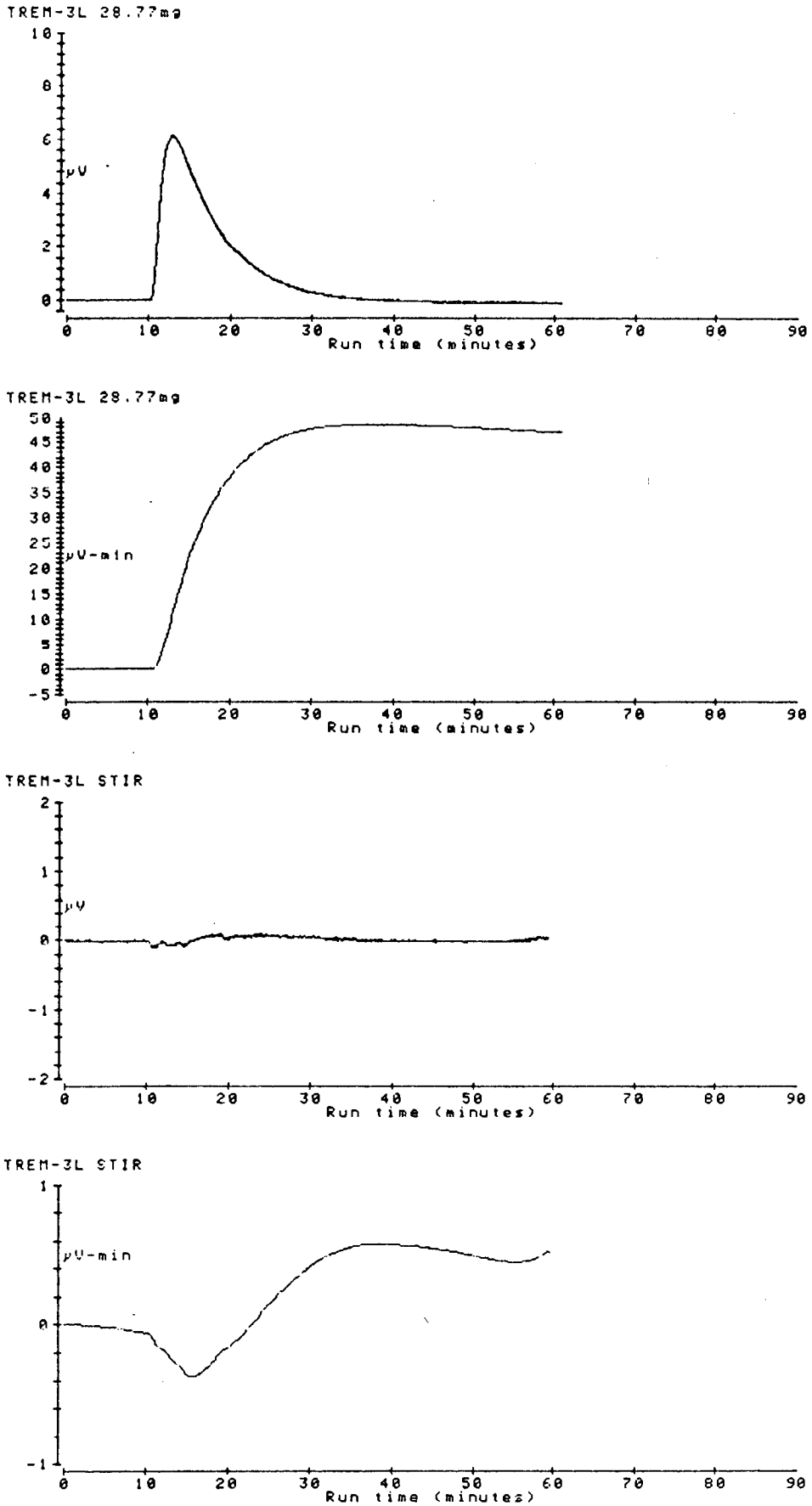

The stirring sequence used for this experiment, and all others, was:

t = 10 minutes: 3 stirs
t = 12 minutes: 2 stirs
t = 14 minutes: 2 stirs
t = 19 minutes: 2 stirs

Calculation of ΔH_{sol} is given below:

Run:

$$V_0 = (.034 - .000)/10 = .0034$$
$$V_f = (47.218 - 48.042)/10 = -.0824$$
$$\Rightarrow \bar{V} = -.0395$$
$$t = 36$$
$$NET_r = 48.042 - t\bar{V} - 10\,V_0$$
$$= 49.4300\ \mu V.min$$

Stirring effect:

$$V_0 = (-.057 - .000)/10 = -.0057$$
$$V_f = (.451 - .537)/10 = -.0086$$
$$\Rightarrow \bar{V} = -.0071$$
$$t = 36$$
$$NET_s = 0.537 - t\bar{V} - 10\,V_0$$
$$= 0.8514\ \mu V.min$$

$$49.4300 - 0.8514 = 48.5786$$
$$\times 0.2828871 \text{ (calibration factor)} = 13.7423\ J$$
$$\div 28.77 \text{ (mass of sample, mg)} = 0.4777\ J\ mg^{-1}\ (kJ\ g^{-1})$$
$$\times 812.4103 \text{ (molecular mass of tremolite, g)} = 388.0554\ kJ\ mol^{-1}$$
$$= \Delta H_{sol} \text{ [tremolite].}$$

2.5. PREPARATION OF STARTING MATERIALS

All starting materials for synthesis experiments were gels prepared using the method of Biggar & O'Hara (1969). They were made in 10 g batches, comparison of observed and theoretical yields providing a check against weighing errors. A further compositional check was made using x-ray fluorescence (XRF) analysis, and in some instances electron microprobe analysis of fused samples of the gel.

2.6. XRF ANALYSIS

Fused discs were made using 1 g samples of gels for major element analysis. Totals tended to be on the low side due to incomplete dehydration of the gel in the drying oven or subsequent rapid absorption of water.

2.7. OTHER TECHNIQUES

Three other techniques were used specifically in the characterisation of tremolite$_{92}$-magnesio-cummingtonite$_{8}$ – richterite amphiboles (Chapter 4):

transmission electron microscopy,

vibrational spectroscopy,

and H_2O-content determination by the hydrogen-extraction method.

These are discussed in detail in that chapter.

CHAPTER 3

EXPERIMENTAL STUDY OF NYBÖITE, WITH IMPLICATIONS FOR GLAUCOPHANE STABILITY

CONTENTS

3.1. INTRODUCTION

Amphiboles rich in the glaucophane component are products of the high-pressure/low-temperature "blueschist facies" metamorphism associated with plate collision and subduction. Their widespread presence in these rocks makes them potentially very useful indicators of the P-T conditions attained during metamorphism. But their usefulness depends on how accurately their stability range is known, and therefore much effort over the last 25 years has been put into attempting an experimental determination of glaucophane stability relations.

As no analysed natural amphiboles are of ideal composition $Na_2Mg_3Al_2Si_8O_{22}(OH)_2$, experimental attempts to determine the phase relations of the pure end-member have been forced to use synthetic materials. The claims of successful synthesis of glaucophane have been the subject of debate and experimental re-investigation for many years, a brief resumé of which will be given below. To assist in the interpretation of these results and the understanding of the problems involved, it would be constructive at this point to consider the potential phase relations of end-member glaucophane, as well as the deviations from ideality which may be expected in the synthetic amphibole composition. Previous experimental results and observations have shown that other phases involved in glaucophane stabilty relations are Qz/Co, Jd, En, Ab, Tc, Sp (see Table 3.1 for a list of all mineral abbreviations used in this Chapter). Their compositions are plotted on a Na_2O-MgO-Al_2O_3-SiO_2 (NMAS) tetrahedron in Fig. 3.1(a). But because most of these phases are related by simple exchange vectors, they can be plotted on a vector cage (Fig. 3.1(b)) or a projection thereof (Fig. 3.1(c)). Fig. 3.1 demonstrates the enormous potential for synthetic amphibole compositions to be displaced from the glaucophane stoichiometry at which the various experimental studies have aimed, and unless 100% yields can be obtained, or reliable compositional analyses of the samples, all claims of success must be treated with caution. From a compilation of previous experimental results and observations (Fig. 3.2), Welch (1987) constructed a Schreinemakers net of reactions relevant to glaucophane stability, the numbered ones of which have been located, correctly or otherwise, in experiments (Fig. 3.3). Numbered reactions in the text also refer to these.

Successful synthesis was first claimed by Ernst (1961), in experiments conducted at 0.2-35 kbar, at temperatures below 875°C, on the bulk composition $Na_2Mg_3Al_2Si_8O_{23}$ + excess H_2O. However he was unable to obtain yields of more than 10-20% amphibole, nor any analyses of these amphiboles. But on the basis of x-ray unit cell data, he proposed a polymorphic transformation between a low pressure polymorph (Gl I) with Mg and Al randomly distributed on octahedral sites and a high

Table 3.1. Abbreviations used in Chapter 3.

Ab	Albite	$NaAlSi_3O_8$
Am	Amphibole	
Br	Magnesio-barroisite	$NaMg_4Al_3Si_7O_{22}(OH)_2$
Co	Coesite	SiO_2
Ek	Eckermannite	$Na_3Mg_4AlSi_8O_{22}(OH)_2$
En	Enstatite	$Mg_2Si_2O_6$
Fo	Forsterite	Mg_2SiO_4
Gl	Glaucophane	$Na_2Mg_3Al_2Si_8O_{22}(OH)_2$
Jd	Jadeite	$NaAlSi_2O_6$
L	Liquid	
Mk	Magnesio-katophorite	$Na_2Mg_5Al_2Si_7O_{22}(OH)_2$
Ne	Nepheline	$NaAlSiO_4$
Ny	Nyböite	$Na_3Mg_3Al_3Si_7O_{22}(OH)_2$
Pw	Preiswerkite	$NaMg_2Al_3Si_2O_{10}(OH)_2$
Qz	Quartz	SiO_2
Sc	Sodium magnesio-cummingtonite	$Na_2Mg_6Si_8O_{22}(OH)_2$
Sp	Sodium phlogopite	$NaMg_3AlSi_3O_{10}(OH)_2$
Ss	Sheet silicate	
Tc	Talc	$Mg_3Si_4O_{10}(OH)_2$
V	Vapour	
$NaAlSi_{-1}$	$Na^{A}Al^{T(1)}\square^{A}_{-1}Si^{T(1)}_{-1}$	'Edenite' exchange
$AlAlMg_{-1}Mg_{-1}$	$Al^{M(2)}Al^{T(1)}Mg^{M(2)}_{-1}Si^{T(1)}_{-1}$	'Tschermaks' exchange
$MgMgNa_{-1}Al_{-1}$	$Mg^{M(4)}Mg^{M(2)}Na^{M(4)}_{-1}Al^{M(2)}_{-1}$	
$MgMgSi_{-1}$	$Mg^{M(4)}Mg^{M(2)}Si^{T(1)}_{-1}$	
$CaMgNa_{-1}Al_{-1}$	$Ca^{M(4)}Mg^{M(2)}Na^{M(4)}_{-1}Al^{M(2)}_{-1}$	

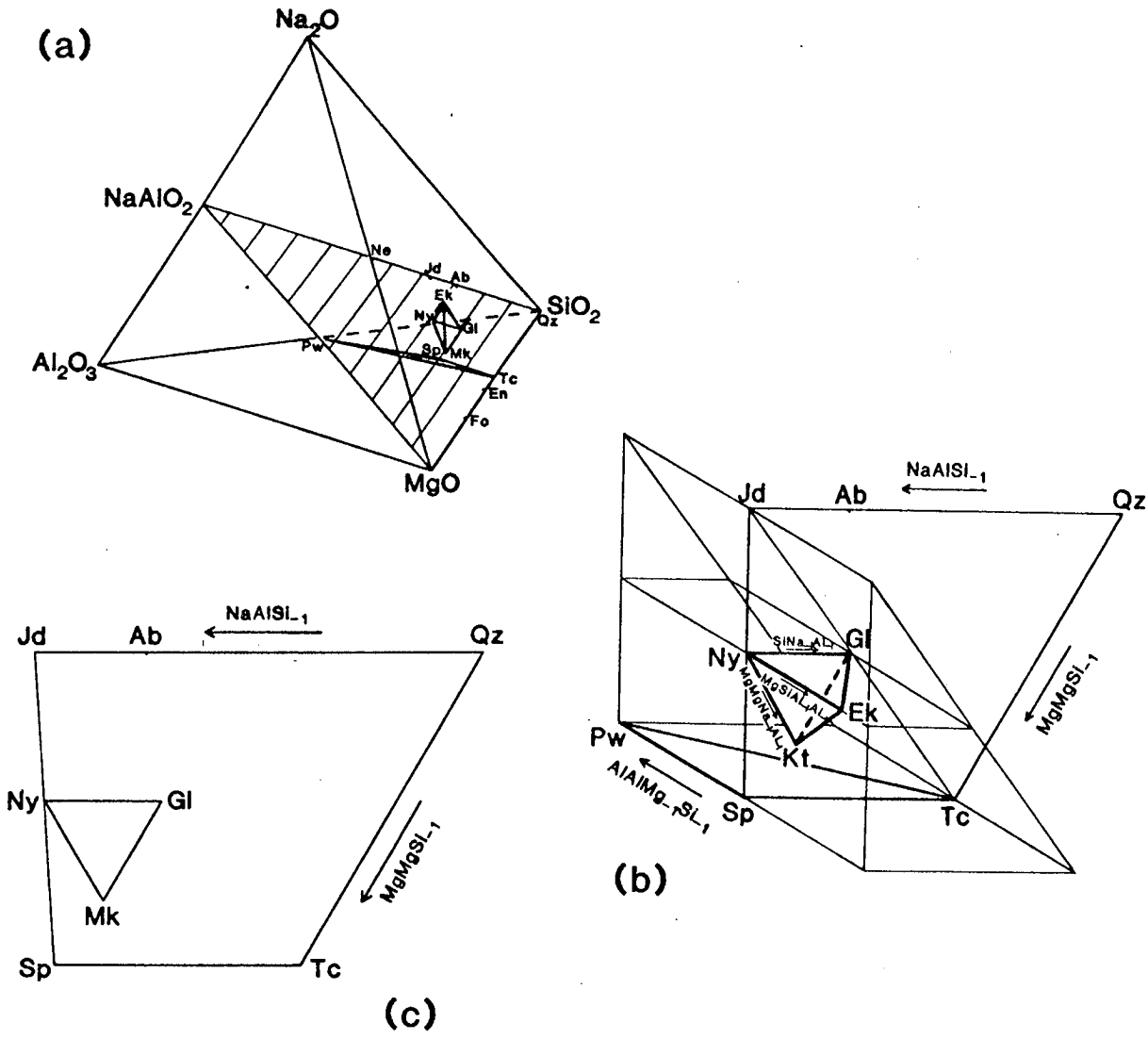

Fig. 3.1.

(a) Projection from H_2O in the system Na_2O-MgO-Al_2O_3-SiO_2-H_2O, showing compositions of phases relevant to glaucophane stability and to this study. All lie on the shaded plane $NaAlO_2$-MgO-SiO_2, except Ek (above) and Pw (below).

(b) The SiO_2-saturated portion of Fig. 3.1.(a) redrawn as a vector cage of the exchanges $NaAlSi_{-1}$, $MgMgSi_{-1}$ and $AlAlMg_{-1}Si_{-1}$, showing the tetrahedron of amphibole compositions and triangle of sheet silicate compositions most relevant to this and previous studies. Amphibole composition space in fact extends beyond the tetrahedron, eg. Sc is related to Ek in the same way as Kt is to Ny, ie. through the exchange $MgMgNa_{-1}Al_{-1}$. Compositions outwith this tetrahedron were not encountered in this study, nor were conclusively demonstrated in previous studies on glaucophane.

(c) Projection from $MgSiAl_{-1}Al_{-1}$ of the vector cage of Fig. 3.1.(b). Ek lies above Ny, and Pw below Sp.

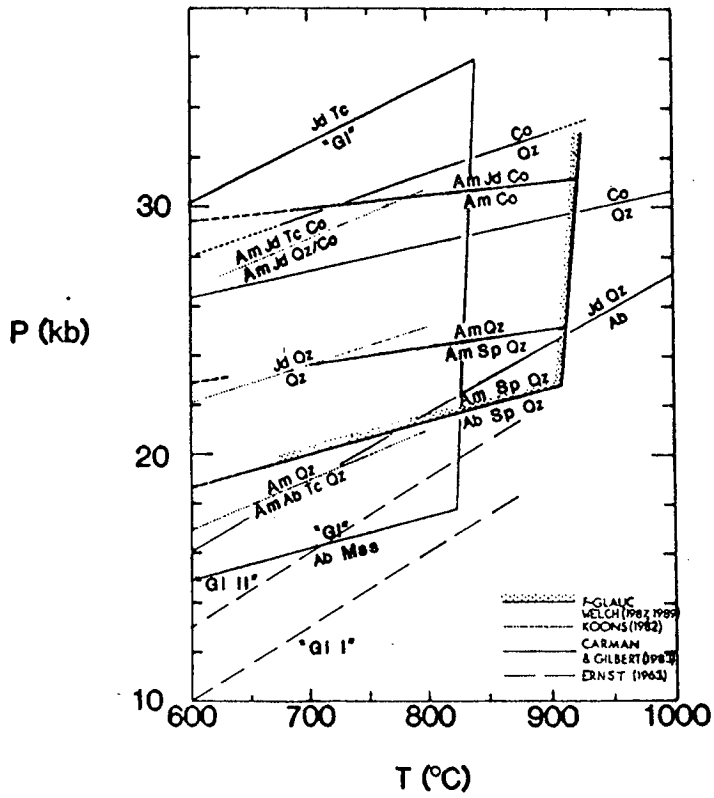

Fig. 3.2. Compilation of glaucophanic amphibole phase relations of Ernst (1963), Koons (1982), Carman & Gilbert (1983) and Welch (1987, 1989). From Welch (1987).

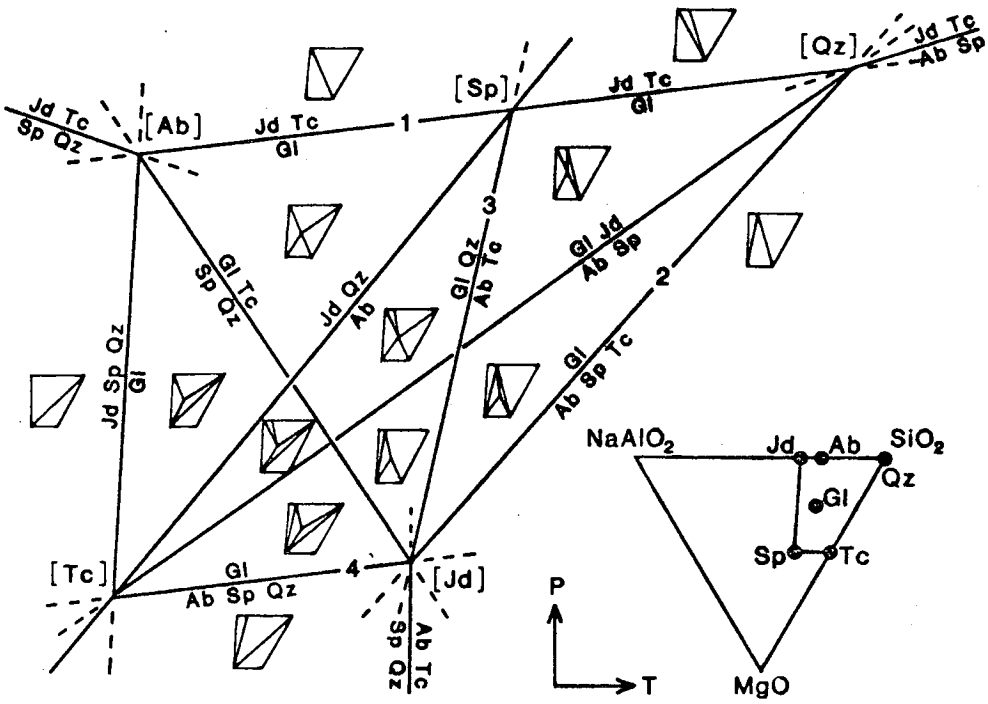

Fig. 3.3. Chemographic relations relevant to glaucophane stability in the systems Na_2O-MgO-Al_2O_3-SiO_2-H_2O and Na_2O-MgO-Al_2O_3-SiO_2-F_2. All reactions are vapour conserving. Numbers refer to reactions studied experimentally:

(1) Koons (1982), Carman & Gilbert (1983),

(2) Carman & Gilbert (1983),

(3) Koons (1982),

(4) Welch (1987,1989) (fluorine analogue system).

From Welch (1987).

pressure form (Gl II) supposedly with Al ordered on M(2) sites (Ernst, 1963, Fig. 1 – his polymorphic transition zone is shown in Fig. 3.2). But subsequent experimental investigation of Ernst's claims (Iiyama 1963, Carman 1969, Maresch 1973, 1974) failed to yield anything approaching glaucophane. Maresch (1977) deduced that neither of Ernst's polymorphs were on-composition, Gl I, significantly off-composition, being at least ternary (ie. situated on a plane in amphibole space defined by three end-members) and probably close to magnesio-richterite or eckermannite in composition (Fig. 3.1), though the high pressure form might closely approach the end-member composition. Two, more recent, studies gave conflicting results: Carman & Gilbert (1983) claimed to have synthesised end-member glaucophane, and to have demonstrated its stability in the pressure range 10-35 kbar, bounded by the high-pressure reaction:

$$Gl = 2\,Jd + Tc \qquad (1)$$

and low pressure reaction:

$$Gl = Ab + Sp + Tc \qquad (2)$$

(reactions (1) and (2) respectively in Fig 3.3) with complete solid solution between the sheet silicates such that the reaction actually located was Gl = Ab + Mss (Mss (their terminology) = sodium phlogopite-talc solid solution). However they also failed to synthesis 100% amphibole, and their 'limited probe analyses' are presented in such a way as to hide potential deviation from ideal stoichiometry along the exchange vectors $NaAlSi_{-1}$ and $MgMgNa_{-1}Al_{-1}$ (Fig. 3.4).

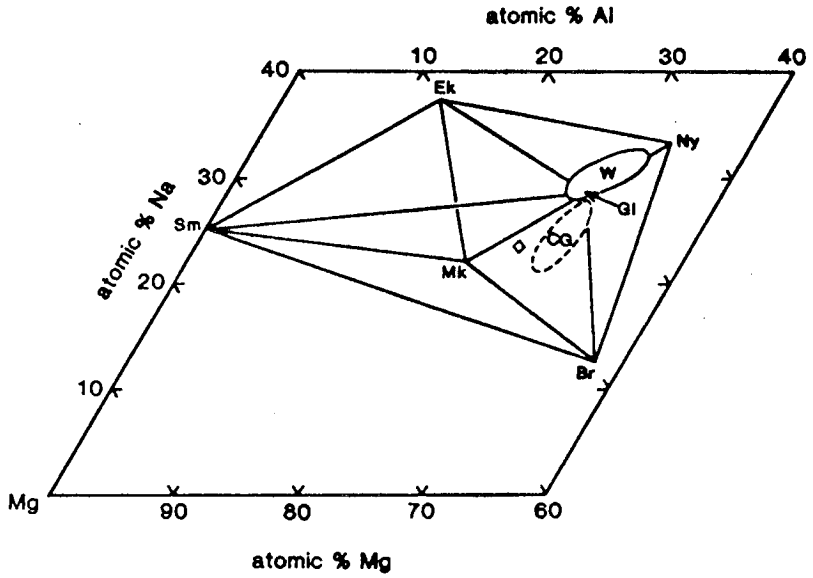

Fig. 3.4. Na-Mg-Al atomic % plot showing the compositions of synthetic glaucophane-rich amphiboles from high-pressure studies of glaucophane stability. CG = Carman & Gilbert (1983) (NMASH); W = Welch (1987, 1989) (NMASF); ◇ = average "glaucophane" of Koons (1982) (NMASH). From Graham et al. (1989).

In contrast to their claims, Koons (1982) demonstrated, through observation of the phases coexisting with amphibole grown from glaucophane bulk composition at 15-35 kbar/550-800°C, that the amphibole could not be end-member glaucophane, but must show solid solution towards nyböite $Na_3Mg_3Al_3Si_7O_{22}(OH)_2$ and Mg-katophorite $Na_2Mg_5Al_2Si_7O_{22}(OH)_2$, ie. along the exchange vectors $NaAlSi_{-1}$ and $MgMgSi_{-1}$ respectively (Fig. 3.1(c)), to an extent largely dependent on pressure. He did not obtain any definitive products of the high- or low-pressure breakdown of his glaucophane-like amphibole, but the high-pressure assemblage of Am, Jd, Tc, Qz was interpreted to contain reactants and products of the divariant equivalent of reaction (1) and the low-pressure assemblage Am, Ab, Tc, Qz, likewise of the reaction

$$Gl + Qz = Ab + Tc \qquad (3)$$

Further evidence against the ability to synthesise glaucophane came from a detailed study by Welch (1987, 1989) in the system Na_2O-MgO-Al_2O_3-SiO_2-F_2 (NMASF). By working in the fluorine-analogue system he was able to conduct experiments at higher temperature and hence obtain coarser-grained samples, more amenable to electron microprobe analysis (EMPA). In experiments on the F-glaucophane bulk composition at 18-32 kbar/680-950°C, he observed phase relations analogous to those of Koons, except that F-talc was not stable, the low pressure stability of F-Gl being defined by the reaction

$$F\text{-}Gl = Ab + Sp + Qz \qquad (4)$$

He obtained amphibole electron microprobe (EMP) analyses, all of which were displaced from glaucophane along the same exchange vectors as suggested by Koons (Fig. 3.5). The dominant exchange was $NaAlSi_{-1}$, which increased significantly with decreasing synthesis pressure such that the lowest pressure amphibole synthesised (at 21 kbar/800°C) contained up to 75% nyböite component. Welch's amphibole compositions plotted, as Carman & Gilbert present their EMP data, on a Na-Mg-Al atom plot, show a similar spread, suggesting that Carman & Gilbert's so-called glaucophane is also at least ternary and of variable composition (Fig. 3.4).

Realising that bulk synthesis of an amphibole approaching glaucophane is impossible, two more recent studies have made use of natural samples close to end-member composition to obtain thermodynamic data for glaucophane. Holland (1988) obtained heat capacity (C_p) and cell volume data, and made reasonable estimates of entropy and thermal expansion and compressibility. Gillet et al. (1989) obtained C_p data from calorimetric and spectroscopic measurements. But the most useful thermodynamic property, the enthalpy of formation ($\Delta H°_f$), cannot be estimated to the accuracy required for phase diagram calculations, nor do there exist any calorimetric

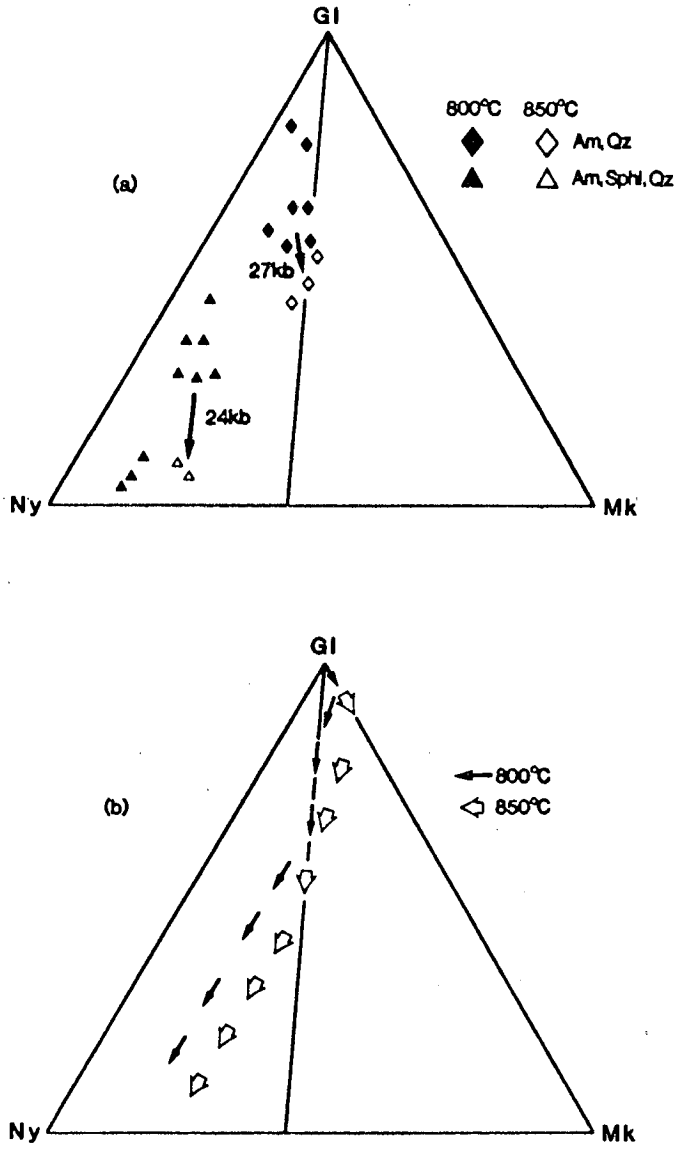

Fig. 3.5. Compositions of amphiboles synthesised by Welch (1987, 1989) (NMASF): (a) EMP analyses, (b) Compositional trends as a function of decreasing pressure. From Welch (1987).

data for glaucophane, which would have been the most direct method of obtaining $\Delta H°_f$. Thus it must be derived from phase equilibrium experiments, and both studies used the data of Carman & Gilbert (1983) on reaction (1), making the assumption that the glaucophane was almost ideal in composition. The two values differ by 9.1 kJ

mol^{-1}, due to small differences in entropy and C_p. The value of $\Delta H°_f$ which Holland extracted, when included in the dataset of Holland & Powell (THERMOCALC, in press) along with the other thermodynamic data for glaucophane, allows a pressure calculation for the Tauern eclogites which is consistent with previous estimates (Holland, 1979). But the uncertainty in the glaucophane composition cannot be ignored. The effect of non-stoichiometry on the calculated $\Delta H°_f$ can be estimated by using THERMOCALC to calculate the positions of glaucophane-bearing equilibria with glaucophane activities <1. For example a reduction in a_{Gl} of 0.1 shifts the position of the reaction Gl = Jd + Tc by a little over 2 kbar at 800°C from 36.0 kbar to 38.2 kbar. Thus, were the mole fraction of glaucophane of the amphibole synthesised by Carman & Gilbert to be $X_{Gl} = 0.9$, ie. $a_{Gl} \approx 0.9$, the reaction Gl = Jd + Tc would be located 2 kbar too high. An activity of 0.8 would of course lead to misplacing of the reaction by 4 kbar, and so on.

In the above-mentioned studies the inability to synthesise end-member glaucophane was taken to reflect problems inherent in the experimental conditions required, eg. rapid nucleation and growth, and persistence, of metastable phases during low-temperature runs. But there is theoretical evidence that pure Mg-glaucophane is in fact unstable under all conditions, and to be stable must contain at least 0.5 Fe per formula unit. The crystal chemical reason for the stabilising effect of Fe on the structure (Ungaretti, in prep.) is that the Al^{3+}, occupying both M(2) sites, attract the O(1) oxygens in opposite directions, causing the M(3) sites to expand to such an extent that the substitution of some Fe^{2+} for Mg in M(2) is necessary to maintain stability.

Thus any attempt to synthesise glaucophane must fail, and the thermodynamic data required to calculate phase relations must be obtained using amphiboles of other compositions. The original aim of this study was therefore to synthesise an amphibole related to glaucophane by a simple exchange, the enthalpy of which could be independently determined, derive $\Delta H°_f$ for the amphibole from phase equilibria, and add to this the exchange enthalpy to obtain $\Delta H°_f$ for end-member glaucophane. Nyböite was selected for two reasons. Firstly, it is related to glaucophane by the "edenite" exchange $NaAlSi_{-1}$, which has been investigated experimentally in fluor-tremolite – fluor-edenite amphiboles by Graham & Navrotsky (1986); and secondly, Welch (1987, 1989) suggested it would be stable at lower pressures than glaucophane, allowing for routine synthesis.

The experiments failed to yield end-member nyböite; nevertheless the results can be usefully applied to natural glaucophane-bearing assemblages.

3.2. PREDICTED PHASE RELATIONS OF NYBÖITE

Because nyböite is compositionally quite similar to glaucophane (Fig. 3.1), its phase relations may be expected to resemble those already determined experimentally for "glaucophane" (Figs. 3.2, 3.3), although silica-undersaturated phases such as nepheline will play a more important role. Bearing this in mind, two Schreinemakers nets were constructed of nyböite phase relations, the first for a silica-undersaturated system, and the second for a system with silica in excess, as is common for "glaucophane"-bearing assemblages (Fig. 3.6). Some of the experimentally determined stability limits of the non-amphibole phases likely to be involved in the reactions with nyböite are depicted in Fig. 3.7.

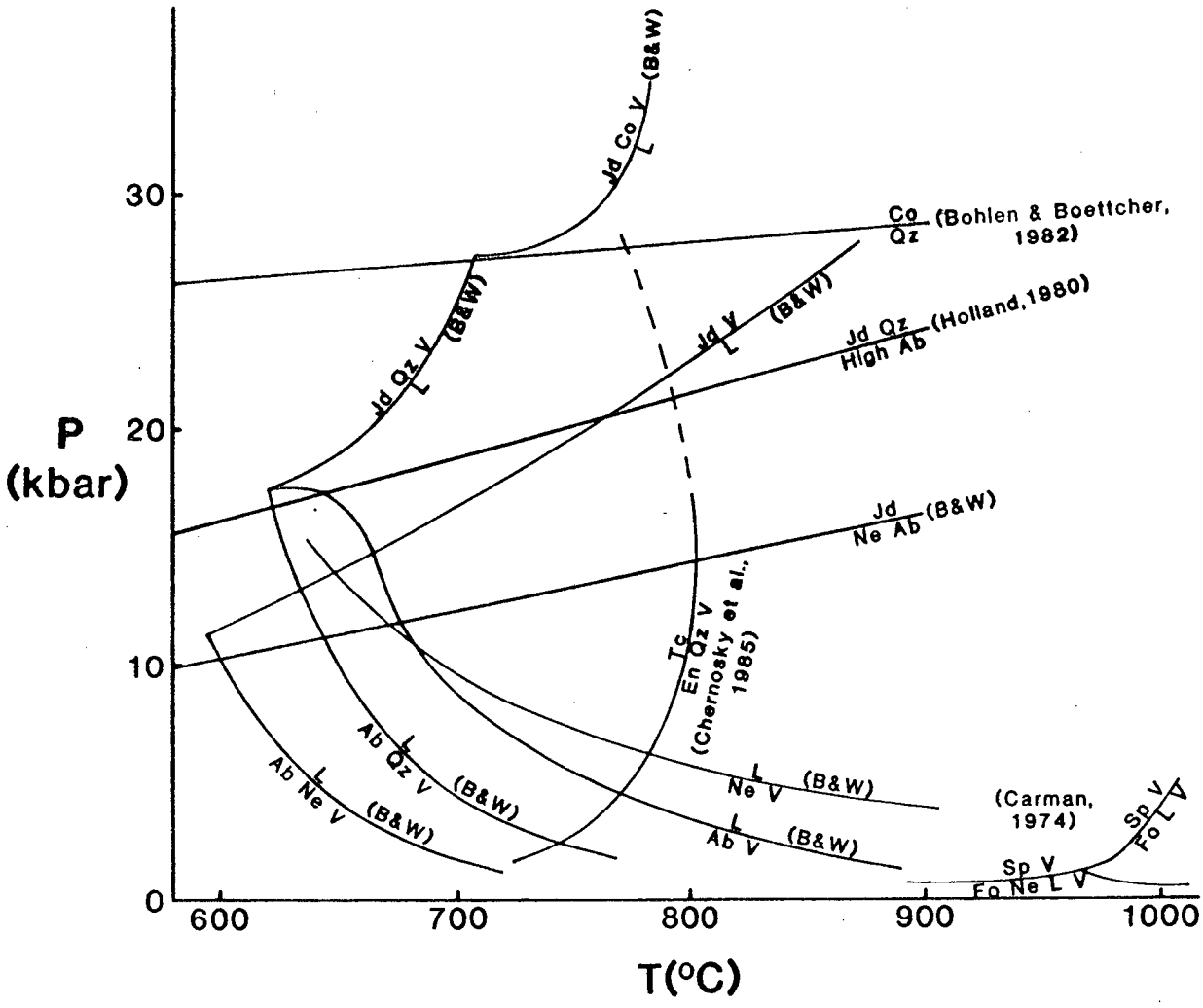

Fig. 3.7. Some important equilibria in the system Na_2O-MgO-Al_2O_3-SiO_2-H_2O relevant to glaucophane and nyböite experiments. B&W = Boettcher & Wyllie (1969).

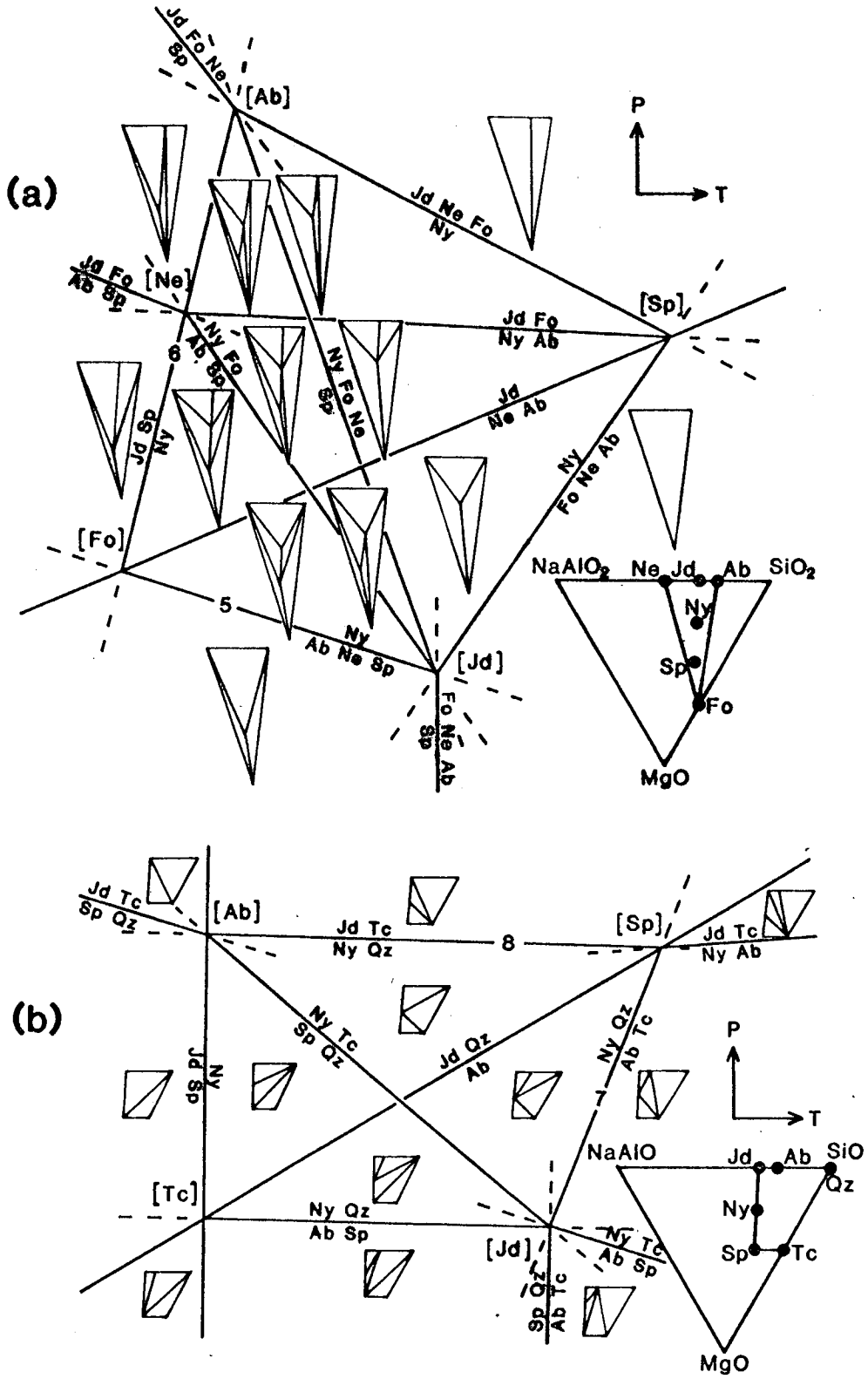

Fig. 3.6. Schreinemakers nets of reactions relevant to nyböite stability in the system $NaAlO_2$-MgO-SiO_2:
(a) SiO_2-undersaturated, H_2O in excess,
(b) SiO_2 and H_2O in excess.
Numbered reactions approximate those investigated in this study, which may contain additional phases due to the non-stoichiometry of the nyböite.

3.3. EXPERIMENTAL

3.3.(i). Procedure

A piston-cylinder apparatus of Boyd and England design was used for all except five experiments. Initially 1/2" diameter furnace-assembly cells were used: talc/boron nitride for runs at temperatures below 750°C and a few higher temperature runs, and talc/pyrex for the majority of high temperature runs. However there were three drawbacks associated with these cells which necessitated the development of the 3/4" salt-cell used for all subsequent experiments. Firstly, despite consistently following the same assembly procedure, and ensuring that every experiment was run "piston-out", the pressure experienced was not reproducible. For example, though a run at 720°C and nominally 28.9-31.4 kbar (OH-Q 1) yielded coesite among its products, a subsequent experiment at the same temperature but a higher pressure (31.5-32.5 kbar) using silica-gel as starting material, yielded quartz. The actual pressure during this run was clearly less than for the previous run, and in fact the underpressure experienced must have been at least 4 or 5 kbar, as at 720°C the quartz-coesite boundary occurs at 27.5 kbar (Bohlen & Boettcher, 1982). For most experiments the actual pressure could not be tightly constrained by its relation to such well-determined univariant reactions as Qz = Co or Ab = Jd + Qz. Therefore the calibration used by Welch (1989) was applied to give the corrected pressures listed in Table 3.2. The second drawback was a sample size limitation of ~10mg. This is enough for run product characterisation by XRD and EMPA, but makes precise addition of water and synthesis of sufficient material for re-runs difficult. This was in any case not feasible because of the third drawback, namely that it was never possible to recover the sample entirely free of contamination by corundum from the recrystallised alumina sleeve surrounding the capsule. The 3/4" salt-cell, described in Chapter 2, overcomes these problems, but can only be used at pressures <~22 kbar.

3.3.(ii). Starting materials

The starting materials, of compositions "A" to "H", representing the nyböite-glaucophane solid-solution (Fig. 3.8), are decarbonated mechanical mixtures of gels, deficient in Na_2O, and Na_2CO_3. Their compositions, determined by x-ray fluorescence (XRF) analysis, are presented in Appendix Table A3.1. Although none of the samples give ideal analyses, for most elements the deviation from ideality is <1%, while the maximum deviation as a percentage of the cation total is <0.3%. A deficiency of 2 Na p.f.u. allowed for fluorine-analogue compositions also to be made,

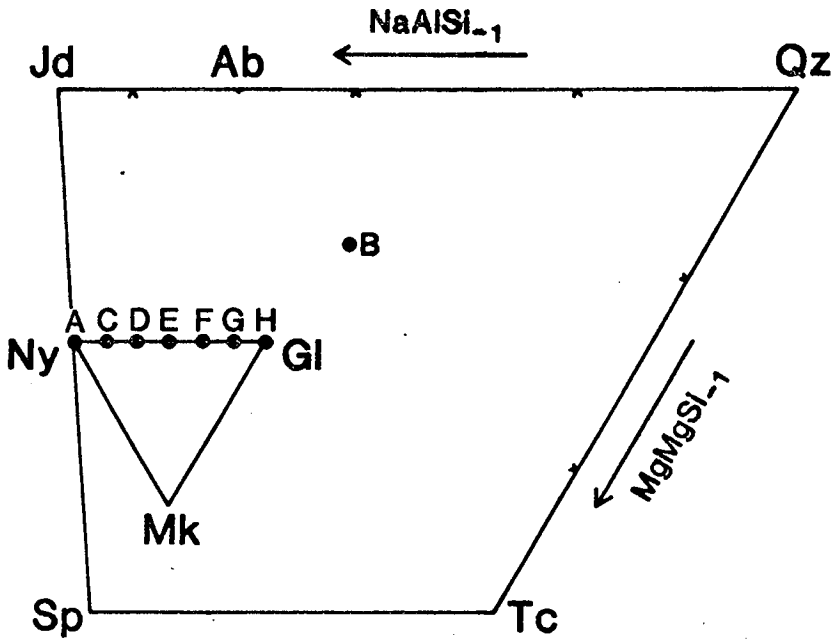

Fig. 3.8. Plot of compositions of gels used as starting materials in this study.

simply by adding 2NaF to the raw gels. "B" is a mechanical mixture of "A" and silica-gel, in the molar ratio $Na_3Mg_3Al_3Si_7O_{23}$: $7SiO_2$.

Attempts to fuse the gel mixtures at 1450°C to make glasses for EMPA were frustrated by the presence of quench crystals of forsterite, or, in the one case where fusion did occur, by subsequent rapid sodium loss under the electron beam.

3.3.(iii). Run product identification

Run products were characterised by optical microscopy, powder x-ray diffraction (XRD) and electron microprobe analysis (EMPA).

Optical microscopy

The crushed run products were mounted in a range of refractive index (RI) oils, and phase identification attempted on the basis of relief, crystal habit and extinction angle. Amphibole crystals were characteristically acicular, submicron to

40μm long × 6μm wide, with RI 1.600-1.620 and $\gamma \wedge z \sim 10\text{-}13°$. RI proved to be the most reliable means of identification, particularly for the microcrystalline phases frequently encountered.

XRD

This technique was particularly useful for identifying fine-grained run-products, though a trace amount of amphibole in one sample was not detected by XRD and therefore the optical examination was necessary. Changes in peak height ratios were used as indicators of reaction direction in mineral-mix experiments, and variations in peak positions demonstrated the presence of solid solution in the sheet silicates – phases often too fine-grained to analyse by EMP.

EMPA

Polished grain mounts in epoxy were made of most of the run products. A 15kV accelerating voltage was used instead of the usual 30kV to decrease the x-ray excitation volume so that it was more likely to lie wholly within the grain being analysed; and low beam currents (5-10 nA) and short peak count times (10-15 seconds) were used in an attempt to minimise damage from the electron beam, under which sodium can be lost rapidly. Because the width of amphibole crystals in the samples was often no more than 5μm, the back-scattered electron imaging facility proved to be essential in order to "see" the area of analysis. 5μm was wide enough to give fairly consistently good analyses, with totals of 96-98% (~2% of the amphibole is H_2O, which is not analysed) and little evidence of contamination by neighbouring grains. However the maximum grain size of most samples was less than 5μm, so that contamination by other phases was common, as were low oxide totals arising from the x-ray excitation volume incorporating epoxy as well as sample.

3.3.(iv). Recognising contamination of EMP analyses

Contamination was a particular problem in runs on the bulk composition Ny.7SiO_2 ("B" in Fig. 3.8) because of the fine amphibole grain-size and abundant fine-grained quartz crystals. For example Fig. 3.9 is a plot of the "amphibole" EMP analyses obtained from sample OH-Q 8. The data points define a band between Gl-poor (SiO_2-poor) and Gl-rich compositions, which actually extends beyond the limits of amphibole space towards Qz. The SiO_2-rich analyses are clearly contaminated, and even the least SiO_2-rich could be contaminated to some extent such that the true amphibole compositions lie closer to the Ny-Mk join. But in this sample there were at

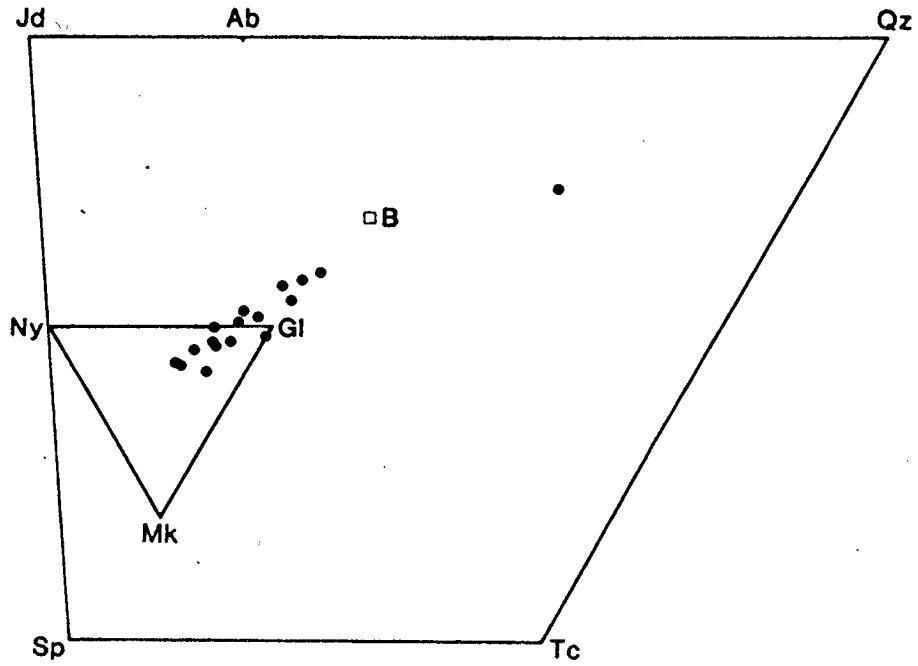

Fig. 3.9. Electron microprobe analyses of OH-Q 8 "amphiboles".

least a few grains large enough for reliable EMPA, and so some analyses must be accepted as being uncontaminated. Such was also the case for samples OH-Q 6, 8 and 15a. Therefore analyses with low Gl-content were accepted as representing the true composition, and those with X_{Gl} >70% rejected.

Although no obvious contamination trends were observed in the other samples, some yielded such a wide spread of compositions that contamination was inferred, and interpretation of analyses was therefore not attempted (eg. sample G-N 7).

3.3.(v). Recalculating amphibole formulae

All amphiboles obtained in this study are Gl-Ny-Mk-Ek solid solutions, ie. their compositions fall in the amphibole tetrahedron shown in Fig. 3.1(b). Their compositions in terms of proportions of the exchange vectors $SiNa_{-1}Al_{-1}$ (Gl),

$MgMgNa_{-1}Al_{-1}$ (Mk) and $MgSiAl_{-1}Al_{-1}$ (Ek) relative to the additive component Ny (terminology of Thompson, 1981) are calculated as follows:

Amphibole composition : $Na_{3-p}Mg_{3+q}Al_{3-r}Si_{7+s}O_{22}(OH)_2$

Cation total : 16-t

$n(SiNa_{-1}Al_{-1}) = t = X_{Gl}$

$n(MgMgNa_{-1}Al_{-1}) = p-t = X_{Mk}$

$n(MgSiAl_{-1}Al_{-1}) = s-t = X_{Ek}$

$\Rightarrow X_{Ny} = 1 - (X_{Gl} + X_{Mk} + X_{Ek})$

The calculated mole proportions may be checked against the values of q and r:

$q = 2X_{Mk} + X_{Ek}$

$r = X_{Gl} + X_{Mk} + 2X_{Ek}$

As a worked example, the first amphibole analysis of sample OH-NY1 is

$Na_{2.87}Mg_{3.34}Al_{2.56}Si_{7.19}$ Cation total 15.96

$\Rightarrow p = 0.13 \quad q = 0.34 \quad r = 0.44 \quad s = 0.19 \quad t = 0.04$

$X_{Gl} = 0.04$

$X_{Mk} = 0.09$

$X_{Ek} = 0.15$

$X_{Ny} = 1 - (0.04 + 0.09 + 0.15) = 0.725$

Checking these against q and r:

$2X_{Mk} + X_{Ek} = 0.33 \qquad (q = 0.34)$

$X_{Gl} + X_{Mk} + 2X_{Ek} = 0.43 \qquad (r = 0.44)$

Agreement is to within rounding error.

3.3.(vi). Sheet silicate compositions

Sheet silicates have been important products in previous studies relating to glaucophane; for example Carman & Gilbert (1983) report the presence of a Sp-Tc solid solution in many of their runs, and Tc or Sp in others. Koons (1982) encountered Tc in most of his "H_2O-undersaturated" experiments, and both Tc and "Na-mica" in his "H_2O-excess" experiments. Welch (1989) found that F-Tc was unstable and the only sheet silicate in his experiments in the system NMASF was F-Sp. The sheet silicates encountered in this study were Tc, Sp and Tc-Sp-Pw solid solutions, their compositions estimated by EMPA and by XRD.

EMPA

Sp suffers rapid sodium loss under the electron beam, resulting in low Na counts and hence increased Mg, Al and Si counts. Analysis of synthetic end-member Sp demonstrates this clearly (Table 5.4, Chapter 5). But Na must occupy the A-site in

the structure only, requiring the sum of the other cations to be 7. Therefore assuming that their counts are all increased by the same proportion, the sum is normalised to 7 and Na added to make the charge up to 22. This procedure gives a satisfactory composition for the pure Sp, and it is assumed also to work for the solid solutions obtained in this study.

The resulting compositions may be recast in terms of the additive component Sp and exchange vectors $SiNa_{-1}Al_{-1}$ (Tc) and $AlAlMg_{-1}Si_{-1}$ (Pw) in a manner analogous to the amphibole compositions:

Sheet silicate composition : $Na_{1-p}Mg_{3-q}Al_{1+r}Si_{3+s}O_{10}(OH)_2$

$$n(SiNa_{-1}Al_{-1}) = p = X_{Tc}$$

$$n(AlAlMg_{-1}Si_{-1}) = q = X_{Pw}$$

$$\Rightarrow X_{Sp} = 1 - (X_{Tc} + X_{Pw})$$

Checking against r and s:

$$r = 2q - p$$

$$s = p - q$$

It is interesting that the lower the Sp content (or higher the Pw content) the less the difference between observed Na and calculated Na (compare Appendix Tables A3.3 and A3.6). For example the observed Na of the analyses of sample OH-NY1 are close to the observed excess over 7 in the cation total, and when recalculated in terms of Sp, Tc and Pw have the lowest Sp content and highest Pw content. Clearly the Pw structure allows for stronger Na-bonding than does the Sp structure.

XRD

The most intense sheet silicate diffraction maximum is usually the (001) peak at 9.4°2θ for Tc, 8.7°2θ for Sp (Carman, 1974) and around 9.2°2θ for Pw (Keusen & Peters, 1980). However at low temperature Sp hydrates (Carman, 1974) and the 8.7°2θ peak shifts to 7.4°2θ (higher-temperature hydrate HI) at 75 ± 5°C under typical laboratory conditions, and 6.0°2θ (low-temperature hydrate HII) at 40 ± 3°C.

All sheet silicates coexisting with amphibole, but without Qz, occur as hydrates at room temperature, their (001) diffraction maxima at 7.4-7.6°2θ. On heating for a few minutes on a hot-plate at ~150°C, (001) peaks shift to 8.9-9.1°2θ, values too high for Sp but too low for Tc, which in any case does not hydrate. Therefore all these sheet silicates are inferred to be Sp-Tc-Pw solid solutions, as those probed certainly are.

The only end-member Sp, with a diffraction maximum at 8.7°2θ, occurs in the amphibole-free OH-NY run products, while all sheet silicates coexisting with quartz are end-member Tc, with XRD maxima at 9.4°2θ.

Table 3.2. Experimental results.

Run no.	Starting composition	Pressure cell *	P(kbar) corrected	T(°C)	Duration (hours)	Run products
OH-NY1	A	P	26.1-27.0	830-833	66	Am,Jd,Ss
OH-NY3	A	P	22.3-24.0	748-751	65	Am,Jd,Ss
OH-NY4	A	BN	28.6-30.4	590-598	138	Jd,Ss
OH-NY5	A	BN	19.0-19.8	598-601	141	Am,Jd,Ss
OH-NY6	A	BN	26.6-28.4	700-704	76	Am,Jd,Ss
OH-NY7	A	BN	20.3-20.6	698-700	71	Am,Jd,Ss
OH-NY8	A	BN	24.4-25.2	597-601	142	Am,Jd,Ss
OH-NY9	A	P	31.1-31.3	898-901	45	Am,Jd,Ss
OH-NY10	A	P	15.1-15.4	900	66	Fo,L
OH-NY12	A	BN	27.3-28.1	649-653	92	Am,Jd,Ss
OH-NY14	A	BN	32.2-32.8	648-650	40	Am,Jd,Ss
OH-NY15	A	P	32.2	829-832	41	Am,Jd,Ss
OH-NY16	A	BN	15.2-16.0	648	42	Am,Ab,Ne,Ss
OH-NY17	A	BN	15.0-15.2	698-700	40	Am,Ab,Ne,Ss
OH-NY18	A	P	15.0	750-754	19	Ab,Ne,Sp
OH-NY19	A	NC	15.7-16.3	799-802	98	Am,Jd,Ss
OH-NYG1	A	GB	8.0	800	48	Sp,L
OH-NYG2	A	GB	8.3-8.5	700	70	Sp,L
OH-Q1	B	BN	26.6-28.6	720	70	Am,Co,Jd,Tc
OH-Q2	B	BN	28.3-29.7	601-603	140	Qz,Co,Jd,Tc
OH-Q3	B	P	29.7-31.4	762	116	Am,Co,Jd,Tc
OH-Q5	B	BN	19.3-20.3	601	39	Qz,Ab,Tc
OH-Q6	B	BN	20.4-21.1	746-749	138	Am,Qz,Jd
OH-Q7	B	BN	21.5-22.1	800	66	Am,Qz,Jd
OH-Q8	B	BN	19.6-20.5	798-801	72	Am,Qz,Ab
OH-Q9	B	BN	20.2-20.5	850	50	Ab,En,L
OH-QG1	B	GB	8.0	800	48	En,L
OH-QG2	B	GB	8.0-9.0	744-757	43	Qz.,Ab,Tc
OH-QG4	B	GB	8.4-9.4	650	22	Qz,Ab,Tc
OH-Q10	OH-QG4	P	17.1-18.2	801	48	Qz,Ab,En
OH-Q11	OH-QG4	P	19.9-20.3	780	33	Am,Qz,Ab
OH-Q13	B	NC	19.0	801	3	Am,Qz,Ab,En
OH-Q14a	B	NC	19.5-20.1	800	80	Am,Qz,Ab,En

(Table 3.2 continued)

Run no.	Starting composition	Pressure cell *	P(kbar) corrected	T(°C)	Duration (hours)	Run products
OH-Q14b	OH-QG4	NC	19.5-20.1	800	80	Am,Qz,Ab,Tc,En
OH-Q15a	B	NC	22.2	825	37	Am,Qz,Ab
OH-Q15b	OH-QG4	NC	22.2	825	37	Am,Qz,Ab,En
OH-Q16a	B	NC	21.0-21.3	800	36	Am,Qz,Ab
OH-Q16b	OH-QG4	NC	21.0-21.3	800	36	Am,Qz,Ab,Tc,En
OH-Q17	B	NC	17.0-17.5	700	44	Am,Qz,Ab,Tc
OH-Q18a	B	NC	18.5-18.9	700	47	Am,Qz,Ab,Tc
OH-Q18b	OH-Q17	NC	18.5-18.9	700	47	Am,Qz,Ab
OH-Q19	B	NC	17.0-17.3	648-650	66	Am,Qz,Ab,Tc
OH-Q21a	B	NC	14.3-14.8	700	82	Am,Qz,Ab,Tc
OH-Q21b	OH-Q19	NC	14.3-14.8	700	82	Am,Qz,Ab,Tc#
OH-Q26	B	NC	17.5-18.0	770	65	Am,Qz,Ab,Tc
OH-Q27	OH-Q26	NC	15.9-16.7	770	44	Am,Qz,Ab,Tc#
OH-Q28	B	NC	17.7-18.4	790	90	Am,Qz,Ab,Tc,En
OH-Q31	B	NC	18.8-19.2	770	48	Am,Qz,Ab,Tc
G-N1	D	NC	17.5-18.0	770	65	Am,Jd,Ss
G-N2	E	NC	15.9-16.7	770	44	Am,Ab,Ss
G-N3	F	NC	17.7-18.4	790	90	Am,Ab,Ss
G-N4	E	NC	17.7-18.3	770	78	Am,Ab,Ss
G-N5	F	NC	17.7-18.3	770	78	Am,Ab,Ss
G-N6	C	NC	15.7-16.3	799-802	98	Am,Ab,Jd,Ss
G-N7	E	NC	18.8-19.2	770	48	Am,Ab,Ss
G-N8	G	NC	18.0-18.4	771	95	Am,Ab,Ss
G-N9	H	NC	18.0-18.4	771	95	Am,Ab,Ss
G-N10	G	NC	16.0-16.4	770	49	Am,Ab,Ss
G-N11	H	NC	16.0-16.4	770	49	Am,Ab,Ss
G-N12	H	NC	21.9-22.1	750?	47	Am,Qz,Jd,Tc

* P . . talc-pyrex BN . .talc-boron nitride

NC . .NaCl GB . .internally heated gas pressure vessel

Reaction Am + Qz → Ab + Tc determined from XRD peak height ratios.

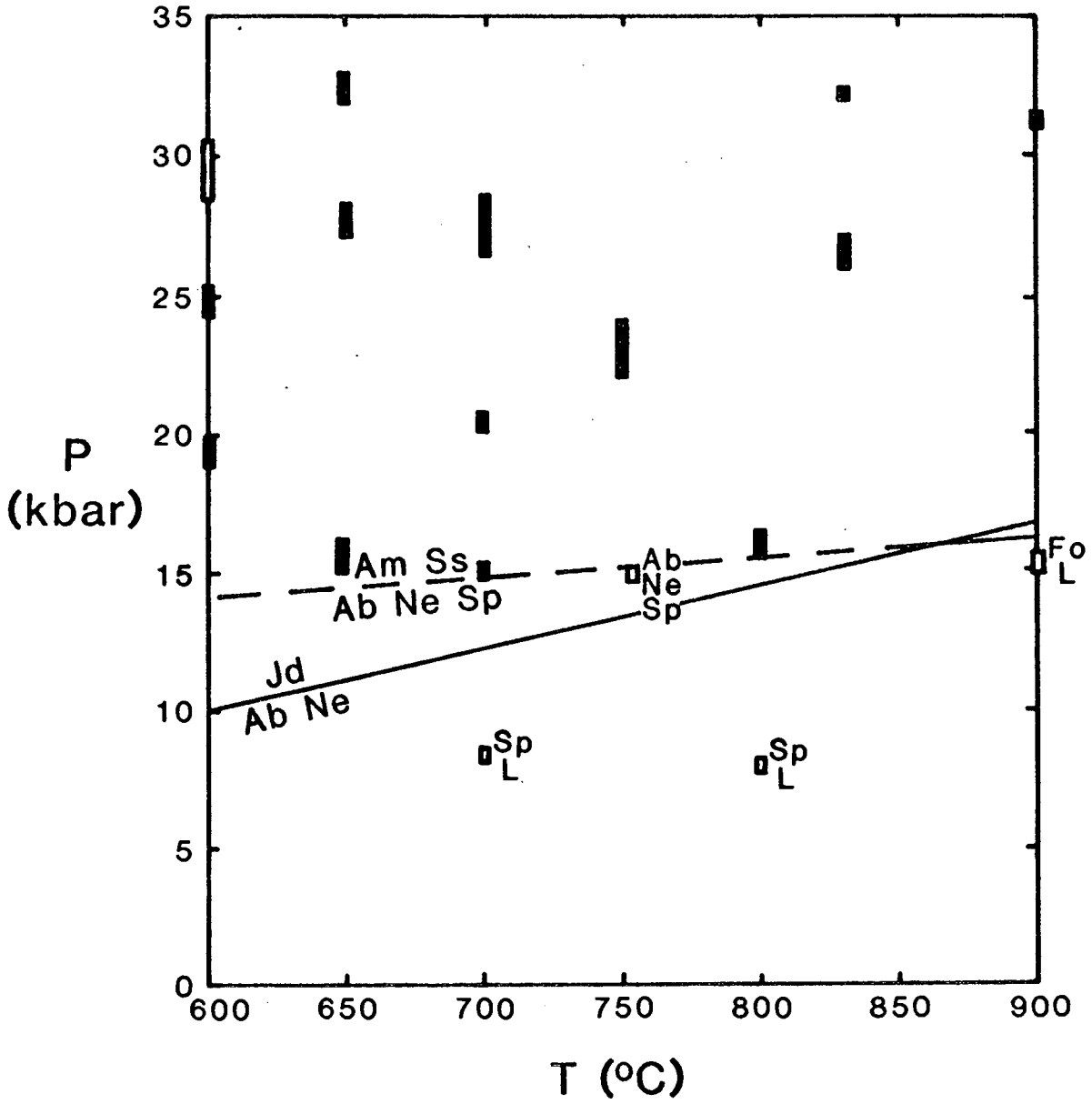

Fig. 3.10. Results of OH-NY experiments. Filled symbols are amphibole-bearing assemblages: Am, Jd, Ss or Am, Ab, Ne, Ss. Open symbols are amphibole-free.

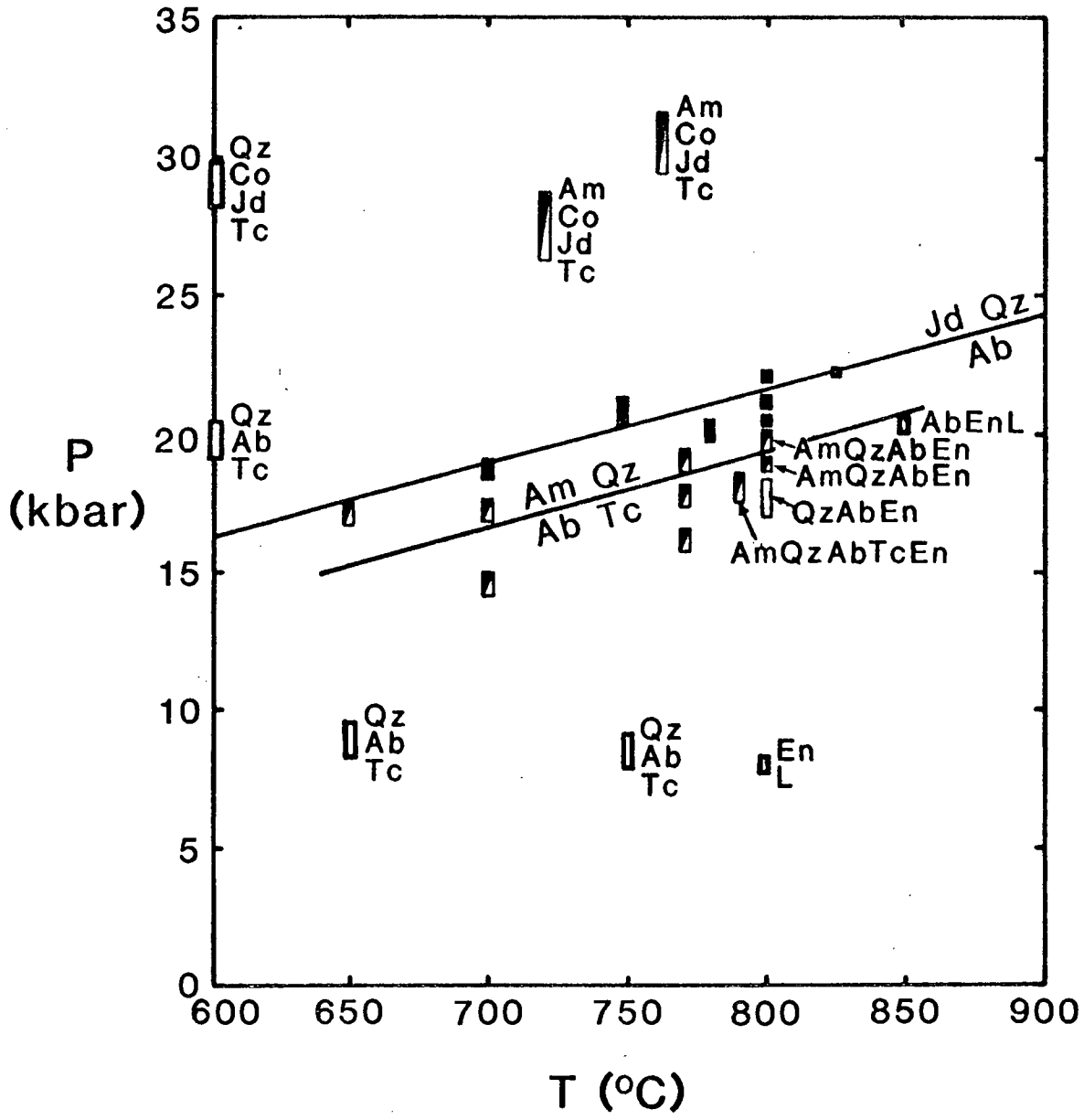

Fig. 3.11. Results of OH-Q experiments. Filled symbols are amphibole-bearing 3-phase assemblages: Am, Qz, Jd or Am, Qz, Ab. Half-filled symbols are amphibole-bearing 4- or 5-phase assemblages: Am, Qz, Ab, Tc, unless otherwise indicated. Open symbols are amphibole-free.

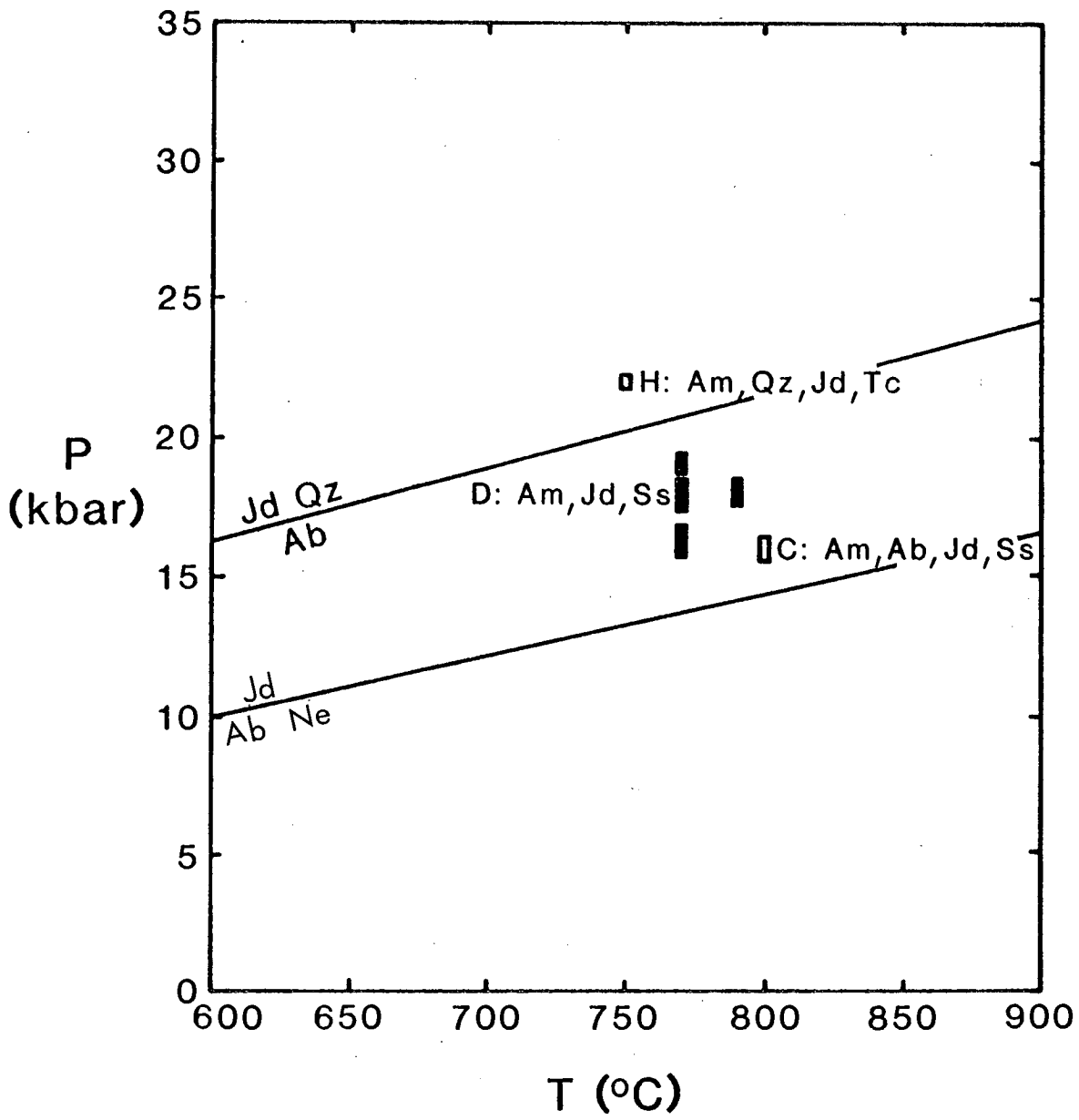

Fig. 3.12. Results of G-N experiments. Filled symbols represent conditions where runs yielded Am, Ab, Ss. Other assemblages as indicated, from bulk compositions indicated.

Table 3.3. Mean EMP analyses of NMASH amphiboles.

Sample	Bulk composition	P (kbar)	T (°C)	N	Na	Mg	Al	Si	X_{Gl}	X_{Mk}	X_{Tk}	X_{Ny}
OH-NY 1	Ny_{100}	27	829	24	2.84	3.30	2.59	7.20	.07	.09	.13	.71
					(3)	(3)	(3)	(2)	(3)	(2)	(2)	
OH-NY 9	Ny_{100}	31	900	12	2.75	3.49	2.70	7.05	.02	.23	.03	.72
					(3)	(7)	(10)	(4)	(1)	(2)	(4)	
OH-NY 15	Ny_{100}	32	830	9	2.78	3.53	2.52	7.15	.02	.20	.13	.65
					(4)	(10)	(9)	(3)	(2)	(4)	(4)	
OH-NY 19	Ny_{100}	16	800	12	2.85	3.24	2.57	7.24	.10	.05	.14	.71
					(3)	(7)	(5)	(2)	(4)	(2)	(4)	
OH-Q 6	$Ny_{100}.7SiO_2$	21	750	4	2.40	3.26	2.22	7.61	.51	.09	.09	.31
					(7)	(9)	(5)	(6)	(7)	(4)	(2)	
OH-Q 7	$Ny_{100}.7SiO_2$	22	800	4	2.25	3.42	2.10	7.66	.58	.17	.08	.17
					(6)	(5)	(7)	(3)	(3)	(3)	(5)	
OH-Q 8	$Ny_{100}.7SiO_2$	20	800	6	2.26	3.33	2.25	7.59	.58	.16	.01	.25
					(5)	(5)	(14)	(13)	(8)	(5)	(1)	
OH-Q 15a	$Ny_{100}.7SiO_2$	22	825	2	2.13	3.54	2.09	7.63	.61	.26	.02	.11
					(12)	(10)	(2)	(6)	(14)	(2)	(6)	
G-N 1	$Ny_{67}Gl_{33}$	18	770	3	2.77	3.45	2.25	7.39	.14	.10	.25	.51
					(9)	(18)	(16)	(9)	(5)	(8)	(4)	
G-N 2	$Ny_{50}Gl_{50}$	16	770	6	2.69	3.82	1.78	7.58	.13	.18	.45	.24
					(3)	(14)	(8)	(2)	(6)	(5)	(5)	
G-N 4	$Ny_{50}Gl_{50}$	18	770	4	2.54	3.43	2.11	7.57	.35	.11	.22	.32
					(2)	(3)	(6)	(4)	(2)	(2)	(3)	
G-N 6	$Ny_{83}Gl_{17}$	16	800	10	2.79	3.26	2.50	7.29	.15	.06	.14	.65
					(4)	(5)	(4)	(2)	(3)	(2)	(3)	

Numbers in parentheses are errors in last digits (2s of mean).

3.4. RESULTS

All experimental run conditions and results are listed in Table 3.2 and plotted in Figs. 3.10-3.12 (for the experiments on Ny, Ny.7SiO_2 and $Ny_{17}Gl_{83}$-Gl bulk compositions respectively, hereafter referred to as OH-NY, OH-Q and G-N). All successful EMP analyses of amphiboles, sheet silicates and pyroxenes are listed in Appendix Tables A3.2-A3.4 respectively, and the recalculated amphibole formulae in Appendix Table A3.5. Averages of uncontaminated analyses are listed in Table 3.3.

3.4.(i). OH-NY experiments

Runs OH-NY 1-19 and OH-NY G1 and G2 (Fig. 3.10) used the gel mixture "A" as starting material. Most runs were conducted below the wet jadeite solidus (see Fig. 3.7); nevertheless the volume of distilled water added to the gel for each run was kept low in an effort to avoid amphibole dissolution in the fluid (usually ~9wt% distilled water was added, anticipating some loss during welding). Because sample OH-NY 19 was run in the salt-cell just 3wt% H_2O was added and there was no evidence of melting even though the temperature exceeded the wet jadeite solidus. Samples OH-NY 17 and 18, run in the 1/2" talc cell with 9wt% H_2O, surprisingly also showed no signs of melting. But more significant was the occurrence of Ab + Ne in the run products of these samples and OH-NY 16, at nominal corrected pressures well above Ab + Ne = Jd (see Fig. 3.7). It is conceivable that the underpressures experienced were much greater (~3 kbar) than anticipated by the calibration, but it is more likely that jadeite failed to nucleate during the runs and metastable Ab + Ne grew instead. This would be consistent with the observations of Boettcher & Wyllie (1968), who in their experimental determination of the reaction Ab + Ne = Jd, found Jd very slow to react from a starting mix of crystalline Ab + Ne at low temperature, and unable to crystallise outside its stability field, while Ab + Ne crystallised readily, both stably and metastably. Another factor which should be considered is the likely solid solution between Ab and Ne, which will decrease the free energy of the low pressure assemblage and hence increase its stability field. Thus the gel starting materials used in this study may initially crystallise to Ab_{ss} + Ne_{ss}, which will be more likely to persist than if pure crystalline Ab + Ne were used.

The most common assemblage encountered in runs on this bulk composition was Am, Jd, Ss. EMPA was successful for amphiboles in four samples: OH-NY 1, 9, 15 and 19. Their compositions, expressed in terms of Gl, Ny, Mk and Ek components, are plotted in Fig. 3.13. Clearly none of them is end-member nyböite, the maximum Ny content of a single analysis being only 0.87, and the maximum mean Ny content 0.72 (both values from sample OH-NY 9). The mean analyses of these amphiboles

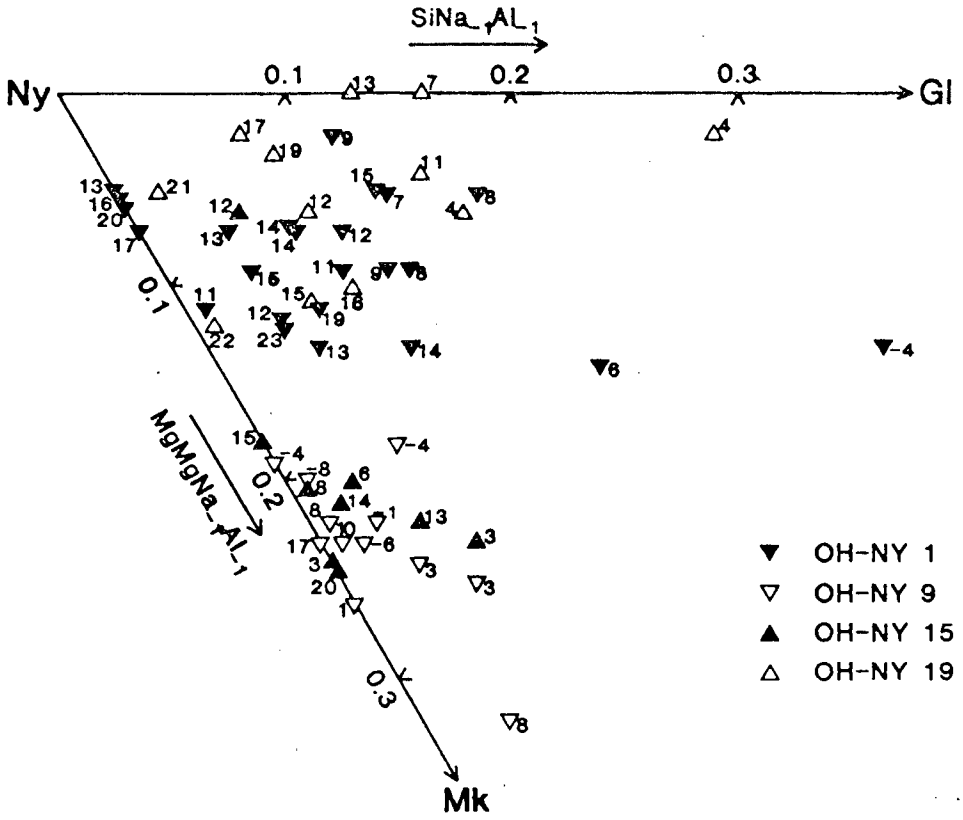

Fig. 3.13. Projection from $MgSiAl_{-1}Al_{1}$ of OH-NY amphibole EMP analyses, with %Ek content given for each analysis.

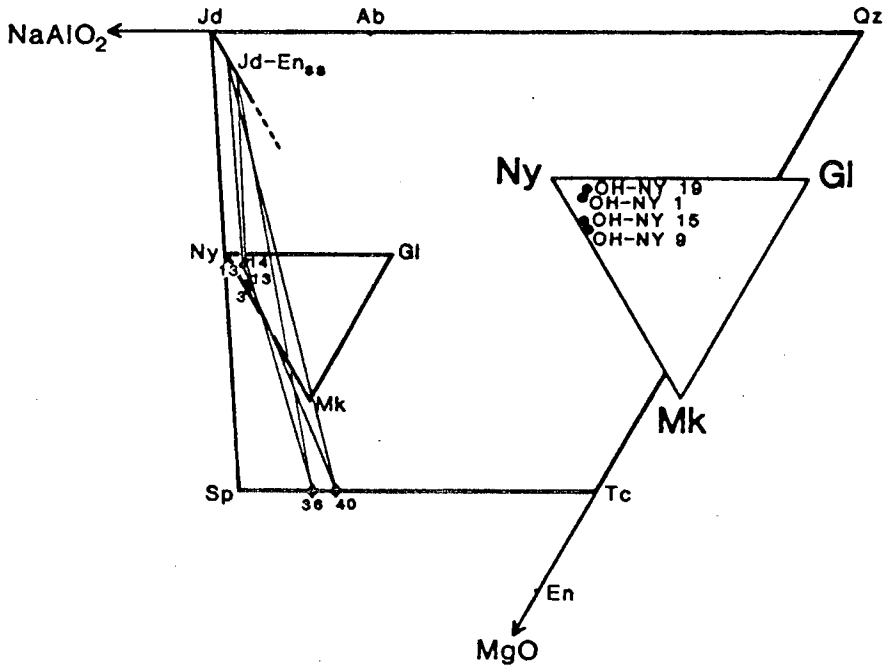

Fig. 3.14. Mean EMP analyses of OH-NY amphiboles (circles, with %Ek contents), sheet silicates (triangles, with %Pw contents) and pyroxenes. Amphibole compositions lie above the plane, and sheet silicates below. Inset indicates from which sample analyses were obtained.

are plotted in Fig. 3.14 together with the mean pyroxene and sheet silicate analyses and appropriate tie-lines. The amphiboles for which EMPA was unsuccessful must also be "off-composition", as otherwise the coexisting sheet silicate and pyroxene would have to have the compositions Sp and Jd, with the bulk composition lying on the tie-line between them. All the pyroxenes are close in composition to Jd, with X_{En} no more than 0.14. However XRD indicates that the sheet silicates are complex solid solutions, and the maximum analysed X_{Sp} is only 0.55.

Despite considerable scatter of analyses, from only four samples, two compositional trends in the amphiboles are apparent. Firstly there is an increasing Mk component and decreasing Gl component with increasing pressure, corresponding to a filling of the A-site through the coupled substitution $MgMgSi_{-1}$ (=$NaAlSi_{-1}$ + $MgMgNa_{-1}Al_{-1}$). Samples OH-NY 9 and 15 have almost full A-sites, with Na^{A} averaging 0.99 and 0.98 respectively. Secondly, with increasing temperature there is an apparent decrease in Ek component through the Tschermak's exchange $AlAlMg_{-1}Si_{-1}$. The orientations of these two exchange vectors in P,T space are shown schematically in Fig. 3.15.

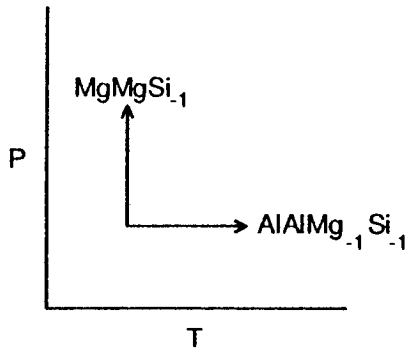

Fig. 3.15. Possible orientations in P-T space of exchange vectors affecting quaternary amphibole compositions.

The absence of amphibole in the product of run OH-NY 4 could lead to the interpretation that it is no longer stable at these conditions (28.6-30.4 kbar, 600°C), but this would require the reaction Am = Jd + Ss to have a much steeper slope than expected from a comparison with previous experimental results on "glaucophane". A more plausible explanation is that the kinetics of amphibole nucleation and growth are prohibitively slow at such a low temperature.

The other amphibole-absent runs were OH-NY 10, 18, G1 and G2. OH-NY G1 and G2 contained a melt, the product of the reaction Ab + Ne + V = L (see Fig. 3.7). They were run in internally heated gas pressure vessels, which allowed the use of larger samples than the piston-cylinder apparatus, and hence the water content to be more accurately controlled. The amount in excess of that needed to grow amphibole was small, and the absence of amphibole in the run products is likely to be

a true indication of its instability, rather than a reflection of an insurmountable kinetic barrier to its nucleation from the melt.

The absence of amphibole in OH-NY 10 may reflect its instability at 15 kbar and 900°C. However, in this case an imprecisely controlled water content may have resulted in an excess of H_2O and hence rapid melting, with amphibole unable to nucleate from the melt. Forsterite is present here as the temperature is above the Sp melting reaction (see Fig. 3.7).

Low pressure amphibole breakdown

While OH-NY 17 contains Am, Ab, Ne, Ss, the higher-temperature OH-NY18 contains Ab, Ne, Sp. These two runs therefore bracket the low-pressure reaction by which nyböitic amphiboles coexisting with Ab, Ne, Ss break down:

$$Ny\text{-}Gl\text{-}Ek\text{-}Mk_{ss}\ (Am) + Sp\text{-}Tc\text{-}Pw_{ss}\ (Ss) \rightarrow Ne + Ab + Sp \qquad (5)$$

(equivalent to reaction (5) in Fig. 3.6(a)), to a pressure of ~15 kbar at 700-750°C. It must be remembered that in containing Ne + Ab, these two assemblages are probably metastable with respect to Jd-bearing assemblages, and therefore it is the metastable extension of reaction (5) which has been located. Run OH-NY 19, in yielding Am, Jd, Ss at ~16 kbar, 800°C, must be close to the low-pressure amphibole limiting reaction:

$$Ny\text{-}Gl\text{-}Ek\text{-}Mk_{ss}\ (Am) + Sp\text{-}Tc\text{-}Pw_{ss}\ (Ss) \rightarrow Jd + Sp \qquad (6)$$

The Schreinemakers construction dictates that this reaction must occur at a higher pressure than the metastable extension of reaction (5), but solid solution between Ab and Ne might raise the pressure of reaction (5) to such an extent that this rule is not obeyed.

3.4.(ii). OH-Q experiments

Clearly most experiments on OH-NY yielded an amphibole with a component of Ek in solid solution. However previous experiments on the glaucophane bulk composition (Koons, 1982; Welch, 1987, 1989) produced amphiboles which could only lie on the plane containing the phases with which they coexisted (Jd, Tc, Qz/Co, Ab, Sp) and hence have zero Ek component. It became apparent, therefore, that as the main difference between these two bulk compositions was the silica content, a bulk composition displaced from Ny towards Qz should yield an amphibole with no Ek component, and hence closer in composition to end-member Ny. And if the two-phase assemblage Am + Qz was produced, EMPA would not be necessary to confirm that the amphibole was Ny, this being the only amphibole on the Qz-Ny tie-line. This was the reason behind the use of bulk composition "B" when "A" yielded amphiboles that were either "off-composition" or too fine-grained to probe.

As before, the addition of minimal excess H_2O was easier when the 3/4" salt-cell or the internally heated gas pressure vessels were used, in which case just 3wt% H_2O was added.

In only one experiment was there obviously an underpressure greater than that expected from the calibration: sample OH-Q 2 contained Qz at a pressure nominally 2-3 kbar above Qz = Co. However this sample did also contain Co, and therefore its true pressure bracket is assumed to straddle the Qz = Co reaction at ~25.8-27.2 kbar. It contained no amphibole, nor did the other sample run at 600°C, again interpreted to be the result of prohibitively sluggish amphibole nucleation and growth.

A number of stable(?) amphibole-bearing assemblages are observed in run products on this bulk composition. At high pressures the 4-phase assemblage Am, Co, Jd, Tc is present. At lower pressures, Co is replaced by Qz, and the assemblage Am, Jd, Qz is stable above Ab = Jd + Qz, while Am, Ab, Qz is stable below Ab = Jd + Qz. At still lower pressures a 4-phase assemblage reappears: Am, Ab, Qz, Tc.

Amphiboles coexisting with quartz and jadeite or albite

The absence of a 2-phase, Am + Qz, assemblage in any of the run products was evidence that these experiments again failed to produce Ny. But the presence of only one other phase – Jd or Ab (at pressures above and below Ab = Jd + Qz respectively) – over a broad region of P-T space implies that the amphibole is no longer quaternary, but must lie within the Ny-Gl-Mk triangle, as predicted. However the successful amphibole analyses obtained are much lower in Ny content than the previous ones, the maximum Ny content of a single analysis being only 0.37 (samples OH-Q 6 and 8), and the maximum mean Ny content only 0.31 (sample OH-Q 6).

The Ek content of the analyses is non-zero for most samples. As OH-Q 8 and 15a average to within one standard deviation of zero, this implied Ek component has been ignored.

EMPA was successful for 4 of these samples (Fig. 3.16). Unfortunately the analyses occupy too small a region of P-T space for any rigorous conclusions to be drawn concerning amphibole compositional variation. There is an apparent, though subtle, trend of decreasing Ny content and increasing Mk content with temperature and pressure, ie. increasing $MgMgNa_{-1}Al_{-1}$, from a composition close to the Gl-Ny join to one close to the Gl-Mk join (Fig. 3.17).

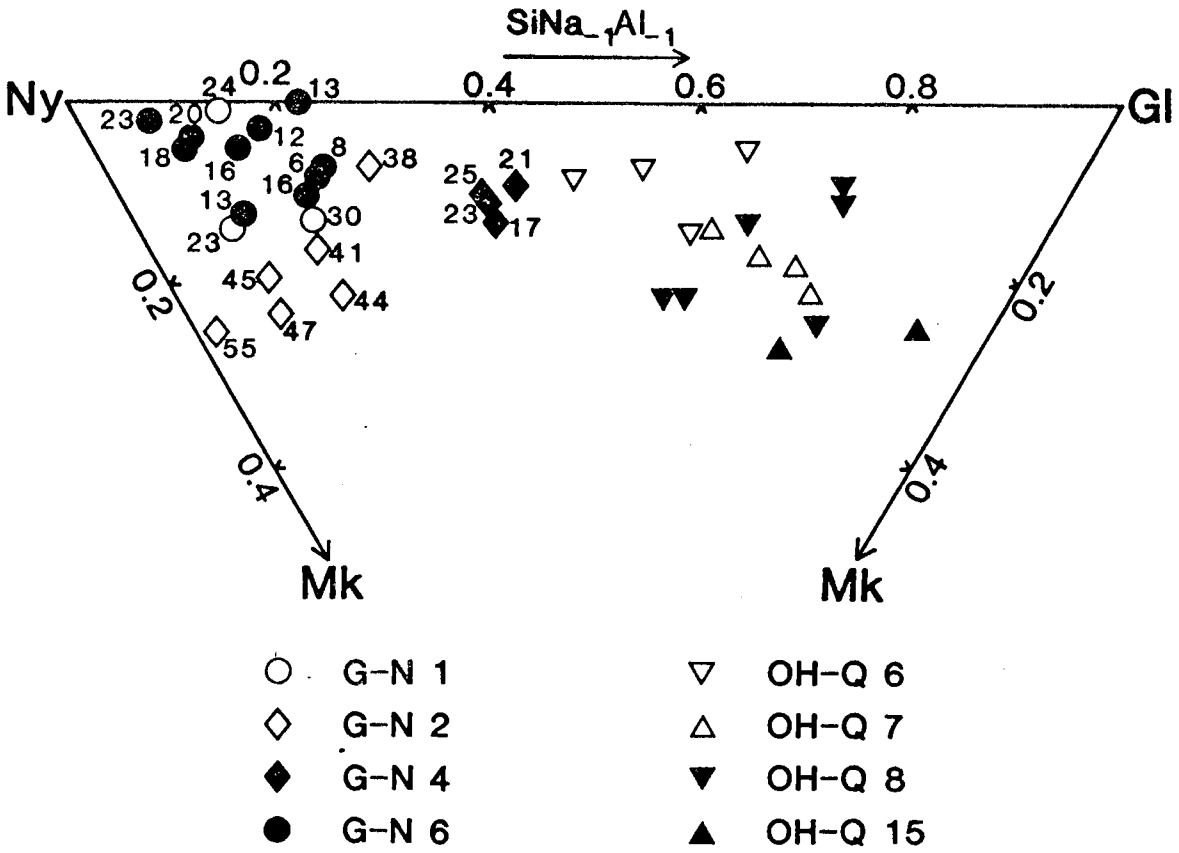

Fig. 3.16. Projection from $MgSiAl_{-1}Al_{-1}$ of OH-Q amphiboles (triangles, < 10% Ek content) and G-N amphiboles (%Ek content given for each analysis).

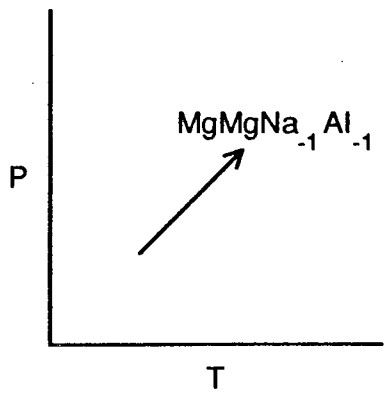

Fig. 3.17. Exchange vector affecting compositions of ternary OH-Q amphiboles.

Amphiboles coexisting with jadeite, talc and quartz or coesite

At 26-32 kbar, amphiboles coexist with Co, Px and Ss. XRD and EMPA indicate that the sheet silicate is very close in composition to Tc (Appendix Table A3.3), while the pyroxene is Jd with X_{En} up to 0.20 (Appendix Table A3.4).

Amphiboles coexisting with albite, quartz and talc

The assemblage Am, Ab, Qz, Tc occurs below 18-19 kbar, occupying a broad region of P-T space in initial runs. Re-runs demonstrate that talc is metastable at higher pressures (sample OH-Q 18b) and amphibole at lower pressures (OH-Q 21b, 27). Thus the assemblage comprises both reactants and products of the low-pressure Gl-Ny-Mk breakdown reaction:

$$\text{Gl-Ny-Mk}_{ss} + \text{Qz} = \text{Ab} + \text{Tc} \qquad (7)$$

(see Fig. 3.6(b), and also analogous to reaction (3), Fig. 3.3), which is constrained to ~15 kbar at 650°C and ~20.5 kbar at 850°C.

At temperatures above ~780°C, En is present in some runs as a product of the reaction Tc = En + Qz + H_2O. Its presence does not obscure the phase relations of the amphibole as it occurs only in products that otherwise would have contained Tc. For example, sample OH-Q 15 is clearly above the Tc dehydration reaction, yet contains only Am, Ab, Qz. Sample OH-Q 13, however, contains the 4-phase asemblage Am, Ab, En, Qz, equivalent to the lower-temperature assemblage Am, Ab, Qz, Tc. The assemblage Ab, En, Qz of sample OH-Q 10 is equivalent to assemblage Ab, Tc, Qz. While the stability of amphibole is not affected by the presence of En, EMP analyses of amphiboles in samples OH-Q 15b and 16 (Appendix Table A3.2) indicate that they are more magnesian than amphiboles in En-free samples.

The high-temperature, melt-bearing sample OH-Q 9 is analogous to OH-NY 10 in containing no amphibole. Here the absence of amphibole is interpreted as reflecting its instability, as the P-T conditions are not far removed from those of amphibole-bearing OH-Q 15, which showed no signs of melting.

3.4.(iii). G-N experiments

With the failure of the OH-Q experiments to yield end-member nyböite, came the suspicion that it could not be synthesised under any condition. The emphasis of the study therefore shifted towards a more detailed investigation of the variations in amphibole composition, particularly as a function of pressure. This had been hampered in the OH-Q experiments by grain sizes too small for EMPA. However it was observed in the OH-NY and OH-Q experiments that amphibole grain size was

related to its proportion in the run product, which was largely dependent on the closeness of the amphibole composition to the bulk composition, so one purpose of the G-N experiments was to attempt to synthesise "probe-able" amphiboles of the same composition as those previously obtained.

Runs G-N 1-12 used the gels of compositions from $Ny_{83}Gl_{17}$ to Gl as starting materials. All experiments were run in the 3/4" salt-cell, with H_2O contents of ~3wt%. The most common product assemblage was Am, Ab, Ss, encountered in the runs on the more Gl-rich bulk compositions, while Jd replaced Ab at the Ny-rich end of the join, and the only run above 20 kbar, on the Gl bulk composition (G-N 12) yielded Am, Jd, Qz, Tc. EMP analyses were obtained of amphiboles from runs G-N 1-7, four of which samples gave the uncontaminated analyses plotted in Fig. 3.16.

Amphiboles coexisting with sheet silicate, albite and/or jadeite

All compositions run at low pressures (ie. above Ab + Ne = Jd and below Ab = Jd + Qz) yielded the assemblage Am, Ss, Ab/Jd. The occurrence of Ab or Jd depends on the amphibole composition relative to the bulk composition. For example in the hypothetical situation in Fig. 3.18, a stable amphibole composition "P" might coexist with Ab and Ss "Q" for bulk compositions "E", "F", "G", "H", but with Jd and Ab for bulk composition "D", while for bulk composition "C" it might coexist with Jd and Ss "R". If the amphibole and sheet silicate are displaced from this plane, a 4-phase assemblage including both Jd and Ab could occur for any of these bulk compositions. Therefore the other reason for these experiments was that even if EMPA was unsuccessful, the amphibole compositions could be more tightly constrained than before.

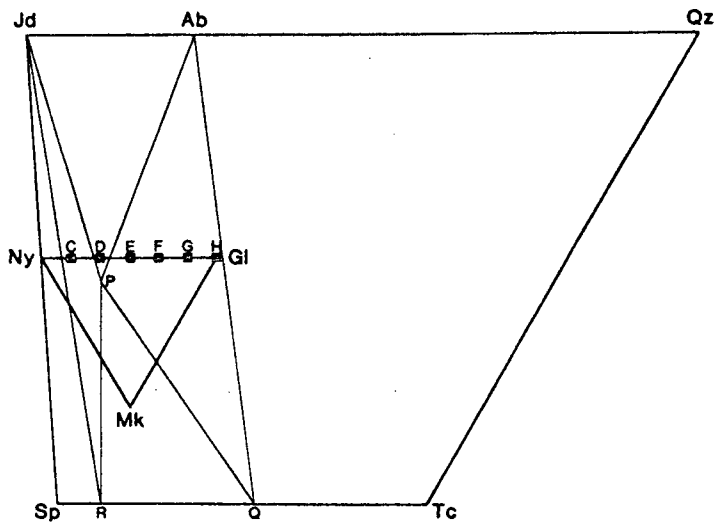

Fig. 3.18. Hypothetical phase relations at fixed P,T, illustrating the stable assemblages for bulk compositions C to H. In reality P will be a 3-dimensional field rather than a point on the Ny-Gl-Mk plane.

The run conditions may be grouped into four regions of P-T space: I: ~18 kbar, 770°C; II: ~16 kbar, 770°C; III: ~16 kbar, 800°C; IV: ~18 kbar, 790°C. Schematic phase relations for Regions I-III are depicted in Fig. 3.19, making use of the available microprobe data.

Region I All compositions between Gl and $Ny_{50}Gl_{50}$ inclusive yielded Am, Ab, Ss (G-N 4, 5, 7, 8, 9), while $Ny_{67}Gl_{33}$ yielded Am, Jd, Ss (G-N 1). Not surprisingly, the more Ny-rich bulk composition yielded more Ny-rich amphiboles (G-N 1) than did the more Gl-rich bulk composition (G-N 4).

Region II All three bulk compositions yielded Am, Ab, Ss. The analysed amphibole of G-N 2 is significantly more Ek-rich than that from the same bulk composition in Region I, or from any other analysed sample (see Table 3.2). The analysed sheet silicates in Region II display an increase in Sp content and decrease in Tc content with increasing Ny content of the bulk composition. This is consistent with the fact that for the Gl bulk composition the sheet silicate must have a higher Tc content than Sp content, as the tie-line from Ab through Gl bisects the Sp-Tc join. As the bulk composition moves towards Ny, more Sp-rich sheet silicates are allowed. The same trend in sheet silicate compositions is inferred in Region I. As the analysed sheet silicates all have a Pw component, and analysed amphiboles have an Ek component, it is inferred that all amphiboles coexisting with Ss and Ab or Jd are quaternary.

Region III A single run (G-N 6) on $Ny_{83}Gl_{17}$ bulk composition yielded Am, Ab, Jd, Ss, analogous to bulk composition "D" in Fig. 3.18. The amphibole is rich in Ny component and the sheet silicate in Sp component.

Region IV A run (G-N 3) on $Ny_{33}Gl_{67}$ bulk composition yielded the same assemblage (Am, Ab, Ss) as the same bulk composition in Region I, 20° lower in temperature .

Amphibole coexisting with jadeite, quartz and talc

The assemblage Am, Jd, Qz, Tc was obtained at 22 kbar and ~750°C from the Gl bulk composition. The temperature uncertainty was due to breaking of the thermocouple during pressurisation of the assembly, requiring the temperature to be estimated from the power consumption.

Fig. 3.19. Schematic phase relations of G-N amphiboles at 3 different P,T conditions.
□ = bulk composition, showing run number,
● = analysed amphibole composition, with %Ek content,
○ = estimated amphibole composition,
◆ = analysed sheet silicate composition, with %Pw content,
◇ = estimated sheet silicate composition.
All amphibole compositions lie above the plane, and all sheet silicate compositions below the plane. Solid lines represent tie-lines between coexisting phases for each bulk composition. Dotted line shows minimum extent of amphibole solid solution. Solid solution may extend further towards Ek.

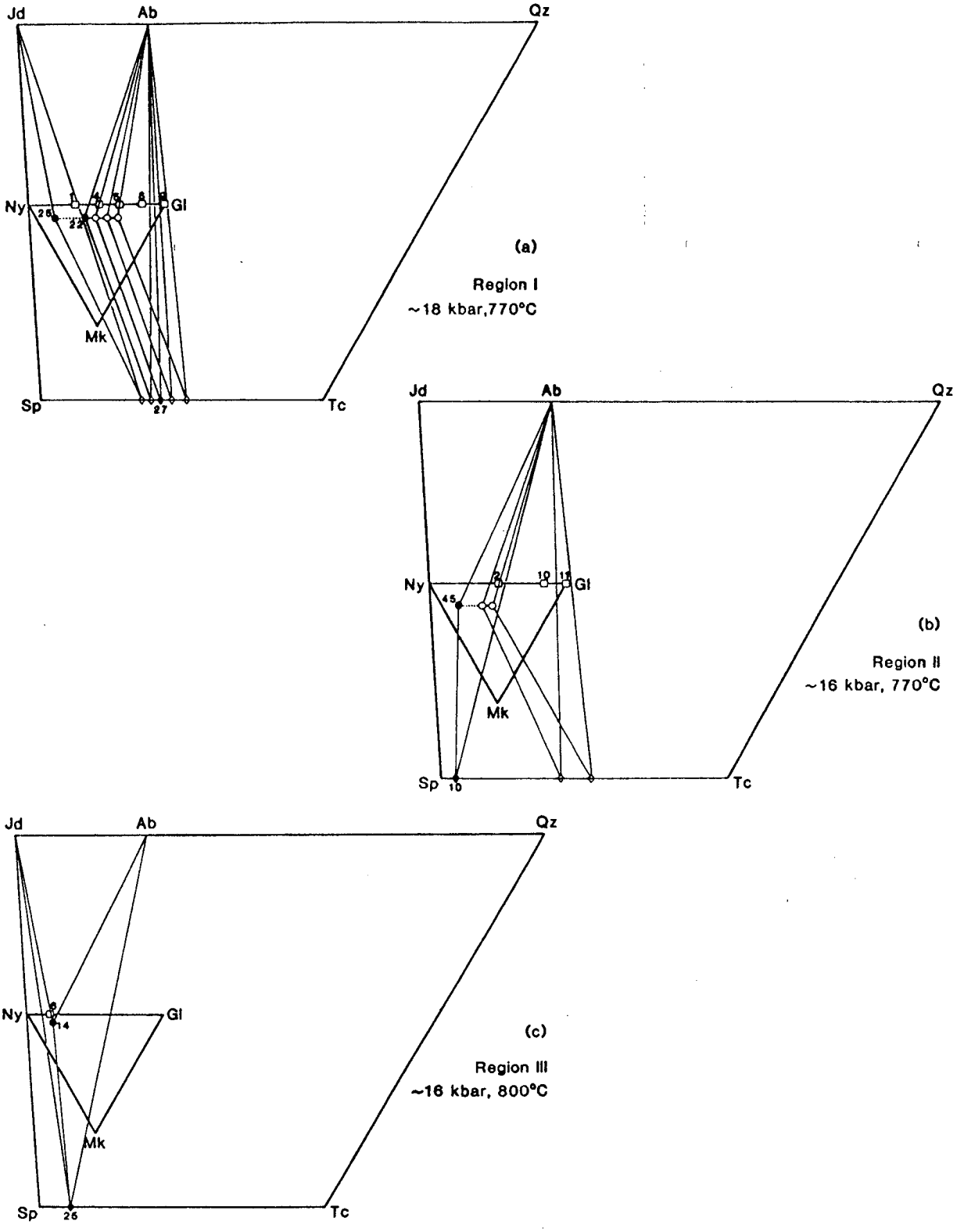

3.5. DISCUSSION AND COMPARISON WITH PREVIOUS RESULTS

3.5.(i). OH-NY experiments

Amphiboles coexisting with jadeite and sheet silicate

Although the experimental evidence for the two compositional trends observed in the amphiboles, ie. increasing $MgMgSi_{-1}$ with pressure and increasing $AlAlMg_{-1}Si_{-1}$ with temperature, is slim, both find support elsewhere. For example, a continuous reaction affecting these amphibole compositions will be Gl + Sp = Ny + Tc, such that as amphibole compositions move along $NaAlSi_{-1}$, sheet silicate compositions move along $SiNa_{-1}Al_{-1}$. A significant factor in determining the slope of this reaction is the volume change. As discussed by Thompson (1981), A-site empty amphiboles are not as compressible as A-site empty sheet silicates. Thus at high pressure the continuous reaction Gl + Sp $\rightarrow$ Ny + Tc will have a negative ΔV and hence Ny + Tc on the high-pressure side, with the result that a filling of the A-site of these amphiboles with increasing pressure is to be expected. The second trend is also observed in natural samples (eg. Black, 1977).

There is no obvious reason why no high pressure amphibole comprises >~80 mol% Ny. Three possible explanations present themselves: some crystal chemical factor may make the Ny structure intrinsically unstable; Mk may become more stable with respect to Ny with increasing pressure; or there may have been an unrecognised kinetic or compositional problem with the experiments. This might then account for the fact that the amphibole, pyroxene and sheet silicate compositions always lie on the SiO_2-rich side of the Jd-Ny-Sp join (see Fig. 3.14), ie. for the Ny bulk composition, either some dissolution in the fluid or an undetected phase forces the bulk composition away from Ny, preventing its formation. Significant dissolution is unlikely considering the small quantities of water added, and thorough examination of run products did not reveal any additional phases.

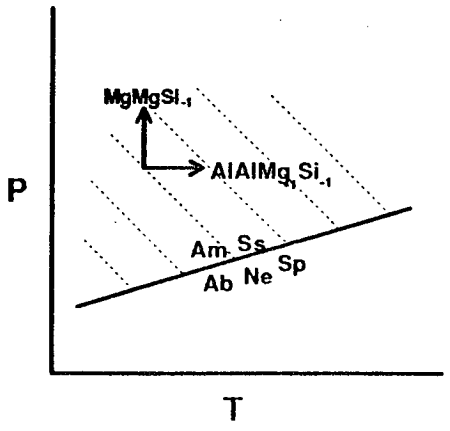

Fig. 3.20. Schematic illustration of the relationship of quaternary OH-NY amphibole compositional isopleths to the low pressure amphibole breakdown reaction.

Low pressure amphibole breakdown

The limiting amphibole composition at the breakdown reaction (5) has not been determined, but is unlikely to be an end-member. The observed compositional trends suggest that cross-cutting isopleths will cause it to change along the boundary, as illustrated schematically in Fig. 3.20. The experimental constraint on the P-T position of this reaction is poor, but a variety of factors may be expected to prevent a precise location, eg. the problem of the failure of jadeite to nucleate leading to the location of a metastable reaction at low temperatures but probably the stable Am + Ss = Jd + Sp reaction at higher temperatures; the unknown extent of solid solution between Ab and Ne at reaction (5), which is likely to change along the reaction; and the changing amphibole composition along the reaction. The last two factors will have the effect of making what should be a univariant reaction of constant slope into a multivariant curve.

3.5.(ii). OH-Q experiments

Amphiboles coexisting with quartz and jadeite or albite

The observation of negligible Ek content in these amphiboles is consistent with previous results for SiO_2-excess experiments (Koons, 1982; Welch, 1987, 1989), while that of increasing $MgMgNa_{-1}Al_{-1}$ with temperature agrees with the results of Welch (1987, 1989), who observed that amphiboles synthesised from the F-glaucophane bulk composition showed a small displacement towards Mk with increasing temperature. The rigidity of the tetrahedral chains in the C2/m structure limits the extent of Mg substitution for Na (Papike et al., 1969). With increasing temperature, greater thermal vibrations will allow for more substitution, which may explain the increase in Mk content with temperature observed here. The increase of Mk content with pressure tentatively suggested is consistent with that observed by Koons (1982) on passing from an Am + Qz field to an Am + Jd + Qz field.

Amphiboles coexisting with jadeite, talc and quartz or coesite

The compositions Jd, Tc, Qz/Co are coplanar with the bulk composition, and thus the 4-phase assemblage disobeys the phase rule for a field with H_2O in excess, whatever the amphibole composition. Koons (1982) obtained the same assemblage in his runs at 30 and 35 kbar on the Gl bulk composition. If his results may be applied to this bulk composition, they imply that the assemblage, whether stable or metastable, occupies a broad region of P-T space. Here it is interpreted to comprise both reactants and products of the limiting Gl-Ny-Mk amphibole reaction:

$$Gl\text{-}Ny\text{-}Mk_{ss} + Qz + H_2O = Jd + Tc \quad (8)$$

(see Fig. 3.6(b), but also approximately equivalent to reaction (1), Fig 3.3), with Tc metastable at lower pressures and Am metastable at higher pressures.

Amphiboles coexisting with albite, quartz and talc

Again, Koons (1982) obtained the same low-pressure assemblage as observed in this study. But in this case mineral-mix experiments have demonstrated the metastability of one or other of Am and Tc.

EMPA was unsuccessful for both the high- and the low-pressure 4-phase assemblages, and hence the amphibole composition cannot be constrained except that it must lie on the Gl-Ny-Mk plane. Again this is in agreement with the results of Koons (1982) and of Welch (1987, 1989). As with the amphiboles synthesised from bulk composition "A", the compositional isopleths are expected to be cut by the limiting amphibole reactions (eg. Fig. 3.21).

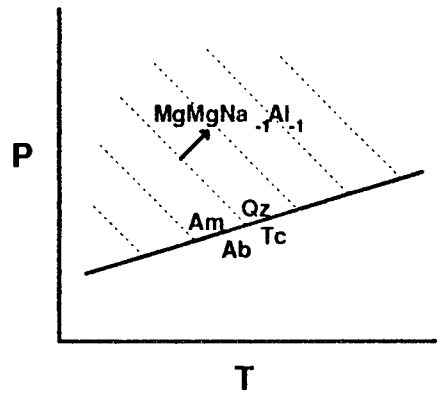

Fig. 3.21. Schematic illustration of the relationship of ternary OH-Q amphibole compositional isopleths to the low pressure amphibole breakdown reaction.

3.5.(iii). G-N experiments

In the G-N experiments EMPA was again not very useful. However, it did support two observations already made for the OH-NY experiments, firstly that amphiboles coexisting with a sheet silicate which is not Tc are quaternary, and secondly that the highest Ek content is found in the lowest-temperature amphiboles (eg. G-N 2). EMPA was not necessary to demonstrate the close relationship between amphibole composition, sheet silicate composition and the presence or absence of Qz. The experiments on Gl bulk composition show this clearly. The assemblage Am, Jd, Qz, Tc is the same as that of Koons' high-pressure runs and the high-pressure OH-Q runs (with Co replaced by Qz). Therefore again a phase must be metastable, and this could be Tc or Jd, depending on how Mk-rich the amphibole is. Again the amphibole must have a zero Ek component, and so will have the same composition as one

synthesised from bulk composition "B" at the same conditions. This amphibole coexists with Qz and Tc, while at lower pressures a quaternary amphibole coexists with ternary Ss and Ab. The presence of Qz favours the growth of Tc by inhibiting the formation of Sp (Na et al., 1986). The amphibole composition is therefore buffered onto the Gl-Ny-Mk plane. With decreasing pressure reaction (7) (Am + Qz = Ab + Tc) is encountered for the OH-Q amphiboles, and hence also for this amphibole. But whereas for bulk composition "B" Qz is still stable below this reaction, for Gl bulk composition it is not. Hence a ternary sheet silicate can grow, resulting in a quaternary amphibole. Thus sample G-N 9, in comprising Am, Ab, Ss (ie. a quaternary amphibole grown from the Gl bulk composition) provides a further bracket on reaction (7). The position of this reaction is remarkably close to Ernst's "polymorphic" reaction between low-pressure "Gl I" and high-pressure "Gl II" (Fig. 3.22). Thus not only are the results obtained here in agreement with the generally accepted theory that that reaction is not a polymorphic reaction, and that the low-pressure amphibole is not glaucophane (eg. Maresch, 1977), but also they go further in proving that neither amphibole is glaucophane. "Gl II" is ternary, though its composition may approach pure Gl at some P-T condition, whilst "Gl I" is quaternary with only a small Gl-component under all conditions of pressure and temperature.

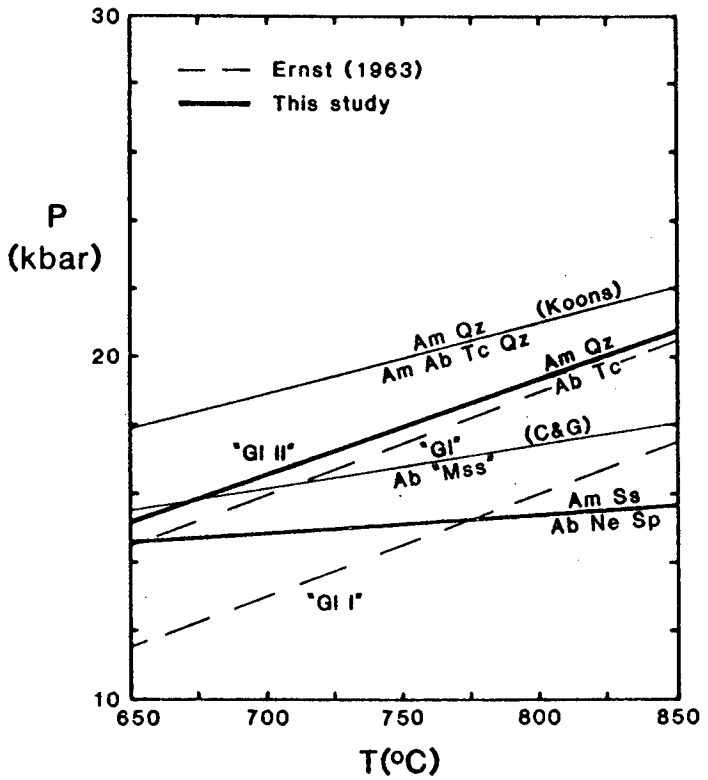

Fig. 3.22. Compilation of low pressure limiting reactions of glaucophane-nyböite amphiboles. Koons = Koons (1982), C&G = Carman & Gilbert (1983).

For a more silica-rich bulk composition than Gl, such as "B", Qz is always stable and thus low-pressure quaternary amphiboles cannot grow. On the other hand, for a silica-poor bulk composition such as "A", stable Ab + Ne at low pressure react to Jd at high pressure, with the result that Qz is never stable, and the amphibole is always quaternary.

At pressures well below Am + Qz = Ab + Tc, Koons' experiments on Gl still yielded the assemblage Am, Qz, Ab, Tc, the amphibole presumably therefore being metastable. A possible cause of the formation of this metastable ternary amphibole is the nature of the starting material, which was a mixture of Ab glass + MgO + SiO_2 (presumably silica gel) in Gl proportions. The SiO_2 would grow rapidly to Qz during the run-up to temperature in the experiments, and Qz would have buffered the first-formed sheet silicate onto Tc composition, thereby forcing the amphibole composition onto the Gl-Ny-Mk plane.

The low-pressure amphiboles synthesised by Carman & Gilbert (1983), on the other hand, coexist with a Sp-Tc (and probably Pw) solid solution sheet silicate, as do those obtained here. Carman & Gilbert's high-pressure amphiboles generally coexist with Qz + Jd ± Tc, and are therefore ternary, and therefore their claim to have synthesised close to end-member Gl is unfounded. Their low-pressure amphibole stability limit defined by the reaction "Gl" = Ab + Mss is approximately parallel to the low pressure quaternary amphibole reaction Am + Ss = Ab + Ne + Sp, but ~2 kbar higher (Fig. 3.22), implying that this reaction is indeed divariant, more Gl-rich compositions breaking down at higher pressure.

As previously mentioned, probably the main effect of the substitution of F^- for OH^- in this system is the destabilisation of Tc (Welch, 1987, 1989), allowing F-Sp to coexist with Qz at high temperatures. The sheet silicate no longer exhibits solid solution towards Pw, with the result that the amphibole composition is buffered onto the Gl-Ny-Mk plane. Another effect is that the stability field of F-Am + Qz is shifted to higher pressures with respect to OH-Am + Qz.

The main compositional variation observed within the F-amphiboles was a decrease in Gl-content and increase in Ny-content with decreasing pressure. There is no reason to suspect that such variation does not occur in the OH-Q system, as EMP analyses could only be obtained over a limited pressure interval. A likely continuous reaction relating Gl to Ny in the Qz-bearing system is Gl + Jd = Ny + 3 Qz, involving a change in Al coordination from VI (Jd) to IV (Ny), with a corresponding entropy increase. The volume change is also positive, therefore the slope of the reaction will be positive, such that amphiboles become progressively more nyböitic with

decreasing pressure and increasing temperature, in agreement with the results of Welch (1987,1989).

3.6. SUMMARY OF RESULTS FOR ALL BULK COMPOSITIONS

The stability fields for Qz-saturated and Qz-undersaturated amphiboles are illustrated in Fig. 3.23. The 4 reactions define 5 pressure-dependent regions of changing phase relations and amphibole compositions:

Region A At pressures above Jd + Qz = Ab (and therefore also above Am + Qz = Ab + Tc) there are 2 fields of stable amphibole composition, one a Ny-rich quaternary amphibole and the other a more Gl-rich ternary amphibole. The quaternary amphibole field has tie-lines to Jd and a field of Sp-rich ternary sheet silicates, while the ternary amphibole has tie-lines to Jd, Qz and end-member Tc. There are insufficient EMP data to determine whether solid solution exists between the 2 amphibole fields, or between the 2 sheet silicate fields. The effect of temperature at this pressure is to increase the stability of the ternary amphibole towards Mk, and to increase the extent of Tschermak's substitution ($AlAlMg_{-1}Si_{-1}$) in the quaternary amphiboles, while with increasing pressure the substitution $MgMgNa_{-1}Al_{-1}$ increases for both amphiboles and concurrently the edenite substitution increases for the quaternary amphiboles.

Region B With a decrease in pressure, Jd + Qz react to give Ab. The 2 amphibole fields still exist, though presumably their compositions are continuously changing.

Region C With the reaction Am + Qz = Ab + Tc, the ternary amphibole breaks down, and all compositions for which Qz is absent and hence a ternary sheet silicate is stable yield a quaternary amphibole.

Region D The quaternary amphibole finally breaks down in a continuous reaction, either the metastable reaction Am + Ss = Ab + Ne + Sp or the stable reaction Am + Ss = Ab + Jd + Sp. Silica-poor bulk compositions now yield Ab + Ne + Sp (or Ab + Jd + Sp), while more silica-rich bulk compositions (such as Gl) yield Ab + Sp + Tc, with probable solid solution between the 2 sheet silicates.

Fig. 3.23. P,T location of amphibole breakdown reactions obtained in this study. Schematic phase relations at three different pressures are also shown. Squares are bulk compositions, circles amphibole compositions and triangles sheet silicate compositions. Solid symbols represent quaternary, and open symbols ternary, phase relations. Dotted line indicates amphibole solid solution, with a question mark where uncertain.

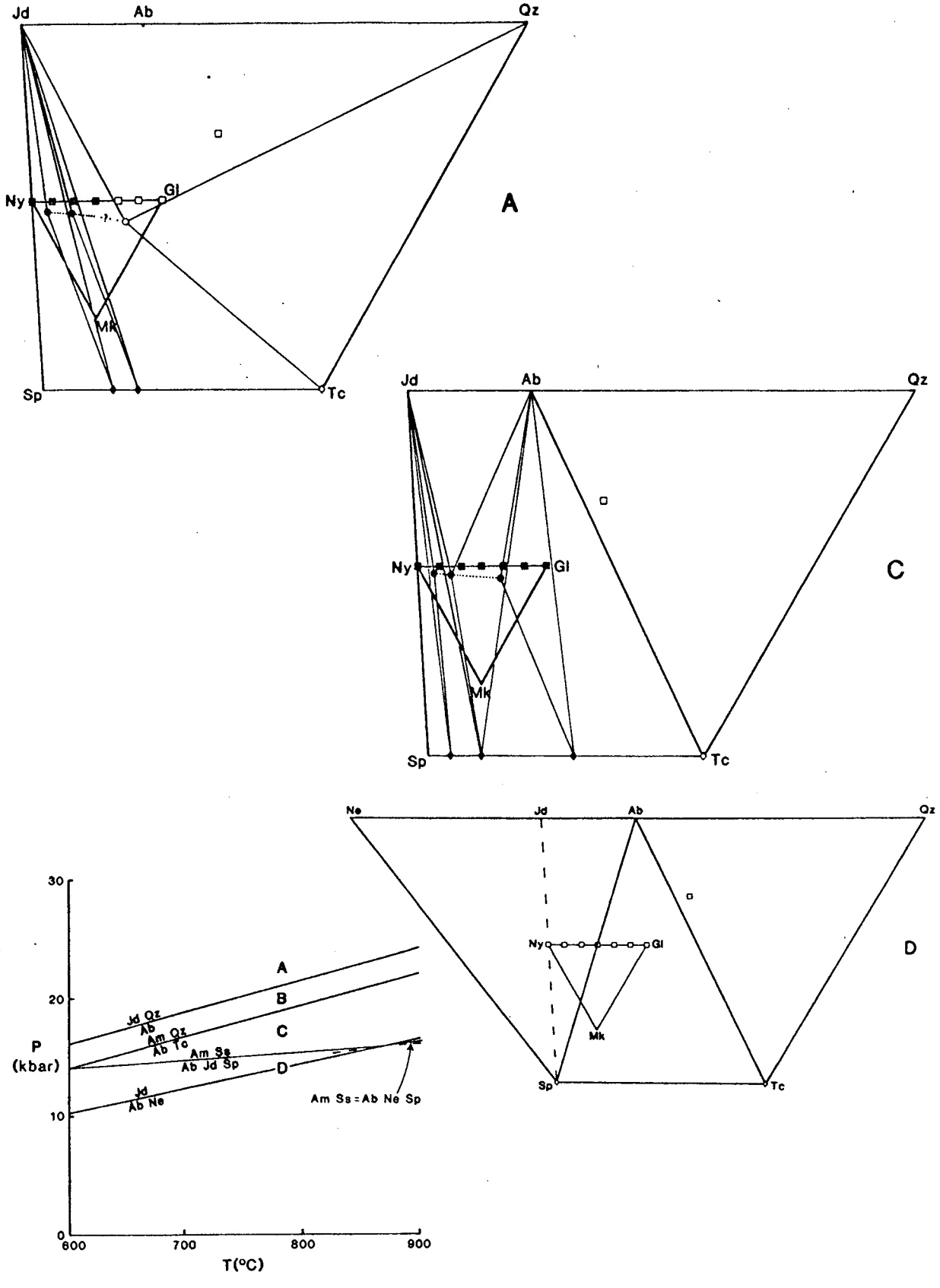

3.7. APPLICATION TO NATURAL ASSEMBLAGES

A number of compositions of glaucophanic amphiboles from blueschists and eclogites obtained from the literature are presented in terms of mole fractions of the exchange vectors $SiNa_{-1}Al_{-1}$, $MgSiAl_{-1}Al_{-1}$, $MgMgNa_{-1}Al_{-1}$ and $CaMgNa_{-1}Al_{-1}$ (Fe^{3+} is included with Al^{3+}, and Fe^{2+} with Mg^{2+}) in Table 3.4. Although phase assemblages are varied, all contain Qz. Combining $CaMgNa_{-1}Al_{-1}$ with $MgMgNa_{-1}Al_{-1}$, the compositions may be plotted in the same way as those of the synthetic amphiboles of this study, projecting from $MgSiAl_{-1}Al_{-1}$ (Fig. 3.24). Several important observations may be made:

(i). Only 2 amphiboles contain >8 mol% Ek component. This is entirely consistent with the results obtained for Qz-bearing assemblages in this study. However some analyses contain a significant negative Ek component, that is a barroisitic component. This is possible because natural assemblages often contain a paragonitic sheet silicate, rather than Tc or Sp, whose composition can be displaced along $MgSiAl_{-1}Al_{-1}$ (towards phengite), ie. in the opposite direction to the Tschermak's exchange (towards Pw) exhibited by the synthetic sheet silicates of this study.

(ii). Very few amphiboles contain a significant Mk component. Thus the apparently high Mk contents in Fig. 3.24 are products of the exchange $CaMgNa_{-1}Al_{-1}$, with the larger Ca^{2+} substituting into M(4) rather than Mg^{2+}. The small Mk content is in keeping with the results obtained in both the silica-saturated and Qz-absent experiments.

(iii). Iron is an important constituent of glaucophanic amphiboles, as already suggested.

The compositional changes observed during progressive high-pressure metamorphism of natural amphiboles often involve an increase in Tschermak's substitution with temperature (Robinson et al., 1982). Though these natural samples tend to be calcic amphiboles, this is again consistent with the results from the silica-undersaturated experiments of this study.

Helper's analysis is from a blueschist terrain whose P,T-evolution can be traced in the amphibole crystals through a zonation from crossite core to ferroglaucophane rim, interpreted as recording a path of decreasing pressure during uplift and erosion following subduction. The exchange reactions occurring from core to rim are ($CaMgNa_{-1}Al_{-1}$ and) $NaAlSi_{-1}$, ie. an increase in Ny content with decreasing pressure, agreeing with Welch's experimental results. One of the explanations Ungaretti et al. (1981) give for the high Ny content in amphiboles from

Table 3.4 Compositions of some natural high-pressure amphiboles expressed in terms of mole fractions of glaucophane, nyböite, eckermannite, Mg-katophorite and katophorite.

	X_{Gl}	X_{Ny}	X_{Ek}	X_{Mk}	X_{Kt}	$\frac{Mg}{Mg+Fe}$		X_{Gl}	X_{Ny}	X_{Ek}	X_{Mk}	X_{Kt}	$\frac{Mg}{Mg+Fe}$
1	.90	-.02	.04	.02	.06	.71							
2	.98	-.11	-.01	.04	.10	.63	24	.96	.0	-.02	.0	.06	.61
3	1.00	-.13	-.05	.0	.18	.74	25	.99	.04	-.07	.0	.04	.62
4	.97	-.08	-.27	.21	.17	.96	26	.99	.03	-.05	.0	.03	.62
5	.72	-.16	-.12	.01	.55	.37	27	.95	.03	-.03	.0	.05	.63
6	1.00	-.13	-.04	.0	.17	.85	28	1.00	-.09	-.10	.02	.17	.77
7	1.00	-.03	-.07	.0	.10	.85	29	1.00	-.03	-.09	.0	.12	.78
8	.61	.10	-.19	.0	.48	.55	30	1.00	-.02	.0	.0	.02	.77
9	.57	.02	.0	.0	.41	.58	31	.38	.06	-.05	.0	.61	.88
10	.62	-.04	.03	.0	.39	.63	32	.44	.03	.04	.03	.46	.90
11	.75	.14	-.30	.0	.41	.59	33	.40	.09	.06	.0	.45	.84
12	.72	.12	-.20	.0	.36	.56	34	.37	.05	.06	.0	.52	.89
13	.78	-.03	-.16	.0	.41	.59	35	.26	.43	-.02	.0	.33	.84
14	.80	-.08	-.02	.02	.28	.59	36	.38	.22	.01	.0	.39	.86
15	.93	.04	-.24	.11	.16	.72	37	.30	.35	.11	.0	.24	.80
16	.80	-.06	.02	.09	.15	.78	38	.35	.31	.0	.0	.34	.83
17	.93	-.15	-.01	.03	.20	.70	39	.36	.25	-.08	.0	.47	.83
18	.94	.04	-.11	.01	.12	.62	40	.17	.36	.02	.0	.45	.85
19	.98	.05	-.08	.0	.05	.60	41	.17	.34	.08	.0	.41	.85
20	.89	.02	-.18	.01	.26	.60	42	.19	.29	.03	.0	.49	.86
21	.85	.02	-.14	.0	.27	.61	43	.93	-.07	-.01	.0	.15	.68
22	.94	.01	-.07	.0	.12	.63	44	.95	-.02	-.03	.0	.10	.67
23	.96	.0	-.07	.01	.10	.63	45	1.00	-.06	.0	.0	.06	.51

Sources of data with estimated P,T conditions of metamorphism and typical assemblages where specified:

1,2: Barr (unpubl. data): >14 kbar/450-500°C: Gl-Qz-Ph-Chl-Gt-Sph-Rut-Pg-Cb-Ep
3: Brown & Forbes (1986): 15 kbar/600°C: Gl/Cr-Qz-Ab-Ep-Om-Gt-Rut-Mag
4: Chopin (1986): 25 kbar/700°C: Ell-Gt-Co-Tc-Chl-Gl-Rut-Ky-Zc
5: Helper (1986): >6 kbar/360-410°C: Am-Ep-Chl-Ab-Qz
6: Holland (1979): 19.5 kbar/620°C: Gl-Gt-Om-Ky-Qz-Pg-Mag-Rut
7: Holland (1988): as 6 above
8-14: Holland & Richardson (1979): 15 kbar/200°C: Am-Ep-Chl-Ab-Gt-Qz-Rut-Pg-Ox-Cb
15: Maresch (1977)
16: Maruyama et al. (1986)
17: Papike & Clark (1968): Gl-Laws-Gt-Ph-Qz-Sph
18-29: Ridley & Dixon (1984): >14 kbar/450-500°C: Gl-Ep-Gt-Om-Ph-Pg-Qz-Sph
30: Ungaretti (unpubl. data)
31-42: Ungaretti et al. (1981): 15-28 kbar/700-850°C: Am-Gt-Cpx
43-45: Ungaretti et al. (1983): 15 kbar/500-600°C: Qz-Gl-Pg-Ph-Gt

Additional abbreviations: Cr=crossite, Ep=epidote, Om=omphacite, Gt=garnet, Rut=rutile, Mag=magnetite, Ell=ellenbergerite, Chl=chlorite, Ky=kyanite, Zc=zircon, Pg=paragonite, Ox=oxides, Cb=carbonates, Ph=phengite, Sph=sphene, Cpx=clinopyroxene

Fig. 3.24. Projection from $MgSiAl_{-1}Al_{-1}$ of some natural glaucophanic amphibole compositions, contoured for %Ek content:

- ■ Barr (unpubl. data)
- ▽ Brown & Forbes (1986)
- ▣ Chopin (1986)
- ▼ Helper (1986)
- □ Holland (1979)
- ✡ Holland (1988)
- △ Holland & Richardson (1979)
- ◉ Maresch (1977)
- ▲ Maruyama et al. (1986)
- ◈ Papike & Clark (1968)
- ○ Ridley & Dixon (1984)
- ◆ Ungaretti (unpubl. data)
- ● Ungaretti et al. (1981)
- ◇ Ungaretti et al. (1983)

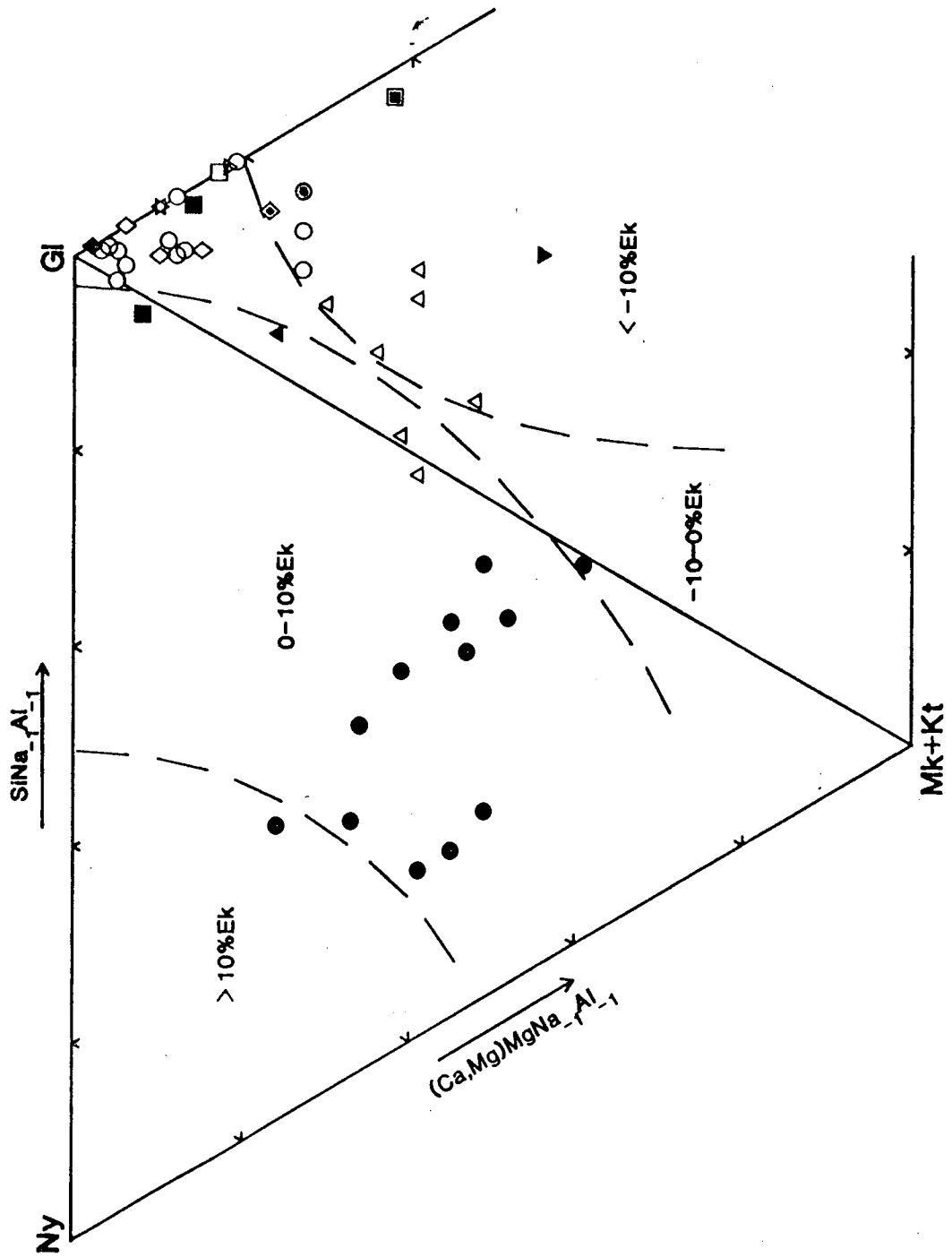

the Nybö eclogite pod is that the temperature (700-850°C) was too high for glaucophane formation, implying that $NaAlSi_{-1}$ is also favoured with increasing temperature. In fact $NaAlSi_{-1}$ is known to increase with temperature in natural high-pressure amphiboles (Robinson et al., 1982). Thus Ny is apparently stable to a lower pressure and higher temperature than Gl. The low-pressure stability limit of the Ny-rich synthetic amphiboles obtained in the SiO_2-undersaturated system is indeed extended to a lower pressure and higher temperature than for the SiO_2-saturated system. Because Qz and Ny are on the same side of the reaction Gl + Jd = Ny + 3 Qz, an increase in silica-activity will favour the formation of more Gl-rich amphiboles, as found experimentally. If Qz is absent altogether, a nyböitic amphibole should be stable over the whole amphibole stability field, perhaps even to a higher pressure than the glaucophanic amphibole, as suggested by Ungaretti (in prep.) and by the results of this study, inasmuch as even at the highest run pressures there is no evidence of nyböitic amphibole breakdown, whereas the presence of a 4-phase assemblage in the high-pressure OH-Q experiments implies close proximity to its breakdown reaction. A thorough literature search has failed to unearth any study of glaucophanic amphiboles in rocks which do not contain Qz, but these should be less Gl-rich, more Ek-rich, and stable over a wider P-T range than their silica-saturated counterparts.

Finally, the literature survey has not revealed any evidence concerning the effect on $MgMgNa_{-1}Al_{-1}$ of changing pressure and temperature in natural samples, partly because one of the methods of recalculating amphibole formulae assumes no $MgMgNa_{-1}Al_{-1}$, ie. no $Mg^{M(4)}$.

3.8. CONCLUSIONS

1. Nyböite, like glaucophane, cannot be synthesised from its own or any other bulk composition. Compositions closest to nyböite, obtained in experiments on its own bulk composition, are quaternary Ny-Gl-Mk-Ek solid solutions, with Ny contents up to ~70 mol%. The Ek contents decrease with increasing temperature through the Tschermak's exchange $AlAlMg_{-1}Si_{-1}$, while with increasing pressure there is a filling of the A-site through the exchange $MgMgSi_{-1}$. The amphiboles are stable to pressures above 32 kbar at 600-900°C, and break down below ~14 kbar/600°C - 15.5 kbar/800°C to Ab + Ne + Sp (probably metastable with respect to Ab + Jd + Sp). They generally coexist with Sp-Tc-Pw sheet silicates, and jadeitic pyroxenes.

2. Amphiboles coexisting with Qz are ternary Gl-Ny-Mk solid solutions, Mk-contents of which are low but increase with pressure and temperature through the exchange $MgMgNa_{-1}Al_{-1}$. The upper pressure stability limit of these amphiboles is

above 30 kbar in the temperature range studied, above which they break down by the reaction Am + Qz/Co = Jd + Tc. The low-pressure breakdown reaction, at ~14 kbar/600°C - 22 kbar/900°C, is Am + Qz = Ab + Tc. As well as with Qz, the amphiboles commonly coexist with Ab + Tc, though Tc may be metastable.

3. Amphibole composition is determined to a large extent by the presence or absence of Qz. When Qz is present, the composition of the sheet silicate is constrained to be Tc, and the slower growing amphibole is buffered onto the Gl-Ny-Mk plane. When Qz is absent, the sheet silicate composition is free to move along $NaAlSi_{-1}$ and $AlAlMg_{-1}Si_{-1}$, and the amphibole composition is no longer buffered.

4. The reaction interpreted by Ernst (1963) to be a polymorphic reaction between low and high pressure polymorphs of glaucophane is in fact the reaction Am + Qz = Ab + Tc located in this study, above which amphiboles synthesised from the glaucophane bulk composition are ternary Gl-Ny-Mk solid solutions, and below which they are quaternary Gl-Ny-Mk-Ek solid solutions.

5. Amphiboles coexisting with Qz show compositional trends in agreement with previous experimental results (Koons, 1982; Welch, 1987, 1989), and consistent with compositional trends observed in natural sodic amphiboles.

CHAPTER 4

SYNTHESIS, CHARACTERISATION AND THERMOCHEMISTRY OF TREMOLITE-RICHTERITE AMPHIBOLES

CONTENTS

4.1. INTRODUCTION

Description of the diverse compositional and structural variation exhibited in amphibole-group minerals, which accounts for their ability to crystallise under a wide range of geologic conditions, is a necessary but daunting task. However the variation may in fact be considered in terms of a small number of simple site-specific coupled ionic substitutions acting on only a few important end-members. Thermochemical data relating to these substitutions is necessary to determine the stability of any non-end-member phase, ie. any solid solution. However problems with synthesis have meant that to date the only substitution which has been adequately investigated in amphiboles is the A-site filling "edenite" substitution $Na^{A}Al^{T}\square^{A}_{-1}Si^{T}_{-1}$ (A = A-site, T = tetrahedral site, $\square$ = vacancy) between F-tremolite and F-edenite (Graham & Navrotsky, 1986). In that study heats of mixing were obtained using high temperature solution calorimetry, from which activity-composition relationships were derived. Fluorine-analogues were used as they were more amenable to synthesis than their hydroxy-counterparts, for which at the time the solubility of H_2O in the calorimeter flux was also uncertain. However more recent calorimetric studies have indicated that the enthalpy of solution of H_2O-bearing minerals can be directly measured (Kiseleva & Ogorodova, 1984; Clemens et al., 1987).

Recent experimental studies on amphiboles have also demonstrated, through a range of novel techniques such as high resolution transmission electron microscopy (HRTEM) and vibrational and nuclear magnetic resonance spectroscopy, as well as the more traditional methods of electron microprobe analysis (EMPA) and x-ray diffraction (XRD), that apparently ideal compositions and structures are in fact frequently non-ideal (Graham et al., 1989, and references therein). Therefore it is imperative that an amphibole's composition and structure are fully characterised to reveal any potential sources of uncertainty in calorimetric and other experimental results. Thus for this study, in which it was intended to obtain activity-composition relations from high temperature solution calorimetric measurements of a synthetic hydroxy-amphibole solid solution, it was realised that complete characterisation of the samples by all available means was absolutely necessary.

Another A-site filling substitution is $Na^{A}Na^{M(4)}\square^{A}_{-1}Ca^{M(4)}_{-1}$, which is of some importance in calciferous amphiboles, defining the solid solution between tremolite (Tr) $Ca_2Mg_5Si_8O_{22}(OH)_2$ and richterite (Ri) $Na_2CaMg_5Si_8O_{22}(OH)_2$ in the system

Table 4.1. Mineral abbreviations used in Chapter 4.

Cpx	Clinopyroxene	
Di	Diopside	$CaMgSi_2O_6$
En	Enstatite	$Mg_2Si_2O_6$
Fo	Forsterite	Mg_2SiO_4
Mc	Magnesio-cummingtonite	$Mg_7Si_8O_{22}(OH)_2$
Opx	Orthopyroxene	
Qz	Quartz	SiO_2
Ri	Richterite	$Na_2CaMg_5Si_8O_{22}(OH)_2$
Sc	Sodium magnesio-cummingtonite	$Na_2Mg_6Si_8O_{22}(OH)_2$
Tr	Tremolite	$Ca_2Mg_5Si_8O_{22}(OH)_2$

Na_2O - CaO - MgO - SiO_2 - H_2O (NCMSH). It was chosen for study here, firstly to complement the results of the investigations of the "edenite" substitution in glaucophanic amphiboles (Chapter 3) and between F-tremolite and F-edenite (Graham & Navrotsky, 1986), secondly because such a study may help to clarify the nature of site-splitting and disorder on the A-site and the energetic importance of interactions between A-site cations and other crystallographic sites (eg. O(3), T) for the stabilisation of A-site-full amphiboles, and thirdly because it was expected that both synthesis of the solid solution and thermodynamic interpretation would be comparatively simple as the reaction involves only 2 cations substituting on 2 sites. In fact previous studies had implied that richterite and intermediate compositions towards tremolite are easily synthesised (eg. Rowbotham and Farmer, 1973: Ri_{100}, $Tr_{25}Ri_{75}$, $Tr_{75}Ri_{25}$; Welch, 1987: Ri_{100}, $Tr_{50}Ri_{50}$). However as will become apparent, the substitution $Mg^{M(4)}{}_2Ca^{M(4)}{}_{-2}$ is also important in this system, with the result that clino-amphibole compositions may contain components of the end-members:

magnesio-cummingtonite (Mc, $Mg_7Si_8O_{22}(OH)_2$)

$$= Tr + Mg_2Ca_{-2}$$

sodium-magnesio-cummingtonite (Sc, $Na_2Mg_6Si_8O_{22}(OH)_2$)

$$= Tr + Na_2Ca_{-1} + 0.5Mg_2Ca_{-2} \qquad \text{(Fig. 4.1)}$$

Fortunately amphibole electron microprobe (EMP) analyses may easily be converted into mole proportions of the additive component Tr* and the two exchange

* using the terminology of Thompson (1981)

vectors* Na_2Ca_{-1} and Mg_2Ca_{-2}, from which proportions of the end-members may be calculated to determine the extent of their deviation from ideality.

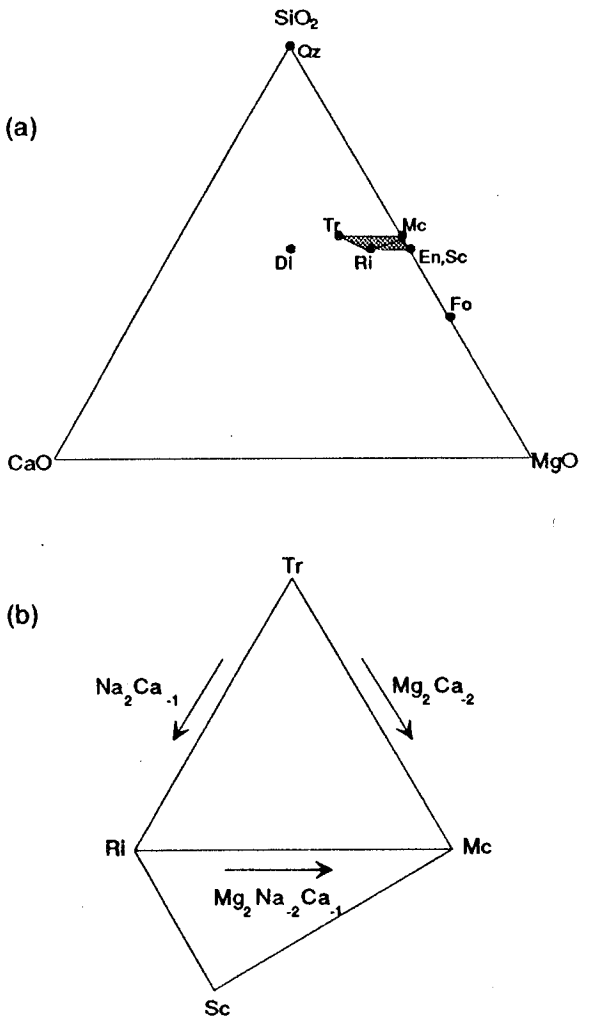

Fig. 4.1. (a) Projection from $Na_2Si_2O_5 + H_2O$ of phases in the system NCMSH relevant to this study. The shaded quadrilateral represents the plane of legitimate clino-amphibole compositions. See Table 4.1 for a list of abbreviations.

(b) The amphibole quadrilateral redrawn with unit vectors between Tr, Ri and Mc.

A natural tremolite was to be used as the other end-member for this study as all previous attempts at synthesis had yielded an amphibole coexisting with Di ± Qz that was clearly off-composition (eg. Boyd, 1959; Jenkins, 1983, 1987), for which

metastable persistence of diopside was blamed. However Jenkins (1987) demonstrated that end-member Tr is in fact not stable at 750-850°C. In experiments at this temperature on a series of bulk compositions along the Tr-Mc join between Tr_{100} and $Tr_{75}Mc_{25}$, a single stable amphibole composition – 90 ± 3 mol% Tr, 10 ± 3 mol% Mc – was produced. In addition to amphibole, more Tr-rich bulk compositions yielded Cpx (Di) ± Qz, while more Mc-rich bulk compositions yielded Opx (En) ± Qz. Tr_{100} must be stable at the lower temperatures of greenschist facies metamorphism for an almost pure natural sample to be found, and so the following temperature-dependent continuous reaction accounts for the observed synthetic assemblages:

$$Tr = Tr\text{-}Mc_{ss} + Di + Qz + H_2O \qquad (1)$$

Jenkins also observed that Tr was stabilised by the presence of silica in the coexisting fluid. Hydrothermal treatment of natural tremolite in a slightly silica-undersaturated fluid led to partial dissolution by the reaction:

$$Tr = Opx + Cpx + SiO_2(aq) + H_2O \qquad (2)$$

which could be almost completely reversed by re-running with sufficient additional quartz to saturate the fluid in silica.

Reactions (1) and (2) will be seen to have affected amphibole compositions obtained in initial synthesis experiments in this study, such that a change of bulk compositions became necessary.

4.2. EXPERIMENTAL

4.2.(i). Procedure

Experiments were conducted at 2 kbar, in externally heated cold-seal pressure vessels, and at 6 kbar, in internally heated gas vessels. A discussion of the operation and calibration of these is given in Chapter 2.

Compositions of starting materials are shown in Fig. 4.2. TR100, TR83, TR67, TR50, TR33, TR17, RI100, RI92 and MC100 were gels prepared on-composition. Approximately 1 g of each of the first six of these was dried at 400°C, accurately weighed and mixed with MC100 gel by grinding under acetone for 15 minutes. In order that experiments could be run with excess water for reaction-rate enhancement, but with no possibilty of incongruent dissolution of amphibole occurring, the resulting gel mixes – TR92MC8, RI16, RI31, RI48, RI65, RI82 – were mixed with silica-gel in increasing proportions from RI65 (2 wt%) to TR92MC8 (10 wt%) (RI82 already contained an excess of 0.4 wt% SiO_2). Compositions determined by XRF analysis of

the raw gels, and EMPA of glasses of the gel mixtures (Appendix Tables A4.1 and A4.2), are close to ideal.

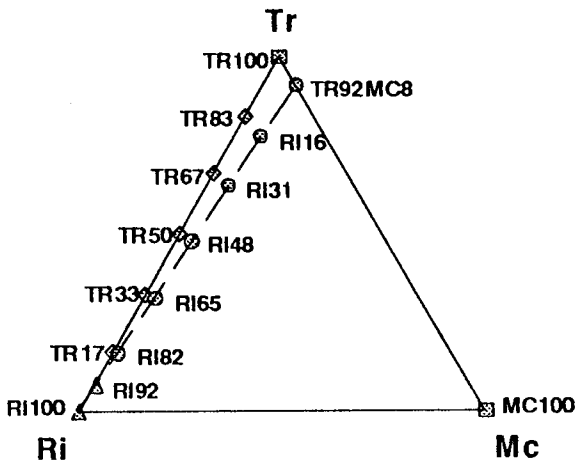

Fig. 4.2. Plot of compositions of gels and gel-mixes used as starting materials in this study, in terms of Tr, Ri and Mc components.
◈ Gels used in initial attempts to synthesise Tr_{100}-Ri_{100} amphiboles;
◬ Gels used in synthesis of $Tr_{92}Mc_8$-Ri_{100} amphiboles;
⊛ Gel-mixes used in synthesis of $Tr_{92}Mc_8$-Ri_{100} amphiboles;
▩ Gels used in mixes only.

Samples were sealed in 4 mm diameter annealed Pt capsules with between 0.5 and 30 wt% distilled H_2O. At the conclusion of each experiment the capsule was weighed both before and after puncturing with a needle to confirm that excess H_2O had been present throughout the run.

Samples were examined by optical microscopy and powder x-ray diffraction (XRD), and the majority also by electron microprobe analysis (EMPA). Optical identification was based on crystal habit, extinction angle and refractive index (RI). Amphibole crystals were prismatic to acicular, sub-micron to tens of microns long and up to 20 microns wide. Extinction angle varied from 12° for Ri_{100} to 17° for $Tr_{92}Mc_8$. Occasionally microcrystalline amphibole aggregates were present, in which case detection of impurities on the basis of relief in an oil of RI close to that of the amphibole was necessary. For example in an oil of RI 1.632, Tr-rich amphiboles had a low negative relief, pyroxenes a positive relief and quartz a high negative relief. Amphibole RI decreased with increasing Ri content, such that an oil of RI 1.600 was the most useful for detecting impurities in end-member Ri_{100}.

XRD was unable to yield additional information to that obtained by optical microscopy, being able only to detect phases present in more than trace amounts.

The Cameca Camebax system, with back-scattered electron imaging facility, was used for EMPA. Within each sample there were enough large grains for contamination of analyses by epoxy or neighbouring grains not to be a problem. But low accelerating voltage (15 kV), beam current (10nA) and peak count times (20 seconds for Mg, Si, Ca; 15 seconds for Na) were required to minimise Na loss under the electron beam.

Analyses were rejected if the oxide total was less than 95 wt%, that is 2.8-2.0 wt% below the ideal H_2O-free total.

4.2.(ii). Results

All pertinent run conditions and products are listed in Table 4.2. Optical examination revealed that the only sample on the Ri-Tr binary which yielded >99% amphibole was RI100. Runs T-R 2(a) to (e), comprising predominantly amphibole, also contained Di in increasing proportions, Qz increased from (b) to (e), and En occurred in (e) and possibly (d). No Na-bearing phases were detected other than amphibole, implying that the non-amphibole phases were not congruent breakdown products of the theoretical amphibole, and that the amphibole itself was therefore "off-composition". Its decreasing abundance with increasing Tr content of the bulk composition suggests that displacement from ideal composition increases along the join, such that Ri_{100} is the only "on-composition" sample. Therefore just as Jenkins' synthetic "tremolite" was displaced from ideal composition through reaction (1), so also are the Tr components of all the amphiboles along the Ri_{100}-Tr_{100} binary, with the result that all assemblages also contain Di + Qz.

The presence in the Tr-rich bulk compositions of amphibole and Di + En + Qz also suggests partial amphibole dissolution in a silica-undersaturated fluid through reaction (2), followed by Qz precipitation on H_2O-evaporation. It is inferred that all the T-R 2 run products contain at least a trace of Qz + En.

EMP analyses of the amphiboles obtained in the experiments on the Ri_{100}-Tr_{100} binary are plotted in Fig. 4.3. As expected, with increasing Tr content of the bulk composition, the analyses are increasingly displaced from the binary join. The displacement vectors are made up of 2 components, reaction (1) causing the amphibole composition to move along the exchange vector $MgCa_{-1}$, ie. parallel to the Tr-Mc join, and reaction (2) resulting in a decrease of the Tr content of the amphibole and hence a shift in the composition towards Ri.

Table 4.2. Results of synthesis experiments on the Ri_{100}-Tr_{100} binary and $Tr_{92}Mc_8$-Ri_{100} pseudo-binary.

Run no.	Starting material	P (kb)	T (°C)	H_2O-content (wt%)	Duration (hours)	Run products#
T-R 2(a)	TR17	2	850	3	160	Am,Di
T-R 2(b)	TR33	2	850	3	160	Am,Di,Qz
T-R 2(c)	TR50	2	850	3	160	Am,Di,Qz
T-R 2(d)	TR67	2	850	3	160	Am,Di,Qz,En?
T-R 2(e)	TR83	2	850	3	160	Am,Di,Qz,En
T-R 31	TR92MC8+QZ	6	850	27	160	Am,Qz,Di,En
T-R 33	RI48+QZ	2	850	12	165	Am,Qz,Di
T-R 34	RI65+QZ	2	850	9	165	Am,Qz
T-R 35	RI16+QZ	2	840	21	165	Am,Qz,Di,En
T-R 36	RI82	2	850	3	166	Am,Qz
T-R 38(a)	T-R 31*	6	850	24	160	Am,Qz
T-R 38(b)	TR92MC8+QZ	6	850	22	160	Am,Qz,Di,En
T-R 39	RI31+QZ	2	850	15	160	Am,Qz
T-R 41	T-R 33*	2	850	13	188	Am,Qz,Di
T-R 42	T-R 35*	2	840	3	188	Am,Qz,Di,En
T-R 43	T-R 42*	6	850	17	161	Am,Qz
T-R 44	T-R 31+T-R 38(b)*	6	850	24	165	Am,Qz
T-R 49	RI92	2	850	3	162	Am,Di,Qz
T-R 55	RI100	6.3-7.0	850	3	284	Am,Di
T-R 56	T-R 55*	6.3-7.0	850	0.5	159	Am,Di

In order of decreasing abundance, with minor phases (~1%) underlined and trace phases (<~1%) double underlined.

* Repeat runs of products containing suspected metastable phases, which were ground under acetone for ~15 minutes. Quoted H_2O-content is the wt% added to the run.

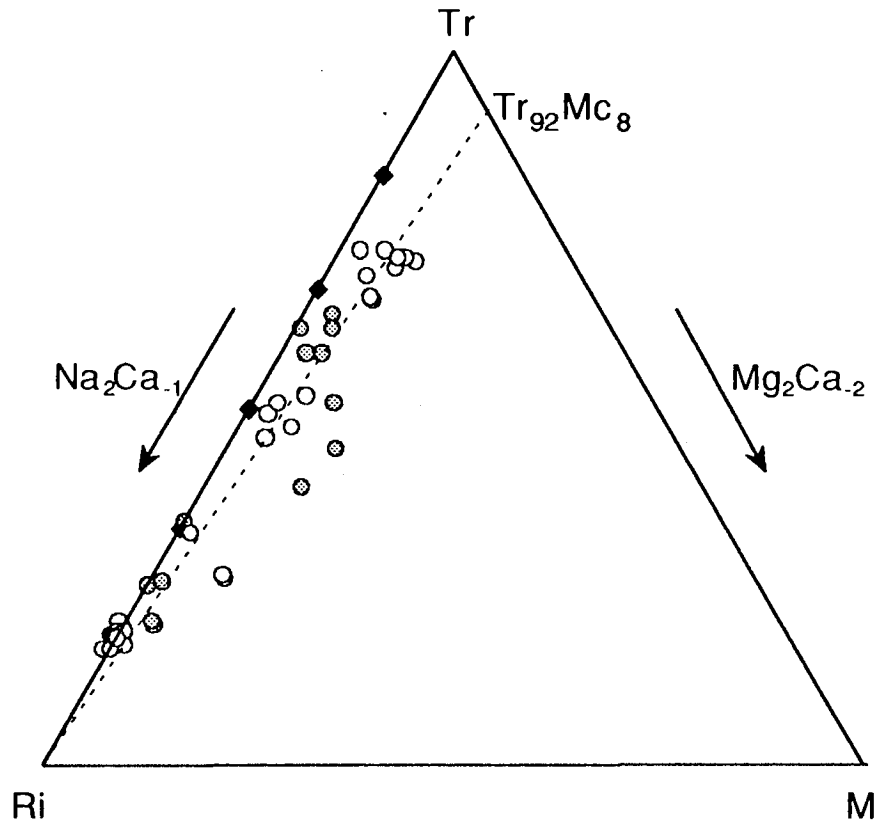

Fig. 4.3. Compositions determined by EMPA of amphiboles synthesised from the bulk compositions ◆ (+ Qz) on the Ri_{100}-Tr_{100} binary. Analyses for each bulk composition are shown by alternating groups of open and filled circles. Dotted line is join Ri-$Tr_{92}Mc_8$, the best-fit straight line through the analyses.

There is significant scatter of analyses reflecting inter-grain variation which increases towards Tr_{100}. However, the best-fit straight line through the points extends from Ri_{100} to $Tr_{92}Mc_8$, ie. to a point very close to Jenkins' stable amphibole composition. Therefore, apart from Ri_{100} itself, and despite the reported syntheses by Rowbotham & Farmer (1973) and Welch (1987), the whole Ri_{100}-Tr_{100} binary is inferred to be unstable at 850°C. It may be stable at the lower temperatures of greenschist facies metamorphism under which the purest natural tremolites are formed, but low-temperature synthesis is subject to kinetic problems which make it impractical. In any case, the join Ri_{100}-$Tr_{92}Mc_8$ is not far displaced from Ri_{100}-Tr_{100}. Therefore it was decided to continue the study treating the "pseudo-binary" as a real

binary. New starting materials on this join were made up, to which silica-gel was added to prevent amphibole dissolution through reaction (2).

Synthesis conditions and results are displayed in Table 4.2. The gel mixes, though supposedly amorphous, in fact contained substantial pyroxene which had crystallised on sintering the gels during their preparation, reaction of which was slow in the Tr-rich samples. But it was enhanced by the presence of a large volume of fluid, and by grinding incompletely reacted samples and re-running with additional H_2O.

Reaction was considered complete when either a pyroxene-free assemblage (Am + Qz) was obtained, or when re-running did not reduce the amount of pyroxene. For example an optical examination of samples T-R 33 and 41 (RI48+QZ) suggested comparable amounts of Di in both, and similarly in T-R 55 and 56 (RI100). Thus these two bulk compositions cannot be stoichiometric. However such small percentages of impurities will have negligible effect on the sample's measured bulk properties.

4.3. AMPHIBOLE CHARACTERISATION

4.3.(i). Optical Microscopy and Scanning Electron Microscopy (SEM)

The use of optical microscopy to search for impurities in the samples and to determine the degree of crystallinity was followed up by SEM examination. Images of $Tr_{92}Mc_8$, Ri_{65} and Ri_{100} obtained using the two techniques are compared in Plate 4.1. Crystal habit is clearly composition-dependent, eg. the Ri-rich samples are the most prismatic and the Tr-rich samples the most acicular of the solid solution. No impurities were detected in any sample by either method of examination, suggesting that the amphiboles are on-composition.

4.3.(ii). EMPA

EMPA was required to confirm the stoichiometry of the amphiboles, as microcrystalline or amorphous impurities might easily go undetected optically. Individual analyses are presented in Appendix Table A4.3, which also shows the calculated proportions of the exchange vectors Na_2Ca_{-1} and Mg_2Ca_{-2} with respect to Tr_{100}. These are plotted in Fig. 4.4 in terms of Tr, Ri and Mc components.

Plate 4.1. Optical and scanning electron micrographs of synthetic $Tr_{92}Mc_8$-Ri_{100} amphiboles:

(a) $Tr_{92}Mc_8$,

(b) Ri_{65},

(c) Ri_{100}.

Scale bar represents 20μm.

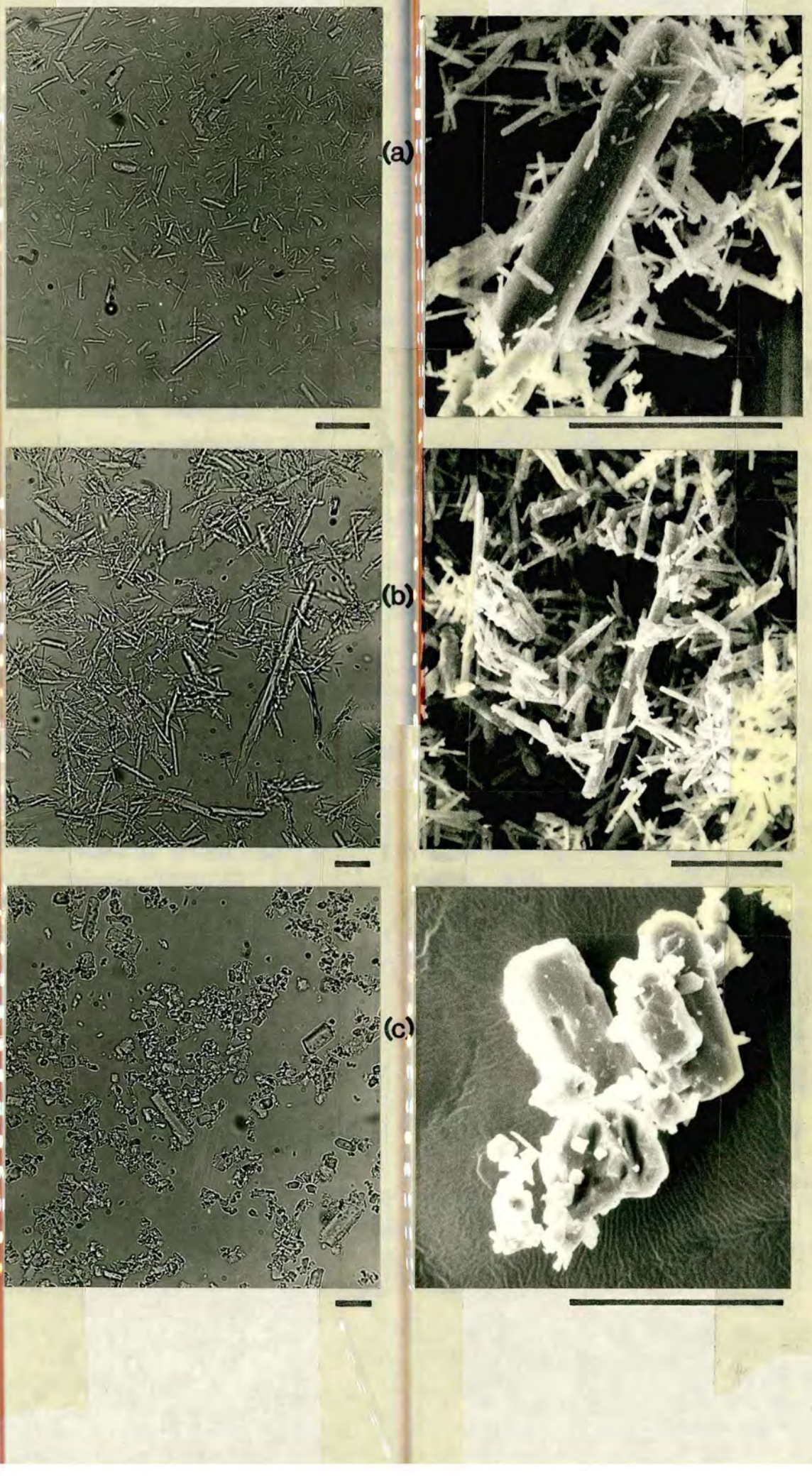
(a)
(b)
(c)

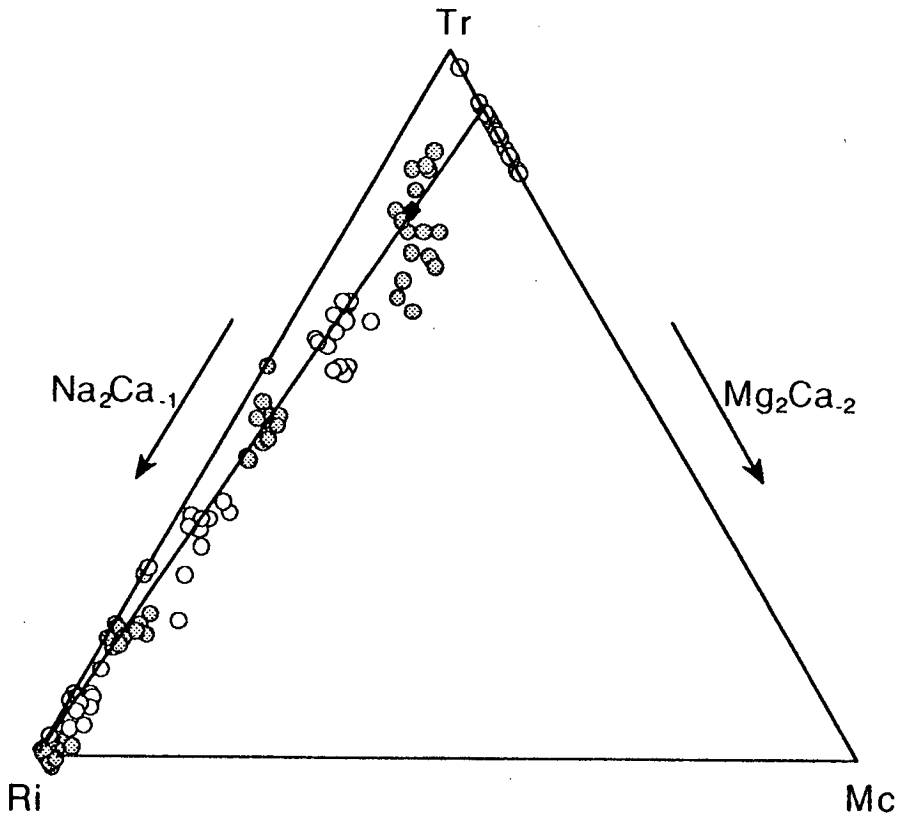

Fig. 4.4. Compositions determined by EMPA of amphiboles synthesised from the bulk compositions ◆ (+ Qz) on the $Tr_{92}Mc_8$-Ri_{100} pseudo-binary.

For each sample the scatter of analyses exceeds analytical error, and increases with increasing Tr-content. Clearly the sluggish reaction kinetics associated with the persistence of metastable pyroxene have prevented compositional homogenisation in the Tr-rich samples. Nevertheless the envelopes of analyses are discrete, and the mean analyses are in close agreement with the theoretical values (Table 4.3, Fig. 4.5).

The observed intra-grain compositional variation is in most cases less than the inter-grain variation, suggesting within-grain chemical homogeneity. However multiple analyses were generally obtained only at points along the axis of long grains, almost all grains being too small for analysis of both core and rim, between which any variation would be most expected.

Table 4.3. Mean compositions of synthetic $Tr_{92}Mc_8$ - Ri_{100} amphiboles determined by electron microprobe analysis.

Sample	No. of analyses (N)		Cations per formula		
			Ideal	Mean analysis	$2s/\sqrt{N}$
$Tr_{92}Mc_8$	15	Ca	1.84	1.78	0.03
		Mg	5.16	5.23	0.06
		Si	8.00	7.99	0.02
Ri_{16}	17	Na	0.32	0.35	0.04
		Ca	1.71	1.67	0.05
		Mg	5.13	5.18	0.04
		Si	8.00	7.98	0.01
Ri_{31}	14	Na	0.62	0.68	0.03
		Ca	1.58	1.52	0.03
		Mg	5.11	5.14	0.04
		Si	8.00	8.00	0.02
Ri_{48}	12	Na	0.96	0.99	0.04
		Ca	1.44	1.43	0.03
		Mg	5.08	5.08	0.03
		Si	8.00	8.00	0.01
Ri_{65}	11	Na	1.30	1.32	0.05
		Ca	1.29	1.27	0.04
		Mg	5.06	5.08	0.04
		Si	8.00	7.99	0.02
Ri_{82}	12	Na	1.64	1.63	0.03
		Ca	1.15	1.16	0.02
		Mg	5.03	5.04	0.03
		Si	8.00	7.99	0.01
Ri_{92}	14	Na	1.84	1.86	0.03
		Ca	1.07	1.06	0.02
		Mg	5.01	5.04	0.02
		Si	8.00	7.98	0.01
Ri_{100}	16	Na	2.00	2.00	0.01
		Ca	1.00	1.00	0.01
		Mg	5.00	5.05	0.01
		Si	8.00	7.98	0.01

Microprobe operating conditions: accelerating voltage 15kV
beam current 7.6nA
count time on peaks 20s (Ca,Mg,Si), 15s (Na).

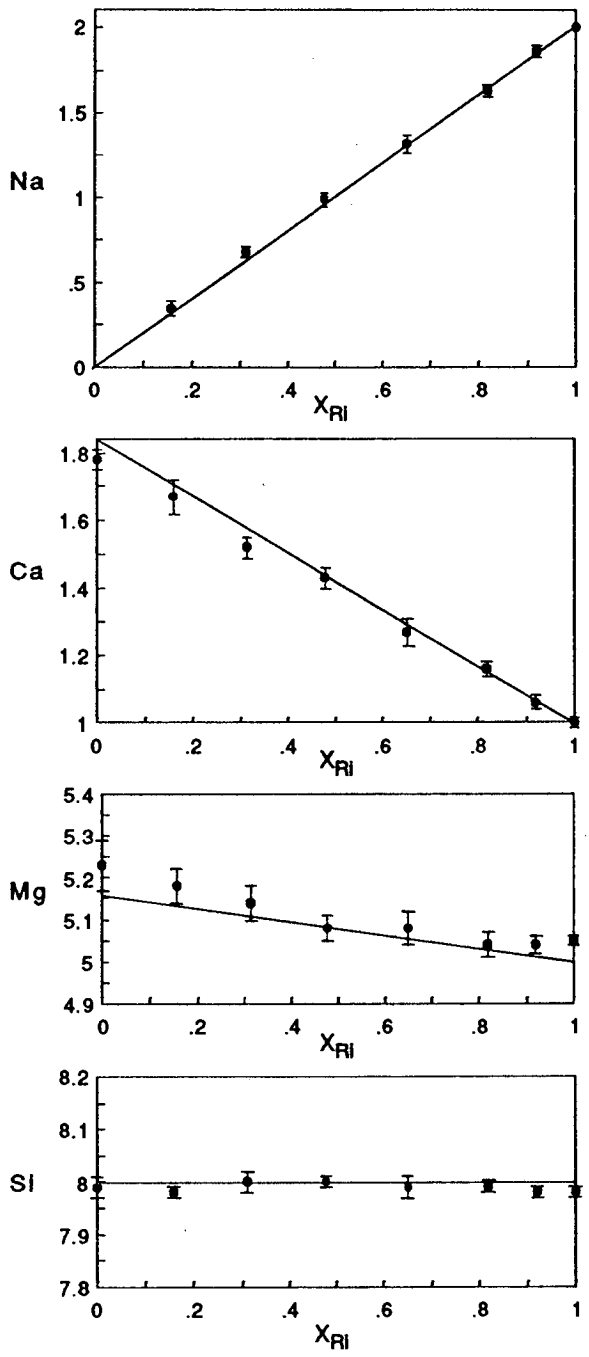

Fig. 4.5. Mean cations per formula determined by EMPA versus theoretical X_{Ri} of synthetic $Tr_{92}Mc_8$-Ri_{100} amphiboles. Error bars represent 2 standard deviations of the mean, and the solid lines define the ideal ratios.

4.3.(iii). Unit-cell parameters

In order to derive the thermodynamically important parameter ΔV_{mix}, unit-cell parameters of the 8 amphiboles were determined by least-squares refinement of powder XRD patterns. Finely ground sample, mixed with powdered silicon, was spread as a paste onto 'mylar' film and mounted in a Guinier Camera. Monochromatic CuKα_1 radiation and 24 hour exposures were used, and the silicon acted as an internal standard (strongest peak at 28.442°2θ). 29 to 48 sharp reflections in the range 10 - 70°2θ were indexed on the basis of a monoclinic unit cell, and used in the refinement program. Deviations of <0.02° between observed and calculated 2θ were considered acceptable.

Cell parameters are listed in Table 4.4 and plotted as a function of composition in Fig. 4.6.

Table 4.4. Unit cell parameters of synthetic $Tr_{92}Mc_8$-Ri_{100} amphiboles.

Sample	a(Å)	b(Å)	c(Å)	β(deg)	asinβ(Å)	V(Å^3)	V(cm^{3}mol^{-1})
$Tr_{92}Mc_8$	9.8079 ±.0012	18.0513 ±.0011	5.2767 ±.0004	104.553 ±.008	9.4932	904.235 ±.150	272.291
Ri_{16}	9.8322 ±.0010	18.0444 ±.0017	5.2755 ±.0005	104.552 ±.013	9.5168	905.931 ±.114	272.802
Ri_{31}	9.8466 ±.0008	18.0368 ±.0009	5.2735 ±.0003	104.488 ±.005	9.5335	906.805 ±.115	273.065
Ri_{48}	9.8623 ±.0004	18.0232 ±.0005	5.2720 ±.0002	104.450 ±.003	9.5503	907.451 ±.066	273.259
Ri_{65}	9.8749 ±.0010	18.0101 ±.0009	5.2696 ±.0004	104.389 ±.006	9.5651	907.783 ±.134	273.359
Ri_{82}	9.8927 ±.0007	17.9997 ±.0008	5.2693 ±.0003	104.328 ±.005	9.5850	909.090 ±.108	273.753
Ri_{92}	9.9028 ±.0008	17.9930 ±.0009	5.2687 ±.0005	104.284 ±.006	9.5967	909.768 ±.150	273.957
Ri_{100}	9.9050 ±.0009	17.9829 ±.0010	5.2691 ±.0005	104.260 ±.006	9.5998	909.611 ±.152	273.910

Quoted uncertainties are standard errors.

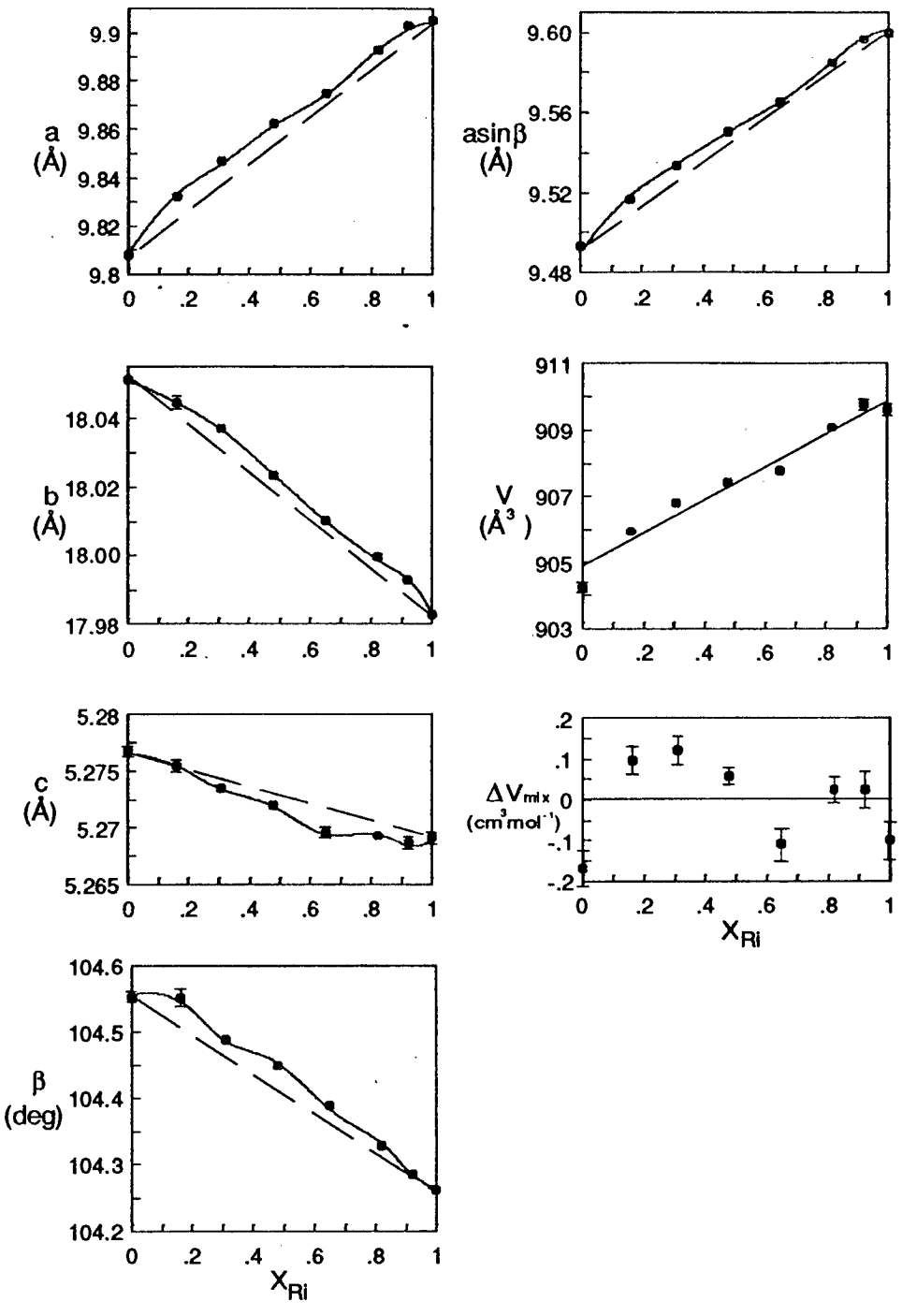

Fig. 4.6. Unit cell parameters and volume of mixing of synthetic $Tr_{92}Mc_8$-Ri_{100} amphiboles. Straight line in volume plot is least squares fitted, and ΔV_{mix} points were calculated relative to this line. ± 1 standard error bars are shown where they are larger than the point markers; those on ΔV_{mix} are the same magnitude as those on V.

The trends of increasing **a** and decreasing **b**, **c** and β from $Tr_{92}Mc_8$ to Ri_{100} are consistent with the differences between F-tremolite (Cameron & Gibbs, 1973) and F-richterite (Cameron et al., 1983). The large increase in **a** and decrease in β is primarily a result of the substitution of Na into the empty A-site, though β also decreases as Na substitutes for Ca on M(4) (Papike et al., 1969). The expansion of **a** (and asinβ) causes the cell volume to increase, allowing the structure to contract a little in the **b** and **c** dimensions.

All parameters show a slight deviation from ideality, **a**, **b** and β a positive deviation and **c** a negative deviation. The deviation in **a** is the main cause of what is perhaps a positive excess ΔV_{mix}. A positive ΔV_{mix} is not uncommon in mineral solid solutions (eg. F-tremolite - F-edenite, Graham & Navrotsky, 1986). In this case it is probable that in order to relieve the strain arising when just a few Na are substituted randomly into the A-sites of $Tr_{92}Mc_8$, the whole structure expands by a disproportionally high amount. With further substitution the rate of expansion can then decrease.

It is not clear why the volume of A-site-full Ri_{100} is less than that of Ri_{92}, nor why ΔV_{mix} decreases at the composition Ri_{65}. However experience suggests the existence of additional errors to those given in the cell refinement program, and so attempts to explain these anomalies are considered unnecessary.

The cell volumes were fit by linear regression to a straight line:

$$V(Å^3) = 904.80 + 5.1430\ X_{Ri}$$

$$V(cm^3mol^{-1}) = 272.46 + 1.5487\ X_{Ri}$$

Because of the possibility of additional errors, and also because deviations are in fact very small (< 1%), a more precise fit was not undertaken.

Zero ΔV_{mix} implies no pressure effect on the activity-composition relationships, while the approximately continuous variation in cell parameters is further evidence for complete solid solution.

4.3.(iv). H_2O-determination

When an amphibole is analysed by EMP, it is usually assumed that there are two OH groups per formula unit, occupying the 2 structural O(3) sites, and the analysis is normalised to 23 oxygens. But when H_2O is analysed by some other means, it is not uncommon to find an excess (eg. Kuroda et al., 1975; Maresch & Langer, 1976), which may have a significant effect on the amphibole's thermochemistry. This may be the result of proton-bearing coupled substitutions (eg. Welch & Graham, 1988).

Fig. 4.7. Layout of the hydrogen-extraction line at SURRC. From Welch (1987).

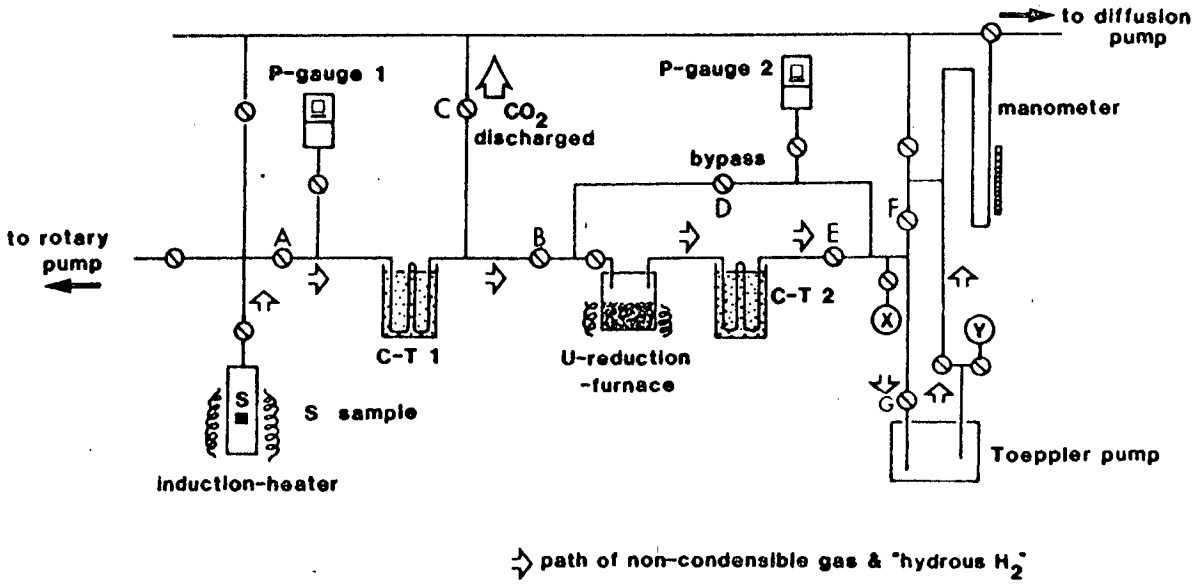

Table 4.5. H_2O-contents of synthetic $Tr_{92}Mc_8$ - Ri_{100} amphiboles (+ quartz) determined by hydrogen - extraction.

Sample	Mass (mg)	µmol H	wt% H_2O	Ideal wt% H_2O
$Tr_{92}Mc_8$	35.7	43.9	2.22 ± .12	2.10
Ri_{16}	35.5	38.6	1.96 ± .13	2.02
Ri_{31}	35.8	36.8	1.85 ± .14	2.02
Ri_{48}	35.7	39.4	1.99 ± .13	2.10
Ri_{65}	38.0	44.0	2.09 ± .11	2.16
Ri_{82}	35.9	44.7	2.25 ± .11	2.20
Ri_{100}	35.8	42.4	2.14 ± .12	2.20

Uncertainties on H_2O-contents derived from 95% confidence brackets on measured µmol H.

H_2O-contents of the synthetic $Tr_{92}Mc_8$-Ri_{100} amphiboles of this study were determined by hydrogen extraction using the facility at the Scottish Universities' Research and Reactor Centre at East Kilbride (Fig. 4.7). Radio-frequency induction heating under vacuum results in decomposition of the sample and release of structural H_2O at ~1500°C. This condenses in cold-trap 1 (C-T 1) along with any CO_2 released, while non-condensible gases such as hydrogen pass straight through to the manometer. The CO_2 is then removed by raising the temperature of the cold-trap above its boiling-point. Further heating causes the water to boil off, and the steam is reduced to hydrogen by passing over uranium (at 750°C) in the U-reduction furnace. The hydrogen is collected in C-T 2, and then its volume measured in the manometer calibrated for μmol H. The sample may be re-heated to release any H_2O not given off initially.

Before any measurements were made on the synthetic $Tr_{92}Mc_8$-Ri_{100} amphiboles, the calibration was checked by measuring the H_2O-content of a sample of known H_2O-content. The sample used was the same natural tremolite as used in a previous determination (Graham et al., 1984). The two results were in good agreement. This also served as a check that the system was leak-proof. H_2O-contents of the synthetic amphiboles are presented in Table 4.5. All except one (Ri_{31}) are ideal within the 95% confidence brackets. The low value for Ri_{31} is probably a result of incomplete sample decomposition or H_2O-reduction.

4.3.(v). HRTEM

The ideal amphibole structure consists of double chains of SiO_4 tetrahedra, 9Å wide along **y**, extending infinitely along **z** (Fig. 4.8). But this is simply an intermediate member of the continuous polysomatic "biopyribole" series between single-chain pyroxenes and infinite-chain sheet silicates, which also includes triple-chain and mixed-chain silicates (eg. jimthompsonite $Mg_{10}Si_{12}O_{32}(OH)_4$ and chesterite $Mg_{17}Si_{20}O_{54}(OH)_6$). Therefore it is not uncommon for so-called "amphiboles" in fact to incorporate chains of width $m \neq 2$, which are referred to as chain multiplicity faults (CMFs). The compositions of these will be different from the compositions of the double chains. However overall amphibole stoichiometry may be maintained provided the number of CMFs with $m > 2$ are balanced by an appropriate number with $m = 1$.

Such structural disorder is more common in synthetic amphiboles than natural ones (cf. synthetic and natural tirodites, Maresch & Czank, 1983), arising as it probably does from factors in the nucleation and growth mechanism. Therefore, although little is known of its effect on the thermodynamic properties of the phase,

detailed characterisation of any synthetic amphibole should be undertaken before applying its thermochemistry to natural assemblages.

As well as CMFs, amphiboles may contain stacking faults, or chain arrangement faults (CAFs), in which the regular stagger of tetrahedral chains along a* is disrupted. But because these do not affect the chemical composition, their effect on amphibole thermodynamic properties will be considerably less than any effect produced by CMFs.

A transmission electron microscope may be used to obtain high resolution images of, for example, CMFs and CAFs, low resolution images and electron diffraction patterns simply by interchanging lenses and apertures. The flexibility of the technique arises from the ability of the sample to diffract electrons, which may be described in the same way as x-ray diffraction, the important difference being that the wavelength of electrons is much smaller than that of x-rays, and therefore considerably more lattice planes in a single crystal under an electron beam simultaneously satisfy the Bragg condition for reflection. This is demonstrated in the Ewald sphere construction, in which the short wavelength means that the surface of the sphere is essentially flat over a large part of the reciprocal lattice, which is imaged when the microscope is being operated in diffraction mode. The diffraction pattern contains much useful information regarding lattice spacings and crystallographic orientations, and because it is not averaged over as many unit cells as in x-ray diffraction, small areas of crystals, such as intergrowths or antiphase domains, may be examined individually. Furthermore it can reveal structural disorder within the sample which disrupts the regular lattice repeat and gives rise to diffuse spots, or streaking.

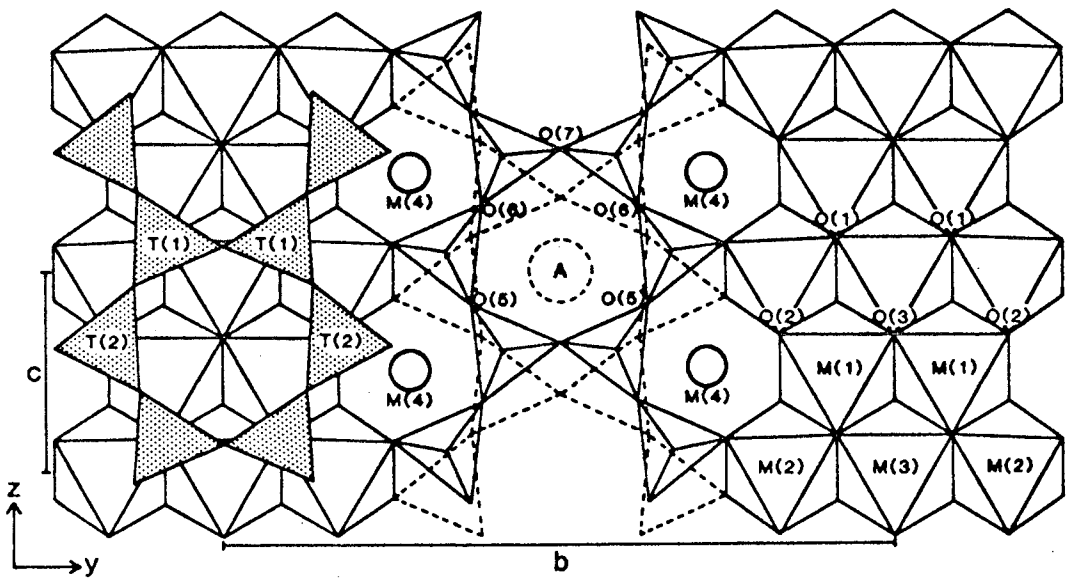

Fig. 4.8. (100) projection of the C2/m amphibole structure.

In high resolution transmission electron microscopy (HRTEM), some of the diffracted beams are recombined to form an image of the crystal, the resolution of which increases with the number of beams being used. Caused by phase contrast between the beams, the image is a projection of the electrostatic potential within the crystal, which is high where the density of atoms is high (eg. the silicate double chain in the amphibole structure) and low where there are few or no atoms (the pseudo-hexagonal holes). Modern instruments are capable of imaging structural detail to a resolution of 2Å.

If only the transmitted beam is allowed to pass through the objective aperture, the resulting lower magnification bright field image arises from diffraction contrast. Diffracted beams do not pass through the aperture, and therefore diffracting planes appear dark. Dark field images are produced when a diffracted beam forms the image.

The microscope used to image the synthetic $Tr_{92}Mc_8$-Ri_{100} amphiboles in this study was a JEOL JEM 100CX, operated at 100 kV, and fitted with a cartridge allowing a ± 10° tilt about 2 orthogonal axes. A suspension of the sample in ethanol was deposited onto 'holey' carbon film over a 2 mm diameter copper grid. Crystals were small enough that thin edges over holes in the film, essential for high resolution imaging, were quite common. However their acicular habit generally resulted in sedimentation with **c** in the plane of the carbon film and **b** frequently also in this plane, the crystals being flatter in the **b** dimension than in **a**. Hence whilst **b***-**c*** images showing (0k0) fringes were easily obtained, **a***-**c*** images were more difficult and **a***-**b*** images virtually impossible to obtain.

A 40 μm objective aperture allowed 5 (0k0) beams to form a **b***-**c*** image, in which the 9Å repeat (0k0) fringes were resolvable at the typical 220,000× magnification.

In contrast to certain other synthetic amphiboles, eg. anthophyllite - tirodite (Maresch & Czank, 1983, 1988) the amphiboles of this study are highly ordered. The Tr-rich compositions contain a few CMFs (Plate 4.2(a)), which decrease in abundance towards Ri_{100}, which is apparently CMF-free (Plate 4.2(b)). (h00) fringes in **a***-**c*** images were occasionally observed, and their regular spacing indicated complete order with no CAFs.

All diffraction patterns were sharp, with no streaking of reciprocal lattice points. Furthermore the general similarity of the patterns of all the samples confirmed that there are no major changes in lattice spacings along the join.

Plate 4.2 (a). HRTEM image of (0k0) fringes in synthetic $Tr_{92}Mc_8$. CMFs indicated by arrows.

(b). HRTEM image of (0k0) fringes in synthetic Ri_{100}. No CMFs visible. Inset is electron diffraction pattern.

(c),(d). Bright field images showing CMFs in an amphibole synthesised from the bulk composition $Na_3Mg_3Al_3Si_7O_{23} + H_2O$, and in a natural glaucophane.

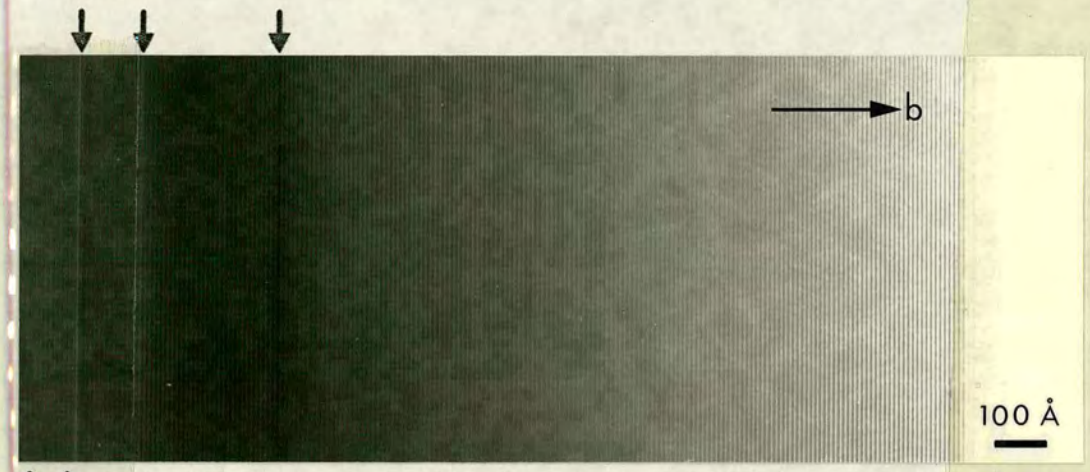

(a)

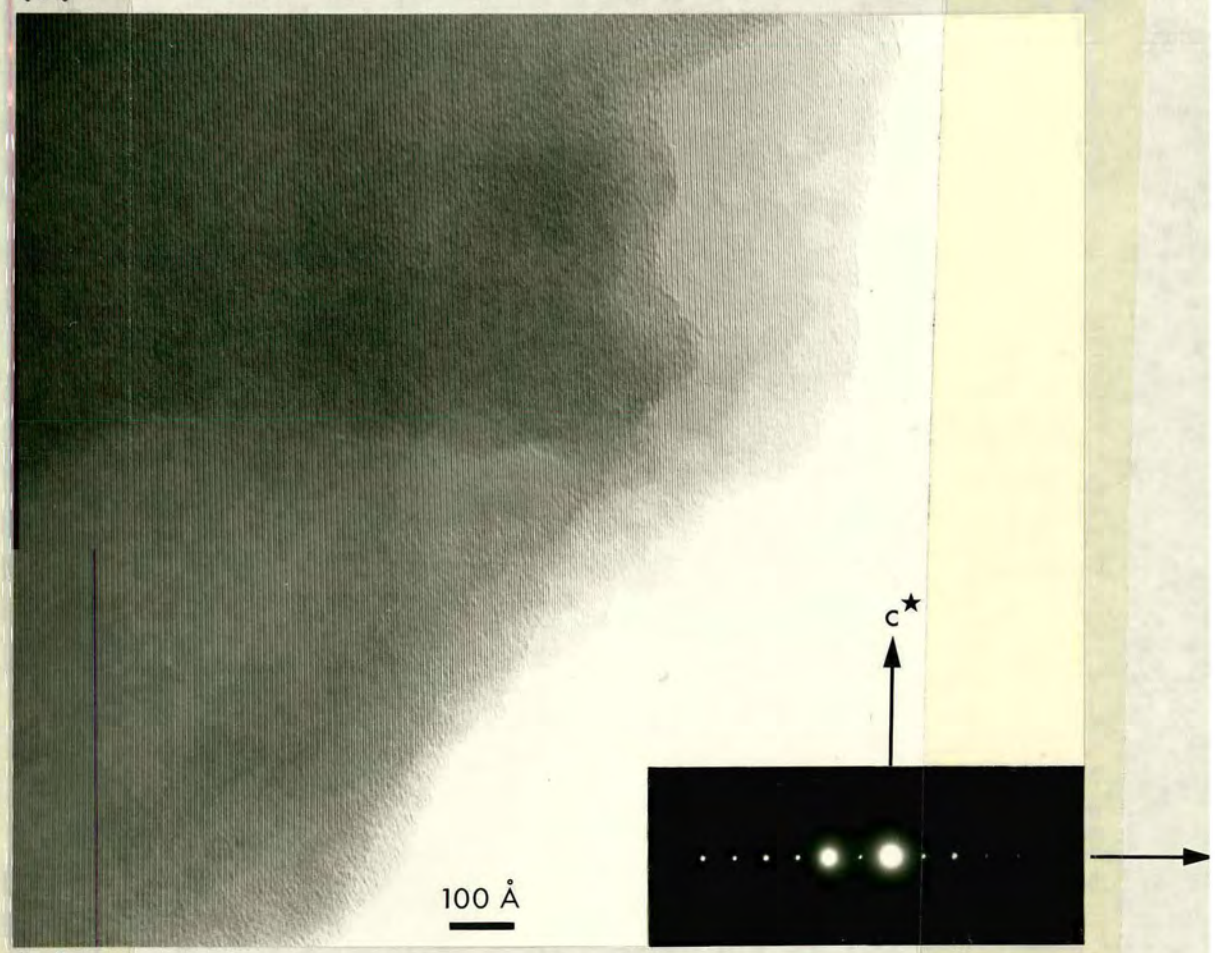

(b)

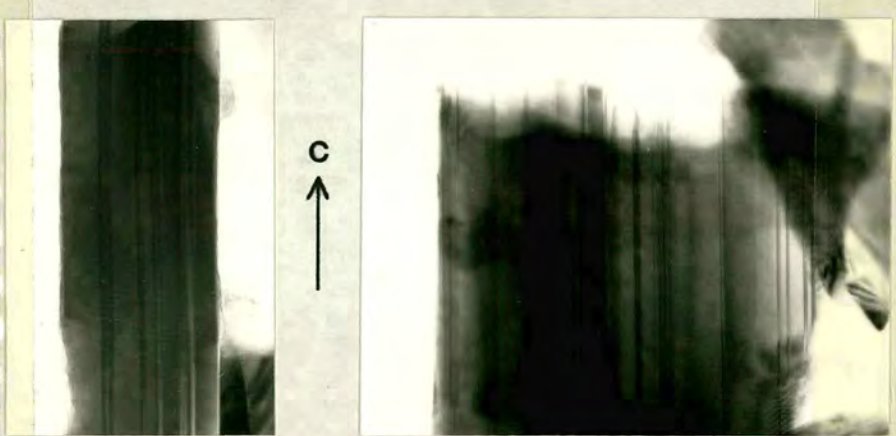

(c) (d)

It has been observed that alkali-rich amphiboles may be less susceptible to CMFs than other compositions (eg. Koons, 1982; Maresch & Czank, 1983). Certainly it is the most alkali-rich composition here (Ri_{100}) which contains the fewest defects. But even in the Na-free endmember $Tr_{92}Mc_8$ the number is significantly less than appears to be the case for eg. (Mn,Mg)-amphiboles (Maresch & Czank, 1988), and also less than for an alkali-rich amphibole synthesised from the bulk composition $Na_3Mg_3Al_3Si_7O_{23} + H_2O$ (OH-nyböite) and a natural glaucophane (Plate 4.2(c), (d)). In common with the increase in compositional variation, the increase in CMF density along the join Ri_{100}-$Tr_{92}Mc_8$ is almost certainly related to rate of synthesis kinetics, with the most Tr-rich amphiboles still containing a minor component of pyroxene in the form of CMFs.

It is interesting to note that while $Tr_{92}Mc_8$ does contain a few CMFs, the number is probably much less than in "tremolite" synthesised from the bulk composition $Ca_2Mg_5Si_8O_{23} + H_2O$. Maresch & Czank (1988) report an "A"-value (A = width of ideal undisturbed amphibole structure / width of crystal) of ~0.70 for synthetic "tremolite", indicating significant structural disorder. They also suggest that silica-activity plays an important part in determining the A-value of synthetic amphiboles, high a_{SiO_2} favouring high A-values. This could account for the greater degree of order of $Tr_{92}Mc_8$, synthesised with 10% excess Qz, than "tremolite". Furthermore, as the synthetic "tremolite" coexists with diopside, it is also more likely to contain m = 1 CMFs with the composition of diopside.

4.4. VIBRATIONAL SPECTROSCOPY

4.4.(i). Introduction

While EMPA provides a valuable means of characterising average chemical composition over a large number of unit cells, it does not give direct information regarding specific site occupancies or cation order-disorder in a mineral, which may have a significant effect on its thermochemistry. Vibrational spectroscopy, however, provides an easy-to-use means of investigating these and other properties of the mineral.

Vibrational spectroscopy is the interaction of light with vibrational motions of molecules or structural groups in a crystal. The energies of these motions (0 - 60 kJ mol^{-1}) are of the same order as infrared (IR) radiation, hence in an IR absorption experiment, incident radiation is absorbed directly by the vibrations. In a Raman scattering experiment, incident light of a higher frequency (visible light) excites the vibrations and is inelastically scattered at a lower energy.

The vibrational frequencies are functions of force constants, which vary considerably from one type of bond to another, and are affected by the surrounding structural environment. Coupling of vibrations results in vibrational modes arising from very complex motions within the crystal.

The amount of information that can be obtained from spectra is varied and depends on how well the peaks can be assigned to specific vibrations. At the simplest level, spectral "fingerprinting" allows mineral identification without any understanding of the vibrations. By observing spectral changes with composition, it may then be possible to assign peaks to particular vibrations, to give information regarding site occupancies and the nature of interatomic forces and bond strengths.

On a more advanced level, *ab initio* molecular orbital calculations of force constants have recently been used to determine frequencies of simple vibrations, which may then be compared with observed frequencies to explore the nature of other forces acting on the vibration. From a set of force constants, an entire vibrational spectrum may be calculated.

Thus as the great potential for sample characterisation offered by vibrational spectroscopy is increasingly realised, the resulting larger number of experimental data and theoretical calculations allows assignment of more and more vibrational frequencies in even quite complex minerals, with the result that their thermodynamic behaviour can be better understood and quantified.

4.4.(ii). Previous work on amphiboles

A typical amphibole IR or Raman spectrum is extremely complex, consisting of a large number of bands which are difficult to resolve and most of which are impossible to assign to specific vibrational modes. The exception is the O-H stretching frequency, at 3600 - 3750 cm^{-1}, which has been studied quite extensively.

The hydroxyl ion occupies the O(3) site in the amphibole structure (Figs. 4.8 and 4.9) which is coordinated by two M(1) and one M(3) cations in a pseudo-trigonal arrangement around the orthogonal O-H vector, such that the hydrogen points directly towards the centre of a pseudo-hexagonal hole in the silicate double-chain. The frequency of the O-H stretch depends on its bond strength, which is influenced by the local environment of the hydroxyl group. Thus the M(1) and M(3) site occupancies are important in determining the O-H stretching frequency. It has been suggested that the mean covalency of the octahedral cation - hydroxyl bond is a significant factor in determining the bond strength, such that the more electronegative the M(1)/M(3) cation the lower the frequency (Hawthorne, 1983). The A-site occupancy is also important, as this site lies directly behind the 6-membered ring; and though not

actually coordinated to O(3), both the M(2) and M(4) site occupancies also influence the O-H stretching frequency.

Thus the spectrum of a typical amphibole composition, in which there is mixing on most, if not all, of these sites, will comprise several bands in the O-H stretching region, each assignable to a particular cation configuration around a hydroxyl group.

In ordered end-member tremolite, with all of the octahedral sites occupied by Mg, the M(4) sites by Ca, and the A-sites empty, all of the OH groups are in identical environments, and there is therefore just one O-H stretching frequency, at 3674 cm^{-1}. The substitution of Mg at M(4) through the exchange $MgCa_{-1}$ causes a frequency shift of ~-2 cm^{-1} for each of the 4 M(4) sites around the A-site (Hawthorne, 1983), and the substitution of Na into the A-site (here through the reaction $NaNaCa_{-1}$) results in a frequency increase of 56 cm^{-1} (Rowbotham & Farmer, 1973). This shift is large because the A-site Na repels the H atoms, and so shortens the length and increases the strength of the O-H bond.

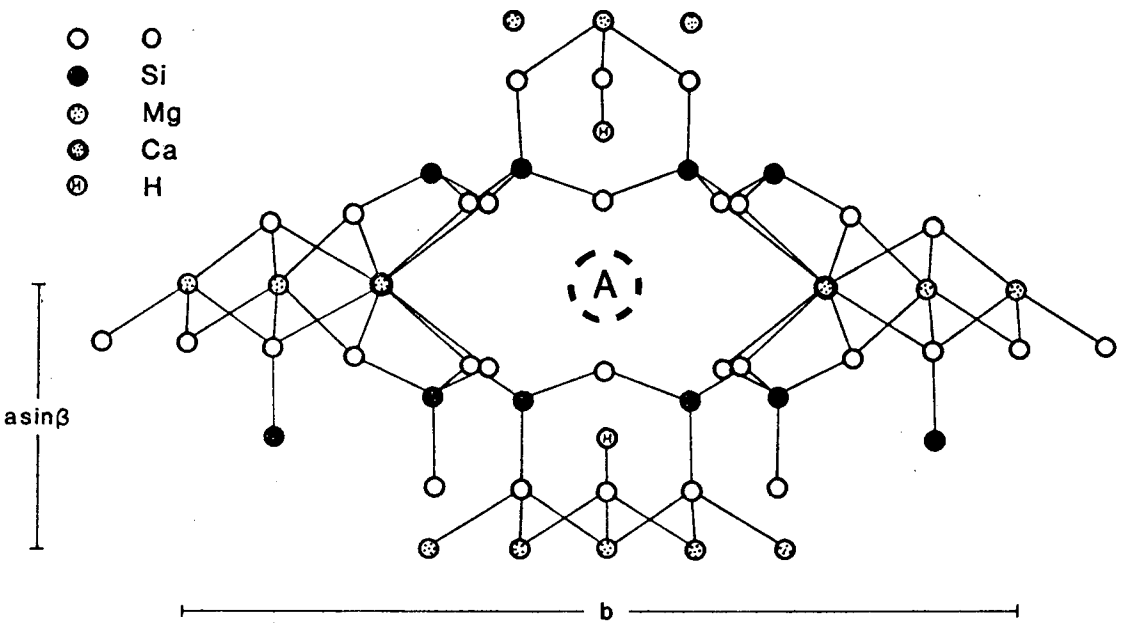

Fig. 4.9. (001) projection of the structure of tremolite (calculated in the program VIBRAT (Dowty, 1987) from an input of atomic coordinates, bond lengths and bond angles).

Few data have been published concerning the lower frequency part of IR spectra. Kukovskii & Litvin (1970) and Barabanov et al. (1974) have published spectra for a number of well-characterised natural amphiboles, but only a couple of bands could be assigned to specific vibrations.

Very little Raman spectroscopy has been done on amphiboles. However the O-H stretching band occurs at the same frequency as in IR experiments, eg at 3674 cm^{-1} in tremolite (Sheu & McMillan, 1988) and therefore direct comparisons may be made between spectra obtained by the two techniques.

4.4.(iii). Instrumentation

Nowadays most IR studies on minerals use Fourier Transform instruments to obtain powder transmission spectra in the mid-IR range (4000 - 400 cm^{-1}). Sample preparation and data collection are straightforward. Only 1 - 2 mg of sample is required, which is supported as a finely ground powder in a compressed alkali halide disc, chemically inert and transparent to the IR beam in this frequency range.

In a Fourier Transform experiment, the entire spectrum may be sampled in a fraction of a second and hence a large number of scans collected in a few minutes and the signals summed to reduce the noise level. Furthermore, sensitivity is high as energy throughput is not limited by instrumental slit widths, and stray radiation will not interfere with the signal.

The spectra obtained in powder IR studies are transmission spectra, in which minima are taken to correspond to bulk sample absorption maxima. However spurious bands and increased band-widths often arise as a result of the small particle sizes involved (McMillan & Hofmeister, 1988). It may be possible to remove these; otherwise though still very useful, it must be realised that the spectra are not true absorption spectra. These problems are not encountered in micro-FTIR spectroscopy, in which reflection spectra may be obtained from single crystals by focussing the IR beam onto the sample through a microscope and sampling the reflected beam. Again a portion of the incident radiation is absorbed by the crystal rather than reflected, and the resulting spectrum is quite complex. But an absorption or transmission spectrum may be derived from this by applying a set of "Kramers-Kronig" dispersion relations.

Two further advantages of micro-IR are that preparation of fine-grained samples is minimal, and most importantly it can be used for single crystal studies on samples 10 μm diameter or less. However this technique has only recently begun to be applied to the study of geological materials.

Fourier Transform Raman spectroscopy is also still in its infancy, and therefore most instruments currently in use incorporate a "monochromator" with slits

and diffraction gratings for wavelength selection. Gas lasers with lasing transitions in the visible region of the spectrum are the most common sources in Raman experiments, the 488 nm and 514.5 nm lines of argon ion (Ar^+) lasers being the most popular. In a micro-Raman experiment, this light is focussed through the objective lens of a microscope onto the sample and the scattered light passing back through the lens is directed into the spectrometer. A photomultiplier, which amplifies the weak signal, is a common detector for the entire spectrum. However it is essential that the elastically scattered laser line is not allowed to reach the sensitive detector and hence the spectrum below ~20 cm^{-1} cannot be sampled.

Sample preparation is as simple as for micro-IR, and again studies of single crystals only a few μm diameter are possible. Better quality spectra are obtained for large crystals as the signal intensity and hence signal to noise ratio is increased. The signal may also be increased by using larger monochromator slit sizes, but in so doing the resolution decreases and the edge of the laser line may overlap and obscure the signal at low wavenumbers. The signal to noise ratio can be improved by increasing the count time on each point and by co-adding more than one spectrum from the same sample.

In this study, powder IR transmission spectra of all 8 synthetic amphiboles were obtained using a Nicolet 10-MX FTIR spectrometer. 2 mg of crushed sample was mixed with 180 mg KBr, pressed into a disc and dried in a vacuum oven to remove adsorbed water before collecting the spectra. These are shown in Fig. 4.10, replotted as absorption spectra.

Single crystal micro-infrared reflectance spectra of 2 sub-50 μm crystals of Ri_{100} were obtained using a Digilab FTS-40 infrared bench with UMA-300 microscope system, and a broad band MCT detector. The spectra were transformed to absorption spectra through application of the Kramers-Kronig dispersion relations (Fig. 4.11).

Single crystal micro-Raman spectra were obtained using an Instruments S.A. U-1000 micro-Raman system, and the 514.5 nm lasing line of a Coherent Innova 90-4 Ar^+ laser for sample excitation. The crushed sample was sprinkled onto a glass slide, and the laser beam focussed onto the largest crystal visible in each sample, which was typically ~6 - 10 μm wide. 200 - 300 μm slits were used, and a counting time of 5 - 10 seconds/point, with points spaced by 1 cm^{-1}. 6 - 15 scans were co-added for each crystal. Spectra were obtained for $Tr_{92}Mc_8$, Ri_{48}, Ri_{82} and Ri_{100} (Fig. 4.12 (a), (b)).

Fig. 4.10. Infrared absorption spectra of synthetic $Tr_{92}Mc_8$-Ri_{100} amphiboles: (a) hydroxyl stretching region, (b) the region 850-1200 cm^{-1}, (c) the region 630-820 cm^{-1}.

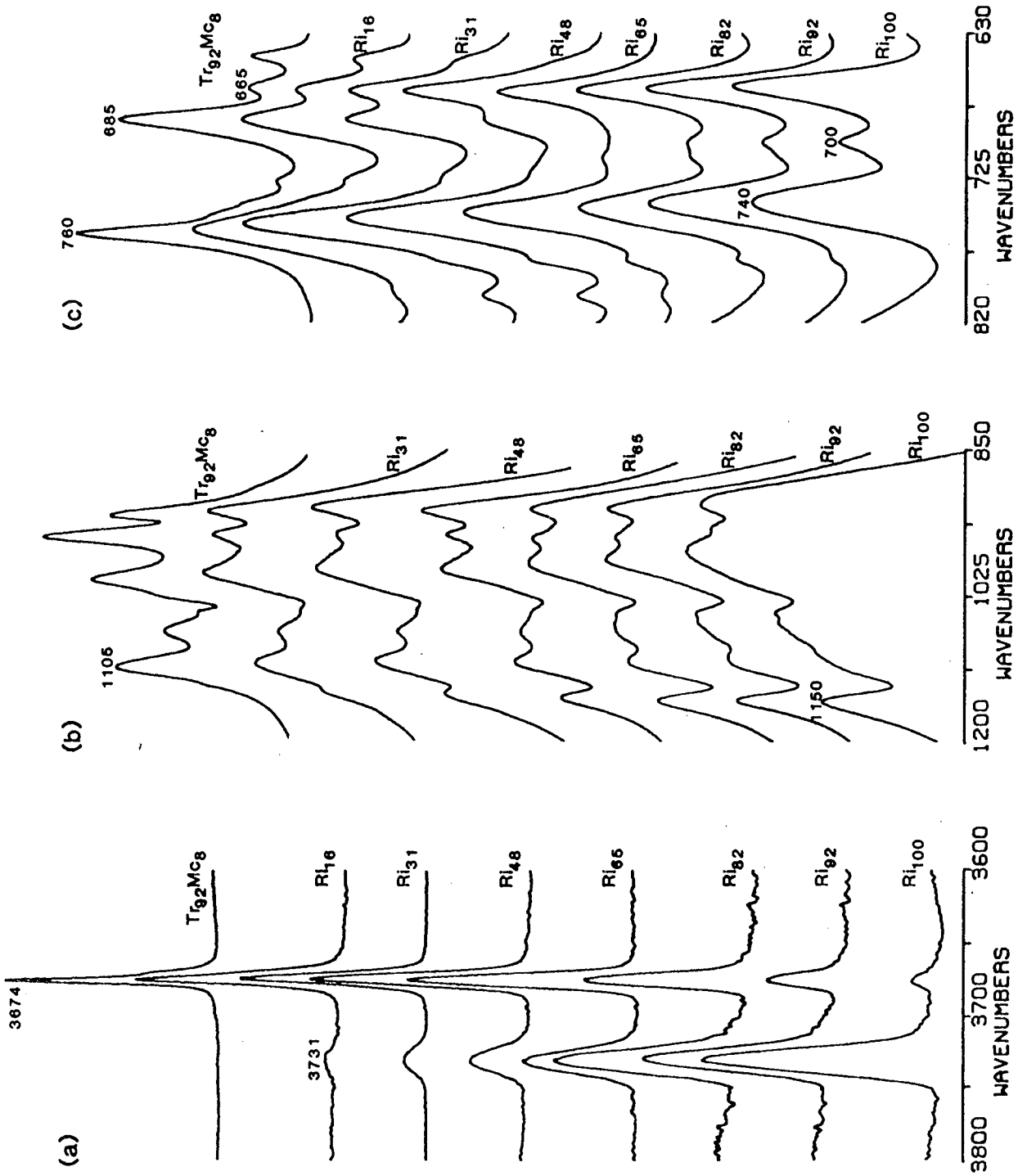

Fig. 4.11. (a) Infrared reflection spectra of two crystals of synthetic richterite.
(b) The same spectra transformed to absorption spectra by the "Kramers-Kronig" dispersion relations.

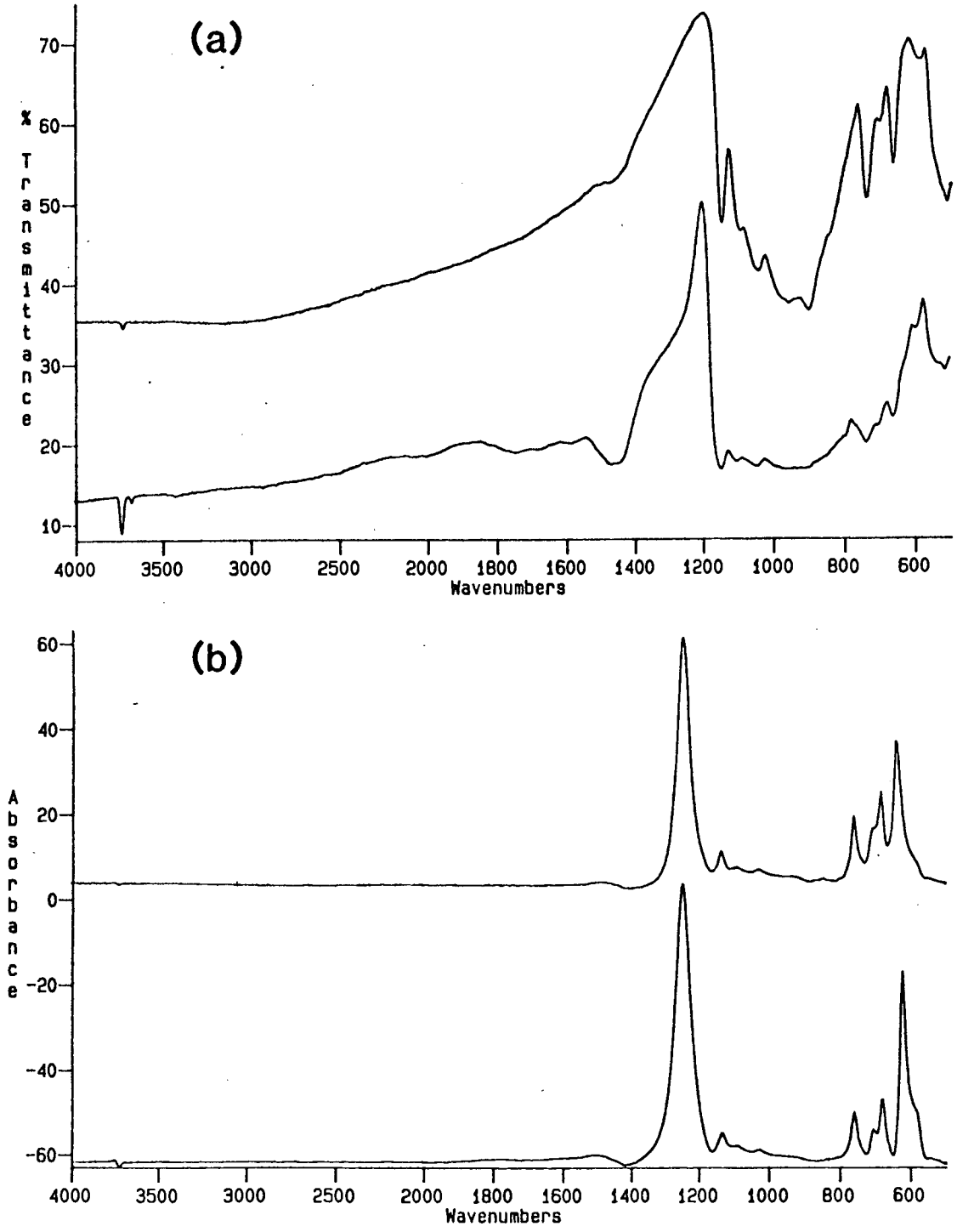

Fig. 4.12. (a) Single crystal micro-Raman spectra of synthetic $Tr_{92}Mc_8$, Ri_{48}, Ri_{82} and Ri_{100} amphiboles: hydroxyl stretching region.

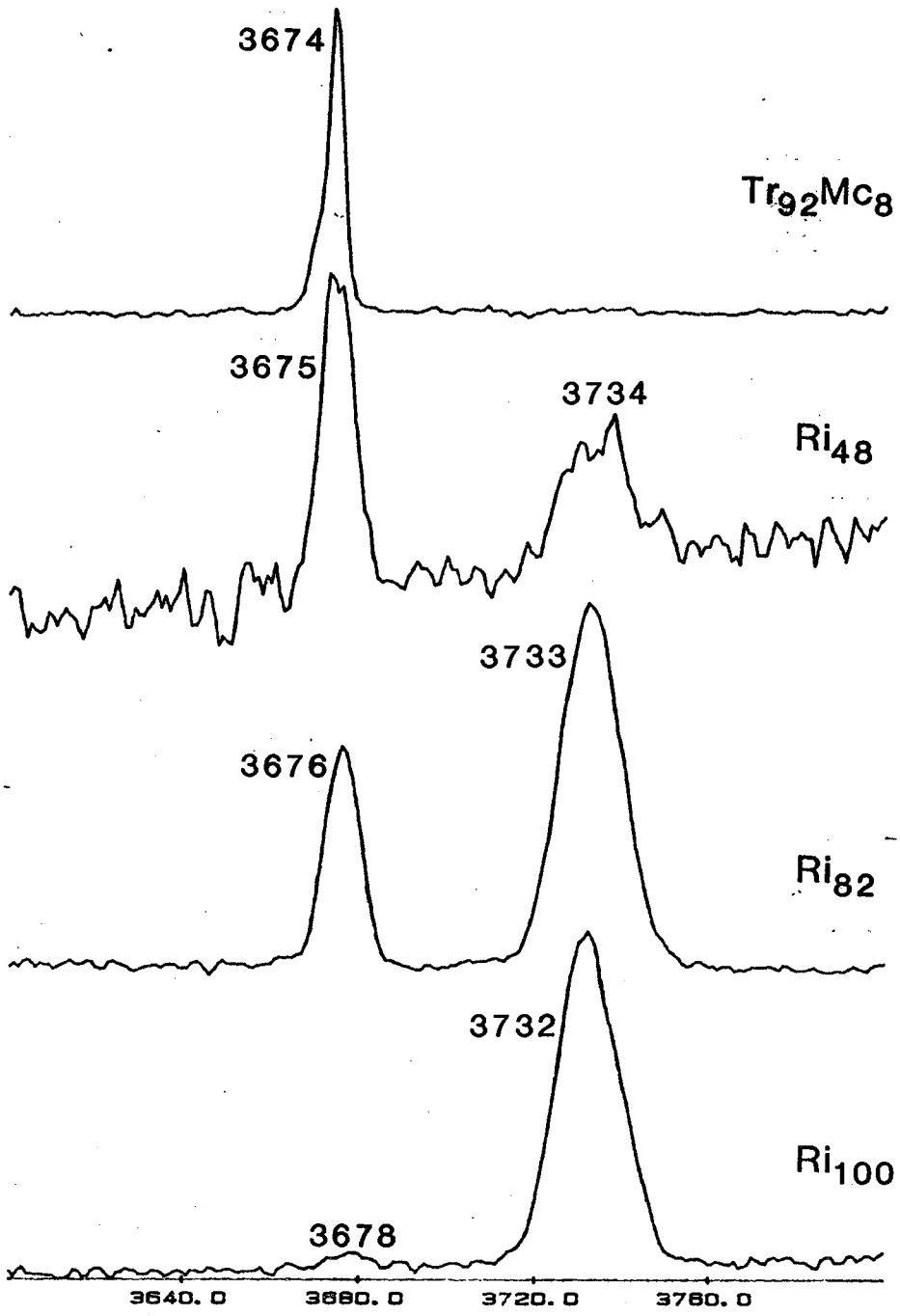

Fig. 4.12. Single crystal micro-Raman spectra of
(b) synthetic $Tr_{92}Mc_8$ and Ri_{100} (this study),
(c) natural tremolite (Sheu & McMillan, unpubl. data),
(d) synthetic pargasite (McMillan & Graham, unpubl. data).

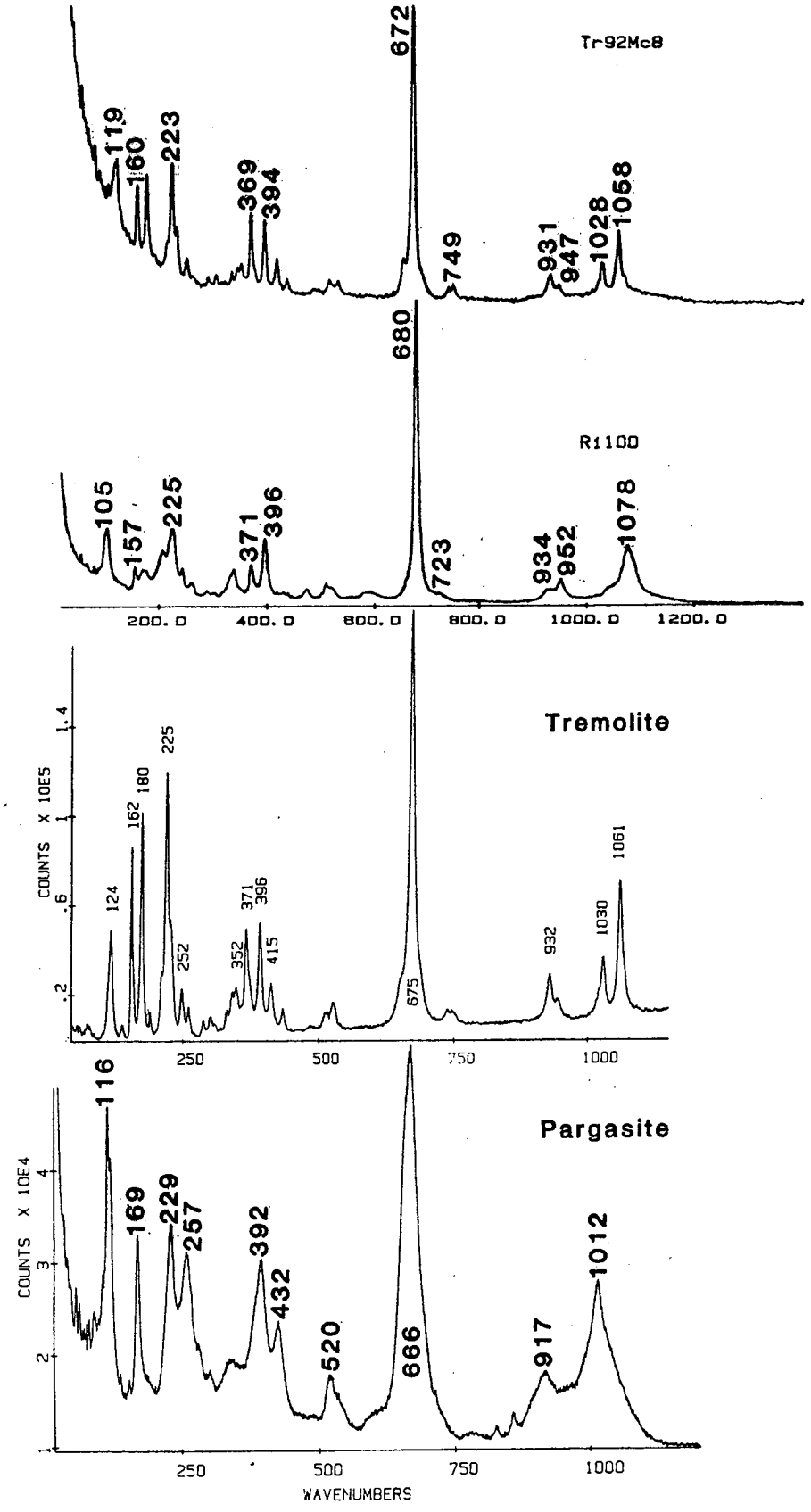

4.4.(iv). Results

Powder Infrared

Hydroxyl stretching region (Fig. 4.10(a))

The peak in the spectrum of $Tr_{92}Mc_8$ at 3674 cm^{-1} is clearly the A-site empty tremolite band, while the absence of a peak at ~3730 cm^{-1} confirms that all of the A-sites are vacant. There is, however, a shoulder in the sharp 3674 cm^{-1} band at ~3670 cm^{-1}, which must, in the absence of A-site effects, arise from the occupancy of some M(4) sites by Mg rather than Ca.

With the substitution of Na into the A-site, a band appears at 3731 cm^{-1}, while the 3674 cm^{-1} band decreases in intensity. The shoulder at 3670 cm^{-1} is no longer visible as the main band has broadened out, implying that, though the vacant A-site hydroxyls still share the same immediate environment, there are slight variations in longer range forces. The A-site full band is much the broader of the two. The reason for this may be understood by considering Fig. 4.9, in which it may be seen that two hydroxyl groups, related by the diad parallel to **b**, are associated with a single A-site. When the A-site is empty the hydroxyl groups vibrate independently of each other. But Na occupying an A-site interacts with both hydroxyl groups and their vibrations become coupled. Two different vibrational frequencies result, depending on whether the vibrations are in phase or exactly out of phase (Fig. 4.13), and the broad band actually consists of two closely overlapping bands.

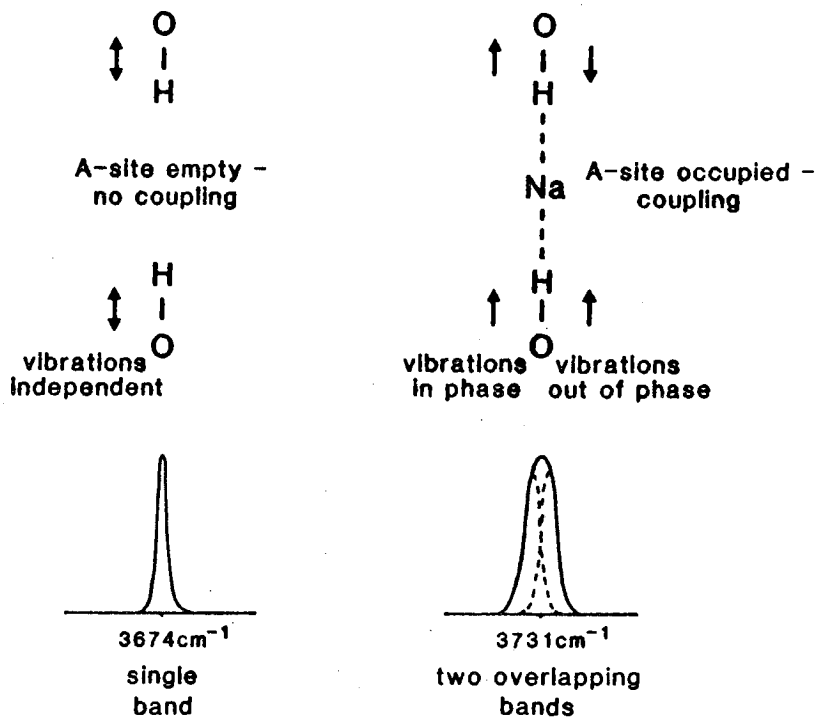

Fig. 4.13. Effect of A-site occupancy on O-H stretching frequency band width.

In end-member Ri_{100} all of the A-sites should be occupied by Na, and there should therefore be only one O-H stretching band. However the spectrum obtained here contains a small peak at 3674 cm^{-1}, corresponding to a few vacancies on the A-site. This peak is considerably smaller than that obtained in previous studies of synthetic richterite (Rowbotham & Farmer, 1973; Robert et al, 1989). However in neither of those studies were any results of optical examination or EMPA reported, and therefore non-stoichiometry of the sample is possible. Furthermore, the A-site vacant peak in the Ri_{100} spectrum obtained by Robert et al. (1989), rather than being at 3674 cm^{-1}, is in fact at 3670 cm^{-1} (with only a shoulder at ~3674 cm^{-1}), ie. at the same frequency as the shoulder in the 3674 cm^{-1} band of the $Tr_{92}Mc_8$ spectrum, and hence must be associated with Mg in M(4) sites. In richterite these sites should only be occupied by Na and Ca, and therefore the amphibole must be off-composition.

In an attempt to estimate the proportion of vacant A-sites in Ri_{100}, based on the assumption that the site-occupancies are proportional to the relative peak intensities, the areas under the two O-H stretching peaks were measured for each sample, and a proportionality constant relating the intensities derived. Using this the percentage of A-site vacancies in Ri_{100} was estimated as 2.5 %, ie. a very small percentage which may have gone undetected by EMPA.

At lower frequencies than the O-H stretch, the IR spectra contain several strong bands between 850 and 1200 cm^{-1} (Fig. 4.10(b)) and some weaker bands at 630-820 cm^{-1} (Fig. 4.10(c)), which, by analogy with other mineral spectra, may be associated with Si-O stretching and Si-O-Si bending vibrations. In common with the O-H stretching regions, there is systematic variation from one end-member to the other. Some bands in $Tr_{92}Mc_8$ decrease in intensity towards Ri_{100}, eg. those at 685 cm^{-1} and 1105 cm^{-1}; while others increase in intensity, eg. the 665 cm^{-1}, 700 cm^{-1} and 1150 cm^{-1} bands. Frequency shifts also occur, eg. from 760 cm^{-1} in $Tr_{92}Mc_8$ to 740 cm^{-1} in Ri_{100}.

Micro-infrared

Fig. 4.11(a) shows the raw reflection spectra of the two crystals of Ri_{100}, and Fig. 4.11(b) the Kramers-Kronig transformed absorption spectra. In the latter spectra the peaks are clearly sharper and fewer in number than in the former, and than in the powder IR spectra (Fig. 4.10), demonstrating the effectiveness of this technique in providing quality mid-IR spectra.

Without spectra for the other members of the solid solution, no interpretation of those of Ri_{100} is possible, but given the effectiveness of the techniques of powder

IR and Raman spectroscopy in demonstrating continuous variation along the solid solution, the collection of further micro-IR spectra was considered unnecessary.

Raman

The O-H stretching bands in the Raman spectra are similar in all respects to those in the IR spectra (Fig. 4.12(a)), and in common with those of the IR spectra the lower frequency portions of the Raman spectra display continuous variation from one end-member to the other. Changes in band intensity are not pronounced, but there are some significant shifts in peak positions, eg. the peaks at 1058 cm^{-1} and 749 cm^{-1} in $Tr_{92}Mc_8$ move to 1078 cm^{-1} and 723 cm^{-1} respectively in Ri_{100}, the latter becoming a shoulder in the strong 680 cm^{-1} band (Fig. 4.12(b)).

A comparison of the Raman spectrum of $Tr_{92}Mc_8$ with that of natural tremolite (Fig. 4.12(c)) shows a closer similarity than might be expected between synthetic and natural samples. Peaks for synthetic samples are often broadened by structural disorder (eg. synthetic pargasite, Fig. 4.12(d)), but the only significant difference between the two spectra of "tremolite" is the laser line overlap on the synthetic spectrum, its presence due to the reduced size of this sample.

In common with the results of the IR experiments, the absence of any dramatic variations between the Raman spectra makes peak assignments very difficult, and without detailed study of other simple synthetic solid solutions, or some sort of vibrational modelling, only the same general peak assignments may be made, namely Si-O stretching in the 850 - 1100 cm^{-1} region and Si-O-Si bending in the 600 - 700 cm^{-1} region.

One of the potential uses of vibrational spectra is in the calculation of heat capacity and third-law entropy (eg. Kieffer, 1985). However this requires all IR- and Raman-active vibrational modes to be known (determined experimentally or modelled), which has not been possible in this study. However the relative insensitivity of the frequencies to composition implies little variation in these thermodynamic properties. Therefore the main variable component of the entropy of $Tr_{92}Mc_8$-Ri_{100} amphiboles, ie. the main contribution to the entropy of mixing, will be a configurational entropy term, the significance of which will be discussed later.

Interestingly, the Raman spectrum of pargasite is not very different from that of tremolite or richterite, again suggesting a relative unimportance of the third-law term in the entropy of mixing of, for example, the tremolite-pargasite solid solution.

4.4.(v). Calculation of vibrational spectra

Vibrational frequencies are functions of force constants, and so in theory a complete vibrational spectrum may be calculated from a set of atomic positions and a set of force constants for two-atom bonds, three-atom angles and interactions between these. However in practice the calculations are extremely complex, and for all but the simplest of spectra require lengthy computation. The program VIBRAT (Dowty, 1987) allows atomic motions and spectral intensities as well as vibrational frequencies to be calculated for a structure containing up to 50 atoms in the primitive unit cell, from an input of the above-mentioned two sets of information. The calculated spectrum is a better approximation for Raman and single crystal IR spectra than for powder IR absorption spectra, due to the complexities of the latter caused by the problems mentioned in Section 4.4.(iii).

Calculation of a vibrational spectrum has been attempted for tremolite. Unit cell parameters and atomic positions were taken from the x-ray refinement of Hawthorne & Grundy (1976). Also required were the equivalent general positions for the C2/m space group, these being the set of positions produced by the operation of the symmetry elements of the space group upon an initial position chosen at random, and which are contained in the International Tables for X-ray Crystallography. But there do not exist any force constant data for tremolite other than for the O-H stretch, determined by an *ab initio* molecular orbital calculation (Sheu & McMillan, 1988). Though force constants for bonds and angles in some simple structures such as quartz and forsterite have been calculated, they are not transferable to minerals with different structures. But it was hoped that a spectrum calculated using such force constants would be similar enough to the observed spectrum that it was clear which band frequencies were incorrect, and the calculated atomic motions for these bands would indicate which force constants should be adjusted to shift them towards their observed frequencies.

To obtain the correct O-H stretching frequency (3674 cm^{-1}) in the calculated spectrum, a force constant of 9 mdyn $Å^{-1}$, corresponding approximately to the value calculated by Sheu & McMillan (1988), was used. However this yielded a frequency too high, and so was adjusted to 7.5 mdyn $Å^{-1}$, which gave a frequency of 3678 cm^{-1}. The calculated atomic motions confirmed that this is the O-H stretching frequency. These motions are displayed on a projection of the structure (eg. Fig. 4.9), which may be rotated about two axes, as vectors of magnitude proportional to the actual vibrational amplitude. Fig. 4.14(a) shows such a displacement for O(3) and H during the O-H stretch.

Fig. 4.14. Atomic motions calculated in the program VIBRAT for various vibrational frequencies. Broad lines show direction and relative magnitude of motion of the atoms from which they originate. See text for further discussion.

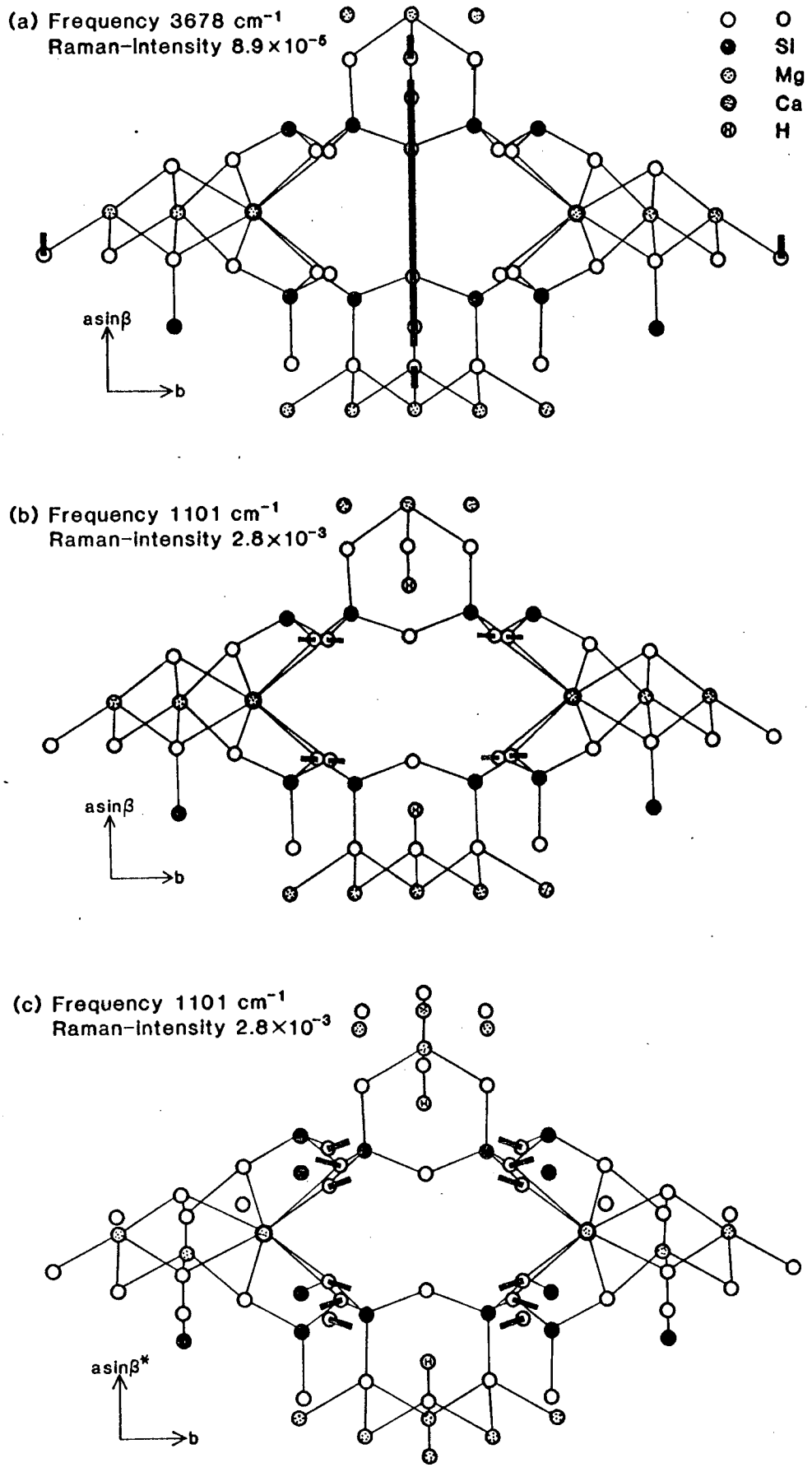

(Fig. 4.14 continued)

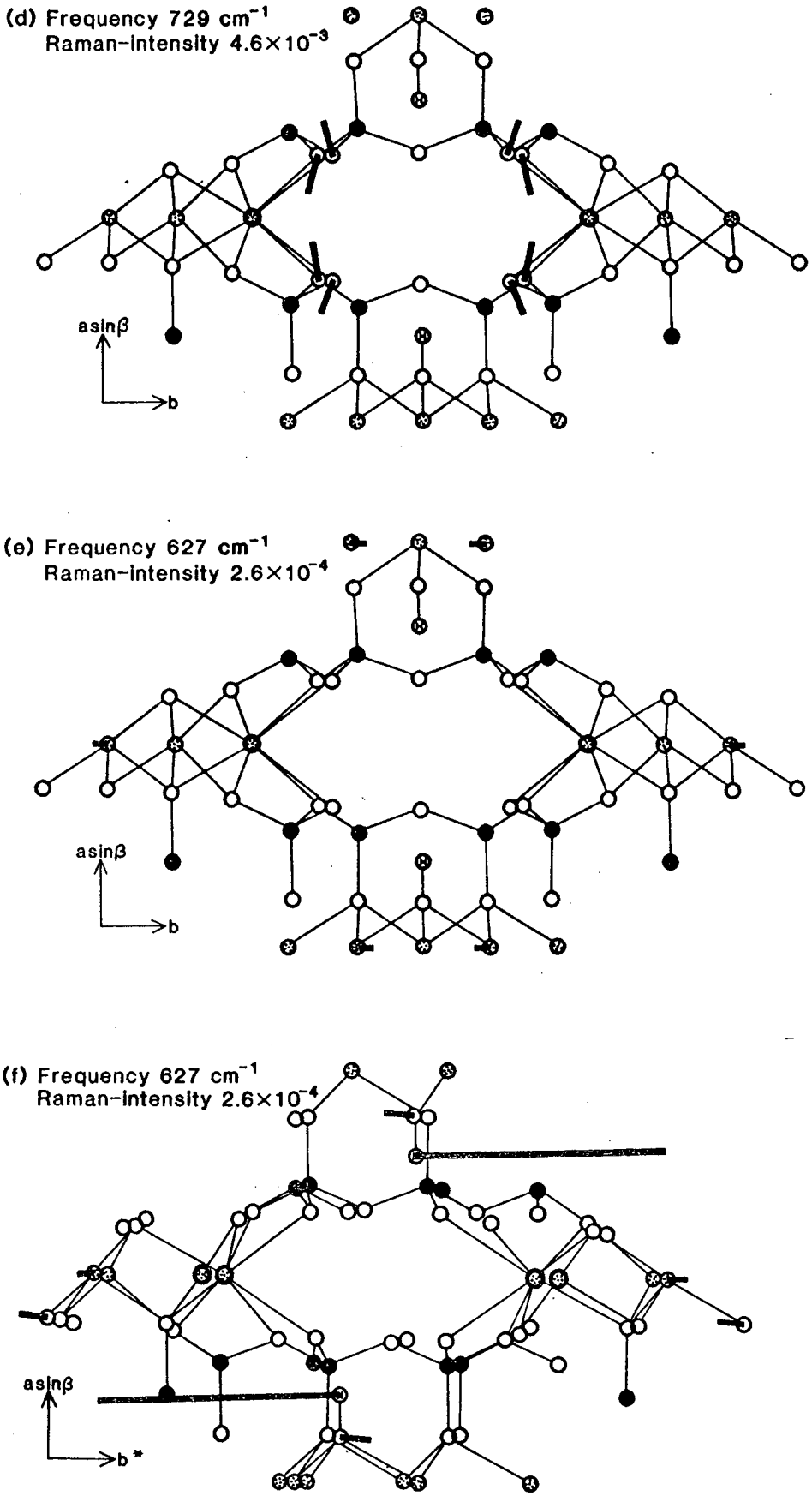

(Fig. 4.14 continued)

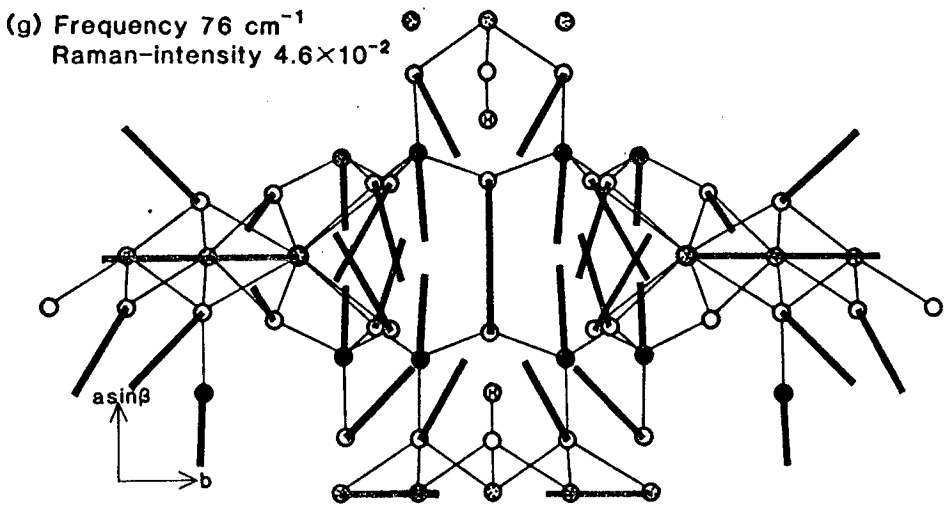

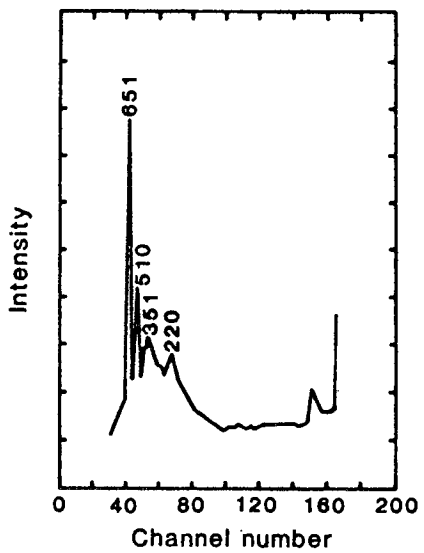

Fig. 4.15. Inelastic neutron scattering spectrum of tremolite (Naumann et al., 1966).

The hydroxyl group may also vibrate as a rigid group in the amphibole structure. The frequencies of these "librations" may be determined in Inelastic Neutron Scattering (INS) experiments, the strongest peaks in the spectra arising from the motion of H-bearing groups. Naumann et al. (1966) report a spectrum for tremolite (Fig. 4.15), which consists of two sharp peaks at 651 and 510 cm^{-1}, and two much broader and less intense peaks at 351 and 220 cm^{-1}, probably consisting of a number of small overlapping peaks.

Librations are easily recognisable in calculated atomic motions. For example Fig. 4.14(e) and (f) are, respectively, a projection down **c** of the atomic motions of the highest frequency Raman-active O-H libration and the same image rotated by a small amount about $a\sin\beta$. The motion of the OH group is clearly parallel to **c**. The value of the Mg-O-H bending force constant was adjusted to bring this band near 650 cm^{-1} (the highest INS frequency), and a frequency of 627 cm^{-1} was obtained for a force constant of 0.1 mdyn $Å^{-1}$. Several of the lower frequency modes involved O-H motions coupled with motions of other atoms. With this force constant they occurred at 492 and 476 cm^{-1}, 364 and 355 cm^{-1}, 326 and 311 cm^{-1}, and some frequencies between 250 cm^{-1} and the lowest band at 76 cm^{-1}. The number and frequency of peaks are in good agreement with the INS data.

As most vibrational frequencies involve the coupling of more than one type of motion, eg. Si-O stretching and O-Si-O bending, the fitting of calculated to observed spectra was far from easy. A trial-and-error approach had to be adopted, initially using various published and estimated force constants in the calculation, and adjusting them one at a time and repeating the calculation, until the closest agreement was obtained. With the force constants listed in Table 4.6, some derived from published values and others estimated, the Raman-active frequencies listed in Table 4.7 were obtained. These are not equal to the observed frequencies, but can be seen to fall into groups occupying approximately the same regions of the spectrum. The frequencies between 895 and 1101 cm^{-1} probably correspond to the observed frequencies between 932 and 1061 cm^{-1}. The atomic motions of some of these are relatively simple, eg. the 1101 cm^{-1} motion involves vibration of the O(5) and O(6) bridging oxygens approximately parallel to **c** (Fig. 4.14(b) and (c), rotated about **b**); the 1077 cm^{-1} band involves motion of bridging and non-bridging oxygens and silicon; and the 1069 cm^{-1} motion consists mainly of $Si\text{-}O_{non\text{-}bridging}$ stretching.

The calculated frequencies in the range 571-729 cm^{-1} may correspond to those around the strongest peak in the observed Raman spectrum at 675 cm^{-1}. In fact the 682 cm^{-1} frequency varies little with change of force constants, and may therefore be this strong band. Its vibration involves complex Si-O motions and a small component

Table 4.6. Force constants (mdyn Å^{-1}) used to calculate vibrational frequencies of tremolite in the program VIBRAT (Dowty, 1987).

Bonds		Angles	
O-H	7.5	OSiO	0.5*
Si-O_{nb}	5.5*	OMgO	0.1
Si-O_b	4.5*	MgOH	0.1
Mg-O	0.9	SiOSi	0.05*
Ca-O	0.4	MgOSi	0.05
		MgOMg	0.05
		CaOSi	0.03
		MgOCa	0.02
		OCaO	0.01

nb non bridging

b bridging

* from Furukawa et al. (1981); Si-O force constants increased by 0.5 mdyn Å^{-1}.

Table 4.7. Calculated Raman-active vibrational frequencies.

Frequency (cm^{-1})	Principal vibrating species	Frequency (cm^{-1})	Principal vibrating species
3678	O-H	355	MgOH
1101	Si-O_b, OSiO?	340	
1077	Si-O_{nb}, Si-O_b	326	
1069	Si-O_{nb}	311	MgOH
1007	Si-O_{nb}	281	
895	Si-O_{nb}, Si-O_b	267	
729	Si-O_b? OSiO	250	
682	SiOSi, OSiO	232	
627	MgOH	216	
571	OSiO, SiOSi	169	
492	MgO, MgOH	153	
476	MgOH, MgO	144	
410	OSiO, OMgO?	134	
388		112	
364		76	

of Mg-O vibrations. Although VIBRAT calculates band intensities, they are dependent on input values of bond polarisability, and very sensitive to small changes in these. Thus they do not assist in matching calculated and observed frequencies.

The atomic motions of the 729 cm^{-1} band are relatively simple, comprising vibration of the O(5) and O(6) bridging oxygens approximately parallel to asinβ (Fig. 4.14(d)).

Many of the vibrations below 492 cm^{-1} involve O-H librations, as already mentioned. They also involve more motion of Mg and Ca than those at higher frequencies, and thus involve the whole structure. The lowest frequency vibration, at 76 cm^{-1}, which may correspond to the observed band at 82 cm^{-1}, involves flexing of entire silicate double chains such that the A-site cavities between their backs are alternately contracted and expanded again (Fig. 4.14(g)). That such motions are possible has implications for the vibrational modes of wider chain biopyriboles, eg. triple chain silicates, for which lower frequency vibrations should be the result of triple chains vibrating as single groups.

After the calculation for tremolite, a trial calculation of the vibrational spectrum of richterite was made using the same atomic positions and force constants, but with the addition of an A-site position and a force constant for the Na-O bond. The resulting spectrum is almost identical to that for tremolite, and therefore it can be concluded that the substitution of Na has little effect on vibrational behaviour, the same observation as was made in the comparison of observed spectra.

4.5. SOLUTION CALORIMETRY

4.5.(i). Introduction

Most natural minerals, including almost all amphiboles, are solid solutions. Solid solutions occur because free energy (G_{ss}) is reduced with respect to mechanical mixtures of the end-member phases.

$$G_{ss} = \Sigma X_i \mu_i$$

where X_i is the mole fraction of component i in the solid solution phase,

μ_i is the chemical potential of component i in the solid solution phase, and

$$\mu_i = G^\circ_i + RT\ln a_i$$

where G°_i is the molar free energy of pure end-member component i,

and a_i is the activity of component i in the solid solution phase.

For the solid solution to be stable, the free energy of mixing, G_{mix}, must be less than zero.

$$\text{Now } G_{mix} = G_{ss} - G_{endmembers}$$
$$= \Sigma X_i\mu_i - \Sigma X_i G^\circ_i$$
$$= \Sigma X_i RT\ln a_i$$

If no enthalpy change is involved in forming the solid solution, ie. $\Delta H_{mix} = 0$, then $a_i = X_i$

In this ideal solution the reduction in free energy arises only from a configurational entropy of mixing term:

$$\Delta S_{mix} = -\Sigma X_i R\ln X_i.$$

The behaviour of most solid solutions is in fact non-ideal, eg. volume mismatches result in increased strain energies of mixing. An activity coefficient γ_i relates activity to composition:

$$a_i = X_i\gamma_i$$
$$\Rightarrow G_{mix} = \Sigma X_i RT\ln X_i + \Sigma X_i RT\ln\gamma_i$$

An accurate thermodynamic treatment of any solid solution then requires γ_i to be described as a function of X_i through some kind of mixing model.

The regular solution model, though fairly simplistic in its approach, describes many solid solutions well. Only nearest neighbour interaction energies contribute to the symmetrical excess energy, and

$$G^{ex}_{mix} = X_i(1-X_i)W_G$$
$$RT\ln\gamma_i = W_G(1-X_i)^2$$

where G^{ex}_{mix} is the excess free energy of mixing,

and W_G is the interaction, or Margules, parameter, and may be expanded thus:

$$W_G = W_H - TW_S + PW_V.$$

W_H, W_S and W_V then have to be obtained from experiment. W_S can be obtained from combined phase equilibrium experiments and calorimetry. However for binary mineral solid solutions it is likely only to be significant if substitution of ions of large size difference occurs on sites which are anomalously large for the smaller ion, or if temperature-dependent short range order is important (Newton et al., 1981). In this study W_S is assumed to be zero as no phase equilibrium data exist, and the relative insensitivity of vibrational frequencies to composition implies little change in vibrational entropies and hence minimal excess vibrational entropy (configurational entropy of mixing is not included in W_S).

W_V is obtained from cell volume data. In this study $\Delta V_{mix} = 0$ and hence $W_V = 0$.

W_H is obtained by solution calorimetry. The enthalpies of solution of a number of members of the solid solution are fitted to a quadratic equation which is subtracted from the 'ideal' ΔH_{mix} defined by the straight line connecting the enthalpy

of solution of the end-members to give H^{ex}_{mix}.

Other mixing models (eg. the subregular solution model with two interaction parameters) may describe the thermodynamic behaviour of a solid solution more accurately, but the quality of experimental data is often not sufficiently accurate to warrant the increased complexity involved.

4.5.(ii). Application to $Tr_{92}Mc_8$-Ri_{100} amphiboles

A Calvet-type twin microcalorimeter was used for the measurement of ΔH_{sol} of the synthetic $Tr_{92}Mc_8$-Ri_{100} amphiboles (+ quartz). A detailed description of the operation of this is given in Chapter 2.

No change in mass and x-ray diffraction pattern occurred after suspending a sample over the flux overnight, confirming the stability of each sample at calorimeter temperature. The samples were sieved to <100 mesh and any aggregates not passing through initially were further crushed until they did.

A 25-30 mg sample was used in each solution experiment. It dissolved readily, in 30-40 minutes, in an endothermic reaction with a large enthalpy of 40-50 μV.min. The flux was replaced after every three experiments, during each set of which no systematic trends in ΔH_{sol} measurements indicated that infinite dilution of the solution could be assumed throughout. 7-13 measurements for each of the synthetic amphiboles (+ quartz) were made (Table 4.8). It is immediately apparent that the mean ΔH_{sol} [Ri_{100}] is considerably lower than ΔH_{sol} of any of the other samples, and more than 50 kJ mol^{-1} less than ΔH_{sol} [Ri_{92}]. Also there is considerable scatter in the data for end-member Ri_{100} (the standard deviation of the mean of the first eight values obtained is 9.83, ie. larger than for any of the other samples), suggesting an anomaly. ΔH_{sol} [Ri_{100}] was therefore re-determined by drop-solution calorimetry, by S. Circone at Princeton University. She obtained the values of $\Delta H_{drop\text{-}sol}$ [Ri_{100}] and $\Delta H_{dry\text{-}drop}$ [Ri_{100}] given in Table 4.8, from which

$$\Delta H_{sol}\,[Ri_{100}] = \Delta H_{drop\text{-}sol} - \Delta H_{dry\text{-}drop}$$
$$= 441.073 \pm 9.835 \text{ kJ mol}^{-1}.$$

This value is almost 100 kJ mol^{-1} more than the previous value, and now implies a positive ΔH_{mix} (Fig. 4.16), more in keeping with thermochemical data on other mineral solid solutions (eg. Newton et al., 1981), as well as continuing the trend of increasing ΔH_{sol} along the join. Furthermore, though the standard deviation of the mean is still higher than for the other samples, the scatter of $\Delta H_{drop\text{-}sol}$ [Ri_{100}] values is actually significantly less than for the earlier ΔH_{sol} [Ri_{100}] measurements.

Table 4.8. Calorimetric data for synthetic $Tr_{92}Mc_8$-Ri_{100} amphiboles.

Sample	ΔH_{sol} (kJ mol^{-1})	Mean	$2s/\sqrt{N}$
$Tr_{92}Mc_8$	367.57, 359.59, 373.87, 366.20, 353.13, 368.39, 352.31 353.92, 353.13, 352.03, 376.42, 366.64, 360.57	361.83	4.76
Ri_{16}	367.36, 365.23, 368.96, 365.30, 369.11, 374.65, 365.71	368.05	2.53
Ri_{31}	384.98, 375.57, 375.28, 376.84, 383.74, 373.69, 375.05 385.51	378.83	3.53
Ri_{48}	382.36, 382.45, 383.41, 367.33, 370.10, 384.91, 391.77 401.85	383.02	7.79
Ri_{65}	399.73, 378.08, 395.84, 389.64, 385.39, 375.93, 388.85 375.87	386.17	6.40
Ri_{82}	398.81, 403.55, 393.35, 395.82, 388.54, 396.00, 410.17 392.12	397.29	4.86
Ri_{92}	388.58, 389.71, 400.90, 403.83, 402.84, 395.54, 409.07 404.51, 414.01	401.01	5.62
Ri_{100}	343.77, 335.33, 361.58, 357.35, 345.25, 329.39, 340.06 370.02, 335.62, 364.25, 355.65, 354.53, 348.43, 339.69	348.64	6.52
	$\Delta H_{drop-sol}$ (kJ mol^{-1})		
Ri_{92}	1026.76		
Ri_{100}	1037.48, 1048.84, 1023.61, 1026.56, 1024.08, 1043.56 1044.33, 1055.86	1038.04	8.62
	$\Delta H_{dry-drop}$ (kJ mol^{-1})		
Ri_{100}	593.15, 606.79, 595.76, 597.41, 589.77, 598.91	596.97	4.74

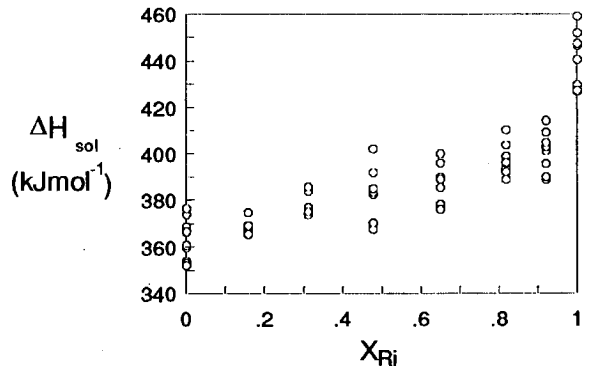

Fig. 4.16. Enthalpy of solution data of synthetic Tr_{92}-Mc_8 – Ri_{100} amphiboles (data for Ri_{100} from drop-solution measurements).

A decomposition or disordering process occurring during thermal equilibration in the calorimeter is suggested to explain the low ΔH_{sol} [Ri_{100}], for which the scatter arises from variable degrees of decomposition in each experiment. However an examination by XRD and EMPA, and comparison of mass, of a sample removed from the calorimeter after overnight thermal equilibration revealed no difference from the original sample. Therefore the change must involve a very subtle, and possibly non-quenchable, "intracrystalline" process. Annealing of synthetic minerals at elevated temperatures below their synthesis temperatures sometimes increases structural or cation order. However the decrease in ΔH_{sol} observed here implies destabilisation of the sample with time at 976 K, ie. disordering. The nature of this is unknown. Na/Ca disordering on M(4) can be ruled out on two counts. Firstly, the temperature is actually lower than during synthesis. Secondly, considering that previous characterisations of cation ordering in synthetic amphiboles (eg. Raudsepp et al., 1987) demonstrate that disorder on crystallographically distinct sites in synthetic amphiboles (eg. M(1,2,3)) is not uncommon, disorder on a unique crystallographic site may be expected to be commonplace, with the result that synthetic end-member richterite is likely to have a disordered Na/Ca distribution on M(4).

A more uncertain candidate for order-disorder in richterite involves positional disorder of Na on the A-site. This has been recognised in synthetic and natural amphiboles since Papike et al. (1969) observed highly anisotropic electron density at the A-site in an x-ray refinement of K-richterite, which they interpreted as positional disorder about the A(2/m) (**2b**) position, mainly confined to the mirror plane A(m) (**4i**), but with residual density along the diad A(2) (**4g**). Hawthorne & Grundy (1978) proposed that the nature of the disorder is composition-dependent, with Na ordering into A(2) and K into A(m), while Cameron et al. (1983) suggested that cation bond-

strength requirements are important, so that Na occupies the general position (**8j**) and K **4i**. More recently, Docka et al. (1987), using model energy calculations, suggested that in richterite and edenite the most probable position for the A-site cation is **8j**, though a significant number will occupy **2b**, **4g** and **4i** positions. Their predictions disagree with the observations of some of the previous studies. Single crystal x-ray studies would be useful to test these theories, but the synthetic amphiboles of this study are too fine-grained for this. It may be expected that splitting of the O-H stretching band in vibrational spectra should occur, depending on the position of the A-site cation interacting with the OH-group, but this band is already broadened through interaction of one A-site cation with two OH-groups (Fig. 4.13), so that further splitting may not be resolvable. It is also difficult to interpolate any of the end-member studies to the intermediate members of the $Tr_{92}Mc_8$-Ri_{100} solid solution. However it is interesting to note that the energy minimisations of Docka et al. (their Table 1) stabilise richterite relative to a structure in which all A-sites are in the **2b** position by ~100 kJ mol^{-1}, remarkably similar to the difference between the two values of ΔH_{sol} [Ri_{100}]. Such a coincidence is certainly not proof that the A-site positions in the calorimetrically heat-treated richterite have migrated from the minimum-energy positions, as there is no experimental evidence of this having occurred. Moreover, the structure refinements by Cameron et al. (1983) of synthetic fluor-richterite at a series of temperatures up to 800°C demonstrate only small variations with temperature of the split A-site positions, such that the 24°C **8j** position moves slightly closer to the mirror plane and further from the diad as the temperature is increasd to 800°C, lending no support to the hypothesis of anomalous behaviour at high temperatures. But hydroxy-richterite may not behave in the same way as fluor-richterite, or the possible presence of flux vapour may influence its behaviour in the calorimeter. Thus such anomalous behaviour cannot be ruled out, and the calculations do indicate that energy changes associated with A-site positional variations could be sufficiently large that they should not be ignored.

Not only may shifts in A-site positions be potential causes of changing enthalpy of solution of Ri_{100}, but also disordering of Na over more than one A-site position from an initially ordered distribution may be important. For example, the energetics of the movement of Na between A-site positions will be quite different from that of Ca/Na interdiffusion. Therefore while it appears unlikely that there should be any Ca/Na order in Ri_{100}, it may be that on synthesis, richterite contains an ordered distribution of Na over the A-site positions. For example occupancy of an A(2) site could alternate with occupancy of an A(m) site along **y**. Alternatively all of the A(2) sites could be occupied and none of the A(m) sites. On heating, disorder

could occur over all A-site positions. It appears unlikely that such a disordering on its own would be able to destabilise the sample by as much as 100 kJ mol^{-1}. But it may occur in conjunction with shifts in the position of the Na away from the minimum-energy position. In fact it will be seen later that a degree of order in synthetic richterite is inferred from the enthalpy of mixing data of the whole solid solution.

From Fig. 4.16 it is apparent that ΔH_{sol} [Ri_{92}] is further removed from the 'ideal' ΔH_{mix} line between the two end-members than is ΔH_{sol} [Ri_{82}]. Therefore it is possible that this sample is beginning to disorder in the same way as is Ri_{100}, though the considerably smaller scatter suggests a much lesser extent. A single measurement of $\Delta H_{drop\text{-}sol}$ [Ri_{92}] was made, which together with a value of $\Delta H_{dry\text{-}drop}$ = $\Delta H_{dry\text{-}drop}$ [Ri_{100}], yielded ΔH_{sol} [Ri_{92}] = 429.794 kJ mol^{-1}, ie. 29 kJ mol^{-1} higher than the previous determination. Though one measurement is not statistically significant (more measurements were precluded by lack of sample) an anomaly in the original measurements of ΔH_{sol} [Ri_{92}] is evident, and therefore these data are not included in the thermodynamic treatment. While a check on the data for the rest of the solid solution by drop-solution calorimetry would be worthwhile, the fact that any disordering effect in the richterite-rich members diminishes dramatically from Ri_{100} (94 kJ mol^{-1}) to Ri_{92} (29 kJ mol^{-1}) leads to the conclusion that by Ri_{82} it should have disappeared altogether, and therefore the calorimetric data for Ri_{82} and less richterite-rich compositions must be accepted. No explanation can be given for the anomalous behaviour occurring only in Ri_{100} and, to a lesser extent, in Ri_{92}.

4.5.(iii). Results

The individual ΔH_{sol} measurements of $Tr_{92}Mc_8$ to Ri_{82}, together with data-points for Ri_{100} obtained by subtracting the mean $\Delta H_{dry\text{-}drop}$ from each $\Delta H_{drop\text{-}sol}$ measurement, were fit by least squares to a quadratic equation:

$$\Delta H_{sol}\ (\text{kJ mol}^{-1}) = 364.21\ (\pm 3.86) + 67.56\ (\pm 8.12)X^2 \qquad \text{(Fig. 4.17)}$$

where $X = X_{Ri}$ and errors correspond to 2σ*. This curve is shown superimposed on the mean data in Fig. 4.18(a). ΔH_{mix} calculated relative to the 'ideal' straight line obtained from the above equation is shown in Fig. 4.18(b). The interaction parameter, W_H, is then

$$W_H = 67.56 \pm 8.12\ \text{kJ mol}^{-1}$$

---

* The regression program used gives standard errors on the coefficients of the fitted equation, assumed to equal 1σ.

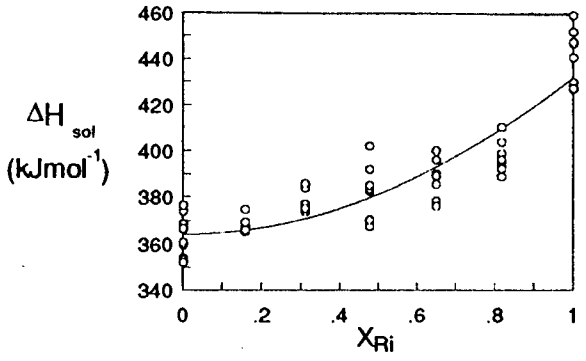

Fig. 4.17. Enthalpy of solution data (excluding Ri_{92} data) with least squares fitted quadratic equation: $\Delta H_{sol} = 364.21 + 67.56\ X^2$.

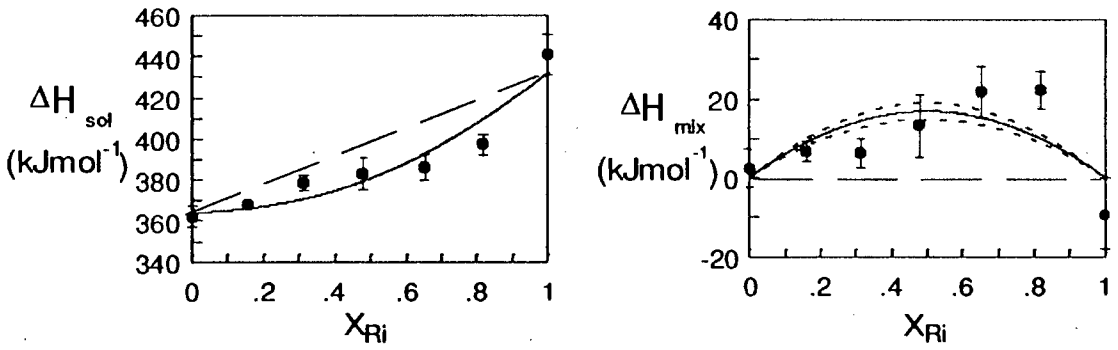

Fig. 4.18. (a) Mean enthalpy of solution data (excluding Ri_{92} data) with $2s/\sqrt{N}$ error bars, 'ideal' mixing line, and least squares fitted quadratic curve.

(b) Enthalpy of mixing curve, and limiting curves (dotted) defined by 95% confidence limits on W.

Although the quadratic curve does not pass through every error bracket, to fit a cubic equation (corresponding to a subregular solution model) would yield a region of negative ΔH_{mix} at the tremolite-rich end of the solid solution, ie. a convex upwards ΔH_{sol} curve, which the raw data as plotted in Fig. 4.16 do not suggest. Furthermore, the datum which deviates most from the regular solution curve is the Ri_{82} value, for which a small effect of disordering in the calorimeter is conceivable. Therefore bearing in mind this possible error and the already relatively large uncertainties on the ΔH_{sol} data, the regular solution model is considered to be adequate to describe this solid solution.

4.5.(iv). Discussion

In the following discussion, it will be assumed for simplicity that the ΔH_{mix} curve obtained for the $Tr_{92}Mc_8$-Ri_{100} solid solution may be directly applied to the Tr_{100}-Ri_{100} solid solution. This is probably justified when the errors on the ΔH_{sol} data are considered along with the fact that the range of substitution of Mg for Ca on M(4) is minor compared to the other two substitutions (Na for Ca on M(4) and Na for □ on A). Therefore Tr_{100} and $Tr_{92}Mc_8$ are interchangeable in the discussion.

Many mineral solid solutions can be approximated by the regular solution model, for which W_H is typically positive because mixing of cations of different sizes increases structural strain energies (eg. $CaMgSi_2O_6$-$Mg_2Si_2O_6$ clinopyroxenes: Newton et al., 1979; $CaMgSi_2O_6$-$NaAlSi_2O_6$ clinopyroxenes: Wood et al., 1980).

A large ΔH_{mix} in intermediate compositions, relative to end-member tremolite, might be expected to arise mainly from the strain involved in substituting Na into empty A-sites. Relative to richterite, it is likely still to be the A-site substitution which contributes the most strain energy, probably having more effect than the substitution of Ca for Na on M(4) into a structure already with an assumed random distribution of these cations.

At high temperatures the unfavourable enthalpy of mixing is usually offset by configurational entropy of mixing to give a stable solid solution with a negative ΔG_{mix}:

$$\begin{aligned} G_{mix} &= H_{mix} - TS_{mix} \\ &= WX(1-X) - TS_{mix} \\ &< 0 \\ \Rightarrow TS_{mix} &> WX(1-X) \end{aligned}$$

At the synthesis temperature used in this study (1123 K), all the characterisation evidence (EMPA, TEM, spectroscopy) indicates the entire solid solution to be stable. However the value of W (67.56 ± 8.12 kJ mol^{-1}) is high, eg. for the composition Ri_{50},

$$\begin{aligned} H_{mix} &= 0.5 \times 0.5 \times 67.56 \\ &= 16.89 \text{ kJ mol}^{-1} \\ \Rightarrow \text{at } T &= 1123\text{K}, \\ S_{mix} &\geq 16.89/1123 \\ &\geq 15.0 \text{ J K}^{-1} \text{ mol}^{-1}. \end{aligned}$$

Calculation of configurational entropies

Configurational entropy is calculated from the relationship:

$$S_{cfg} = -\sum_j n_j R(\Sigma X_i^j \ln X_i^j)$$

where n_j is the number of sites j on which mixing occurs,

and X_i^j is the mole fraction of species i on site j.

In the Tr_{100}-Ri_{100} solid solution there is potential for configurational entropy to arise from random mixing on two sites – M(4) and A – as well as from positional disorder of the A-site.

(1). Na-Ca mixing on M(4) (curves (1), Fig. 4.19)

The two M(4) sites per formula unit are occupied by two Ca in Tr_{100}, and one Na, one Ca in Ri_{100}. Assuming that Na-Ca mixing is random and independent of mixing on the A-site, its contribution to S_{cfg} of the solid solution is given by:

$$S_{cfg} = -2R[X_{Na}^{M(4)} \ln X_{Na}^{M(4)} + X_{Ca}^{M(4)} \ln X_{Ca}^{M(4)}]$$

where $X_{Na}^{M(4)} = 1 - X_{Ca}^{M(4)} = 0.5\, X_{Ri}$

eg. $S_{cfg}\,[Ri_{50}] = 9.35$ J K^{-1} mol^{-1}.

S_{mix} is calculated relative to the straight line between $S_{cfg}\,[Tr_{100}]$ and $S_{cfg}\,[Ri_{100}]$, and therefore $S_{mix}\,[Ri_{50}] = 3.59$ J K^{-1} mol^{-1}.

(2). Na-□ mixing on A (curves (2), Fig. 4.19)

If the single A-site, vacant in Tr_{100} and occupied by Na in Ri_{100}, is assumed for the moment not to be positionally disordered, then considered on its own, Na-□ mixing on the A-site contributes a configurational entropy to the solid solution of:

$$S_{cfg} = -R[X_{Na}^{A} \ln X_{Na}^{A} + X_{□}^{A} \ln X_{□}^{A}]$$

where $X_{Na}^{A} = 1 - X_{□}^{A} = X_{Ri}$

$S_{cfg} = 0$ for Tr_{100} and Ri_{100}, and therefore $S_{mix} = S_{cfg}$. Thus $S_{mix}\,[Ri_{50}] = S_{cfg}\,[Ri_{50}] = 5.76$ J K^{-1} mol^{-1}.

If both Na-Ca mixing on M(4) and Na-□ mixing on A occur entirely independently of each other, ie. the occupancy of an M(4) site is not influenced by that of the nearest A-site, and vice versa, then the configurational entropy of the solid solution will be the sum of the above two terms (curves 3, Fig. 4.19), eg. $S_{cfg}\,[Ri_{50}] = 15.11$ J K^{-1} mol^{-1} and $S_{mix}\,[Ri_{50}] = 9.35$ J K^{-1} mol^{-1}. However bearing in mind the charge imbalance imposed by mixing of cations (and vacancies) of different charges,

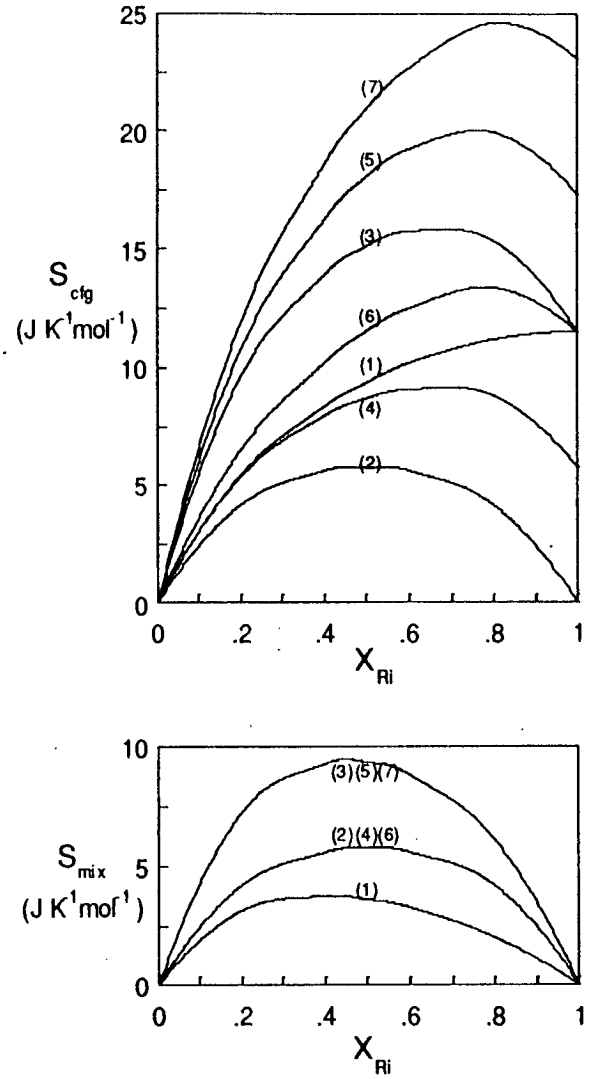

Fig. 4.19. Configurational entropy (S_{cfg}) and entropy of mixing (S_{mix}) of Tr_{100}-Ri_{100} amphiboles for various mixing models:

(1) Na-Ca mixing on M(4), with short range Na-□ order on A;

(2) Na-□ mixing on A, with short range Na-Ca order on M(4);

(3) Na-Ca mixing on M(4), plus Na-□ mixing on A;

(4) Na-□ mixing on an A-site split into two positions, with short range Na-Ca order on M(4);

(5) Na-□ mixing on an A-site split into two positions, plus Na-Ca mixing on M(4);

(6) Na-□ mixing on an A-site split into four positions, with short range Na Ca order on M(4);

(7) Na-□ mixing on an A-site split into four positions, plus Na-Ca mixing on M(4).

it is likely that one substitution follows the other, resulting in short range order. S_{cfg} would then reduce to S_{cfg} of the controlling substitution, whichever that is.

(3). Na-□ mixing on a positionally disordered A-site

A further complication and source of uncertainty in configurational entropy calculations comes from the possibility of positional disorder of Na on the A-site. As already mentioned, although modelled for Ri_{100} (Docka et al., 1987) and measured for F-Ri_{100} (Cameron et al., 1983), it has not been measured for the hydroxy end-member, and no data exist for intermediate compositions between tremolite. Furthermore, it is uncertain as to firstly, whether positional disorder arises only because of asymmetric charge distribution, ie. is entirely dependent on M(4) site occupancy, and secondly, whether the different A-site positions are energetically sufficiently dissimilar for random mixing on these sites to contribute any entropy at all. Nevertheless it is instructive to calculate S_{cfg} for a number of hypothetical mixing models involving A-site positional disorder. The simplest model comprises Na-□ mixing on an A-site split into A(2) (4g) and A(m) (4i) sites (following the model of Hawthorne and Grundy, 1972). These should perhaps themselves be considered as being split into two symmetrically related positions, though it may be that the A-site cation vibrates between the two. Na-Ca mixing on M(4) is neglected for the moment.

In end-member richterite, each formula unit can thus be considered to contain one A(2) and one A(m) site. Both sites within a single cavity cannot be occupied simultaneously, as then for every doubly-occupied A-site a vacant A-site would be expected, which would give rise to a second OH-stretching frequency in the vibrational spectra of richterite, at 3674 cm^{-1}. Although there is a peak at this frequency (Fig. 4.10(a) and 4.12(a)), the probability of its being as small as is observed if random mixing of Na and □ on two A-sites occurs is extremely low. Therefore the occupancy of one site (say A(m)) must be coupled to that of the other (A(2)), such that if A(2) is occupied by Na, A(m) must be vacant, and if A(2) is vacant, A(m) must be occupied by Na. The configurational entropy is then given by:

$$S_{cfg} = -R[X_{Na}^{A(2)} \ln X_{Na}^{A(2)} + X_{\square}^{A(2)} \ln X_{\square}^{A(2)}]$$
$$= -R[X_{Na}^{A(2)} \ln X_{Na}^{A(2)} + X_{Na}^{A(m)} \ln X_{Na}^{A(m)}]$$

S_{cfg} is a maximum (5.76) when $X_{Na}^{A(2)} = X_{Na}^{A(m)} = 0.5$.

This model differs from that of Westrich & Holloway (1981) for S_{cfg} [pargasite], as they did not exclude the possibility of more than one Na occupying the same A-site, and of Graham & Navrosky (1986) for S_{cfg} [edenite], as they did not

consider that the random distribution of Na on the two different site positions will contribute a configurational entropy.

In intermediate compositions along the solid solution the occupancy of A(m) is still coupled to that of A(2), but now there are three permitted combinations for the occupancy of a single A-site cavity:

	A(2)	A(m)
(1)	Na	□
(2)	□	Na
(3)	□	□

where $X_{Na}^{A(2)} + X_{Na}^{A(m)} = X_{Na}^{A} = X_{Ri}$

The calculation of S_{cfg} therefore reduces to a model involving mixing of three species on one site (each of the above combinations being considered as a single species).

$$\Rightarrow S_{cfg} = -R[\underbrace{X_{Na}^{A(2)} \ln X_{Na}^{A(2)}}_{(1)} + \underbrace{X_{Na}^{A(m)} \ln X_{Na}^{A(m)}}_{(2)} + \underbrace{(1 - X_{Ri})\ln(1 - X_{Ri})}_{(3)}]$$

$$\Rightarrow S_{cfg}^{max} = -R[0.5X_{Ri}\ln(0.5X_{Ri}) + 0.5X_{Ri}\ln(0.5X_{Ri}) + (1-X_{Ri})\ln(1-X_{Ri})]$$

eg. S_{cfg} [Ri_{50}] = 8.64 J K^{-1} mol^{-1}.

S_{mix} turns out to be the same as for simple Na-□ mixing on one A-site (curves (4), Fig. 4.19).

When Na-Ca mixing on M(4) is included (curves (5), Fig. 4.19), S_{cfg} increases with increasing richterite content and S_{mix} is again equivalent to the curve calculated assuming no positional disorder. Thus S_{cfg} [Ri_{50}] = 17.99 J K^{-1} mol^{-1} and S_{mix} [Ri_{50}] = 9.35 J K^{-1} mol^{-1}.

Similar curves may be calculated for a configurational entropy model involving positional disorder of Na over four A-site positions (eg. **2b**, **4g**, **4i**, **8j**) (curves (6) and (7), Fig. 4.19). These lead to increasingly higher configurational entropies at the richterite end of the solid solution, but again reduce to the S_{mix} curves calculated assuming no positional disorder.

An examination of Fig. 4.19 shows that none of the values of S_{mix} [Ri_{50}] approach 15.0 J K^{-1} mol^{-1} (the minimum for stabilisation at 1123 K implied by the calorimetric data) and the maximum values are almost 4 J K^{-1} mol^{-1} less than the minimum allowed by the 95% confidence limits on W (13.2 J K^{-1} mol^{-1}).

The M(4) site-only mixing configurational entropy model (curves (1), Fig. 4.19) clearly vastly underestimates S_{mix} as allowed by the calorimetric data. A model which does not include Na-Ca mixing on M(4) does not yield very much higher S_{mix} values, while the models involving both Na-Ca and Na-□ mixing still yield values of S_{mix} which are too low. However the latter models do yield S_{cfg} [Ri_{50}] > 15.0 J K^{-1}

mol^{-1}. If S_{cfg} [Ri_{100}] was substantially less than calculated in these models, S_{mix} for intermediate compositions would be higher. S_{cfg} [Ri_{100}] could be reduced in a number of ways. For example in Ri_{100} there could be random mixing on A but complete short range order of Na and Ca on M(4), which would drop the Ri_{100} end of S_{cfg} curve (3) down to zero. Or there could be random mixing on M(4) and complete A-site positional order, which would drop the end of S_{cfg} curve (7) down to S_{cfg} [Ri_{100}] of curve (3). Alternatively there could be partial order on both sites in Ri_{100}. Any of these models would confer sufficient S_{mix} on intermediate compositions provided they contained no short range order. Alternatively there could be considerable order on both M(4) and A in Ri_{100}, which decreased only slowly along the solid solution, such that Ri_{50} still contained some short range order.

A-site positional order in Ri_{100} was in fact one of the hypotheses suggested to explain the anomalous calorimetric behaviour of this sample (and to a lesser extent of the Ri_{92} sample), and therefore it is inferred that whatever the ordering scheme, short range A-site positional order in Ri_{100} plays an important part.

So far, the possibility of metastability of the solid solution at the synthesis temperature has not been considered. If this temperature was below the crest of the solvus, though for intermediate compositions two amphiboles should crystallise, smaller activation energy barriers might lead to crystallisation of a disordered phase, which would persist if the kinetics of Na/Ca and Na/□ interdiffusion were too slow (as discussed for other mineral systems in Putnis & McConnell, 1980). In this case the solid solution could be considered to represent the stable join at a higher temperature. The crest of the solvus calculated for S_{mix} curves (3), (5) and (7) is at 2440 K (2160°C), and so if there is no short range order in richteritic compositions this is the minimum temperature for stabilisation of the whole solid solution. However this temperature seems unrealistically high, and considering the run durations of the synthesis experiments (eg. a total of two weeks for Ri_{48}) and the sensitive analytical techniques used to characterise the samples (TEM, vibrational spectroscopy), both unmixing in a metastable composition and its detection (streaking of electron diffraction patterns, modulations of high resolution fringes, vibrational band-splitting) would be expected. Therefore the solid solution is accepted as being stable at 850°C and is concluded to be stabilised by configurational entropy arising from Na-Ca mixing on M(4) and Na-□ mixing on A, with some short range order in the richteritic compositions.

At temperatures not very much lower than 850°C, it is predicted that a solvus will appear and unmixing of the solid solution will occur. Lower temperature annealing experiments of intermediate compositions, followed by characterisation by

transmission electron microscopy and spectroscopy, would be instructive to test this prediction.

4.5.(v). Comparison with F-tremolite - F-edenite solid solution

ΔH_{mix} obtained for tremolite-richterite amphiboles contrasts strongly with that obtained by Graham & Navrotsky (1986) for the F-tremolite – F-edenite solid solution. Here the data have been fitted by a regular solution model with $W_{Tr} = W_{Ri} = 67.56 \pm 8.12$ kJ mol^{-1}. In contrast, a subregular solution model was fitted to the F-tremolite – F-edenite data to account for the asymmetry of calorimetric data along the solid solution, with $W_{Tr} = 74.73 \pm 48.87$ kJ mol^{-1} and $W_{Ed} = -70.12 \pm 47.49$ kJ mol^{-1}, the lower magnitude limits of which were used in the activity-composition calculations. It can be seen that though the magnitudes of W are all very similar, W_{Ed} is of opposite sign to W_{Tr} and W_{Ri}.

In this study, the magnitude of W_{Tr} is assumed to relate to the strain energy involved in substituting vacancies into the A-site. If such is the case for tremolite-edenite, then the question arises as to why W_{Ed} is not also positive. Graham & Navrotsky relate it to preferential ordering of Na into A(2) sites during the initial stages of substitution. This must be associated with either Al/Si order-disorder on tetrahedral sites, or be related to O(3) site occupancy, the two factors which distinguish the F-tremolite – F-edenite from the tremolite-richterite solid solution. The latter, though of importance as far as A-site positional order-disorder is concerned (Docka et al., 1987), is fixed in the entire solid solution, and if occupancy by F somehow favours that of Na on the A(2) position, this would be expected along the whole join, not just at the tremolite-rich end. The Al/Si distribution, on the other hand, must change along the solid solution as the ratio of Al to Si increases. Al is generally assumed to substitute into the larger T(1) site, of which there are four per formula unit. This must influence the environment of a neighbouring A-site in such a way that it is enthalpically very favourable for Na to enter that site. However when half of the A-sites are occupied, it no longer becomes enthalpically favourable, and according to Graham & Navrotsky Na now begins to enter A(m).

Clearly during the richterite substitution the M(4) site occupancy does not exert as much influence on the A-site environment, and though A-site Na may be positionally disordered and interact with M(4) Na, the substitution is never enthalpically favourable.

Though ΔH_{mix} for the two solid solutions contrasts strongly, the difference in ΔH_{sol} between end-members for the two series are similar. For tremolite-richterite amphiboles the difference is 60 kJ mol^{-1}, while for F-tremolite – F-edenite

amphiboles it is 84 kJ mol^{-1}. The substitution taking place in the latter solid solution is a stuffed silica substitution ($Si^{4+}_T \rightarrow Al^{3+}_T + 1/nN^{n+}_A$) which occurs in a variety of other mineral and glass systems (eg. framework silicates and aluminosilicate glasses). For an ion N of low ionic potential (z/r, where z = charge and r = ionic radius), eg. K or Na, enthalpy of solution data indicate stabilisation of the stuffed phase by an approximately constant amount for different N, eg. ~ -90 kJ mol^{-1} for N = K and ~ -80 kJ mol^{-1} for N = Na, implying that the energetics of the substitution are controlled by the immediate environment of the sites on which substitution is occurring (Navrotsky, 1985). The substitution $NaNaCa_{-1}$, defining the solid solution between tremolite and richterite, is also a stuffing substitution, with one Na being stuffed into the vacant A-site, while another substitutes for Ca on M(4) rather than Al substituting for Si on T(1). It is therefore not surprising that the stabilisation energy of the two substitutions are similar. In fact richterite is related to edenite by the plagioclase exchange $NaSiCa_{-1}Al_{-1}$, the enthalpy of which is only 2 kJ mol^{-1} in high structural state plagioclases (Newton et al., 1980), ie. small compared to the enthalpy of stuffing substitutions involving Na. This has implications for all A-site filling substitutions in amphiboles and sheet silicates, suggesting that A-site full compositions are stabilised with respect to A-site empty phases, though clearly the stability of intermediate compositions varies from one solid solution to another.

4.5.(vi). Implications for the stability of natural richteritic amphiboles

While tremolitic amphiboles are common in nature, compositions approaching end-member richterite are likely to be very rare because of the special bulk compositions required. However even relatively small components of richterite in solid solution with tremolite have seldom been reported. A notable exception is the amphibole found in kimberlite from Buell Park, Arizona (Aoki et al., 1972), a solid solution of 57 mol% tremolite, 31 mol% richterite and 12 mol% other components. This was interpreted to be a primary phase in the kimberlite magma, and therefore its stability field must extend to high temperatures and pressures. A high pressure stability is supported by experiments on the stability of synthetic $Tr_{50}Ri_{50}$ (Hariya & Terada, 1973), in which the amphibole was found to be stable up to 40 kbar at 700°C. Tremolite, however, breaks down at ~ 28 kbar at 700°C (see Chapter 5, Fig. 5.5) through the biopyribole reaction tremolite = 2 diopside + talc. But comparisons of volume of dissociation of various biopyribole reactions suggest that while amphiboles with vacant A-sites are destabilised by increasing pressure, those with filled A-sites are stabilised until the greater compressibility of the sheet silicates leads to amphibole destabilisation at even higher pressures (Thompson, 1981). Also, a simple biopyribole

reaction involving richterite cannot be written. Therefore richterite should be expected to be stable to higher pressures than tremolite.

The calorimetric data and derived activity-composition relationships of tremolite-richterite amphiboles are consistent with these observations and predictions. The Buell Park amphibole crystallised at a temperature higher than 850°C, the temperature of synthesis at which the entire tremolite-richterite solid solution is stable. However most tremolitic amphiboles crystallise at much lower temperatures, ie. well below the synthesis temperature, where a wide immiscibilty gap is inferred. The tremolite will not tolerate any richterite component in its structure. Given a sufficiently Na-rich and Al-poor bulk composition, a small amount of richterite might be expected to coexist with the predominating tremolite-rich amphiboles, but either such bulk compositions do not exist or proportions of richterite have been too small to be detected.

The negligible volume of mixing of synthetic tremolite-richterite amphiboles implies a minimal pressure effect on the stability of the solid solution. Together with the high stabilisation energy of the A-site filling substitution, this implies that the stability field of end-member richterite will be greater than that of both $Tr_{50}Ri_{50}$ and end-member tremolite.

4.6. CONCLUSIONS

1. At 2 kbar/850°C, bulk compositions along the Tr_{100}-Ri_{100} binary yield amphiboles displaced in composition towards the $Tr_{92}Mc_8$-Ri_{100} "pseudo"-binary. The composition of the tremolitic end-member is the same, within error, as that obtained by Jenkins (1987) in synthesis experiments on part of the join Tr_{100}-Ri_{100}.

2. At 2-6 kbar/850°C, bulk compositions along the join $Tr_{92}Mc_8$-Ri_{100} (plus quartz) react completely to amphibole plus quartz in a single run or in two runs with intermediate grinding.

3. EMPA and hydrogen extraction experiments demonstrate that the amphiboles are essentially on-composition, and contain no excess water.

4. Powder XRD unit cell refinements indicate that the cell parameters vary smoothly with composition, and ΔV_{mix} is approximately linear. Therefore there is no excess volume of mixing and hence no pressure effect on activity-composition relations.

5. All amphiboles are shown in HRTEM images to be structurally well-ordered, with from no CMFs in Ri_{100} to only a few in $Tr_{92}Mc_8$. Their use as analogues for well-ordered natural samples is therefore justified.

6. The A-site of Ri_{100} is essentially full, minor vacancies probably resulting from slight non-stoichiometry of the bulk composition. Its occupancy decreases systematically with decreasing richterite content of the solid solution.

7. No major changes in vibrational frequencies occur along the solid solution, implying minimal structural and vibrational entropy changes, and hence minimal excess entropy of mixing other than that arising from configurational entropy.

8. The vibrational spectrum of tremolite may be modelled with sufficient accuracy to predict to a close approximation the O-H stretching frequency, frequency of O-H librations, frequencies of motions involving predominantly Si-O bonds and angles and the lowest frequency vibrations involving oscillation of the whole structure.

9. The model spectrum of richterite is very similar to that of tremolite, consistent with the experimental observation of little change along the solid solution.

10. During thermal equilibration at 700°C in the solution calorimeter Ri_{100} undergoes an unexplainable disordering transformation, which does not occur in the rest of the solid solution. Its enthalpy of solution has therefore to be determined by drop-solution calorimetry.

11. Enthalpies of solution vary from 361.83 ± 4.76 kJ mol^{-1} for $Tr_{92}Mc_8$ to 441.07 ± 9.84 kJ mol^{-1} for Ri_{100}, and can be fit by a regular solution model with W_{II} = 67.56 ± 8.12 kJ mol^{-1}. Such a large deviation from ideality is due to a high strain energy associated with mixing of Na and vacancies on the A-site.

12. Simple configurational entropy models do not confer sufficient entropy of mixing on intermediate compositions to stabilise the solid solution at 1123 K, the temperature of synthesis at which it must be stable (as it is unlikely to be metastable). Hence significant short range order is inferred in Ri_{100}, involving Na-Ca mixing, Na-□ mixing and/or positional order-disorder of the A-site, which decreases along the solid solution.

13. Short range order and a full A-site in richterite contribute to its stability to high pressures and temperatures, while a wide immiscibility gap expected at low temperatures explains the scarcity of richterite components in natural amphibole solid solutions.

CHAPTER 5

DERIVATION OF THERMODYNAMIC DATA FOR END-MEMBER MINERALS FROM PHASE EQUILIBRIUM AND SOLUTION CALORIMETRIC EXPERIMENTS

CONTENTS

5.1. INTRODUCTION

Reliable thermodynamic data for mineral end-members and solid solutions are essential for the accurate determination of their stabilities and interpretation of geologic processes. The most important data, but also some of the hardest to obtain or estimate with any great certainty, are enthalpies of formation ($\Delta H°_f$) of end-members. Both of the techniques used in the studies of nyböitic and tremolite-richterite amphiboles (Chapters 3 and 4), namely phase equilibrium experiments and high-temperature oxide-melt solution calorimetry, can in fact be used to obtain $\Delta H°_f$ data. However attempts are often frustrated by synthesis problems and lack of necessary additional data such as heat capacities, which therefore limit the range of minerals for which $\Delta H°_f$ may be determined. For example the nyböite study was begun with the intention of extracting $\Delta H°_f$ from phase equilibrium experiments, but this was not feasible as no end-member composition could be synthesised. Neither could stoichiometric tremolite (Tr) be synthesised, and richterite is such a rare component of natural amphibole solid solutions that though its $\Delta H°_f$ could be approximated from the $\Delta H_{drop\text{-}sol}$ data collected for the tremolite-richterite study, the heat capacity (C_p) measurements necessary for extrapolation to other temperatures do not exist. This chapter therefore presents the results of phase equilibrium and calorimetric studies on some important and obtainable end-member compositions. The use of both methods in the determination of $\Delta H°_f$ and other thermodynamic data are compared and their relative merits considered. Although one of the phases investigated is a sheet silicate, its study has broader implications for experimental studies on amphiboles and other complex minerals.

5.1.(i). Tremolite

Tremolite ($Ca_2Mg_5Si_8O_{22}(OH)_2$) is the type end-member of the calciferous amphiboles. Though it cannot be synthesised on-composition, it does occasionally occur naturally in almost pure form. It is important in the greenschist and albite-epidote amphibolite facies metamorphism of a range of lithologies including basic igneous rocks and siliceous marbles, and therefore accurate thermodynamic data would be useful for constraining metamorphic conditions of these rocks. It has already been the object of much experimental investigation, in which heat capacity, entropy and enthalpy data have been derived. But when one considers the compositions of some of the samples used, the quality of most of these data must be doubted. For example Boyd (1959), in one of the earliest phase equilibrium studies of amphibole stability, attempted to bracket the high-temperature tremolite breakdown reaction:

Table 5.1. Mineral abbreviations used in Chapter 5.

Tr	Tremolite	$Ca_2Mg_5Si_8O_{22}(OH)_2$
Mc	Magnesio-cummingtonite	$Mg_7Si_8O_{22}(OH)_2$
Di	Diopside	$CaMgSi_2O_6$
En	Ortho-enstatite	$Mg_2Si_2O_6$
Qz	Quartz	SiO_2
Sp	Sodium phlogopite	$NaMg_3AlSi_3O_{10}(OH)_2$
Sp HI	Sodium phlogopite hydrate I	$NaMg_3AlSi_3O_{10}(OH)_2.2H_2O$
Sp HII	Sodium phlogopite hydrate II	$NaMg_3AlSi_3O_{10}(OH)_2.5H_2O$
F-Sp	Fluor-sodium phlogopite	$NaMg_3AlSi_3O_{10}F_2$
Bru	Brucite	$Mg(OH)_2$
Per	Periclase	MgO
Cen	Clino-enstatite	$Mg_2Si_2O_6$
Tc	Talc	$Mg_3Si_4O_{10}(OH)_2$
Phl	Phlogopite	$KMg_3AlSi_3O_{10}(OH)_2$
Fo	Forsterite	Mg_2SiO_4
Ab	Albite	$NaAlSi_3O_8$
Gl	Glaucophane	$Na_2Mg_3Al_2Si_8O_{22}(OH)_2$
Parg	Pargasite	$NaCa_2Mg_4Al_3Si_6O_{22}(OH)_2$

$$\underset{\text{Tr}}{Ca_2Mg_5Si_8O_{22}(OH)_2} = 2\,\underset{\text{Di}}{CaMgSi_2O_6} + 1.5\,\underset{\text{En}}{Mg_2Si_2O_6} + \underset{\beta\text{-Qz}}{SiO_2} + \underset{\text{vapour}}{H_2O} \qquad (1)$$

at water pressures up to 2 kbar. However 100% synthesis yields of "tremolite" were never obtained, the amphibole always coexisting with pyroxene + quartz and therefore inferred to be displaced from ideal tremolite composition towards magnesio-cummingtonite ($Mg_7Si_8O_{22}(OH)_2$). Thermodynamic data for tremolite based on this experimental determination must therefore be in error, but have in fact been incorporated into more than one thermodynamic dataset (see Table 5.2, from Graham et al., 1989). Table 5.2 also indicates the large number of experimental studies which have been undertaken on tremolite, and the diversity of amphibole compositions (for which ideally Ca/Mg = 0.4) leading to the variations in thermodynamic data listed in Table 5.3.

The only sample of tremolite with Ca/Mg = 0.4 was that used by Welch (1987), in phase equilibrium experiments in the pressure range 0.25-2.00 kbar on reaction (1). The sample was fully characterised by EMPA (Table 5.2), high resolution transmission electron microscopy and infrared and Raman spectroscopy.

Table 5.2. Starting materials used in previous phase equilibrium and calorimetric studies on tremolite. From Graham et al. (1989).

Authors	Reaction/technique	Tremolite composition	Ca/Mg	Data set	Notes
Weeks (1956)	Hf calorimetry	$(Ca_{1.73}Mn_{0.04})(Mg_{5.09}Fe_{0.01})(Si_{8.06}Al_{0.08})O_{22.10}(OH)_{2.06}$	0.34	R	Skarn tremolite, Balmat, New York
Boyd (1959)	Tr=Di+En+Qz+H_2O	Synthetic tremolite (Oxide mix, glass)	<0.40	H, HP	
Robie & Stout (1963)	Low-T calorimetry (Cp)	$(Na_{0.11}K_{0.02})(Ca_{1.90}Mg_{0.10})(Mg_{5.04}Fe_{0.01})(Si_{7.89}Al_{0.08})O_{22}(OH)_{1.94}$	0.37	see Table 3	Falls Village, New York
Metz (1967, 1976)	Tr+Dol = Fo+Cc+CO_2+H_2O	$Na_{0.11}(Ca_{1.73}Mg_{0.27})(Mg_{4.96}Al_{0.14})(Si_{7.93}Al_{0.07})O_{22}(OH)_{1.56}$	0.33	HP, BBG	Natural tremolite, Campo Lungo
Hoschek (1973)	Phl+Cc+Qz = Tr+Ksp+CO_2+H_2O	Synthetic tremolite (gel)	<0.40	HP, BBG	
Hewitt (1975)	Phl+Cc+Qz = Tr+Ksp+CO_2+H_2O	$Na_{0.08}(Ca_{1.94}Mg_{0.05})(Mg_{4.98}Fe_{0.02})(Si_{7.84}Al_{0.10})O_{22}(OH)_{2.14}F_{0.06}$	0.385	HP	Gouverneur, New York
		$(Na,K)_{0.55}(Ca_{1.73}Mg_{0.24})(Mg_{4.76}Fe_{0.05}Al_{0.18})(Si_{7.85}Al_{0.12})O_{22}(OH)_{0.8}F_{0.66}$	0.346		
		Synthetic tremolite (oxide mix)	<0.40		
Slaughther et al. (1975) and Eggert & Kerrick (1981)	Tr+Cc = Dol+Di+CO_2+H_2O Dol+Qz+H_2O = Tr+Cc+CO_2 Tc+Cc+Qz = Tr+CO_2+H_2O Dol+Tc+Qz= Tr+CO_2 Tr+Cc+Qz = Di+CO_2+H_2O	$Ca_{2.16}(Mg_{4.94}Fe_{0.03})(Si_{7.92}Al_{0.01})O_{22}(OH)_{2.0}F_{0.03}$	0.437	BBG, HP	St. Gotthard Switzerland
Jenkins (1983)	Tr+Fo=Di+En+H_2O	Synthetic tremolite (gel, glass, oxide mix)	<0.40	BBG, HP	≤90% synthetic amphibole yield
Yin & Greenwood (1983)	Tr=Di+En+Qz+H_2O	Synthetic tremolite (gel, oxide mix)	<0.40	BBG	
Skippen & McKinstry (1985)	Tr+Fo=Di+En+H_2O	$Ca_{2.16}(Mg_{4.94}Fe_{0.03})(Si_{7.92}Al_{0.01})O_{22}(OH)_{2.0}F_{0.03}$	0.437		St. Gotthard Switzerland
Kiseleva & Ogorodova (1984)	high-T lead borate calorimetry	$Ca_{2.01}Mg_{4.98}Si_{8.02}O_{22}(OH)_{1.95}$	0.404		Marble, Karelia
Welch (1987)	Tr=Di+En+Qz+H_2O	$Na_{0.01}Ca_{2.00}(Mg_{4.98}Fe_{0.02})Si_{8.00}O_{22}(OH)_{2.0}$	0.400		Locality unknown. HRTEM (structurally ordered) IR, Raman.

Abbreviations: Tr = tremolite, Di = diopside, En = enstatite, Qz = quartz, Dol = dolomite, Cc = calcite, Fo = forsterite, Phl = phlogopite, Ksp = K-feldspar, Tc = talc. R = Robie et al. (1978), H = Helgeson et al. (1978), HP = Holland & Powell (1985), BBG = Berman et al. (1985).

To further constrain the values of enthalpy and entropy obtained from those experiments, phase equilibrium experiments using the same sample and on the same reaction were conducted at higher pressure as part of this study.

Tables 5.2 and 5.3 show that there already exists one high-temperature calorimetric determination of $\Delta H°_f$ [Tr] (Kiseleva & Ogorodova, 1984), made using a sample of close-to-ideal composition. However this sample was not well characterised. Therefore as the specimen used for phase equilibrium experiments in this study was suitable for solution calorimetry (separation of a sufficient quantity of impurity-free sample from the hand specimen presenting no problem) another determination of $\Delta H°_f$ [Tr] (calorimetric) was made. This can then be used to further constrain the phase equilibrium thermodynamic data by providing an additional bracket at 0 K on the enthalpy of reaction (1). Ideally $\Delta H°_f$ [Tr] (calorimetric) and $\Delta H°_f$ [Tr] (phase equilibrium) should be equal. However comparisons between phase equilibrium values and enthalpies of formation calculated using pre-existing

Table 5.3. Compilation of enthalpy and entropy data for tremolite.

Source	$\Delta H°_f$ (kJ mol^{-1})	S° (kJ K^{-1}mol^{-1})
Robie et al (1978)	-12355.08 (17.32)$^+$	0.54890
Helgeson et al (1978)	-12319.70	0.54890
Berman et al (1985)	-12311.30	0.51115
Holland & Powell (in press)	-12302.50 (14.12)	0.55000
Kiseleva & Ogorodova (1984)	*(1) -12347.53 (10.88)	-
	*(2) -12336.63 (13.94)	-
This study	**(1) -12300.47 (14.81)	0.55160 (0.00977)
	**(2) -12323.89 (8.93)	-
	**(3) -12310.85 (11.84)	0.54238 (0.00055)

+ Uncertainties in brackets are twice the standard deviation.

* (1) value calculated by Kiseleva & Ogorodova,
(2) value calculated using internally-consistent data from THERMOCALC and the same heat-of-solution data for Di, Per, Bru, β-Qz as for the calculations on the natural tremolite.

** (1) phase-equilibrium,
(2) calorimetric,
(3) combined.

calorimetric data (eg. Kiseleva & Ogorodova, 1984) indicate that this is not always the case. The results of this study may help to clarify whether such discrepancies are always to be expected, ie. whether there is an as yet unrecognised source of systematic error in one or other method of determining $\Delta H°_f$. Previous studies (eg. Jenkins, 1987) have suggested that the tremolite dehydration reaction is divariant (Fig. 5.1), and so non-stoichiometry at the final breakdown reaction may be a reason for discrepancy. Alternatively there may be problems associated with calorimetric experiments on hydrous phases, eg. due to incomplete dissolution of H_2O in the flux. However recent studies (Kiseleva & Ogorodova, 1984; Clemens et al., 1987) suggest that the H_2O dissolves fully and ΔH_{sol} [H_2O] can therefore be measured.

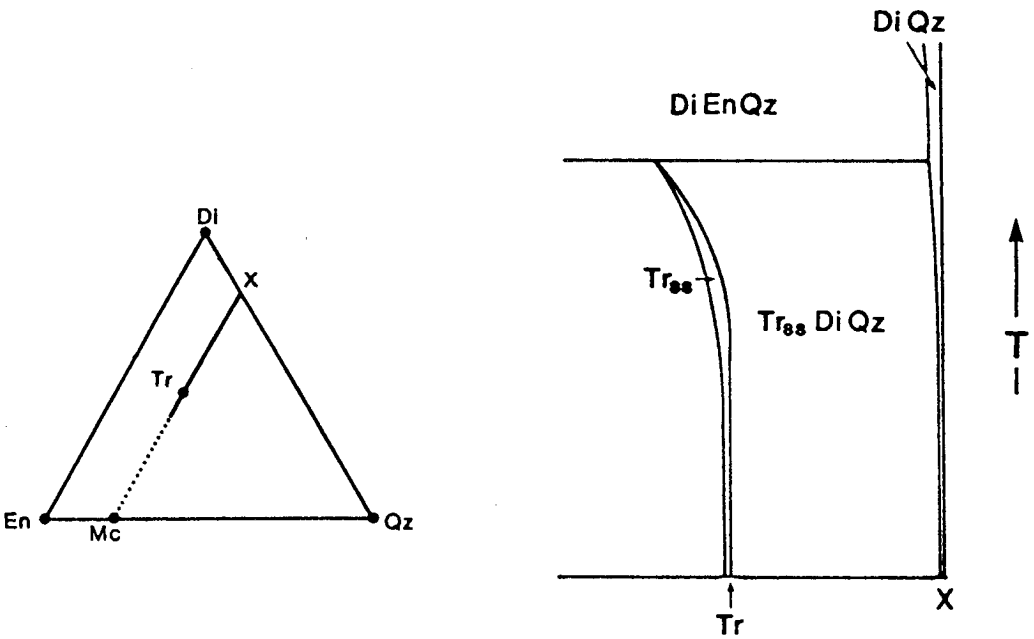

Fig. 5.1. Schematic T-X section along part of the join Mc-Tr-X showing the divariant dehydration of Tr to a Tr-Mc solid solution (Tr_{ss}) + Di + Qz + H_2O, followed by the univariant breakdown of Tr_{ss} to Di + En + Qz + H_2O. H_2O in excess. Abbreviations listed in Table 5.1. From Graham et al. (1989).

The main subject of this chapter is therefore the determination of new enthalpy and entropy data for tremolite from phase equilibrium and calorimetric data. This also forms the subject of a paper in preparation by Welch & Pawley.

Following on from this derivation of data for end-member tremolite, and assuming that in the phase equilibrium study the metastable dehydration reaction of end-member tremolite was in fact located, it would be interesting to compare this with the location of the stable amphibole dehydration reaction. It has already been inferred (Chapter 4) that the high-temperature limiting amphibole composition is $Tr_{92}Mc_8$ ($Ca_{1.84}Mg_{5.16}Si_8O_{22}(OH)_2$). Therefore as part of this study, some phase equilibrium experiments were undertaken on the reaction:

$$Ca_{1.84}Mg_{5.16}Si_8O_{22}(OH)_2 = 1.84\,CaMgSi_2O_6 + 1.66\,Mg_2Si_2O_6 + SiO_2 + H_2O \quad (2)$$
$$Tr_{92}Mc_8 \qquad\qquad Di \qquad\qquad En \qquad\qquad \beta\text{-Qz} \qquad vapour$$

using $Tr_{92}Mc_8$ synthesised for the tremolite-richterite study (Chapter 4).

5.1.(ii). Sodium phlogopite

In contrast to many synthetic amphiboles, sodium phlogopite (Sp, $NaMg_3AlSi_3O_{10}(OH)_2$) is a mineral suitable for calorimetric investigation as 100% on-composition synthesis has been demonstrated (Carman, 1974). Carman located the maximum stability of this sheet silicate at 815°C/250 bars and passing through invariant points at 874°C/530 bars and 960°C/1100 bars. The high-temperature, low-pressure stability field allowed for routine synthesis in cold-seal and internally-heated pressure vessels. However at lower temperatures (below T(°C) = 17.4 P(kbar) + 328) Sp was found to react rapidly with H_2O, forming sodium phlogopite hydrate I (Sp HI, $NaMg_3AlSi_3O_{10}(OH)_2.2H_2O$), and below T = 5.4 P + 82 formed Sp HII ($NaMg_3AlSi_3O_{10}(OH)_2.5H_2O$). Hydration was sufficiently rapid that Sp was not quenchable, but the reaction was also reversible, and at a relative humidity of ~30%, hydration and dehydration at 75 ± 5°C (between Sp and Sp HI) and 40 ± 3°C (between Sp HI and Sp HII) were easily achieved.

Sp is a rare component of natural sheet silicates, requiring unusual bulk compositions (high Na_2O, low SiO_2), but it has been reported in some geological environments, eg. metamorphosed evaporites (Kulke, 1976; Schreyer et al., 1980). It may also be associated with edenitic amphibole, though this too is rare in nature (Na et al., 1986). Its low-temperature hydration will allow for ready weathering to vermiculite or smectite, further decreasing its natural abundance. However estimated thermodynamic data for Sp are included in the revised internally consistent THERMOCALC dataset of Holland & Powell (in press), and a refinement of $\Delta H°_f$ by solution calorimetry, making use of their C_p data, forms part of this study.

Another application of solution calorimetry is in the determination of exchange enthalpies between mineral end-members. As discussed in Chapter 4, the enthalpy of stuffing substitutions (eg. $NaAlSi_{-1}$) is approximately constant between mineral systems, suggesting that measured enthalpies of end-member phases and substitutions may be summed to yield new data for end-members which cannot be synthesised. Amphiboles, though notoriously difficult to synthesise in hydrous form, are sometimes synthesisable as fluorine-analogues, which are readily amenable to calorimetric measurements (eg. F-tremolite and F-edenite, Graham & Navrotsky, 1986). Therefore an independent F-OH exchange enthalpy which could be added to ΔH_{sol} of F-analogues to obtain ΔH_{sol} of the OH-minerals, from which $\Delta H°_f$ could then

be derived, would be widely applicable. To determine whether the enthalpy of the exchange is independent of the mineral system in which it occurs, it must be compared for a number of F-/OH-mineral pairs. Therefore having already synthesised Sp, F-Sp was synthesised as part of this study, its ΔH_{sol} measured, and the derived $\Delta H_{F\text{-}OH}$ compared with pre-existing data.

5.2. EXPERIMENTAL PROCEDURE

5.2.(i). Synthesis of OH-sodium phlogopite (Sp) and F-sodium phlogopite (F-Sp)

Starting materials

Sp was synthesised from a gel prepared by the method of Biggar & O'Hara (1969). Its composition determined by x-ray fluorescence (XRF) analysis (Appendix Table A5.1) is close to ideal. Dried MgO was added to the gel to bring the Mg content up to 3 Mg per 11 O, and mixed by grinding under acetone for 15 minutes. The gel used for synthesis of F-Sp, a mixture of a gel of composition $NaMg_2AlSi_3O_{10}$ and powdered MgF_2, was prepared by M. Welch in a similar manner.

To check their compositions, samples of both gel mixtures (SP and F-SP) were fused at 1650°C for 10 minutes in air, and the glasses analysed by EMPA. Na and F were not analysed as it was impossible to prevent their loss under the electron beam, and so were assumed to be ideal. The mean EMP analyses, though outwith the ideal values by more than two standard deviations of the mean for some elements, actually differ by only ~1 wt% (Appendix Table A5.2) and so the samples are considered to be on-composition.

Experimental conditions

~440 mg of Sp was synthesised from 430 mg of OH-Sp gel + 15 wt% distilled H_2O in a sealed 45 mm long by 4 mm diameter Pt capsule, in a cold-seal pressure vessel at 2 kbar/800°C and for 285 hours. 360 mg of F-Sp was synthesised dry in an internally heated pressure vessel, at 4 kbar/1000°C for 94 hours. The operation and calibration of both types of pressure vessel are described in Chapter 2.

Run product examination

Run products were examined for impurities by optical microscopy, powder XRD and EMPA. Sp crystallised as equant pseudo-hexagonal grains, ~3-80 μm diameter. At room temperature it was present as Sp HII, distinguished from Sp by its lower refractive index – $\gamma = \beta = 1.52$ (cf. 1.57 in Sp) – and higher basal spacing – 15

Å (cf. 10 Å in Sp). A small proportion of Sp HI, with intermediate refractive index and basal spacing, was also present. Dehydration of the sample on a hot-plate (at ~150°C) for 5 minutes transformed the sample to Sp, following which rehydration was rapid. A minor trace of acicular amphibole was present in the sample of Sp, visible optically but not in the XRD pattern.

F-Sp also occurred in pseudo-hexagonal habit, crystals ~3-50 μm diameter, with $\gamma = \beta \approx 1.58$ and (001) diffraction maximum at 9.3°2θ. It too reversibly formed a low temperature hydrate, with $\gamma = \beta \approx 1.54$ and (001) diffraction maximum at 7.4°2θ. No intermediate hydrate was observed. The x-ray diffractogram revealed a trace component of sellaite (MgF_2) in the sample, which was visible optically as anhedral grains up to 15 μm across, with RI much lower than that of the sheet silicate. This could not be removed by grinding and re-running, or running under different P-T conditions. No other impurities were visible.

EMPA of both sheet silicates was subject to the same problems as with the glasses and the Sp-like sheet silicates encountered in the G-N and OH-NY experiments on glaucophane-nyböite amphiboles (Chapter 3), namely low counts on F and Na. Analysis of F was therefore not undertaken. However Na-loss only occurred from Sp, suggesting that interaction with F^- causes Na^+ ions to be more strongly bound within the structure. Table 5.4 shows the analyses obtained for the two sheet silicates. Those of Sp were collected by rastering the beam over the crystal using raster sizes of 15×15 μm^2. But despite this attempt to reduce Na-loss, Na counts were still extremely low, and the method used to estimate the true composition employed for the sheet silicate analyses in Chapter 3 was used here, namely to normalise Mg + Al + Si to 7, and make the charge up to 22 with Na. There is substantial scatter in the recalculated analyses, but the mean values for each element are within 2 standard deviations of the ideal values. An analysis of the trace of amphibole indicated a minor calcium content, presumably present in the starting material and unable to be accommodated in the Sp structure.

The F-Sp analyses display little variation, and the only element for which the ideal value falls outside the error bracket on the mean value is Si, by 0.01 cations per formula unit. The oxide totals, too, occupy a reasonable range. The ideal total is ~94.6 wt%, the microprobe correction procedure assuming an oxygen-equivalent of the non-analysed fluorine.

The observations that both the F-Sp bulk composition and the synthetic sheet silicate are essentially on-composition are incompatible with the presence of sellaite in the sample, particularly considering that no other impurity was detected, either by optical microscopy, XRD or EMPA. In order to correct the bulk enthalpy of solution

Table 5.4. Compositions of synthetic OH- and F- sodium phlogopite determined by electron microprobe analysis.

Sodium phlogopite

Cations				Cations corrected by summing Mg+Al+Si to 7			
Na	Mg	Al	Si	Na	Mg	Al	Si
0.22	3.07	1.06	3.11	0.96	2.96	1.03	3.01
0.16	3.09	1.06	3.12	0.98	2.98	1.02	3.00
0.24	3.11	1.03	3.11	1.01	3.01	1.00	3.00
0.79	3.06	1.04	2.99	1.07	3.02	1.02	2.95
0.26	3.28	1.02	3.03	1.24	3.13	0.98	2.90
0.61	3.15	1.03	3.00	1.14	3.07	1.01	2.93
			μ	1.06	3.03	1.01	2.96
			$2s/\sqrt{6}$	0.09	0.05	0.02	0.04

F-sodium phlogopite

Oxides					Cations			
Na_2O	MgO	Al_2O_3	SiO_2	Total	Na	Mg	Al	Si
7.9	29.3	12.2	44.7	94.0	1.04	2.96	0.97	3.03
7.8	29.4	12.3	43.9	93.5	1.03	3.00	0.99	3.01
7.9	29.1	12.3	44.2	93.5	1.04	2.96	0.99	3.01
7.9	29.4	12.5	44.7	94.4	1.03	2.96	0.99	3.02
7.5	29.2	12.4	44.6	93.6	0.98	2.96	0.99	3.03
7.7	29.6	12.1	44.5	93.9	1.02	2.99	0.97	3.02
7.8	29.9	12.5	44.5	94.6	1.02	3.00	0.99	3.00
				μ	1.02	2.98	0.99	3.02
				$2s/\sqrt{7}$	0.02	0.02	0.01	0.01

Microprobe operating conditions:

accelerating voltage:	15 kV	
beam current:	7 nA	
beam raster area:	15×15 μm^2 (Sp)	
	5×5 μm^2 (F-Sp)	
count time on peaks:	10 secs (Sp)	
	15 secs Na	} (F-Sp)
	20 secs Mg,Al,Si	} (F-Sp)

to that of F-Sp only, an estimation of the proportion of sellaite was necessary, and was therefore attempted by point counting on EMP images. The two phases could not be distinguished in back-scattered electron images, but sellaite appeared very bright in an x-ray image of Mg and was invisible in an image of Si, allowing it to be distinguished from F-Sp and its proportion duly estimated.

Only one grain of sellaite was in fact detected in a careful examination of an area containing 200-300 grains, and so it is inferred that the sample contains ~1 ± 1 wt% sellaite (1 wt% ≡ 0.7 vol%).

5.2.(ii). Phase equilibrium experiments

Starting materials

The same starting materials as used in the experimental study by Welch (1987) of the high-temperature tremolite breakdown reaction

$$Tr = 2\,Di + 1.5\,En + \beta\text{-}Qz + H_2O \qquad (1)$$

were used in the high pressure runs conducted here. The tremolite comes from a siliceous marble (tremolite - calcite - quartz) from the Edinburgh University collection, of locality unknown. Fibres were hand-picked from the specimen, crushed and cleaned of adhering calcite by covering the sample with 30 vol% ethanoic acid, leaving overnight to dissolve the calcite and washing with distilled water. A complete chemical analysis of the amphibole is given in Table 5.5. Pure acid-washed natural α-quartz, and diopside and enstatite synthesised hydrothermally from gel at 4 kbar/ 900°C and 2 kbar/900°C respectively, were used. For each run, twin charges of 85 wt% reactants/15 wt% products and 15 wt% reactants/85 wt% products were used.

The mixtures of reactants and products used in the experiments on the reaction

$$Tr_{92}Mc_8 = 1.84\,Di + 1.66\,En + \beta\text{-}Qz + H_2O \qquad (2)$$

were essentially the same as the above, with $Tr_{92}Mc_8$ in place of Tr_{100}. The $Tr_{92}Mc_8$, synthesised at 6 kbar/850°C in the presence of excess H_2O and SiO_2, was from the well-characterised batch used in the tremolite-richterite study (Chapter 4).

Apparatus and technique

Experiments at 2 kbar and up to 860°C were conducted in cold-seal pressure vessels, whilst those at higher pressure and/or temperature were conducted in internally heated pressure vessels.

15 mg of the two reactant/product mixtures were run side by side in the pressure vessel, in sealed 3 mm diameter Pt capsules with 10 wt% distilled water.

Table 5.5. (a) Wet-chemical analysis of the natural tremolite used in this study. From Welch & Pawley (in prep.).

	wt%	atoms PFU
Na_2O	0.02	0.01
K_2O	n.d.	-
CaO	13.45	2.00
MgO	24.09	4.98
MnO	n.d.	-
FeO*	0.14	0.02
Al_2O_3	n.d.	-
TiO_2	n.d.	-
SiO_2	57.71	8.00
F	0.03	-
H_2O	2.18	2.02
	97.61	17.03

n.d. not detectable.
* All Fe as FeO.

(b) Electron microprobe analysis (20nA, 20kV) of the natural tremolite (average of 12 analyses). From Welch & Pawley (in prep.).

	wt%	$\frac{2s}{\sqrt{12}}$ (sample)	2σ (analytical precision)	atoms PFU
Na_2O	0.01	0.01	0.00	-
K_2O	0.01	0.00	0.00	-
CaO	13.51	0.21	0.13	1.98
MgO	24.74	0.48	0.18	5.05
MnO	0.03	0.00	0.00	-
FeO*	0.25	0.10	0.02	0.04
Al_2O_3	0.04	0.01	0.00	-
TiO_2	0.02	0.01	0.00	-
SiO_2	58.21	0.71	0.71	7.97
	96.82			15.04

Runs were brought up to pressure at room temperature, and then heated isobarically to run-temperature. As discussed in Chapter 2, pressures and temperatures in the cold-seal vessels are believed to be accurate to ± 30 bars and 3° respectively, and in the internally heated pressure vessels to ± 20 bars and 5° respectively.

Isobaric quenching terminated the runs, after which capsule integrity was checked by weighing before and after puncturing with a needle and oven-drying.

Reaction direction was determined from intensity changes in x-ray diffractograms. The unambiguous amphibole and pyroxene peaks listed in Table 5.6 were measured for several x-ray scans of the starting material and the run product, and the ratios of amphibole to pyroxene peak heights averaged for each sample. As changes in ratio were either insignificant or at least 50%, reaction direction was easily determined.

Table 5.6. X-ray peaks used to determine reaction direction in the phase equilibrium experiments on Tr = Di + En + β-Qz + H_2O and $Tr_{92}Mc_8$ = Di + En + β-Qz + H_2O.

In runs on starting mixes comprising 85 wt% reactants, 15 wt% products.

Phase	$2\theta_{CuK\alpha}$	hkl
"Tr"	26.33	131
"Tr"	27.24	240
"Tr"	30.38	221
"Tr"	31.94	330
Di	29.78	$22\bar{1}$
En	31.14	160

In runs on starting mixes comprising 15 wt% reactants, 85 wt% products.

Phase	$2\theta_{CuK\alpha}$	hkl
"Tr"	10.52	110
"Tr"	27.24	240
"Tr"	28.62	310
Di	27.62	220
En	28.16	240
En	31.14	160

5.2.(iii). High temperature solution calorimetry

Apparatus and technique

A Calvet-type twin microcalorimeter, as described by Navrotsky (1977) and in Chapter 2, was used for the measurement of the enthalpy of solution of the natural tremolite and synthetic Sp and F-Sp. It was first calibrated by dropping pieces of Pt from room temperature into the molten $2PbO.B_2O_3$ flux at 976 K and using their known heat contents to obtain a conversion factor for μV.min to joules. Then before undertaking any solution experiments, the stability of the phase at 976 K was checked by suspending a sample over the flux in the calorimeter for ~20 hours, removing it and comparing its x-ray diffraction pattern with that of an untreated sample. As no difference was observed between the two patterns for any phase, it was assumed that during the experiments the sample would not decompose before being dissolved in the flux.

For each solution experiment a 25-30 mg sample, accurately weighed into a perforated Pt sample holder and suspended above 30 g of flux in the calorimeter, was thermally equilibrated overnight before dissolving in the flux by dipping the sample holder in several times. The sample dissolved readily, in 30-40 minutes, in an endothermic reaction with a large enthalpy (50-60 μV.min). The heat effect associated with the stirring procedure was measured separately after each solution experiment. It was typically around 0.5-1.0 μV.min, and the sample enthalpy of solution was corrected for this.

5.3. EXPERIMENTAL RESULTS

5.3.(i). Phase equilibrium experiments

The five reversed experimental brackets on reaction (1) obtained by Welch (1987) were at 250 ± 30 bars (723-760 ± 5°C), 625 ± 30 bars (765-785 ± 5°C), 1025 ± 30 bars (802-831 ± 5°C), 1500 ± 30 bars (828-852 ± 5°C) and 2000 ± 30 bars (842-855 ± 5°C). Run conditions and results of the phase equilibrium experiments obtained in this study, defining a further bracket on reaction (1) at 8020-8060 ± 20 bars (911 ± 5°C) – 7960-7990 ± 20 bars (931 ± 5°C), and two brackets on reaction (2) at 2000 ± 30 bars (841-859 ± 5°C) and 8020-8060 ± 20 bars (911 ± 5°C) – 7960-7990 ± 20 bars (931 ± 5°C), are listed in Table 5.7. Unequivocal reaction occurred in four runs, reaction in the other three runs occurring in only one sample of each pair, this being the charge already containing 85% reaction products, suggesting that there were

Table 5.7. Run conditions and results of phase equilibrium experiments on $Tr = Di + En + \beta\text{-}Qz + H_2O$ and $Tr_{92}Mc_8 = Di + En + \beta\text{-}Qz + H_2O$.

Run	Starting mixes	P (kbar)	T (°C)	Duration (h)	Reaction direction* 85% reactants	85% products
T100.1+	Tr_{100}/Di,En,Qz	8.02-8.06	911	120	H	H
T100.2+	Tr_{100}/Di,En,Qz	7.96-7.99	931	143	D	D
T92.1+	Tr_{92}/Di,En,Qz	2.00	841	336	H	NR
T92.2+	Tr_{92}/Di,En,Qz	2.00	859	96	NR	D
T92.3	Tr_{92}/Di,En,Qz	2.05	877	130	D	D
T92.4+	Tr_{92}/Di,En,Qz	8.02-8.06	911	120	H	NR
T92.5+	Tr_{92}/Di,En,Qz	7.96-7.99	931	143	D	D

* H = hydration, ie. growth of amphibole;
D = dehydration;
NR = no reaction.
\+ Run defining a bracket limit.

Table 5.8. Enthalpy of solution of natural tremolite and synthetic OH- and F-sodium phlogopite.

Sample	ΔH_{sol} (kJmol^{-1})	Mean	$2s/\sqrt{N}$
Tr	374.02, 369.63, 388.05, 372.52, 368.44, 368.97, 385.40 371.56, 378.87, 380.17	375.76	4.43
Sp	217.67, 239.72, 231.24, 227.39, 231.78, 242.95, 221.12 225.45, 234.84, 229.88	230.20	4.94
F-Sp	249.03, 240.27, 240.60, 232.13, 245.51, 230.94, 237.78 244.41	240.08	7.43

F-Sp data corrected for presence of 1±1 wt% MgF_2 in sample (ΔH_{sol} [MgF_2] = 81.840 kJmol^{-1}, Westrich & Navrotsky, 1981). $2s/\sqrt{N}$ includes uncertainty in estimation of MgF_2 content.

insufficient seeds in the other charges to act as nucleation sites for the reaction products.

The limiting brackets obtained in this study on the two reactions are shown in Fig. 5.2, together with the brackets on reaction (1) determined by Welch (1987). They have been expanded by ± 5° and ± 20-30 bars to include the uncertainties in temperature and pressure.

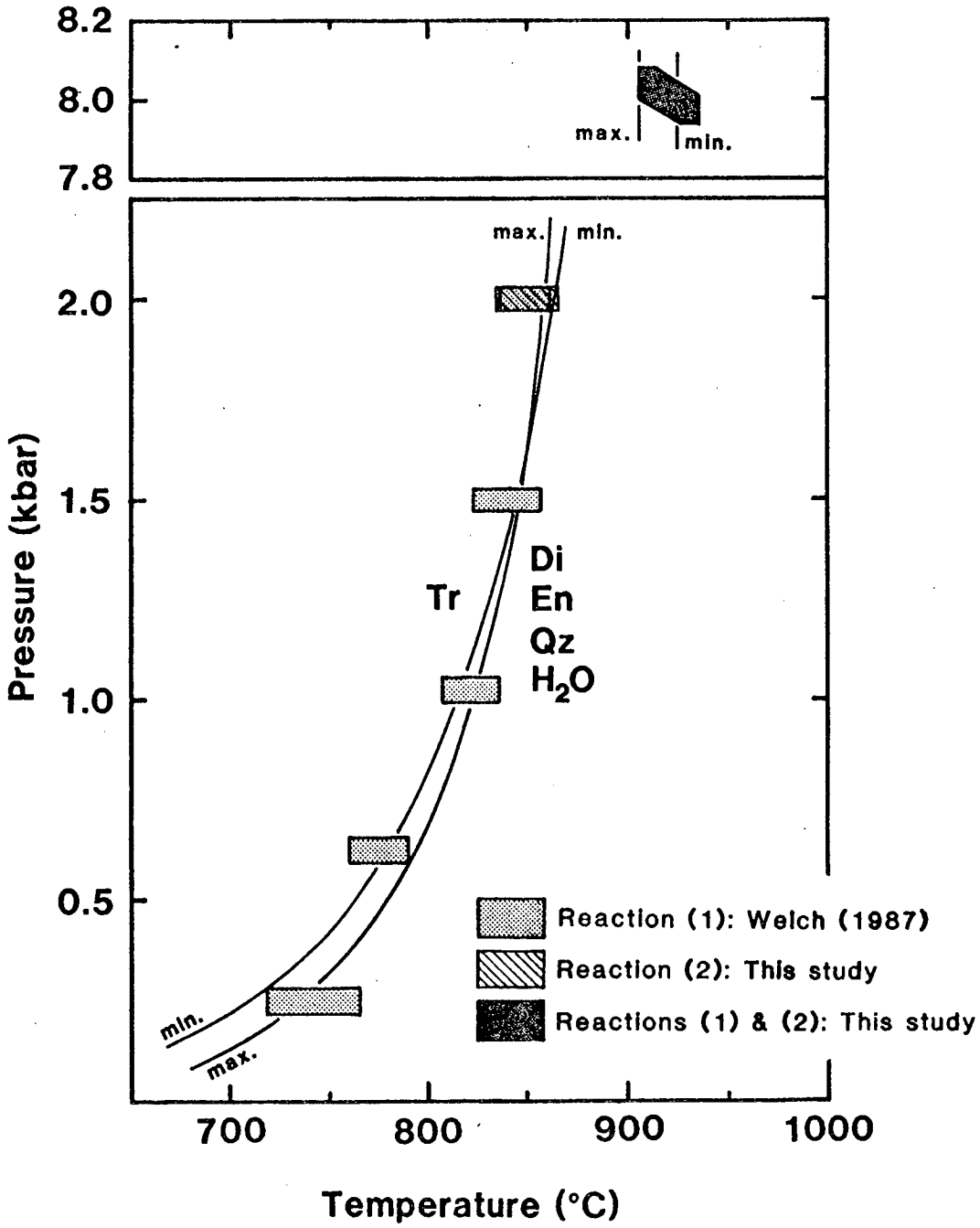

Fig. 5.2. P-T diagram showing the experimental brackets on reactions (1) Tr = Di + En + β-Qz + H_2O and (2) $Tr_{92}Mc_8$ = Di + En + β-Qz + H_2O, and the calculated position of reaction (1) using the maximum and minimum phase equilibrium values of $\Delta H°_r$ and $\Delta S°_r$. Modified from Welch & Pawley (in prep.).

5.3.(ii). Calorimetry

Ten measurements of ΔH_{sol} [Tr] and ΔH_{sol} [Sp], and 8 of ΔH_{sol} [F-Sp], were obtained (Table 5.8). Mean values and errors corresponding to two standard deviations of the mean are:

ΔH_{sol} [Tr] = 375.76 ± 4.43 kJ mol^{-1}

ΔH_{sol} [Sp] = 230.23 ± 4.94 kJ mol^{-1}

ΔH_{sol} [F-Sp] = 240.08 ± 7.43 kJ mol^{-1}

5.4. DERIVATION OF ENTHALPY OF FORMATION OF TREMOLITE

5.4.(i). From phase equilibrium experiments

At each point along a reaction curve, equilibrium exists between reactants and products and the following relation holds:

$$\Delta G_{P,T} = 0$$

$$= \Delta G^\circ_{P,T} + RT\ln K_s$$

$$= \Delta H^\circ_{1,T} - T\Delta S^\circ_{1,T} + \int_1^P \Delta V_s dP + \int_1^P V_{H_2O} dP + RT\ln K_s$$

$$= \Delta H^\circ_{1,298} + \int_{298}^T \Delta C_P dT - T\Delta S^\circ_{1,298} - T\int_{298}^T \Delta C_P/T dT + \int_1^P \Delta V_s dP + \int_1^P V_{H_2O} dP + RT\ln K_s$$

Now $\int_1^P \Delta V_s dP = P\Delta V_{1,298}\{1 + \Delta\alpha(T-298) - \Delta\beta P/2\}$

where α and β are the coefficients of thermal expansion and isobaric compressibility respectively,

and $\int_1^P V_{H_2O} dP = RT\ln f_{H_2O}$

where f_{H_2O} is the water fugacity.

Thus the above equation may be expanded and rearranged in the linear form:

$$T\Delta S^\circ_{1,298} - \Delta H^\circ_{1,298} = \int_{298}^T \Delta C_P dT - T\int_{298}^T \Delta C_P/T dT + P\Delta V_{1,298}\{1 + \Delta\alpha(T-298) - \Delta\beta P/2\}$$

$$+ RT\ln f_{H_2O} + RT\ln K_s$$

$$= G'$$

A plot of G' against T then gives a straight line with slope $\Delta S^\circ_{1,298}$ and intercept $-\Delta H^\circ_{1,298}$.

G' was calculated for the P-T limits of each bracket on reaction (1), using C_P, V*, α and β data from the internally consistent THERMOCALC dataset (Holland & Powell, in press). For $P \geq 2.03$ kbar water fugacities were taken from THERMOCALC, and are correct to within $\pm$ 0.2 kJ. For lower pressures the THERMOCALC polynomial fit to the data of Burnham et al. (1969) becomes poorer ($\pm$ 0.3 - 2.0 kJ) and therefore values were interpolated directly from the Burnham et al. data. EMPA (by M. Welch) of phases from the lowest- and highest- temperature runs indicated that all had close to end-member compositions, and therefore in all calculations $K_s = 1$.

The G'-T data define six parallelograms (Fig. 5.3), and lines of maximum and minimum slope passing through all of these allow calculation of maximum limits of error on $\Delta H°_{reaction}$ and $\Delta S°_{reaction}$ ($\Delta H°_r$ and $\Delta S°_r$):

$\Delta H°_{r,max} = 126.19$, $\Delta H°_{r,min} = 104.25$ $\Rightarrow \Delta H°_r = 115.22 \pm 10.97$ kJ

$\Delta S°_{r,max} = 0.17466$, $\Delta S°_{r,min} = 0.15512$ $\Rightarrow \Delta S°_r = 0.16489 \pm 0.00977$ kJ K^{-1}

In the calculation of uncertainties on $\Delta H°_f$ [Tr] and S° [Tr] which follows, the standard deviations, σ, of $\Delta H°_r$ and $\Delta S°_r$ are required. No rigorous statistical method exists for obtaining σ from "mini-max" errors in such a multi-dimensional problem as this (though it is possible in a one-dimensional situation, eg. Demarest & Haselton, 1981). The mini-max errors may be considered to be 100% confidence limits, but in fact uncertainties on C_p, V, α and β are not included in the calculation of G' limits, and therefore there is a finite chance of values of G' lying outside these limits. Thus while it is realised that this is a gross simplification and leads to an overestimate of σ, because some estimate is necessary, the "mini-max" errors are assumed in the calculation of uncertainties on $\Delta H°_f$ [Tr] and S° [Tr] to equal 2σ, ie. are taken to be 95.5% confidence limits.

The maximum and minimum values, used to calculate the limiting positions of reaction (1), constrain the mean/median curve to within $\pm$ 10° in the pressure range studied (Fig. 5.2).

Enthalpy and entropy data for tremolite calculated from $\Delta H°_r$ and $\Delta S°_r$ are:

$\Delta H°_f$ [Tr] $= \Sigma\Delta H°_f$ [2Di, 1.5En, β-Qz, H_2O]$^+$ - $\Delta H°_r$

$= -12300.47$ kJ mol^{-1}

S° [Tr] $= \Sigma S°$ [2Di, 1.5En, β-Qz, H_2O]$^+$ - $\Delta S°_r$

$= 0.55160$ kJ K^{-1} mol^{-1}

---

* V [Tr] was determined by x-ray cell refinement (= 272.45 cm^3 mol^{-1}).

+ Data taken from THERMOCALC.

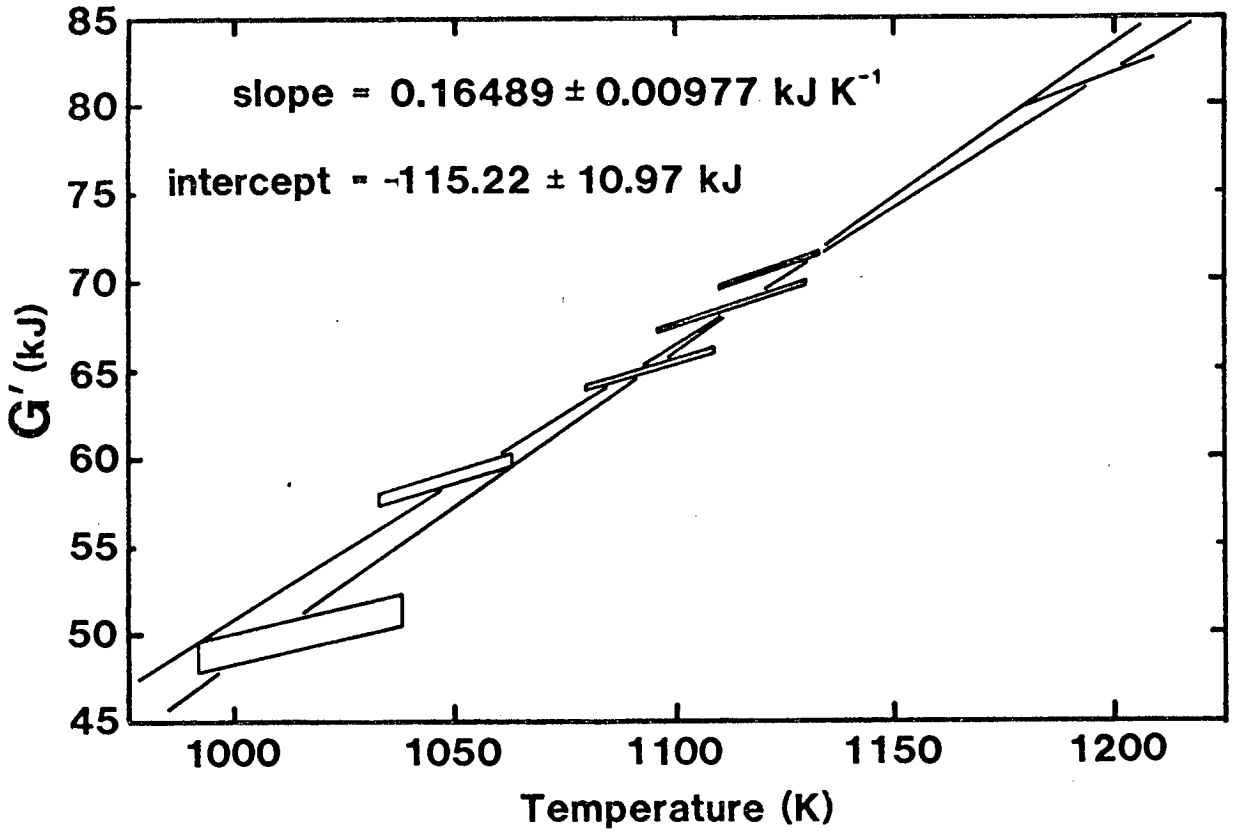

Fig. 5.3. Plot of G' vs. T for the six experimental brackets on the reaction Tr = Di + En + β-Qz + H_2O, showing lines of maximum and minimum slope passing through all six brackets. From Welch & Pawley (in prep.).

Calculation of uncertainties

If $Y = f\{A,B,C,...\}$ is a function relating an unknown Y to measured A,B,C,... with standard deviations $\sigma_A,\sigma_B,\sigma_C,...$, then the standard deviation of Y, σ_Y, is given by the well-known formula

$$\sigma_Y^2 = \left(\frac{\delta Y}{\delta A}\right)^2 . \sigma_A^2 + \left(\frac{\delta Y}{\delta B}\right)^2 . \sigma_B^2 + \left(\frac{\delta Y}{\delta C}\right)^2 . \sigma_C^2$$

eg. for $Y = A + 2B - C$

$$\frac{\delta Y}{\delta A} = 1, \quad \frac{\delta Y}{\delta B} = 2, \quad \frac{\delta Y}{\delta C} = -1$$

$$\Rightarrow \quad \sigma_Y^2 = \sigma_A^2 + 2\,\sigma_B^2 + \sigma_C^2$$

Taking the above-calculated mini-max error on $\Delta H°_r$ to be $2\,\sigma_{\Delta H°_r}$, and using $\sigma_{\Delta H°_f}$ data from THERMOCALC, the above equation gives

$$\sigma_{\Delta H°_f[Tr]} = 7.41$$

$$\Rightarrow \underline{\Delta H°_f\,[Tr] = -12300.47 \pm 14.81\ kJ\ mol^{-1}}$$

There are no errors on entropies in THERMOCALC, therefore $2\,\sigma_{\Delta S°[Tr]}$ was taken to be $2\,\sigma_{\Delta S°_r}$.

$$\Rightarrow \underline{S°\,[Tr] = 0.55160 \pm 0.00977\ kJ\ K^{-1}\ mol^{-1}}$$

5.4.(ii). From calorimetry

To obtain $\Delta H°_f$ from the elements, a reaction is first written in which tremolite is formed from simple oxides or minerals for which ΔH_{sol}, $\Delta H°_f$ and heat content ($\int \Delta C_p dT$) data are available. The reaction used here was:

$$2\,CaMgSi_2O_6 + 2\,MgO + 4\,SiO_2 + Mg(OH)_2 = Ca_2Mg_5Si_8O_{22}(OH)_2$$

diopside periclase β-quartz brucite tremolite

The calorimetric cycle is shown in Fig. 5.4. Now $\Delta H°_f\,[Tr] = \Sigma\ \Delta H°_f\,[reactants] + \Sigma \int \Delta C_p dT\ [reactants] + \Sigma\ \Delta H°_{sol}\ [reactants] - \int \Delta C_p dT\ [Tr] - \Delta H°_{sol}\ [Tr]$, and therefore using enthalpy of formation and heat content data from Table 5.9 and enthalpy of solution data from Table 5.10, this cycle gives

$$\Delta H°_f\,[Tr] = -12323.89\ kJ\ mol^{-1}.$$

It will be noted (Table 5.10) that ΔH_{sol} [Bru] was measured by drop-solution calorimetry rather than ordinary solution calorimetry as used for the other measurements. This was because brucite decomposes near 700°C. But as $\Delta H_{drop\text{-}sol}$ is equal to ΔH_{sol} <u>plus</u> the heat content, the only additional heat content of brucite required in the calculation (-0.20 kJ mol^{-1}, Table 5.9) was that associated with the difference in temperature of 2° between the room temperature from which the drops into the calorimeter were made and standard room temperature (298 K).

Fig. 5.4. Calorimetric cycle used to obtain ΔH°_f [tremolite].

Each arrow represents an enthalpy change: those in the first row enthalpies of formation at 298 K from the elements; those in the second row the heats absorbed by the phases as their temperature is raised to 976 K; and those in the third row the enthalpies of solution of the phases. The sum of the enthalpy changes of the reactants (2 Di + 2 Per + 4 β-Qz + Bru) associated with the transformation from elements at 298 K to solution in the calorimeter at 976 K (= $\Sigma\Delta H$ [reactants]) equals that of tremolite ($\Delta H^\circ_f + \int \Delta C_p dT + \Delta H_{sol}$). Therefore ΔH°_f [Tr] = $\Sigma\Delta H$ [reactants] - $\int \Delta C_p dT$ [Tr] - ΔH_{sol} [Tr]. The reason for the different position of Bru in the cycle is discussed in the text.

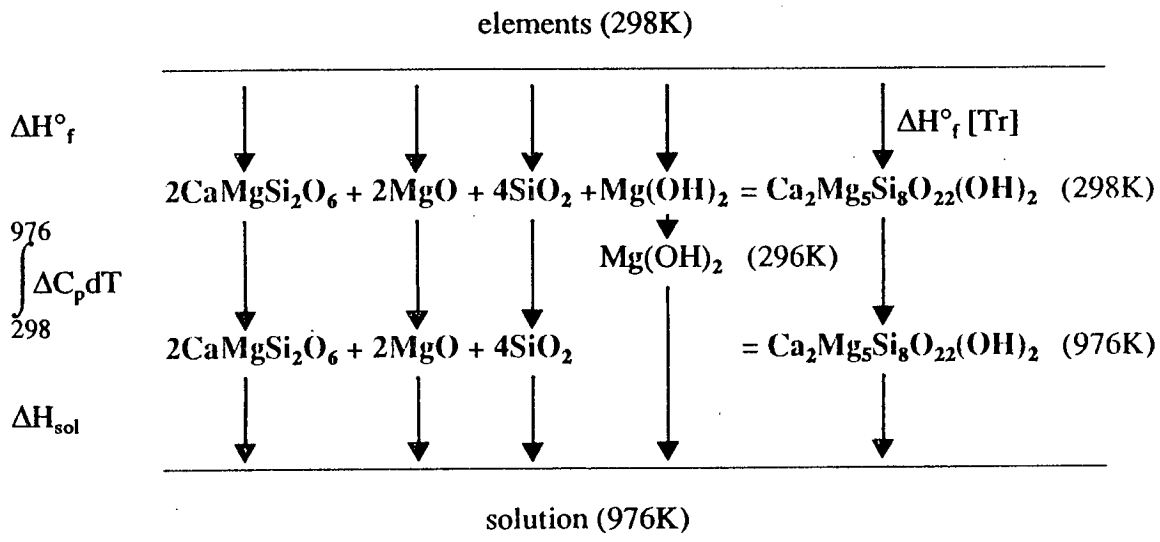

Table 5.9. Thermodynamic data used in the calculation of ΔH°_f [tremolite] and ΔH°_f [sodium phlogopite].

Phase	ΔH°_f (kJmol^{-1})	σ_H	$\int_{298}^{976} \Delta C_p dT$ (kJmol^{-1})
Tremolite	-	-	599.33
Diopside	-3200.15	1.90	150.35
Periclase	-601.41	0.48	31.76
β-Quartz	-909.07	0.74	41.80
Brucite	-925.50	0.57	-0.20 ($= \int_{298}^{296} \Delta C_p dT$)
Ortho-enstatite	-3089.38	2.08	149.75
Water	-241.81	0.03	25.04
Sodium phlogopite	-	-	318.88
Albite	-3937.86	3.72	187.15

All data from THERMOCALC (Holland & Powell, in press).

Table 5.10. Enthalpies of solution in $2PbO.B_2O_3$ used in the calculation of $\Delta H°_f$ [tremolite] and $\Delta H°_f$ [sodium phlogopite].

Phase	ΔH_{sol}(kJmol^{-1})	Source
Tremolite $Ca_2Mg_5Si_8O_{22}(OH)_2$	375.764 ± 4.431 (976K, 10)[a]	This study
Diopside $CaMgSi_2O_6$	85.413 ± 2.946 (985K, 4)	Weill et al. (1980)
Periclase MgO	4.875 ± 0.601 (986K, 14)	Davies & Navrotsky (1981)
β-Quartz SiO_2	-3.510 ± 0.147 (975K, 6)	Akaogi & Navrotsky (1984)
Brucite $Mg(OH)_2$	118.356 ± 1.093[b] (978K, 10)	Circone, unpubl. data
Ortho-enstatite $Mg_2Si_2O_6$	72.677 ± 0.477 (973K, 9)	Ito & Navrotsky (1985)
Water H_2O	-25.799 ± 1.942[c]	-
Sodium phlogopite $NaMg_3AlSi_3O_{10}(OH)_2$	230.203 ± 4.937 (976K, 10)	This study
Albite $NaAlSi_3O_8$	81.652 ± 1.649 (985K, 9)	Navrotsky et al. (1980)

[a] Temperature of $2PbO.B_2O_3$ flux, number of calorimetric measurements.

[b] $(H°_{978} - H°_{296}) + \Delta H_{sol,978}$; obtained by drop-solution calorimetry (= $\Delta H_{drop\text{-}sol}$).

[c] Calculated from ΔH_{sol} [Bru] and ΔH_{sol} [Per] data given here, and ΔH_f and $\int \Delta C_p dT$ data from Table 5.9.

Uncertainties are twice the standard deviation of the mean.

The 2σ error on $\Delta H°_f$ [Tr] was calculated using $\sigma_{\Delta H°_f}$ data from THERMOCALC, together with standard deviations of the means of the calorimetric measurements, $\sigma/\sqrt{N}$, ie. half the errors quoted in Table 5.10. Errors on heat capacity data, though not included in THERMOCALC, are assumed to be small compared to the uncertainties in the calorimetric and $\Delta H°_f$ data. Therefore they have been omitted from the calculation.

$\Rightarrow \sigma^2_{\Delta H°_f}$[Tr] = $\Sigma\, \sigma^2_{\Delta H°_f}$[2Di, Per, β-Qz, Bru] + $\Sigma\, \sigma^2/N_{\Delta H_{sol}}$[2Di, Per, β-Qz, Bru, Tr]

= 10:196 + 9.748

= 19.944

$\Rightarrow \sigma_{\Delta H°_f}$[Tr] = 4.466

$\Rightarrow 2\sigma_{\Delta H°_f}$[Tr] = 8.932

$\Rightarrow$ $\underline{\Delta H°_f \text{ [Tr]} = -12323.89 \pm 8.93 \text{ kJ mol}^{-1}}$

This is not the only calorimetric cycle from which $\Delta H°_f$ [Tr] may be derived. For example the reactions

2 $CaMgSi_2O_6$	+	1.5 $Mg_2Si_2O_6$	+	SiO_2	+	H_2O	=	$Ca_2Mg_5Si_8O_{22}(OH)_2$
diopside		enstatite		β-quartz		steam		tremolite
2 $CaMgSi_2O_6$	+	3 MgO	+	4 SiO_2	+	H_2O	=	$Ca_2Mg_5Si_8O_{22}(OH)_2$
diopside		periclase		β-quartz		steam		tremolite

could be used, but would involve larger uncertainties. For example thermodynamic data for enstatite is dependent on that for periclase and quartz, and ΔH_{sol} [H_2O] is derived from ΔH_{sol} [Br] (Clemens et al., 1987; Circone, unpubl. data).

Another point concerning uncertainties is that it has been assumed that enthalpies of solution at 985 K (Di) and 986 K (Per) are the same as they would be at 976 K (the measurements on Tr). All calorimetric data used should strictly have been obtained under the same conditions, but given that the uncertainties in ΔH_{sol} are already relatively large (3% and 12% for ΔH_{sol} [Di] and ΔH_{sol} [Per] respectively), any extra uncertainty associated with temperature variations should be insignificant.

5.4.(iii). From combined phase equilibrium and calorimetric data

The enthalpy of reaction (1) at 1 bar/298 K may be calculated from enthalpy of solution data. The 2σ error limits are then a bracket on the intercept of the G'-T line:

$$\text{intercept} = -\Delta H°_{r,298} = \Delta H°_{r,976} + \int_{298}^{976} \Delta C_p dT$$

$\Delta H°_{r,976}$ (= 2 ΔH_{sol} [Di] + 1.5 ΔH_{sol} [En] + ΔH_{sol} [β-Qz] + ΔH_{sol} [H_2O] - ΔH_{sol} [Tr]) was calculated using calorimetric data from Table 5.10, and $\int \Delta C_p dT$ using data from Table 5.9. These data were used in preference to the calorimetric $\Delta H°_f$ [Tr] and

$\Delta H°_f$ data for Di, En, β-Qz, H_2O from THERMOCALC as the calculation then involves fewer steps and hence smaller errors.

The value of $\Delta H°_{r,298}$ thus obtained is

$$\Delta H°_r = -130.41 \pm 6.42 \text{ kJ mol}^{-1}$$

This bracket on the intercept overlaps the phase equilibrium limits (104.25-126.19) at 123.99-126.19 kJ, ie. affecting only the line of minimum slope. Combined (phase equilibrium and calorimetric) data are then

$$\Delta H°_r = -125.09 \pm 1.10 \text{ kJ mol}^{-1}$$

and $$\Delta S°_r = 0.17365 \pm 0.00102 \text{ kJ K}^{-1} \text{ mol}^{-1}$$

$$\Rightarrow \Delta H°_f[Tr] = -12310.34 \pm 11.88 \text{ kJ mol}^{-1}$$

and $$S°[Tr] = 0.54238 \pm 0.00102 \text{ kJ K}^{-1} \text{ mol}^{-1}$$

5.4.(iv). Discussion

$\Delta H°_f$ [Tr] derived from phase equilibrium experiments (-12300.47 ± 14.81 kJ mol^{-1}) and calorimetry (-12323.93 ± 8.93 kJ mol^{-1}) differ by ~23 kJ mol^{-1}, with the result that they can only just be reconciled within error. There is no obvious explanation for the discrepancy, as though there do exist a number of potential sources of error, discussed below, removal of any of these would increase the difference rather than decrease it:

(a). The fibrous nature of the tremolite sample may introduce a high surface-energy term (eg. ~5-10 kJ) into ΔH_{sol} [Tr]. This energy, released as the sample dissolved, would lower ΔH_{sol} and hence increase the derived $\Delta H°_f$ [Tr]. The true value would therefore be more negative than the calculated value and further displaced from $\Delta H°_f$ [Tr] (phase equilibrium).

(b). Calorimetric measurements on the hydrous phases (Tr, Bru) may be incorrect due to only partial dissolution of H_2O in the calorimeter flux. However this is more likely to be a problem for brucite than for tremolite, as it has a higher H_2O content and is also less stable at high temperature. Therefore if only a proportion of the water content of brucite dissolves, the magnitude of ΔH_{sol} [H_2O] will be too low. As ΔH_{sol} [H_2O] is negative (-24.85 kJ mol^{-1}), the true ΔH_{sol} [H_2O] will be more negative, the true ΔH_{sol} [Bru] smaller, and the true $\Delta H°_f$ [Tr] also smaller, ie. more negative and further displaced from $\Delta H°_f$ [Tr] (phase equilibrium).

(c). It has already been observed that solid solution towards magnesio-cummingtonite might be expected in tremolite with increasing temperature until it breaks down (Fig. 5.1). A reduction in the activity of tremolite would cause reaction (1) to occur at a higher temperature than the end-member reaction. Between the two, substitution of Mg for Ca might occur in initially pure tremolite, but replacement rims would be too

thin to analyse by EMPA, as would overgrowths on seeds in hydration reactions, and so the compositional change would go undetected. The calculated $\Delta H°_f$ [Tr] would then be too low, and of course an increase would increase the difference from the calorimetric value.

Clearly the difference between the two values of $\Delta H°_f$ [Tr] cannot be explained. In an effort to determine whether there are always systematic differences between $\Delta H°_f$ (calorimetric) and $\Delta H°_f$ (phase equilibrium), these two data are compared for the only hydrous minerals for which both are available (tremolite, phlogopite (Phl), talc (Tc) and sodium phlogopite (Sp)) in Table 5.11. The data for Tr and calorimetric data for Sp are from this study; the phase equilibrium data of Phl, Tc and Sp are from THERMOCALC; and the calorimetric values for Phl and Tc were calculated using ΔH_{sol} [Phl] = 281.88 ± 3.10 kJ mol^{-1} from Clemens et al. (1987) and their calorimetric cycle, with C_P and H_f data from THERMOCALC, and ΔH_{sol} [Tc] = 207.57 ± 3.89 kJ mol^{-1} from Kiseleva & Ogorodova (1984) and an appropriate calorimetric cycle and C_P and H_f data from THERMOCALC. Using a single dataset for all calculations ensured maximum consistency between data.

Table 5.11. A comparison of enthalpy of formation data obtained from phase equilibrium and calorimetric studies.

Phase	ΔH_f (kJ mol^{-1}) (phase equilibrium)	ΔH_f (kJ mol^{-1}) (calorimetric)
Tremolite $Ca_2Mg_5Si_8O_{22}(OH)_2$	-12300.47 ± 14.81	-12323.89 ± 8.93
Phlogopite $KMg_3AlSi_3O_{10}(OH)_2$	-6211.76 ± 7.02	-6215.15 ± 6.57
Talc $Mg_3Si_4O_{10}(OH)_2$	-5895.23 ± 7.40	-5923.57 ± 10.50
Sodium phlogopite $NaMg_3AlSi_3O_{10}(OH)_2$	-6173.64 ± 8.92	-6155.04 ± 9.35

The sign of the difference between the two values of $\Delta H°_f$ [Sp] is the reverse of that for Tr, but here the discrepancy can be explained by poor quality of the phase equilibrium data, as discussed in a later section (5.5.(i)). The phase equilibrium data for Tr, Phl and Tc are much better constrained, and therefore the difference for Sp may be anomalous. For all three of Tr, Phl and Tc, $\Delta H°_f$ (calorimetric) is less than (ie. more negative than) $\Delta H°_f$ (phase equilibrium), though the difference for phlogopite is small. Thus there may be some systematic source of error in one or other method of deriving $\Delta H°_f$. More phase equilibrium and calorimetric studies on hydrous minerals using the same sample are warranted to attempt to shed further light on the problem, but meanwhile one of the methods of derivation of $\Delta H°_f$ must be accepted for use in phase diagram calculations. Table 5.3 compares the $\Delta H°_f$ [Tr] data of this study with pre-existing estimates. Robie et al. (1978) calculated $\Delta H°_f$ [Tr] by integrating the C_P data of Robie & Stout (1963). Their value is clearly anomalous. Of the other three thermodynamic datasets, that of Holland & Powell (THERMOCALC) is the most extensive and with error estimates is more useful than those of Helgeson et al. (1976) and Berman et al. (1985). Their values of $\Delta H°_f$ [Tr] and S° [Tr] are in remarkably close agreement with the phase equilibrium-derived values of this study, which are preferred over the calorimetric data for calculation of tremolite stability relations.

The validity of calculating $\Delta H°_f$ [Tr] and S° [Tr] from combined phase equilibrium and calorimetric data is doubted here, as the large temperature difference between the calorimetric bracket (at 0 K) and the phase equilibrium brackets (at ~1000-1200 K) leads to a bias of the best-fit straight line towards the former bracket. Therefore a systematic error in this will be over-represented in the new value.

5.4.(v). Calculation of tremolite stability relations using the new data

The new values of $\Delta H°_f$ [Tr] and S° [Tr] have been used to calculate the positions of three important tremolite-bearing equilibria: (1) Tr = Di + En + Qz + H_2O, (3) Tr = Di + Tc, (4) Tr + Fo = Di + En + H_2O (Fig. 5.5).

The minimum-maximum envelope shown for reaction (1) is for the phase equilibrium data. The maximum curve is the same as the combined phase equilibrium and calorimetric maximum curve, but the envelope for the combined data is considerably smaller than for the phase equilibrium data alone.

Reaction (3) is a biopyribole reaction, involving H_2O-conserving disproportionation of amphibole to pyroxene plus sheet silicate. $\Delta H°_r$ and $\Delta S°_r$ are very small (4.94 ± 17.41 kJ and -0.0054 ± 0.0097 kJ K^{-1} respectively, calculated using the phase equilibrium data) but their errors are large. Therefore the P-T position of the

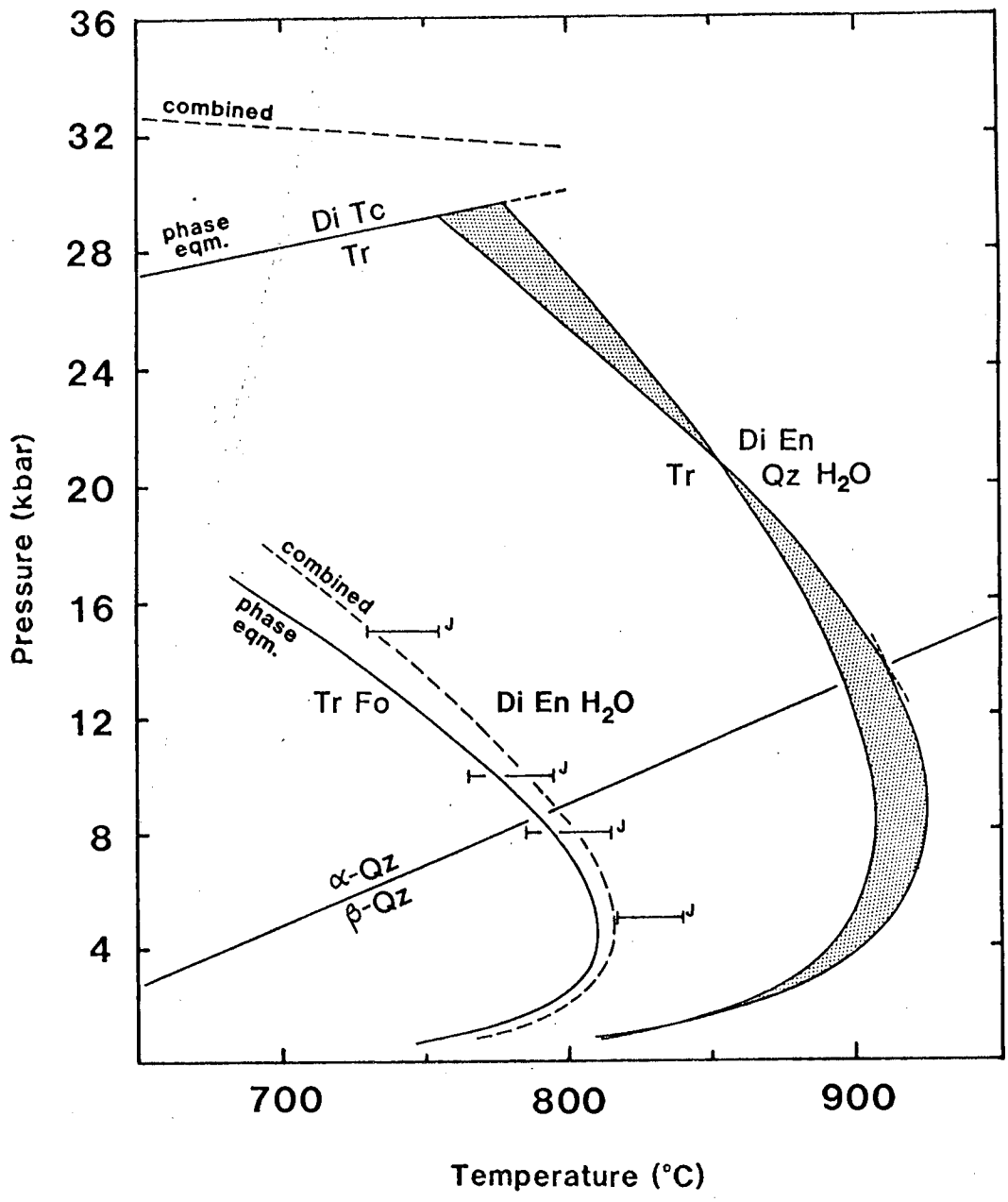

Fig. 5.5. Tremolite stability limits calculated using the enthalpy and entropy data derived from phase equilibrium studies (phase eqm.) and combined phase equilibrium and calorimetric studies (combined). The reaction Tr = Di + En + Qz + H_2O is shown by 'maximum' and 'minimum' phase equilibrium curves; other reactions calculated using mean data. J = experimental brackets of Jenkins (1983) on the reaction Tr + Fo = Di + En + H_2O. Position of α-Qz = β-Qz calculated using THERMOCALC data. Mineral abbreviations given in Table 5.1. From Welch & Pawley (in prep.).

reaction is poorly constrained by these data, and because of the small energy changes involved, would probably be difficult to constrain experimentally.

Reaction (4) has been investigated in hydrothermal experiments by Jenkins (1983), whose brackets, shown in Fig. 5.5, are in good agreement with both the phase equilibrium and combined curves calculated here. The temperature uncertainty on the former curve is ~ ± 90°.

5.4.(vi). Discussion of $Tr_{92}Mc_8$ phase equilibrium results

Experimental brackets on both reactions (1) Tr_{100} = 2 Di + 1.5 En + β-Qz H_2O and (2) $Tr_{92}Mc_8$ = 1.84 Di + 1.66 En + β-Qz + H_2O, were obtained at two pressures: 2 kbar and 8 kbar. The brackets at 8 kbar are the same, while the 2 kbar bracket on reaction (2) is a few degrees wider than that on reaction (1) only because of slight differences in run-temperature. Thus the two reactions may be coincident, though in fact the brackets being 30° wide could conceal differences. An estimate of a possible difference may be made by using THERMOCALC to locate reaction (1) for tremolite with unit activity, and tremolite with a reduced activity. It is found that using a value for a_{Tr} of 0.90 increases the temperature of reaction (1) by 12° at 2 kbar and 15° at 8 kbar, placing it still within the error limits. The actual value of a_{Tr} in $Tr_{92}Mc_8$ is likely to be >0.92, considering that $a_i = \gamma_i X_i$ and γ_i is generally >1, and therefore a shift of >10° is unlikely.

Thus the same experimental brackets on the two reactions may easily be reconciled without requiring the end-member tremolite to be off-composition. But if reaction (1) was incorrectly located, the above calculation demonstrates that the effect on the derived free energy of tremolite would be minimal (a shift of 10° would cause ΔG to change by ~1 kJ mol^{-1}), confirming the reliability of the phase equilibrium-derived values of $\Delta H°_f$ [Tr] and S° [Tr].

5.5. DERIVATION OF ENTHALPY OF FORMATION OF SODIUM PHLOGOPITE FROM CALORIMETRY

Using the calorimetric cycle shown in Fig. 5.6 and enthalpy of solution data from Table 5.10 and $\Delta H°_f$ and heat content data from Table 5.9, the calculated $\Delta H°_f$ [Sp] is

$$\underline{\Delta H°_f [Sp] = -6155.040 \pm 9.354 \text{ kJ mol}^{-1}}$$

Fig. 5.6. Calorimetric cycle used to obtain $\Delta H°_f$ [sodium phlogopite].

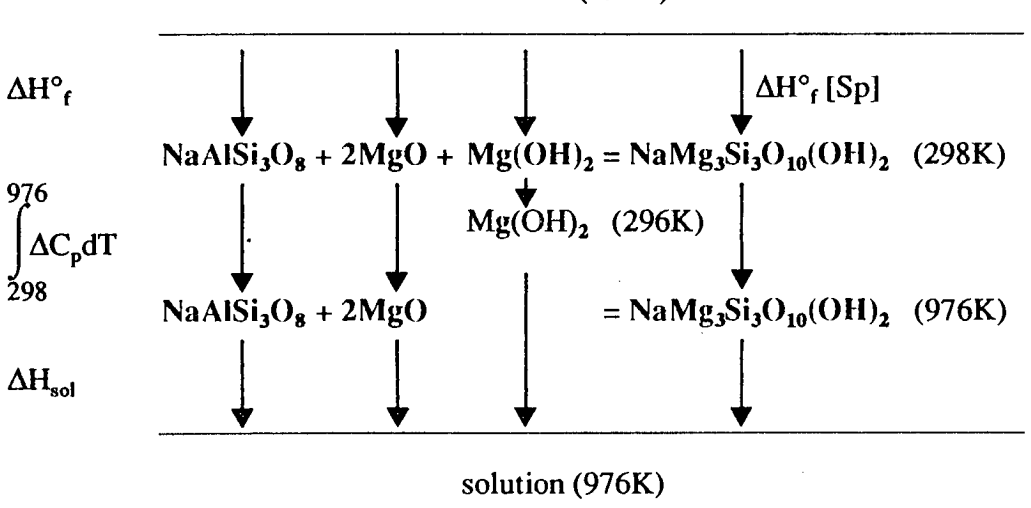

The uncertainty was calculated in the same manner as before. Again, additional uncertainties may arise from differences between calorimeter temperatures used, and in this calculation the heat content of Sp is also likely to be a significant source of error, as it was calculated using estimated heat capacity data from THERMOCALC, rather than measured data as for the other minerals.

5.5.(i). Discussion

The calorimetric value of $\Delta H°_f$ [Sp] may be compared with the phase equilibrium value in THERMOCALC, estimated by Holland & Powell using the experimental data of Carman & Gilbert (1983) on the reaction

$$Sp + 1.5\,En = 3\,Fo + Ab + H_2O \qquad (5)$$

at 0.28-1.55 kbar/800-870°C, and their own estimated C_p data and entropy, which comprises a third-law term predicted from the entropy-volume model of Holland (1989) and a configurational entropy term. They obtain $\Delta H°_f$ [Sp] = -6173.64 ± 8.92 kJ mol^{-1}, ie. almost 20 kJ mol^{-1} below (ie. more negative than) the calorimetric value. The difference is of the opposite sign to that found for tremolite and other hydrous minerals, and may be attributable to one or both of the following:

(a). Although Carman & Gilbert (1983) were able to reverse reaction (5), they were unable to confirm that the sheet silicate was stoichiometric Sp anywhere along it. As they pointed out, the x-ray parameters of Sp and its hydrates are similar to those of their "Mss", nominally a binary solid solution between Sp and Tc (though probably

also comprising a component of preiswerkite when coexisting with amphibole - see Chapter 3). They therefore used the observation that Sp is not glycol-expandable, whereas their "Mss" is, to distinguish between the two sheet silicates. However there is no evidence that end-member Sp is the only composition in this system which is not glycol-expandable. Thus their Sp could be displaced in composition towards Tc along the length of reaction (5), causing it to be displaced to a higher temperature than the dehydration reaction of the pure end-member, and hence yielding a value of $\Delta H°_f$ [Sp] too low. Alternatively the composition of the sheet silicate may change along the reaction, eg. becoming more Tc-rich with increasing temperature, again causing a reaction displacement and reduction in calculated $\Delta H°_f$ [Sp] (Fig. 5.7).

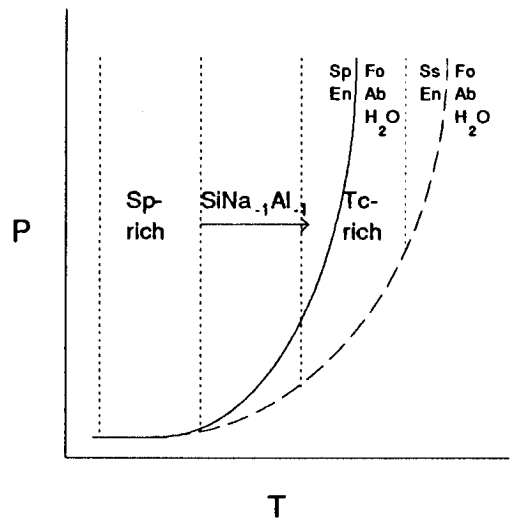

Fig. 5.7. Schematic P-T diagram showing how reduced activity of Sp shifts the sheet silicate breakdown reaction up-temperature. Dotted lines are hypothetical sheet silicate compositional isopleths. Ss = Sp-Tc solid solution.

(b). The value of $S°$ [Sp] used in the calculation of $\Delta H°_f$ [Sp] (phase equilibrium) includes a configurational entropy term arising from Al/Si order-disorder on tetrahedral sites, the extent of which could only be estimated. Because Al/Si interdiffusion is very slow, both synthetic sheet silicates and the first sheet silicates to grow in a metamorphic reaction will be at least partially disordered. But the actual degree of disorder is debatable. Complete Al/Si disorder is usually assumed in minerals on initial crystallisation (eg. high albite, which crystallises even in the stability field of low albite). But strong short range order has been suggested for some minerals (eg. short range Al/Si order in muscovite, Herrero et al., 1987). $S°_{config}$ [Sp]

estimated by Holland & Powell (9 J K^{-1} mol^{-1}) was half of the full value – -4R[0.25ln0.25 + 0.75ln0.75] = 19 J K^{-1} mol^{-1} – obtained by assuming complete Al/Si disorder. If a further 10 J K^{-1} mol^{-1} is added to $S°_{config}$ [Sp], $\Delta H°_f$ [Sp] is increased by ~10 kJ mol^{-1} and the discrepancy between $\Delta H°_f$ (calorimetric) and $\Delta H°_f$ (phase equilibrium) is reduced by about half.

$\Delta H°_f$ [Sp] (calorimetric) may be substituted into the THERMOCALC dataset, and phase equilibria calculated and compared with those determined using the pre-existing data. The dataset loses its internal consistency when a value is altered, but because Sp is not an 'anchor' phase (terminology of Holland & Powell, 1985), consistency among the data for the other phases involved in the calculations should remain more or less intact. Calculations on the reactions:

$$Sp + 1.5\,En = 3\,Fo + Ab + H_2O$$

and

$$2\,Gl = Sp + Tc + 3\,Ab$$

demonstrate that an increase in $\Delta H°_f$ [Sp] of 20 kJ mol^{-1} has the effect of shifting the reactions by approximately 100 and 250°C respectively, while the same increase combined with an increase in entropy of 10 J K^{-1} mol^{-1} causes shifts of half these magnitudes.

Although the loss of internal consistency arising from such alterations to data in the dataset causes these calculations not to be strictly meaningful, the considerable shifts produced in the reactions by changing $\Delta H°_f$ [Sp] and S° [Sp] do demonstrate the need for caution when using datasets such as THERMOCALC to calculate equilibria involving phases whose thermodynamic parameters are poorly constrained. Such is the case for most amphiboles, their compositions in phase equilibrium experiments often not being properly analysed, and their state of cation order/disorder not determined. Seldom are synthetic amphiboles as "on-composition" as Sp, and so their $\Delta H°_f$ cannot be determined by solution calorimetry to compare with phase equilibrium values, errors in which may then not be realised, even though they could dramatically affect calculated equilibria.

5.6. F-OH EXCHANGE ENTHALPY CALCULATIONS

The F-OH exchange enthalpy for sodium phlogopite is

$$\Delta H_{F\text{-}OH} = \Delta H_{sol}\,[F\text{-}Sp] - \Delta H_{sol}\,[OH\text{-}Sp]$$
$$= 9.88 \pm 8.92 \text{ kJ mol}^{-1}$$

It is compared with $\Delta H_{F\text{-}OH}$ calculated for some other hydrous minerals in Table 5.12. The variation in $\Delta H_{F\text{-}OH}$ is considerably greater than for some other substitutions, eg.

Table 5.12. ΔH_{sol} of OH- and F-minerals and calculated F-OH exchange enthalpies.

Phase	ΔH_{sol} (kJ mol^{-1})	Source	$\Delta H_{F\text{-}OH}$ (kJ mol^{-1})
OH-pargasite $NaCa_2Mg_4Al_3Si_6(OH)_2$	415.93 ± 3.43	Ross & Graham (in prep.)	-15.50 ± 6.22
F-pargasite $NaCa_2Mg_4Al_3Si_6F_2$	400.43 ± 5.19	Ross & Graham (in prep.)	
OH-tremolite $Ca_2Mg_5Si_8(OH)_2$	375.76 ± 4.43	This study	7.92 ± 10.64
F-tremolite $Ca_2Mg_5Si_8F_2$	383.68 ± 9.67	Graham & Navrotsky (1986)	
OH-phlogopite $KMg_3AlSi_3(OH)_2$	281.88 ± 3.10	Clemens et al. (1987)	-28.50 ± 3.65
F-phlogopite $KMg_3AlSi_3F_2$	253.38 ± 1.92	Westrich & Navrotsky (1981)	
OH-Na-phlogopite $NaMg_3AlSi_3(OH)_2$	230.20 ± 4.94	This study	9.88 ± 8.92
F-Na-phlogopite $NaMg_3AlSi_3F_2$	240.08 ± 7.43	This study	

the 'edenite' exchange $NaAlSi_{-1}$. However there is agreement between $\Delta H_{F\text{-}OH}$ [Tr] and $\Delta H_{F\text{-}OH}$ [Sp]. Moreover ΔH_{sol} [F-Phl] may be too low, considering that Westrich & Navrotsky (1981) report an average grain size of their synthetic sample of <2 μm, suggesting that it is poorly crystalline and therefore the energy required to dissolve it is too low. The ΔH_{sol} of their synthetic F-pargasite, also very fine-grained, was 55 kJ mol^{-1} lower than that recently obtained by Ross & Graham (in prep) on a well-crystallised sample. Therefore the derived $\Delta H_{F\text{-}OH}$ [Phl] is considered unreliable.

The reason for $\Delta H_{F\text{-}OH}$ [Parg] being negative while $\Delta H_{F\text{-}OH}$ [Tr] and [Sp] are positive is unclear. A-site occupancy cannot be important, as Parg and Sp both have A-sites occupied by Na, while that of Tr is empty. Likewise Tr is the only phase

without tetrahedral Al. However, though in all three minerals the M(1) and M(3) sites should all be occupied by Mg (the octahedral sites in Sp are equivalent to M(1) and M(3) sites in amphiboles), vibrational spectroscopy reveals that the synthetic pargasite has a disordered distribution of Mg and Al over all of the octahedral sites (Graham, pers. comm.), ie. comprising some Al in M(1) and M(3) sites. As these sites are coordinated to the O(3) anion, it may be expected that their occupancy will exert the greatest influence on the strength of the forces holding the O(3) anions within the structure, and hence on $\Delta H_{F\text{-}OH}$. However the observed difference in $\Delta H_{F\text{-}OH}$ is large for what must be a relatively small M(1)/M(3) occupancy by Al, and other structural factors may also be important, or some of the calorimetric data may be incorrect, due for example to poor crystallinity. Therefore until more data are available it is not recommended that any of these F-OH exchange enthalpies be used to predict enthalpies of solution of hydrous minerals on the basis of measurements on their fluorine-analogues alone.

5.7. CONCLUSIONS

1. New enthalpy of formation and entropy data for tremolite have been obtained in experiments on an essentially pure natural sample. Phase equilibrium experiments on the reaction Tr = 2 Di + 1.5 En + β-Qz + H_2O were conducted at 250 bars-8 kbar/700-930°C to yield $\Delta H°_f$ [Tr] and S° [Tr], and high-temperature solution calorimetric measurements on this sample were used to obtain $\Delta H°_f$ [Tr].

(a). The phase equilibrium data – $\Delta H°_f$ [Tr] = -12300.47 ± 14.81 kJ mol^{-1}, S° [Tr] = 551.6 ± 9.8 J K^{-1} mol^{-1} – are in excellent agreement with those in the revised THERMOCALC dataset of Holland & Powell (in press).

(b). The calorimetric $\Delta H°_f$ [Tr] = -12323.89 ± 8.93 kJ mol^{-1} is ~ 20 kJ mol^{-1} more negative than the phase equilibrium value. Conceivable systematic errors in one or other method of derivation cannot explain the discrepancy, but partly because there are more 'unknowns' associated with calorimetry than with phase equilibrium experiments, and partly because the phase equilibrium data agree with those in the THERMOCALC dataset, these are preferred for the calculation of tremolite stability relations.

(c). Data derived by using a calorimetric $\Delta H°_r$ as an additional, 0 K, bracket on the phase equilibrium data – $\Delta H°_f$ [Tr] = -12310.34 ± 11.88 kJ mol^{-1}, S° [Tr] = 542.4 ± 1.0 J K^{-1} mol^{-1} – are biased towards the former data, and so while uncertainty

remains regarding the discrepancy, they are not recommended for use in calculating tremolite stability relations.

(d). P-T positions of some tremolite-bearing equilibria have been calculated using the new data. Those for the reaction Tr + Fo = 2 Di + 1.5 En + H_2O are in good agreement with experimental data (Jenkins, 1983).

(e). Experimental brackets on the reaction $Tr_{92}Mc_8$ = 1.84 Di + 1.66 En + β-Qz + H_2O closely match those on the reaction Tr_{100} = 2 Di + 1.5 En + β-Qz + H_2O, indicating that any shift in composition away from end-member tremolite in the latter reaction will have minimal effect on derived thermochemical data for tremolite.

2. The enthalpy of formation of sodium phlogopite, derived from high-temperature calorimetric measurements, is ΔH°_f [Sp] = -6155.040 ± 9.354 kJ mol^{-1}. This is ~ 20 kJ mol^{-1} less negative than the value in the THERMOCALC dataset. Uncertainty as to the composition and state of Al/Si disorder in the sample from which the phase equilibrium data was derived may account for this discrepancy. Using such poorly constrained thermodynamic data may lead to the misplacing of calculated reactions by up to a few hundred degrees.

3. An F-OH exchange enthalpy has been calculated as the difference in ΔH_{sol} between F-Sp and OH-Sp. Thus $\Delta H_{F\text{-}OH}$ = 9.88 ± 8.92 kJ mol^{-1}, in good agreement with data for tremolite, but ~ 25 kJ mol^{-1} higher than $\Delta H_{F\text{-}OH}$ [pargasite]. The enthalpy depends to some extent on the occupancy of the sites coordinated to O(3), ie. M(1) and M(3), which are occupied solely by Mg in tremolite and sodium phlogopite, but by disordered Mg and Al in pargasite.

CHAPTER 6

CONCLUDING REMARKS

While the experimental studies undertaken for this thesis have yielded their own specific results and conclusions, which have been summarised in the relevant chapters, there have also been some common themes enabling results of one study to be applied to others, and from them all a general picture for the future of experimental studies on amphiboles to be extracted.

The A-site

For example one of the aims which the glaucophane-nyböite and tremolite-richterite studies had in common was that of clarifying and quantifying the extent and importance of the A-site filling substitution in stabilising the respective solid solutions. The two studies were tackled in entirely different ways, and therefore yielded different kinds of information. On the one hand, the glaucophane-nyböite study was begun with the objective of yielding thermodynamic data directly applicable to the interpretation of natural metamorphic assemblages through phase equilibrium experiments. However it was hampered by problems with sample synthesis, a common feature in studies on geologically important amphibole compositions. Therefore only limited data were extracted, though one major conclusion was that the A-site filling 'edenite' exchange, $NaAlSi_{-1}$, increased the pressure-temperature stability field of high-pressure glaucophanic amphiboles, extending it towards lower pressures and higher temperatures.

The tremolite-richterite solid solution, on the other hand, was chosen for study not primarily because of any geological relevance, but because synthesis of most of the solid solution was expected to be possible, and therefore detailed characterisation could be undertaken and the energetics of the A-site filling 'richterite' exchange, $NaNaCa_{-1}$, understood. Despite the minor setback of not being able to synthesise the true binary join, this objective was attained. While end-member richterite does not occur naturally, and few phase equilibrium experiments have been conducted on it, those that have (eg. Charles, 1975) suggest that its stability is increased with respect to tremolite. The results of the glaucophane-nyböite study and the thermochemical study of F-tremolite – F-edenite amphiboles (Graham & Navrotsky, 1986), in both of which increased stability of A-site-full over A-site-empty amphiboles was demonstrated, consolidate the hypothesis that the richterite substitution increases amphibole stability, and indicate that the same may be true for all A-site-filling substitutions. The detailed characterisation and calorimetric study were able to suggest reasons for the increased stability, eg. the presence of significant short range order in A-site full richterite. It may be possible to infer that some of the same factors

are responsible for the increased stability of nyböitic over glaucophanic amphiboles, and will be important in stabilising other A-site full amphiboles.

Thus these two studies together demonstrate how the results of investigations on simple systems, though frequently geologically over-simple, yet often amenable to direct investigation, may be applied to the interpretation of more geologically relevant, but more complex compositions.

Derivation of thermodynamic data

Though the studies described in Chapter 5 are not of direct relevance to the others, the phase equilibrium experiments on tremolite, as well as yielding thermodynamic data for this important mineral, showed how this technique is used to obtain the enthalpy of a reaction, and could have been for the nyböite-bearing reactions if only the amphibole had been of end-member composition. Likewise, the calorimetric studies on tremolite and sodium phlogopite usefully demonstrated this alternative method of deriving enthalpy of formation data, which is particularly useful when 100% synthesis yields can be obtained, but when thermodynamic data for reaction breakdown products are poorly constrained, eg. if a melt is involved, or if the reaction is divariant. For example the nyböite breakdown reaction is at least divariant, and attempting to quantify it for phase equilibrium calculations would be impossible. But had stoichiometric nyböite been synthesised at some other pressure and temperature, solution calorimetry would have enabled its enthalpy of formation to be derived.

Errors

Comparisons between results obtained in these studies have also revealed discrepancies and errors leading to some methods of derivation of thermodynamic data being considered potentially unreliable. For example the large difference between ΔH_{sol} [Ri] obtained in the fairly routine method of solution calorimetry and ΔH_{sol} [Ri] obtained by drop-solution calorimetry suggests that published enthalpies of solution for some other minerals may be in error. Also the difference between ΔH°_f [Tr] (phase equilibrium) and ΔH°_f [Tr] (calorimetric) suggests some previously unidentified systematic source of error in one or other experimental method, more likely the calorimetry. The difference between ΔH°_f [Sp] (calorimetric) and ΔH°_f [Sp] (phase equilibrium, from THERMOCALC) reveals one danger of assuming that all data in tabulated datasets are well-constrained. Finally, the differences between $\Delta H_{F\text{-}OH}$ obtained for sodium phlogopite and from previous studies show that caution must be used when extrapolating exchange enthalpies between mineral systems.

Future studies

The errors revealed by the above comparisons are not entirely bad news for amphibole studies, as they in fact reveal additional information regarding mineral chemistry and influences on mineral stability, eg. the importance of the coordinating cation on the energetics of the F-OH exchange. But at present there are still too many uncertainties as to whether such errors in data are random, caused by, for example, non-stoichiometry or poor crystallinity of the sample. Therefore there is a real need for more amphibole studies to be undertaken, beginning with investigations of simple systems, until their behaviour is understood, before progressing on to more complex systems. In all studies, detailed characteristion is of paramount importance, as only then can similarities and differences between samples be recognised, and the usefulness of one sample as an analogue for another be judged. Fortunately the number of methods available for characterisation, and their precision, are continually increasing. Furthermore, some of the techniques used for characterisation in these studies (eg. IR and Raman spectroscopy) should become less empirical and more quantitative as they are more widely applied, as should magic angle spinning NMR spectroscopy, only briefly mentioned in this thesis and to date seldom used for amphibole characterisation, but likely to prove very useful in the future. Modelling and *ab initio* calculations are also only just beginning to be applied to amphibole studies, but have potential to provide otherwise unobtainable thermodynamic data, and reveal additional information when compared with experimental data. The modelling of heat capacities by vibrational spectra should also prove very useful in the future, particularly if the spectra can themselves be modelled. Finally, if different kinds of experiments are conducted using the same sample, eg. both phase equilibrium and calorimetric experiments, then there is certainly potential for a wealth of information to be extracted from experimental studies on amphiboles, both relating to their microscopic properties and to their application to the interpretation of geological processes.

APPENDIX

X-RAY FLUORESCENCE AND ELECTRON MICROPROBE ANALYSES

Table

Table A3.1. XRF analyses of nyböite - glaucophane gels (-Na_2O).

Ny_{100}				Theoretical
SiO_2	57.54	Si	7.03	7.00
Al_2O_3	20.78	Al	2.99	3.00
MgO	16.22	Mg	2.95	3.00
Na_2O	4.24	Na	1.00	1.00

$Ny_{83}Gl_{17}$				Theoretical
SiO_2	59.95	Si	7.18	7.17
Al_2O_3	20.07	Al	2.83	2.83
MgO	16.63	Mg	2.97	3.00
Na_2O	3.63	Na	0.84	0.83

$Ny_{67}Gl_{33}$				Theoretical
SiO_2	60.21	Si	7.32	7.33
Al_2O_3	18.62	Al	2.67	2.67
MgO	16.68	Mg	3.02	3.00
Na_2O	2.94	Na	0.69	0.67

$Ny_{50}Gl_{50}$				Theoretical
SiO_2	63.08	Si	7.49	7.50
Al_2O_3	17.91	Al	2.51	2.50
MgO	16.88	Mg	2.99	3.00
Na_2O	2.25	Na	0.52	0.50

$Ny_{33}Gl_{67}$				Theoretical
SiO_2	62.76	Si	7.66	7.67
Al_2O_3	16.23	Al	2.34	2.33
MgO	16.50	Mg	3.00	3.00
Na_2O	1.40	Na	0.33	0.33

$Ny_{17}Gl_{83}$				Theoretical
SiO_2	65.16	Si	7.80	7.83
Al_2O_3	15.52	Al	2.19	2.17
MgO	17.03	Mg	3.04	3.00
Na_2O	0.72	Na	0.17	0.17

Gl_{100}				Theoretical
SiO_2	66.38	Si	7.94	8.00
Al_2O_3	14.38	Al	2.03	2.00
MgO	17.21	Mg	3.07	3.00

Table A3.2. Electron microprobe analyses of NMASH amphiboles.

Na_2O	MgO	Al_2O_3	SiO_2	Total	Na	Mg	Al	Si	Total
				OH-NY1 Ny_{100}/26.1-27.0kbar/830-833°C					
11.3	17.2	16.7	55.1	100.3	2.87	3.34	2.56	7.19	15.96
11.4	16.8	17.0	54.8	100.0	2.89	3.28	2.61	7.17	15.96
11.1	17.2	16.7	54.5	99.5	2.85	3.36	2.59	7.16	15.96
11.2	16.4	17.5	55.3	100.4	2.83	3.17	2.69	7.19	15.88
11.0	17.2	16.4	54.3	98.9	2.82	3.38	2.56	7.18	15.95
10.9	17.4	16.1	55.0	99.4	2.78	3.41	2.49	7.23	15.92
11.1	16.6	16.6	54.5	98.8	2.86	3.27	2.59	7.21	15.93
11.2	16.0	17.2	54.5	98.9	2.87	3.14	2.67	7.20	15.89
11.2	16.8	17.0	53.6	98.7	2.87	3.33	2.66	7.12	15.99
11.5	16.6	16.2	53.9	98.3	2.96	3.31	2.55	7.19	16.02
10.8	16.4	16.5	53.4	97.1	2.83	3.29	2.61	7.19	15.92
11.3	16.6	16.5	53.8	98.3	2.93	3.31	2.59	7.17	16.00
11.0	16.4	16.3	53.7	97.5	2.87	3.28	2.58	7.21	15.93
10.8	16.1	16.2	53.1	96.2	2.84	3.27	2.59	7.21	15.91
11.5	16.3	17.1	53.4	98.2	2.97	3.24	2.68	7.12	16.02
11.4	16.4	16.5	53.2	97.5	2.96	3.29	2.61	7.15	16.02
10.9	17.5	15.1	54.4	97.9	2.84	3.48	2.38	7.27	15.96
10.8	16.4	16.6	53.7	97.6	2.81	3.28	2.62	7.19	15.90
11.0	17.3	15.6	54.8	98.7	2.83	3.42	2.44	7.25	15.94
10.6	17.2	16.7	55.4	99.9	2.69	3.34	2.57	7.23	15.83
10.8	16.0	16.8	54.4	98.0	2.79	3.18	2.63	7.24	15.84
9.9	16.0	16.7	54.0	96.6	2.57	3.22	2.65	7.26	15.70
10.9	16.5	16.8	54.2	98.4	2.80	3.27	2.63	7.19	15.89
10.8	16.3	15.8	54.0	97.0	2.83	3.26	2.51	7.27	15.88
				OH-NY9 Ny_{100}/31.1-31.3kbar/898-901°C					
10.6	17.6	17.3	52.5	98.1	2.74	3.51	2.72	7.01	16.00
10.8	17.9	16.6	53.5	98.8	2.77	3.53	2.60	7.09	15.99
10.5	17.7	16.9	53.2	98.4	2.72	3.52	2.65	7.07	15.96
10.3	18.8	15.9	53.7	98.7	2.65	3.72	2.48	7.12	15.96
10.7	17.2	18.5	52.6	99.0	2.75	3.39	2.88	6.96	15.98
10.8	16.7	18.7	51.8	97.9	2.79	3.32	2.95	6.93	15.99
11.0	16.9	18.5	52.4	98.8	2.82	3.34	2.89	6.96	16.01
10.8	16.9	18.1	53.1	99.0	2.76	3.33	2.83	7.02	15.94
10.7	18.4	15.3	53.6	98.0	2.78	3.66	2.42	7.16	16.02
10.7	17.4	17.7	53.0	98.7	2.75	3.44	2.76	7.02	15.97
10.7	18.0	16.3	53.5	98.6	2.76	3.57	2.55	7.11	15.99
10.3	17.7	16.6	53.0	97.6	2.69	3.53	2.63	7.09	15.94
				OH-NY15 Ny_{100}/32.2kbar/829-832°C					
10.8	18.9	14.8	54.9	99.4	2.77	3.71	2.29	7.23	16.01
10.6	17.2	16.7	52.7	97.2	2.78	3.46	2.65	7.09	15.97
10.9	17.6	16.9	53.6	99.0	2.79	3.47	2.64	7.09	15.99
10.8	18.9	15.0	54.4	99.1	2.77	3.71	2.34	7.19	16.02
11.0	17.8	16.1	53.9	98.7	2.83	3.52	2.51	7.15	16.01
10.4	17.6	16.7	53.2	97.9	2.70	3.50	2.63	7.10	15.93
10.8	18.1	15.9	54.0	98.8	2.77	3.57	2.49	7.16	15.98
10.7	18.2	15.8	54.5	99.2	2.73	3.58	2.46	7.18	15.95
11.3	16.4	16.9	54.1	98.7	2.90	3.24	2.64	7.17	15.95

(Table A3.2 continued)

Na_2O	MgO	Al_2O_3	SiO_2	Total	Na	Mg	Al	Si	Total
				OH-NY19 Ny_{100}/15.7-16.3kbar/799-802°C					
10.9	16.8	15.9	54.0	97.5	2.82	3.35	2.50	7.24	15.92
11.1	15.5	17.3	54.7	98.6	2.85	3.06	2.70	7.23	15.84
10.5	15.6	16.8	55.3	98.2	2.70	3.08	2.62	7.32	15.72
10.9	15.5	16.3	53.6	96.3	2.88	3.14	2.60	7.26	15.87
10.9	16.0	16.6	54.3	97.9	2.82	3.18	2.61	7.25	15.86
11.2	16.4	16.0	54.6	98.2	2.89	3.25	2.51	7.27	15.92
11.1	16.0	16.0	53.6	96.8	2.91	3.22	2.55	7.24	15.93
10.7	16.5	15.6	52.7	95.5	2.84	3.37	2.52	7.21	15.94
11.1	17.5	15.4	54.1	98.0	2.87	3.48	2.42	7.23	15.99
11.4	16.8	16.0	54.6	98.8	2.92	3.31	2.51	7.23	15.98
11.0	16.3	16.6	53.9	97.8	2.86	3.24	2.62	7.20	15.92
10.9	16.0	17.4	54.4	98.6	2.79	3.16	2.71	7.19	15.85
				OH-Q6 Ny_{100}.7SiO_2/20.4-21.1kbar/746-749°C					
8.4	15.8	13.8	61.3	99.3	2.08	3.04	2.09	7.89	15.10
9.2	17.3	14.0	58.2	98.7	2.34	3.37	2.16	7.61	15.48
9.4	16.3	14.5	57.2	97.5	2.42	3.22	2.27	7.58	15.49
9.6	16.4	14.3	56.7	97.0	2.49	3.27	2.25	7.56	15.56
9.2	16.2	14.1	58.6	98.0	2.34	3.17	2.18	7.70	15.38
8.1	16.2	13.6	59.5	97.4	2.06	3.17	2.10	7.82	15.15
8.3	15.3	14.5	62.7	100.8	2.03	2.89	2.16	7.93	15.00
8.0	15.4	13.6	57.4	94.5	2.10	3.12	2.18	7.78	15.18
8.2	16.2	14.0	57.7	96.1	2.11	3.23	2.20	7.70	15.25
				OH-Q7 Ny_{100}.7SiO_2/21.5-22.1kbar/800°C					
8.1	19.2	13.4	56.3	97.0	2.09	3.81	2.11	7.49	15.50
8.5	17.6	13.4	57.8	97.4	2.19	3.47	2.09	7.65	15.40
9.0	17.1	13.5	57.5	97.2	2.32	3.38	2.12	7.64	15.46
8.7	17.4	12.8	57.5	96.4	2.26	3.46	2.02	7.69	15.43
8.9	17.5	14.3	59.0	99.7	2.22	3.37	2.19	7.62	15.40
8.0	16.1	12.9	59.5	96.5	2.06	3.17	2.02	7.88	15.13
8.5	16.0	12.9	59.3	96.6	2.18	3.16	2.01	7.86	15.22
				OH-Q8 Ny_{100}.7SiO_2/19.6-20.5kbar/798-801°C					
9.1	16.1	13.7	60.3	99.2	2.28	3.10	2.09	7.81	15.28
8.6	16.3	13.2	58.0	96.1	2.22	3.25	2.09	7.75	15.31
8.7	16.9	13.3	59.5	98.5	2.21	3.29	2.05	7.77	15.31
8.4	16.5	13.8	60.8	99.5	2.09	3.16	2.10	7.83	15.17
9.0	16.9	13.9	58.3	98.1	2.29	3.32	2.15	7.66	15.42
7.9	15.8	14.0	59.9	97.6	2.00	3.07	2.16	7.84	15.07
9.2	17.4	15.9	57.2	99.7	2.31	3.36	2.43	7.42	15.52
9.1	17.3	15.2	56.2	97.7	2.33	3.40	2.37	7.44	15.54
8.4	17.1	15.3	56.5	97.2	2.17	3.37	2.39	7.48	15.41

(Table A3.2 continued)

Na_2O	MgO	Al_2O_3	SiO_2	Total	Na	Mg	Al	Si	Total
				OH-Q15a Ny_{100}+7SiO_2/22.2kbar/825°C					
7.9	17.2	13.1	56.4	94.6	2.07	3.49	2.10	7.66	15.32
8.2	17.2	13.7	60.4	99.5	2.03	3.30	2.08	7.78	15.19
8.5	18.2	13.4	57.5	97.6	2.19	3.59	2.08	7.60	15.45
				OH-Q15b OH-QG4/22.2kbar/825°C					
5.6	22.0	9.4	57.5	94.6	1.46	4.44	1.51	7.78	15.19
6.0	22.2	9.5	57.7	95.4	1.57	4.44	1.51	7.75	15.28
6.8	20.3	9.9	57.1	94.1	1.79	4.13	1.60	7.79	15.30
				OH-Q16b OH-QG4/21.0-21.3kbar/800°C					
5.7	22.2	8.3	57.9	94.1	1.49	4.51	1.34	7.87	15.20
				G-N1 $Ny_{67}Gl_{33}$/17.5-18.0kbar/770°C					
10.5	17.3	14.3	53.9	96.1	2.77	3.52	2.29	7.32	15.91
10.8	16.0	14.6	54.0	95.4	2.85	3.27	2.36	7.38	15.86
10.2	17.5	13.1	54.7	95.5	2.70	3.55	2.10	7.47	15.83
				G-N2 $Ny_{50}Gl_{50}$/15.9-16.7kbar/770°C					
10.2	18.8	11.2	55.2	95.5	2.71	3.83	1.81	7.55	15.90
10.5	18.0	12.3	57.9	98.6	2.68	3.53	1.91	7.63	15.75
10.4	19.9	11.1	57.1	98.5	2.68	3.93	1.73	7.56	15.91
10.5	19.0	12.0	57.4	98.8	2.68	3.73	1.86	7.57	15.84
10.0	19.2	10.9	56.2	96.3	2.63	3.87	1.74	7.60	15.84
10.4	20.1	10.3	56.0	96.8	2.73	4.04	1.64	7.57	15.98
				G-N3 $Ny_{33}Gl_{67}$/18kbar/790°C					
8.5	20.2	11.9	54.6	95.2	2.26	4.10	1.92	7.45	15.72
8.4	18.0	12.9	57.2	96.6	2.18	3.58	2.03	7.64	15.43
				G-N4 $Ny_{50}Gl_{50}$/17.7-18.3kbar/770°C					
9.7	17.1	13.8	56.0	96.6	2.52	3.42	2.18	7.52	15.65
9.8	17.3	12.9	56.7	96.8	2.56	3.45	2.04	7.60	15.65
9.9	17.5	13.4	57.5	98.4	2.54	3.45	2.09	7.58	15.65
9.8	17.0	13.5	56.9	97.2	2.53	3.38	2.12	7.59	15.62
				G-N5 $Ny_{33}Gl_{67}$/17.7-18.3kbar/770°C					
8.0	16.1	13.3	58.4	95.9	2.08	3.20	2.09	7.81	15.19
8.0	17.9	12.5	58.6	97.0	2.06	3.53	1.95	7.75	15.30
8.5	17.6	12.6	58.0	96.8	2.20	3.50	1.97	7.72	15.40
9.1	18.2	11.9	56.5	95.8	2.38	3.68	1.90	7.64	15.60
8.8	17.6	12.4	57.8	96.8	2.28	3.50	1.96	7.71	15.46

(Table A3.2 continued)

Na_2O	MgO	Al_2O_3	SiO_2	Total	Na	Mg	Al	Si	Total
			G-N6 $Ny_{83}Gl_{17}$/15.7-16.3kbar/799-802°C						
10.6	17.1	15.3	55.4	98.3	2.71	3.37	2.39	7.34	15.82
11.0	16.5	16.0	55.3	98.8	2.82	3.25	2.48	7.30	15.86
10.8	15.7	16.1	55.3	97.9	2.79	3.12	2.52	7.35	15.78
10.8	16.0	15.2	53.3	95.4	2.86	3.27	2.46	7.30	15.90
11.2	16.3	15.4	54.4	97.3	2.91	3.27	2.44	7.30	15.93
10.8	17.1	16.0	54.7	98.6	2.76	3.37	2.50	7.24	15.89
10.6	16.3	16.3	54.9	98.2	2.72	3.23	2.55	7.29	15.79
10.7	15.9	16.2	54.3	97.1	2.80	3.18	2.56	7.29	15.83
10.7	16.4	16.8	55.4	99.4	2.72	3.21	2.60	7.26	15.80
10.9	16.3	15.7	53.7	96.6	2.85	3.28	2.51	7.27	15.91
			G-N7 $Ny_{50}Gl_{50}$/18.8-19.2kbar/770°C						
10.4	16.8	14.6	56.6	98.3	2.65	3.30	2.27	7.48	15.71
9.5	18.3	14.1	57.7	99.6	2.40	3.55	2.15	7.51	15.61
9.3	16.9	13.4	57.8	97.4	2.38	3.34	2.09	7.66	15.48
9.9	17.7	12.7	55.6	95.9	2.61	3.58	2.03	7.53	15.76
9.5	18.8	12.6	56.6	97.6	2.46	3.73	1.98	7.53	15.71
9.2	16.6	13.1	58.1	97.0	2.38	3.28	2.06	7.72	15.44
10.2	18.2	13.3	55.7	97.4	2.64	3.63	2.10	7.45	15.82
9.4	17.3	13.6	56.5	97.0	2.44	3.45	2.15	7.55	15.59
10.1	18.3	12.9	56.5	97.9	2.61	3.63	2.03	7.51	15.78

Table A3.3. Electron microprobe analyses of NMASH sheet silicates.

Na_2O	MgO	Al_2O_3	SiO_2	Total	Na	Mg	Al	Si	Total
				OH-NY1 Ny_{100}/26.1-27.0kbar/830-833°C					
6.4	25.7	19.3	42.8	94.2	0.83	2.56	1.53	2.87	7.78
6.0	26.1	19.7	43.9	95.7	0.76	2.56	1.53	2.88	7.73
5.5	25.0	19.7	42.3	92.5	0.73	2.53	1.58	2.87	7.70
3.1	25.0	20.6	44.3	93.0	0.40	2.48	1.61	2.95	7.44
6.0	26.7	20.5	41.5	94.7	0.78	2.65	1.61	2.77	7.81
6.7	26.6	18.4	41.7	93.5	0.88	2.69	1.47	2.83	7.87
6.2	26.5	18.7	42.1	93.5	0.81	2.67	1.49	2.84	7.82
6.7	25.8	18.3	41.4	92.3	0.90	2.64	1.48	2.84	7.86
5.0	27.1	20.7	44.5	97.3	0.62	2.60	1.57	2.87	7.66
				OH-NY19 Ny_{100}/15.7-16.3kbar/799-802°C					
2.0	23.5	17.1	37.7	80.3	0.30	2.70	1.56	2.90	7.47
				OH-Q3 Ny_{100}-7SiO_2/29.7-31.4kbar/601-603°C					
0.2	30.2	0.8	62.7	93.9	0.03	2.88	0.06	4.01	6.98
				G-N2 $Ny_{50}Gl_{50}$/15.9-16.7kbar/770°C					
2.9	21.6	11.2	32.7	68.4	0.51	2.95	1.21	2.99	7.66
1.2	26.3	13.3	40.7	81.5	0.17	2.96	1.19	3.08	7.41
1.0	28.4	13.5	42.4	85.4	0.14	3.06	1.15	3.07	7.43
1.1	25.4	12.8	38.9	78.2	0.18	2.99	1.19	3.07	7.42
0.9	27.0	13.6	40.8	82.4	0.14	3.01	1.20	3.06	7.41
0.9	24.8	12.8	36.7	75.2	0.15	3.03	1.24	3.01	7.44
				G-N3 $Ny_{33}Gl_{67}$/17.7-18.4kbar/790°C					
0.7	26.5	13.2	43.0	83.5	0.10	2.90	1.14	3.16	7.31
1.7	24.4	12.5	42.7	81.2	0.24	2.75	1.11	3.23	7.34
0.6	25.4	12.8	41.0	79.8	0.09	2.91	1.16	3.15	7.31
0.6	24.9	11.5	38.7	75.7	0.10	3.02	1.10	3.14	7.35
1.2	22.5	12.2	38.6	74.6	0.20	2.76	1.18	3.18	7.33
0.7	26.0	13.0	41.6	81.4	0.11	2.93	1.16	3.14	7.34
				G-N5 $Ny_{33}Gl_{67}$/17.7-18.3kbar/770°C					
0.9	22.2	12.3	37.7	72.9	0.15	2.78	1.21	3.17	7.30
1.8	24.2	11.8	41.8	79.6	0.28	2.78	1.08	3.23	7.37
				G-N6 $Ny_{83}Gl_{17}$/15.7-16.3kbar/799-802°C					
1.4	24.8	15.8	38.8	80.8	0.20	2.83	1.42	2.97	7.42
1.2	24.0	14.8	36.8	76.9	0.19	2.88	1.40	2.96	7.43
1.7	25.3	16.4	39.3	82.7	0.25	2.83	1.45	2.94	7.46

(Table A3.3 continued)

Na_2O	MgO	Al_2O_3	SiO_2	Total	Na	Mg	Al	Si	Total
				G-N8 $Ny_{17}Gl_{83}$/18.0-18.4kbar/771°C					
0.9	27.3	11.4	45.5	85.0	0.13	2.93	0.97	3.28	7.30
1.3	23.4	10.2	39.7	74.5	0.21	2.87	0.99	3.27	7.34
0.5	25.7	10.8	42.8	79.7	0.07	2.94	0.97	3.28	7.26
				G-N9 Gl_{100}/18.0-18.4kbar/771°C					
1.3	25.3	10.6	43.4	80.7	0.20	2.87	0.95	3.30	7.32
1.4	26.0	10.2	44.0	81.6	0.21	2.92	0.90	3.31	7.34
0.7	26.6	11.1	44.4	82.8	0.10	2.93	0.97	3.28	7.28
0.6	27.3	11.4	45.8	85.1	0.09	2.92	0.97	3.29	7.27
				G-N10 $Ny_{17}Gl_{83}$/16.0-16.4kbar/770°C					
0.7	24.0	9.7	39.3	73.6	0.12	2.97	0.95	3.27	7.31
0.8	27.9	9.6	46.3	84.6	0.11	3.01	0.82	3.35	7.29
0.9	28.2	9.4	46.2	84.6	0.13	3.04	0.80	3.35	7.32
0.9	27.9	9.0	46.5	84.2	0.13	3.02	0.77	3.38	7.30
0.7	25.8	9.3	40.5	76.3	0.11	3.10	0.88	3.26	7.35
				G-N11 Gl_{100}/16.0-16.4kbar/770°C					
0.7	25.4	7.9	45.8	79.7	0.10	2.89	0.71	3.50	7.20
0.6	24.1	7.9	41.6	74.3	0.10	2.95	0.77	3.42	7.24
1.0	23.6	7.6	38.8	71.0	0.17	3.04	0.78	3.35	7.34
0.6	27.2	7.6	47.3	82.8	0.09	2.99	0.66	3.49	7.23
0.7	26.4	7.1	45.3	79.4	0.10	3.02	0.64	3.48	7.25
0.5	25.7	8.4	42.2	76.8	0.08	3.05	0.79	3.36	7.28

Table A3.4. Electron microprobe analyses of NMASH pyroxenes.

Na_2O	MgO	Al_2O_3	SiO_2	Total	Na	Mg	Al	Si	Total
				OH-NY1 Ny_{100}/26.1-27.0kbar/830-833°C					
14.7	2.5	2.4	60.4	101.7	0.94	0.12	0.94	2.00	4.00
15.4	2.3	24.6	60.4	102.8	0.98	0.11	0.96	1.98	4.03
14.5	2.5	23.5	59.5	100.0	0.95	0.13	0.93	2.00	4.01
14.0	2.1	23.9	59.4	99.4	0.92	0.11	0.95	2.01	3.98
14.7	2.1	23.6	59.5	99.8	0.96	0.11	0.94	2.01	4.01
14.1	1.4	24.3	59.8	99.7	0.93	0.07	0.96	2.01	3.97
14.0	3.9	22.8	59.4	100.1	0.91	0.19	0.90	2.00	4.01
14.8	2.2	24.1	60.9	102.0	0.95	0.11	0.94	2.01	4.00
14.2	2.2	24.2	60.3	101.0	0.92	0.11	0.95	2.01	3.98
14.5	2.3	23.8	59.1	99.7	0.95	0.12	0.95	1.99	4.01
14.1	2.2	23.8	60.0	100.1	0.92	0.11	0.94	2.01	3.98
14.3	2.4	23.4	61.6	101.6	0.91	0.12	0.91	2.03	3.97
				OH-NY15 Ny_{100}/32.2kbar/829-832°C					
13.3	5.5	22.0	60.6	101.4	0.85	0.27	0.86	2.01	3.99
13.6	4.5	22.8	61.1	102.1	0.86	0.22	0.88	2.01	3.98
13.8	6.4	21.9	59.1	101.2	0.89	0.32	0.86	1.97	4.04
				OH-NY19 Ny_{100}/15.7-16.3kbar/799-802°C					
13.9	2.4	23.6	61.1	101.0	0.89	0.12	0.92	2.03	3.96
				OH-Q3 Ny_{100}.7SiO2/29.7-31.4kbar/762°C					
14.0	4.0	22.8	60.4	101.2	0.90	0.20	0.89	2.01	4.00
13.3	4.9	22.1	59.9	100.2	0.86	0.25	0.87	2.01	3.99
13.3	6.2	21.5	59.9	100.9	0.86	0.31	0.84	2.00	4.01
13.3	5.8	21.4	60.0	100.5	0.86	0.29	0.85	2.01	4.00
13.4	5.9	21.9	60.4	101.6	0.86	0.29	0.85	2.00	4.00
12.5	7.8	20.2	60.5	101.0	0.80	0.39	0.79	2.01	3.99
13.7	6.0	22.0	61.0	102.7	0.87	0.29	0.85	2.00	4.01
				OH-Q7 Ny_{100}.7SiO_2/21.5-22.1kbar/800°C					
13.9	3.6	23.4	61.4	102.4	0.88	0.18	0.91	2.01	3.97
				OH-Q15b OH-QG4/22.2kbar/825°C					
5.1	26.5	7.9	59.0	98.5	0.34	1.34	0.32	2.01	4.00

Table A3.5. Compositions of NMASH amphiboles expressed as mole fractions of glaucophane, Mg-katophorite, eckermannite and nyböite.

X_{Gl}	X_{Mk}	X_{Ek}	X_{Ny}
	OH-NY1		
0.04	0.09	0.15	0.72
0.04	0.07	0.13	0.76
0.04	0.12	0.12	0.72
0.12	0.05	0.07	0.76
0.05	0.13	0.13	0.69
0.09	0.13	0.14	0.64
0.07	0.07	0.14	0.72
0.11	0.02	0.09	0.78
0.01	0.11	0.11	0.77
0.00	0.05	0.20	0.75
0.08	0.09	0.11	0.72
0.00	0.07	0.17	0.76
0.07	0.07	0.14	0.72
0.09	0.07	0.12	0.72
0.00	0.05	0.13	0.82
0.00	0.05	0.16	0.79
0.04	0.12	0.23	0.61
0.10	0.09	0.09	0.72
0.06	0.11	0.19	0.64
0.17	0.14	0.06	0.63
0.16	0.05	0.08	0.71
0.30	0.13	-0.04	0.61
0.11	0.09	0.08	0.72
0.12	0.05	0.15	0.68
	OH-NY9		
0.00	0.26	0.01	0.73
0.01	0.22	0.08	0.69
0.04	0.24	0.03	0.69
0.04	0.32	0.08	0.56
0.02	0.23	-0.06	0.81
0.01	0.20	-0.08	0.87
0.00	0.19	-0.04	0.85
0.06	0.18	-0.04	0.80
0.00	0.23	0.17	0.60
0.03	0.22	-0.01	0.76
0.01	0.23	0.10	0.66
0.06	0.25	0.03	0.66

X_{Gl}	X_{Mk}	X_{Ek}	X_{Ny}
	OH-NY15		
0.00	0.24	0.23	0.53
0.03	0.20	0.06	0.71
0.01	0.20	0.08	0.71
0.00	0.24	0.20	0.56
0.00	0.18	0.15	0.67
0.07	0.23	0.03	0.67
0.02	0.21	0.14	0.63
0.05	0.22	0.13	0.60
0.05	0.06	0.12	0.77
	OH-NY19		
0.08	0.10	0.16	0.66
0.16	0.00	0.07	0.77
0.28	0.02	0.04	0.66
0.13	0.00	0.13	0.74
0.14	0.04	0.11	0.71
0.08	0.03	0.19	0.70
0.07	0.02	0.17	0.74
0.06	0.11	0.15	0.68
0.01	0.12	0.22	0.65
0.02	0.05	0.21	0.72
0.08	0.06	0.12	0.74
0.15	0.06	0.04	0.75
	OH-Q6		
0.90	0.02	0.00	0.08
0.52	0.14	0.09	0.25
0.51	0.07	0.07	0.35
0.62	0.05	0.07	0.26
0.84	0.09	-0.01	0.08
0.98	0.00	-0.07	0.09
0.82	0.08	-0.04	0.14
0.75	0.13	-0.04	0.16
0.44	0.08	0.11	0.37
	OH-Q7		
0.50	0.40	0.00	0.10
0.60	0.21	0.05	0.14
0.54	0.14	0.10	0.22
0.60	0.18	0.01	0.21
0.87	0.07	0.02	0.04
0.78	0.03	0.09	0.10
0.87	0.17	0.12	0.14

(Table A3.5 continued)

X_{Gl}	X_{Mk}	X_{Ek}	X_{Ny}
	OH-Q8		
0.72	0.00	0.10	0.18
0.69	0.09	0.07	0.15
0.68	0.11	0.08	0.13
0.82	0.08	0.00	0.10
0.58	0.13	0.07	0.22
0.93	0.07	-0.08	0.08
0.48	0.21	-0.06	0.37
0.46	0.21	-0.02	0.35
0.59	0.24	-0.11	0.28
	OH-Q15a		
0.68	0.25	-0.01	0.08
0.81	0.16	-0.02	0.05
0.54	0.27	0.05	0.14
	OH-Q15b		
0.81	0.73	-0.03	-0.51
0.72	0.71	0.03	-0.46
0.70	0.51	0.09	-0.30
	OH-Q16b		
0.80	0.72	0.06	-0.58
	G-N1		
0.09	0.14	0.23	0.54
0.14	0.01	0.24	0.61
0.17	0.13	0.30	0.40
	G-N2		
0.10	0.19	0.45	0.26
0.25	0.07	0.38	0.30
0.09	0.23	0.47	0.21
0.16	0.16	0.41	0.27
0.16	0.21	0.44	0.19
0.02	0.25	0.55	0.18
	G-N3		
0.28	0.46	0.17	0.09
0.57	0.25	0.07	0.11

X_{Gl}	X_{Mk}	X_{Ek}	X_{Ny}
	G-N4		
0.35	0.13	0.17	0.35
0.35	0.10	0.25	0.30
0.35	0.11	0.23	0.31
0.38	0.09	0.21	0.32
	G-N5		
0.81	0.10	0.00	0.09
0.70	0.24	0.05	0.01
0.60	0.19	0.12	0.09
0.40	0.22	0.24	0.14
0.54	0.17	0.17	0.12
	G-N6		
0.18	0.10	0.16	0.56
0.14	0.05	0.16	0.65
0.22	0.00	0.13	0.65
0.10	0.04	0.20	0.66
0.07	0.02	0.23	0.68
0.11	0.12	0.13	0.64
0.21	0.07	0.08	0.64
0.17	0.03	0.12	0.68
0.20	0.08	0.06	0.66
0.09	0.05	0.18	0.68
	G-N7		
0.29	0.06	0.19	0.46
0.39	0.21	0.12	0.28
0.52	0.10	0.14	0.24
0.24	0.15	0.29	0.32
0.29	0.25	0.24	0.22
0.56	0.06	0.16	0.22
0.18	0.18	0.27	0.37
0.41	0.15	0.14	0.30
0.22	0.17	0.29	0.32

Table A3.6. Sheet silicate analyses recalculated by normalising Mg + Al + Si to 7.

Na	Mg	Al	Si	X_{Tc}	X_{Pw}	X_{Sp}
			OH-NY 1			
0.68	2.57	1.54	2.89	0.32	0.43	0.25
0.68	2.57	1.54	2.89	0.32	0.43	0.25
0.66	2.54	1.58	2.88	0.34	0.46	0.20
0.54	2.47	1.60	2.93	0.46	0.53	0.01
0.88	2.64	1.60	2.76	0.12	0.36	0.52
0.86	2.69	1.47	2.83	0.14	0.31	0.55
0.83	2.67	1.49	2.84	0.17	0.33	0.50
0.80	2.66	1.49	2.86	0.20	0.34	0.46
0.74	2.59	1.56	2.85	0.26	0.41	0.33
			OH-NY 19			
0.80	2.64	1.53	2.84	0.20	0.36	0.44
			G-N 2			
0.96	2.89	1.18	2.93	0.04	0.11	0.85
0.88	2.87	1.15	2.98	0.12	0.13	0.75
0.99	2.94	1.11	2.95	0.01	0.06	0.93
0.92	2.89	1.15	2.96	0.08	0.11	0.81
0.95	2.90	1.16	2.95	0.05	0.10	0.85
0.99	2.89	1.20	2.90	0.01	0.11	0.88
			G-N 3			
0.74	2.82	1.11	3.07	0.26	0.18	0.56
0.52	2.72	1.10	3.19	0.48	0.28	0.24
0.76	2.82	1.12	3.05	0.24	0.18	0.58
0.88	2.91	1.06	3.03	0.12	0.09	0.79
0.58	2.71	1.16	3.13	0.42	0.29	0.29
0.79	2.84	1.12	3.04	0.21	0.16	0.63
			G-N 5			
0.61	2.72	1.18	3.10	0.39	0.28	0.33
0.55	2.74	1.07	3.19	0.45	0.26	0.29
			G-N 6			
0.86	2.74	1.38	2.88	0.14	0.26	0.60
0.92	2.78	1.35	2.86	0.08	0.22	0.70
0.89	2.74	1.41	2.85	0.11	0.26	0.63
			G-N 8			
0.65	2.86	0.95	3.20	0.35	0.14	0.51
0.60	2.82	0.97	3.21	0.40	0.18	0.42
0.66	2.86	0.94	3.19	0.34	0.14	0.52

(Table A3.6 continued)

Na	Mg	Al	Si	X_{Tc}	X_{Pw}	X_{Sp}
			G-N 9			
0.57	2.82	0.93	3.24	0.43	0.18	0.39
0.61	2.87	0.88	3.25	0.39	0.13	0.48
0.65	2.86	0.95	3.20	0.35	0.14	0.51
0.63	2.85	0.95	3.21	0.37	0.15	0.48
			G-N 10			
0.70	2.89	0.92	3.18	0.30	0.11	0.59
0.66	2.93	0.80	3.27	0.34	0.07	0.59
0 69	2.96	0.78	3.26	0.31	0.04	0.65
			G-N 11			
0.39	2.85	0.70	3.45	0.61	0.15	0.24
0.53	2.89	0.75	3.35	0.47	0.11	0.42
0.69	2.97	0.76	3.27	0.31	0.03	0.66
0.50	2.93	0.65	3.42	0.50	0.07	0.43
0.54	2.96	0.63	3.41	0.46	0.04	0.50
0.69	2.97	0.77	3.27	0.31	0.03	0.66

Table A4.1. XRF analyses of tremolite - richterite - magnesio-cummingtonite gels.

TR83				Theoretical
SiO_2	60.35	Si	8.01	8.00
MgO	25.19	Mg	4.98	5.00
CaO	12.80	Ca	1.82	1.83
Na_2O	1.32	Na	0.34	0.34

TR67				Theoretical
SiO_2	59.02	Si	8.01	8.00
MgO	24.67	Mg	4.99	5.00
CaO	11.45	Ca	1.66	1.67
Na_2O	2.50	Na	0.66	0.66

TR50				Theoretical
SiO_2	60.22	Si	8.01	8.00
MgO	25.16	Mg	4.99	5.00
CaO	10.43	Ca	1.49	1.50
Na_2O	3.88	Na	1.00	0.34

TR33				Theoretical
SiO_2	60.18	Si	8.01	8.00
MgO	25.13	Mg	4.99	5.00
CaO	9.20	Ca	1.31	1.33
Na_2O	5.19	Na	1.34	1.34

TR17				Theoretical
SiO_2	60.11	Si	8.02	8.00
MgO	25.06	Mg	4.98	5.00
CaO	8.11	Ca	1.16	1.17
Na_2O	6.41	Na	1.66	1.66

RI92				Theoretical
SiO_2	59.81	Si	8.00	8.00
MgO	25.23	Mg	5.03	5.01
CaO	7.42	Ca	1.06	1.07
Na_2O	7.04	Na	1.82	1.84

RI100				Theoretical
SiO_2	59.47	Si	7.96	8.00
MgO	25.10	Mg	5.01	5.00
CaO	7.18	Ca	1.03	1.00
Na_2O	8.05	Na	2.09	2.00

MC100				Theoretical
SiO_2	61.75	Si	8.00	8.00
MgO	36.28	Mg	7.00	7.00

Table A4.2. Electron microprobe analyses of tremolite - richterite - magnesio-cummingtonite - quartz gel mixes[a].

Sample		Weight percentages of oxides		
		Ideal	Mean of 10 analyses	$2s/\sqrt{10}$
TR92MC8+QZ	CaO	12.0	12.0	0.01
	MgO	24.1	25.1	0.01
	SiO_2	62.9	62.9	0.01
RI16+QZ	CaO	11.2	11.2	0.09
	MgO	24.0	23.9	0.11
	SiO_2	64.8	64.9	0.10
RI31+QZ	CaO	10.4	10.6	0.08
	MgO	24.2	24.1	0.11
	SiO_2	65.4	65.3	0.12
RI48+QZ	CaO	10.0	10.1	0.05
	MgO	25.4	25.2	0.08
	SiO_2	64.6	64.8	0.07
RI65+QZ	CaO	9.3	9.4	0.07
	MgO	26.3	26.0	0.11
	SiO_2	64.4	64.6	0.08
RI82	CaO	8.6	8.7	0.11
	MgO	27.1	26.9	0.17
	SiO_2	64.3	64.4	0.10
RI92	CaO	8.0	8.3 (8.0)[b]	0.01
	MgO	27.2	27.1 (27.3)	0.01
	SiO_2	64.7	64.5 (64.7)	0.01

Microprobe operating conditions: accelerating voltage 15kV
beam current 5.4 nA
beam raster size 20×20 μm^2
count time on peaks 20s

[a] Analyses are of glasses made by fusing gel at 1650°C for 10 mins and quenching in water

[b] Numbers in brackets are XRF analysis of same gel normalised to 100 - Na wt%

Table A4.3. Compositions of $Tr_{92}Mc_8$-Ri_{100} amphiboles determined by EMPA. Bracketed analyses are from the same grain.

Na	Ca	Mg	Si	$X(Na_2Ca_{-1})$	$X(Mg_2Ca_{-2})$
			$Tr_{92}Mc_8$		
0.00	1.81	5.23	7.98	0.00	0.11
0.00	1.77	5.32	7.96	0.00	0.13
0.00	1.81	5.21	7.99	0.00	0.10
0.00	1.80	5.17	8.01	0.00	0.10
0.00	1.73	5.39	7.94	0.00	0.16
0.00	1.74	5.33	7.96	0.00	0.15
0.00	1.73	5.21	8.03	0.00	0.12
0.00	1.71	5.30	8.00	0.00	0.15
0.00	1.62	5.31	8.03	0.00	0.17
0.00	1.83	5.11	8.03	0.00	0.07
0.00	1.81	5.26	7.97	0.00	0.11
0.00	1.80	5.26	7.97	0.00	0.11
0.00	1.88	4.95	8.09	0.00	0.02
0.00	1.84	5.21	7.98	0.00	0.09
0.00	1.83	5.19	7.99	0.00	0.09
			Ri_{16}		
0.27	1.81	5.07	7.99	0.13	0.03
0.37	1.60	5.27	7.97	0.17	0.13
0.44	1.56	5.20	8.01	0.22	0.10
0.33	1.65	5.14	8.03	0.18	0.08
0.42	1.62	5.28	7.95	0.17	0.12
0.28	1.74	5.10	8.01	0.14	0.05
0.28	1.62	5.23	8.00	0.14	0.12
0.26	1.84	5.14	7.94	0.09	0.05
0.49	1.55	5.23	7.99	0.24	0.11
0.35	1.66	5.20	7.98	0.16	0.10
0.42	1.63	5.21	7.97	0.19	0.09
0.39	1.58	5.29	7.96	0.17	0.14
0.36	1.72	5.09	8.01	0.18	0.04
0.46	1.49	5.29	7.99	0.23	0.14
0.36	1.69	5.11	8.01	0.18	0.06
0.29	1.81	5.14	7.95	0.11	0.06
0.29	1.83	5.13	7.95	0.11	0.05

(Table A4.3 continued)

Na	Ca	Mg	Si	$X(Na_2Ca_{-1})$	$X(Mg_2Ca_{-2})$
		Ri_{31}			
0.62	1.53	5.12	8.02	0.32	0.06
0.65	1.53	5.11	8.02	0.34	0.06
0.63	1.50	5.03	8.07	0.37	0.04
0.76	1.48	5.24	7.95	0.35	0.10
0.72	1.52	5.12	8.00	0.36	0.06
0.76	1.46	5.21	7.98	0.36	0.10
0.63	1.55	5.06	8.03	0.33	0.04
0.73	1.53	5.08	8.01	0.37	0.05
0.77	1.46	5.22	7.96	0.36	0.10
0.70	1.45	5.17	8.01	0.36	0.09
0.59	1.59	5.11	8.00	0.30	0.05
0.62	1.59	5.08	8.01	0.31	0.05
0.76	1.46	5.18	7.99	0.37	0.08
0.66	1.54	5.23	7.95	0.29	0.10
		Ri_{48}			
1.00	1.44	5.09	7.99	0.49	0.04
1.03	1.41	5.11	7.98	0.50	0.05
0.89	1.54	4.99	8.01	0.45	0.00
0.90	1.44	5.00	8.06	0.48	0.02
0.98	1.45	5.09	7.99	0.48	0.04
0.94	1.43	5.11	8.00	0.47	0.05
1.00	1.44	5.05	8.01	0.50	0.02
1.06	1.36	5.07	8.02	0.54	0.04
1.02	1.40	5.10	8.00	0.51	0.05
1.09	1.37	5.09	8.00	0.54	0.05
1.03	1.40	5.12	7.98	0.50	0.05
0.98	1.41	5.13	7.98	0.48	0.06

(Table A4.3 continued)

Na	Ca	Mg	Si	$X(Na_2Ca_{-1})$	$X(Mg_2Ca_{-2})$
		Ri_{65}			
1.43	1.22	5.12	7.97	0.70	0.05
1.52	1.12	5.17	7.97	0.74	0.07
1.27	1.31	5.16	7.95	0.60	0.06
1.39	1.21	4.94	8.07	0.74	0.00
1.27	1.34	5.13	7.95	0.60	0.05
1.30	1.32	5.11	7.96	0.63	0.04
1.32	1.24	5.11	7.99	0.66	0.05
1.28	1.31	5.02	8.01	0.65	0.01
1.30	1.28	5.08	7.99	0.65	0.04
1.29	1.31	5.07	7.99	0.64	0.03
1.31	1.30	5.03	8.01	0.66	0.02
		Ri_{82}			
1.66	1.19	5.02	7.97	0.82	0.00
1.62	1.17	5.08	7.97	0.79	0.03
1.63	1.14	5.12	7.96	0.79	0.04
1.50	1.26	5.01	7.99	0.75	0.00
1.68	1.16	5.03	7.99	0.83	0.01
1.63	1.16	5.00	8.01	0.82	0.01
1.66	1.12	5.01	8.02	0.84	0.01
1.57	1.17	5.08	7.98	0.77	0.04
1.63	1.15	5.07	7.98	0.80	0.03
1.65	1.14	4.94	8.05	0.84	0.00
1.63	1.13	5.04	8.01	0.82	0.02
1.65	1.13	5.04	8.00	0.83	0.02

(Table A4.3 continued)

Na	Ca	Mg	Si	$X(Na_2Ca_{-1})$	$X(Mg_2Ca_{-2})$
		Ri_{92}			
1.80	1.04	5.02	8.02	0.91	0.01
1.80	1.07	5.04	7.99	0.90	0.02
1.87	1.09	5.00	7.98	0.92	0.00
1.83	1.06	5.06	7.98	0.90	0.03
1.98	1.03	4.99	7.99	0.98	0.00
1.85	1.04	5.08	7.98	0.91	0.03
1.92	1.02	5.05	7.99	0.95	0.02
1.88	1.06	5.03	7.98	0.93	0.01
1.85	1.08	5.00	8.00	0.93	0.00
1.87	1.07	5.03	7.98	0.92	0.00
1.76	1.12	5.05	7.97	0.87	0.02
1.89	1.07	5.05	7.97	0.92	0.01
1.88	1.05	5.05	7.98	0.93	0.02
1.91	1.02	5.10	7.97	0.93	0.04
		Ri_{100}			
1.97	1.00	5.04	7.98	0.98	0.01
1.96	1.01	5.05	7.98	0.97	0.02
2.00	1.00	5.04	7.98	1.00	0.01
2.00	1.02	5.05	7.96	0.98	0.01
2.03	1.02	5.02	7.97	1.00	0.00
1.97	1.00	5.06	7.98	0.97	0.02
1.99	1.00	5.03	7.99	0.99	0.01
2.01	1.00	5.03	7.98	0.99	0.01
1.98	1.00	5.06	7.97	0.98	0.02
2.01	1.03	5.05	7.96	0.98	0.01
1.97	0.99	5.04	7.99	0.98	0.02
1.97	0.99	5.09	7.97	0.96	0.03
2.01	0.98	5.02	8.00	1.00	0.01
2.03	0.97	5.07	7.97	1.00	0.02
2.03	0.97	5.06	7.97	1.00	0.02
2.06	0.99	5.09	7.95	0.99	0.03

Table A5.1. XRF analysis of sodium phlogopite gel.

				Theoretical
SiO_2	59.19	Si	2.99	3.00
Al_2O_3	16.86	Al	1.00	1.00
MgO	13.36	Mg	1.01	1.00
Na_2O	10.27	Na	1.01	1.00

Table A5.2. Electron microprobe analyses of OH- and F- sodium phlogopite gel mixes*.

Sample		Weight percentages of oxides		
		Ideal	Mean of 10 analyses	$2s/\sqrt{10}$
SP	MgO	34.3	34.3	0.10
	Al_2O_3	14.5	14.7	0.08
	SiO_2	51.2	51.0	0.09
F-SP	MgO	34.3	34.4	0.11
	Al_2O_3	14.5	14.3	0.06
	SiO_2	51.2	51.3	0.13

Microprobe operating conditions: accelerating voltage 15kV
beam current 5.4 nA
beam raster area 20×20 μm^2
count time on peaks 20s

* Analyses are of glasses made by fusing gel at 1650°C for 10 mins and quenching in water.

REFERENCES

AKAOGI, M. and NAVROTSKY, A. (1984): The quartz-coesite-stishovite transformations: new calorimetric measurements and calculation of phase diagrams. *Phys. Earth Planet. Interiors*, **36**, 124-134.

AOKI, K., FODOR, R.V., KEIL, K., DOWTY, E. (1972): Tremolite with high richterite-molecule content in kimberlite from Buell Park, Arizona. *Am. Mineral.*, **57**, 1889-1893.

BARABANOV, A.V., ZORINA, M.L., SOBOLEV, V.K. (1974): Infrared spectra of amphiboles from metamorphic rocks. *Mater. Mineral. Kol'sk. Poluostrova*, **10**, 165-175.

BERMAN, R.G., BROWN, T.H., GREENWOOD, H.J. (1985): An internally consistent thermodynamic data base for minerals in the system Na_2O-K_2O-CaO-MgO-FeO-Fe_2O_3-Al_2O_3-SiO_2-TiO_2-H_2O-CO_2. Scientific Document Distribution Office, Atomic Energy of Canada Ltd., Research Company, Chalk River, Ontario, Technical Record - TR 377.

BIGGAR G.M. and O'HARA M.J. (1969): A comparison of gel and glass starting materials for phase equilibria studies. *Mineral. Mag.*, **37**, 198-205.

BLACK, P.M. (1977): Regional high-pressure metamorphism in New Caledonia: Phase equilibria in the Ouégoa district. *Tectonophysics*, **43**, 89-107.

BOETTCHER, A.L. and WYLLIE, P.J. (1968): Jadeite stability measured in the presence of silicate liquids in the system $NaAlSiO_4$-SiO_2-H_2O. *Geochim. Cosmochim. Acta*, **32**, 999-1012.

BOETTCHER, A.L. and WYLLIE, P.J. (1969): Phase relationships in the system $NaAlSiO_4$-SiO_2-H_2O to 35 kilobars pressure. *Am. J. Sci.*, **267**, 875-909.

BOHLEN, S.R. and BOETTCHER, A.L. (1982): The quartz = coesite transformation: a precise determination and the effects of other components. *J. Geophys. Res.*, **87**, No. B8, 7073-7078.

BOYD, F.R. (1959): Hydrothermal investigations of the amphiboles. *In:* Abelson, P.H. (ed.), Researches in Geochemistry. Wiley and Sons, New York, 377-396.

BOYD, F.R. and ENGLAND, J.L. (1960): Apparatus for phase-equilibrium measurements at pressures up to 50 kilobars and temperatures up to 1750°C. *J. Geophys. Res.*, **65**, No. 2, 741-748.

BROWN, E.H. and FORBES, R.B. (1986): Phase petrology of eclogitic rocks in the Fairbanks district, Alaska. *In:* Evans, B.W. and Brown, E.H. (eds.), Blueschists and Eclogites. *GSA Memoir*, **164**, 155-168.

BURNHAM, C.W., HOLLOWAY, J.R., DAVIS, N.F. (1969): Thermodynamic properties of water to 1000°C and 10,000 bars. *Geol. Soc. Am. Spec. Publ.*, **132**.

CAMERON, M. and GIBBS, G.V. (1973): The crystal structure and bonding of fluor-tremolite: a comparison with hydroxyl tremolite. *Am. Mineral.*, **58**, 879-888.

CAMERON, M., SUENO, S., PAPIKE, J.J., PREWITT, C.T. (1983): High temperature crystal chemistry of K and Na fluor-richterites. *Am. Mineral.*, **68**, 924-943.

CARMAN, J.H. (1969): The study of the system $NaAlSiO_4$-Mg_2SiO_4-SiO_2-H_2O from 200 to 5,000 bars and 800°C to 1,100°C and its petrologic applications. PhD thesis, The Pennsylvania State University.

CARMAN, J.H. (1974): Synthetic sodium phlogopite and its two hydrates: stabilities, properties and mineralogic implications. *Am. Mineral.*, **59**, 261-273.

CARMAN, J.H. and GILBERT, M.C. (1983): Experimental studies on glaucophane stability. *Am. J. Sci.*, **283A**, 414-437.

CHARLES, R.W. (1975): The phase equilibria of richterite and ferrorichterite. *Am. Mineral.*, **60**, 367-374.

CHERNOSKY, J.V., DAY, H.W., CARUSO, L.J. (1985): Equilibria in the system MgO-SiO_2-H_2O: I. Experimental determination of the stability of Mg-anthophyllite. *Am. Mineral.*, **70**, 223-236.

CHOPIN, C. (1986): Phase relationships of ellenbergerite, a new high-pressure Mg-Al-Ti silicate in pyrope-coesite-quartzite from the Western Alps. *In:* Evans, B.W. and Brown, E.H. (eds.), Blueschists and Eclogites. *GSA Memoir*, **164**, 31-42.

CLEMENS, J.D., CIRCONE, S., NAVROTSKY, A., McMILLAN, P.F., SMITH, B.K., WALL, V.J. (1987): Phlogopite: high temperature solution calorimetry, thermodynamic properties, Al-Si and stacking disorder, and phase equilibria. *Geochim. Cosmochim. Acta*, **51**, 2569-2578.

CZANK, M. and LIEBAU, F. (1980): Periodicity faults in chain silicates: a new type of planar lattice fault observed with high-resolution electron microscopy. *Phys. Chem. Minerals*, **6**, 85-93.

DAVIES, P.K. and NAVROTSKY, A. (1981): Thermodynamics of solid solution formation in NiO-MgO and NiO-ZnO. *J. Solid State Chem.*, **38**, 264-276.

DEMAREST, H.H. and HASELTON, H.T. (1981): Error analysis for bracketed phase equilibrium data. *Geochim. Cosmochim. Acta*, **45**, 217-224.

DOCKA, J.A., POST, J.E., BISH, D.L., BURNHAM, C.W. (1987): Positional disorder of A-site cations in C2/m amphiboles: model energy calculations and probability studies. *Am. Mineral.*, **72**, 949-958.

DOWTY, E. (1987): Fully automated microcomputer calculation of vibrational spectra. *Phys. Chem. Minerals*, **14**, 67-79.

EGGERT, R.G. and KERRICK, D.M. (1981): Metamorphic equilibria in the siliceous dolomite system: 6 kbar experimental data and geologic implications. *Geochim. Cosmochim. Acta*, **45**, 1039-1049.

ERNST, W.G. (1961): Stability relations of glaucophane. *Am. J. Sci.*, **259**, 735-765.

ERNST, W.G. (1963): Polymorphism in alkali amphiboles. *Am. Mineral.*, **48**, 241-260.

FORD, C.E. (1972): Furnace design, temperature calibration and seal design in internally-heated pressure vessels. Progress in Exptl Petrol., *NERC Publ. Series D*, No. 2, 89-96.

FURUKAWA, T., FOX, K.E., WHITE, W.B. (1981): Raman spectroscopic investigation of the structure of silicate glasses. III. Raman intensities and structural units in sodium silicate glasses. *J. Chem. Phys.*, **75**, 3226-3237.

GILLET, P., REYNARD, B., TEQUI, C. (1989): Thermodynamic properties of glaucophane: new data from calorimetric and spectroscopic measurements. *Phys. Chem. Minerals*, **16**, 659-667.

GRAHAM, C.M. and NAVROTSKY, A. (1986): Thermochemistry of the tremolite-edenite amphiboles using fluorine analogues, and applications to amphibole-plagioclase-quartz equilibria. *Contrib. Mineral. Petrol.*, **93**, 18-32.

GRAHAM, C.M., HARMON, R.S., SHEPPARD, S.M.F. (1984): Experimental hydrogen isotope studies: hydrogen isotope exchange between amphibole and water. *Am. Mineral.*, **69**, 128-138.

GRAHAM, C.M., MARESCH, W.V., WELCH, M.D., PAWLEY, A.R. (1989): Experimental studies on amphiboles: a review with thermodynamic perspectives. *Eur. J. Mineral.*, **1**, 535-555.

HARIYA, Y. and TERADA, S. (1973): Stability of richterite$_{50}$-tremolite$_{50}$ solid solution at high pressures and possible presence of sodium calcic amphibole under upper mantle conditions. *Earth Planet. Sci. Letters,* **18**, 72-76.

HAWTHORNE, F.C. (1981): Crystal chemistry of the amphiboles. *In:* Veblen, D.R. (ed.), Amphiboles and other hydrous pyriboles – Mineralogy. Mineralogical Society of America. *Reviews in Mineralogy,* **9A**, 1-102.

HAWTHORNE, F.C. (1983): The crystal chemistry of the amphiboles. *Canad. Mineral.*, **21**, 173-480.

HAWTHORNE, F.C. and GRUNDY, H.D. (1972): Positional disorder in the A-site of clino-amphiboles. *Nature,* **235**, 72-73.

HAWTHORNE, F.C. and GRUNDY, H.D. (1976): The crystal chemistry of the amphiboles: IV. X-ray and neutron refinements of the crystal structure of tremolite. *Can. Mineral.*, **14**, 334-345.

HAWTHORNE, F.C. and GRUNDY, H.D. (1978): The crystal chemistry of the amphiboles: VII. The crystal structure and chemistry of potassium ferritaramite. *Can. Mineral.*, **16**, 53-62.

HELGESON, H.C., DELANEY, J.M., NESBITT, H.W., BIRD, D.K. (1978): Summary and critique of the thermodynamic properties of rock-forming minerals. *Am. J. Sci.*, **278A**, 1-229.

HELPER, M.A. (1986): Deformation and high P-T metamorphism in the central part of the Condrey Mountain Window, north-central Klamath Mountains, California and Oregon. *In:* Evans, B.W. and Brown, E.H. (eds.), Blueschists and Eclogites. *GSA Memoir,* **164**, 125-142.

HERRERO, C.P., GREGORKIEWITZ, M., SANZ, J., SERRATOSA, J.M. (1987): ^{29}Si MAS-NMR spectroscopy of mica-type silicates: Observed and predicted distribution of tetrahedral Al-Si. *Phys. Chem. Minerals,* **15**, 84-90.

HEWITT, D.A., (1975): Stability of the assemblage phlogopite-calcite-quartz. *Am. Mineral.*, **60**, 391-397.

HOLLAND, T.J.B. (1979): High water activities in the generation of high pressure kyanite eclogites of the Tauern Window, Austria. *J. Geol.*, **87**, 1-27.

HOLLAND, T.J.B. (1980): The reaction albite = jadeite + quartz determined experimentally in the range 600-1200°C. *Am. Mineral.*, **65**, 129-134.

HOLLAND, T.J.B. (1988): Preliminary phase relations involving glaucophane and applications to high pressure petrology: new heat capacity and thermodynamic data. *Contrib. Mineral. Petrol.*, **99**, 134-142.

HOLLAND, T.J.B. (1989): Dependence of entropy on volume for silicate and oxide minerals: A review and a predictive model. *Am. Mineral.*, **74**, 5-13.

HOLLAND, T.J.B. and POWELL, R. (1989): An enlarged and updated internally-consistent thermodynamic dataset with uncertainties and correlations: the system K_2O-Na_2O-CaO-MgO-MnO-FeO-Fe_2O_3-Al_2O_3-TiO_2-SiO_2-C-H_2-O_2. *J. Metam. Geol.* (in press).

HOLLAND, T.J.B. and RICHARDSON, S.W. (1979): Amphibole zonation in metabasites as a guide to evolution of metamorphic conditions. *Contrib. Mineral. Petrol.*, **70**, 143-148.

HOLLOWAY, J.R. (1971): Internally-heated gas-pressure vessels. *In:* Ulmer, G.C. (ed.), Research techniques for high pressures and high temperatures. Springer-Verlag, New York.

HOSCHEK, G. (1973): Die Reaktion Phlogopit + Calcit + Quarz = Tremolit + Kalifeldspat + H_2O + CO_2. *Contrib. Mineral. Petrol.*, **39**, 231-237.

IIYAMA, J.T. (1963): Synthèse hydrothermale à 750°C, 1000 bars dans le système Na_2O-MgO-Al_2O_3-SiO_2-H_2O d'amphiboles orthorhombiques et monocliniques. *C. R. Acad. Sci. Paris*, **256**, 966-967.

ITO, E. and NAVROTSKY, A. (1985): $MgSiO_3$-ilmenite: calorimetry, phase-equilibria, and decomposition at atmospheric pressure. *Am. Mineral.*, **70**, 1020-1026.

JENKINS, D.M. (1983): Stability and composition relations of calcic amphiboles in ultramafic rocks. *Contrib. Mineral. Petrol.*, **83**, 375-384.

JENKINS, D.M. (1987): Synthesis and characterization of tremolite in the system H_2O-CaO-MgO-SiO_2. *Am. Mineral.*, **72**, 707-715.

JOHANNES, W., BELL, P.M., MAO, H.K., BOETTCHER, A.L., CHIPMAN, D.W., HAYS, J.F., NEWTON, R.C., SEIFERT, F. (1971): An inter-laboratory comparison of piston-cylinder pressure calibration using the albite breakdown reaction. *Contrib. Mineral. Petrol.*, **32**, 24-38.

KEUSEN, H.R. and PETERS, T.J. (1980): Preiswerkite, an Al-rich trioctahedral sodium mica from the Geisspfad ultramafic complex (Penninic Alps). *Am. Mineral.*, **65**, 1134-1137.

KIEFFER, S.W. (1985): Heat capacity and entropy: systematic relations to lattice vibrations. *In:* Kieffer, S.W. and Navrotsky, A. (eds.), Microscopic to macroscopic – Atomic environments to thermodynamic properties. Mineralogical Society of America. *Reviews in Mineralogy*, **14**, 65-126.

KISELEVA, I.A. and OGORODOVA, L.P. (1984): High-temperature solution calorimetry for determining the enthalpies of formation for hydroxyl-containing minerals such as talc and tremolite. *Geochem. Internat.*, **12**, 36-46.

KOONS, P.O. (1982): An experimental investigation of the behaviour of amphibole in the system Na_2O-MgO-Al_2O_3-SiO_2-H_2O at high pressures. *Contrib. Mineral. Petrol.*, **79**, 258-267.

KUKOVSKII, E.G. and LITVIN, A.L. (1970): Infrared spectra of amphiboles. *Konst. Svoistva. Mineral.*, **4**, 81-85.

KULKE, H.G. (1976): Metamorphism of evaporitic carbonate rocks (NW Africa and Afghanistan) and the formation of lapis lazuli. *25th Int. Geol. Congress Abstr.*, **1**, 131.

KURODA, Y., HARIYA, Y., SUZUOKI, T., MATSUO, S. (1975): Pressure effect on water content of amphiboles. *Geophys. Res. Lett.*, **2**, 529-531.

LEAKE, B.E. (1968): A catalog of analysed calciferous and subcalciferous amphiboles with their associated minerals. *Geol. Soc. Am. Mem.*, **92.**

McMILLAN, P.F. and HOFMEISTER, A (1988): Infrared and Raman spectroscopy. *In:* Hawthorne, F.C. (ed.), Spectroscopic methods in mineralogy and geology. Mineralogical Society of America. *Reviews in Mineralogy*, **18**, 99-159.

MARESCH, W.V. (1973): New data on the synthesis and stability relations of glaucophane. *Earth Planet. Sci. Lett.*, **20**, 385-390.

MARESCH, W.V. (1974): Neue Daten zur Stabilität und "Polymorphie" des synthetischen Glaukophans. *Fortschr. Mineral.*, **51**, Beihert 1, 30-31.

MARESCH, W.V. (1977): Experimental studies on glaucophane: an analysis of present knowledge. *Tectonophysics*, **43**, 109-125.

MARESCH, W.V. and CZANK, M. (1983): Problems of compositional and structural uncertainty in synthetic hydroxyl-amphiboles. *Periodico di Mineralogia, Roma*, **52**, 463-542.

MARESCH, W.V. and CZANK, M. (1988): Crystal chemistry, growth kinetics and phase relationships of structurally disordered (Mn^{2+},Mg) amphiboles. *Fortschr. Mineral.*, **66**, 69-121.

MARESCH, W.V. and LANGER, K. (1976): Synthesis, lattice constants and OH-valence vibrations of an orthorhombic amphibole with excess OH in the system Li_2O-MgO-SiO_2-H_2O. *Contrib. Mineral. Petrol.*, **56**, 27-34.

MARUYAMA, S., CHO, M., LIOU, J.G. (1986): Experimental investigations of blueschist-greenschist transition equilibria: pressure dependence of Al_2O_3 contents in sodic amphiboles - a new barometer. *In:* Evans, B.W. and Brown, E.H. (eds.), Blueschists and Eclogites. *GSA Memoir,* **164,** 1-16.

METZ, P. (1967): Experimentelle Bildung von Forsterit und Calcit aus Tremolit und Dolomit. *Geochim. Cosmochim. Acta,* **31,** 1517-1532.

METZ, P. (1976): Experimental investigation of the metamorphism of siliceous dolomites III. Equilibrium data for the reaction: 1 tremolite + 11 dolomite = 8 forsterite + 13 calcite + 9 CO_2 + 11 H_2O for the total pressure of 3000 and 5000 bars. *Contrib. Mineral. Petrol.,* **58,** 137-148.

NA, K.C., McCAULEY, M.L., CRISP, J.A., ERNST, W.G. (1986): Phase relations to 3 kbar in the systems edenite + H_2O and edenite + excess quartz + H_2O. *Lithos,* **19,** 153-163.

NAUMANN, A.W., SAFFORD, G.J., MUMPTON, F.A. (1966): Low-frequency (OH)-motions in layer silicate minerals. *Clays Clay Minerals,* **14,** 367-383.

NAVROTSKY, A. (1977): Progress and new directions in high temperature calorimetry. *Phys. Chem. Minerals,* **2,** 89-104.

NAVROTSKY, A. (1985): Crystal chemical constraints on the thermochemistry of minerals. *In:* Kieffer, S.W. and Navrotsky, A. (eds.), Microscopic to macroscopic – Atomic environments to thermodynamic properties. Mineralogical Society of America. *Reviews in Mineralogy,* **14,** 225-275.

NAVROTSKY, A., HON, R., WEILL, D.F., HENRY, D.J. (1980): Thermochemistry of glasses and liquids in the systems $CaMgSi_2O_6$-$CaAl_2Si_2O_8$-$NaAlSi_3O_8$, SiO_2-$CaAl_2Si_2O_8$-$NaAlSi_3O_8$ and SiO_2-Al_2O_3-CaO-Na_2O. *Geochim. Cosmochim. Acta,* **44,** 1409-1423.

NEWTON, R.C., CHARLU, T.V., ANDERSON, P.A.M., KLEPPA, O.J. (1979): Thermochemistry of synthetic clinopyroxenes on the join $CaMgSi_2O_6$-$Mg_2Si_2O_6$. *Geochim. Cosmochim. Acta,* **43,** 55-60.

NEWTON, R.C., CHARLU, T.V., KLEPPA, O.J. (1980): Thermochemistry of the high structural state plagioclases. *Geochim. Cosmochim. Acta,* **44,** 933-941.

NEWTON, R.C., WOOD, B.J., KLEPPA, O.J. (1981): Thermochemistry of silicate solid solutions. *Bull. Minéral.,* **104,** 162-171.

PAPIKE, J.J. and CLARK, J.R. (1968): The crystal structure and cation distribution of glaucophane. *Am. Mineral.,* **53,** 1156-1173.

PAPIKE, J.J., ROSS, M., CLARK, J.R. (1969): Crystal-chemical characterization of clinoamphiboles based on five new structure refinements. *Mineral. Soc. Amer. Spec. Pap.*, **2**, 117-136.

PUTNIS, A. and McCONNELL, J.D.C. (1980): Principles of mineral behaviour. *Geoscience texts*, **Vol. 1**. Elsevier, New York.

RAUDSEPP, M., TURNOCK, A.C., HAWTHORNE, F.C., SHERRIFF, B., HARTMAN, J.S. (1987): Characterization of synthetic pargasitic amphiboles ($NaCa_2Mg_4M^{3+}Si_6Al_2O_{22}(OH,F)_2$: M^{3+} = Al, Cr, Ga, Sc, In) by infrared spectroscopy, Rietveld structure refinement, and ^{27}Al, ^{29}Si, and ^{19}F MAS NMR spectroscopy. *Am. Mineral.*, **72**, 580-593.

RIDLEY, J. and DIXON, J.E. (1984): Reaction pathways during the progressive deformation of a blueschist metabasite: the role of chemical disequilibrium and restricted range equilibrium. *J. Metam. Geol.*, **2**, 115-128.

ROBERT, J.L., DELLA VENTURA, G., THAURIN, J.L. (1989): The infrared OH-stretching region of synthetic richterites in the system Na_2O-K_2O-CaO-MgO-SiO_2-H_2O-HF. *Eur. J. Mineral.*, **1**, 203-211.

ROBIE, R.A. and STOUT, J.W. (1963): Heat capacity from 12 to 305 K, and entropy of talc and tremolite. *J. Phys. Chem.*, **67**, 2252-2256.

ROBIE, R.A., HEMINGWAY, B.S., FISHER, J.R. (1978): Thermodynamic properties of minerals and related substances at 298.15 K and one atmosphere pressure and at higher temperatures. *U.S. Geol. Surv. Bull.*, **1259**.

ROBINSON, P., SPEAR, F.S., SCHUMACHER, J.C., LAIRD, J., KLEIN, C., EVANS, B.W., DOOLAN, B.L. (1982): Phase relations of metamorphic amphiboles: natural occurrence and theory. *In:* Veblen, D.R. and Ribbe, P.H. (eds.), Amphiboles: Petrology and experimental phase relations. Mineralogical Society of America. *Reviews in Mineralogy*, **9B**, 1-227.

ROWBOTHAM, G. and FARMER, V.C. (1973): The effect of "A" site occupancy upon the hydroxyl stretching frequency in clinoamphiboles. *Contrib. Mineral. Petrol.*, **38**, 147-149.

SCHREYER, W., ABRAHAM, K., KULKE, H. (1980): Natural sodium phlogopite coexisting with potassium phlogopite and sodian aluminium talc in a metamorphic evaporite sequence from Derrag, Tell Atlas, Algeria. *Contrib. Mineral. Petrol.*, **74**, 223-233.

SHEU, J.-L. and McMILLAN, P. (1988): An ab initio study of the O-H stretching frequency in tremolite. *Phys. Chem. Minerals*, **16**, 114-119.

SKIPPEN, G. and McKINSTRY, B.W. (1985): Synthetic and natural tremolite in equilibrium with forsterite, enstatite, diopside and fluid. *Contrib. Mineral. Petrol.*, **89**, 256-262.

SLAUGHTER, J., KERRICK, D.M., WALL, V.J. (1975): Experimental and thermodynamic study of equilibria in the system CaO-MgO-SiO_2-H_2O-CO_2. *Am. J. Sci.*, **275**, 143-165.

THOMPSON, J.B. (1981): An introduction to the mineralogy and petrology of the biopyriboles. *In:* Veblen, D.R. (ed.), Amphiboles and other hydrous pyriboles – Mineralogy. Mineralogical Society of America. *Reviews in Mineralogy*, **9A**, 141-188.

UNGARETTI, L., SMITH, D.C., ROSSI, G. (1981): Crystal chemistry by X-ray structure refinement and electron microprobe analysis of a series of sodic-calcic to alkali amphiboles from the Nybö eclogite pod, Norway. *Bull. Minéral.*, **104**, 400-412.

UNGARETTI, L., LOMBARDO, B., DOMENEGHETTI, C., ROSSI, G. (1983): Crystal-chemical evolution of amphiboles from eclogitised rocks of the Sesia-Lanzo Zone, Italian Western Alps. *Bull. Minéral.*, **106**, 645-672.

WEEKS, W.F. (1956): Heats of formation of metamorphic minerals in the system CaO-MgO-SiO_2-H_2O and their petrological significance. *J. Geol.*, **64**, 456-472.

WEILL, D.F., HON, R., NAVROTSKY, A. (1980): The igneous system $CaMgSi_2O_6$-$CaAl_2Si_2O_8$-$NaAlSi_3O_8$: variations on a classic theme by Bowen. *In:* Hargraves, R.B. (ed.), Physics of magmatic processes. Princeton Univ. Press, 49-92.

WELCH, M.D. (1987): Experimental studies of selected amphiboles in the system Na_2O-CaO-MgO-Al_2O_3-SiO_2-H_2O-F_2 and its subsystems. Unpubl. PhD thesis, Univ. of Edinburgh.

WELCH, M.D. (1989): An experimental study of glaucophane-type amphiboles in the system Na_2O-MgO-Al_2O_3-SiO_2-SiF_4 (NMASF), with implications for natural systems. *Contrib. Mineral. Petrol.* (in press).

WELCH, M.D. and GRAHAM, C.M. (1988): Proton-bearing coupled substitutions in richteritic amphiboles: an experimental study in the system Na_2O-MgO-SiO_2-H_2O (NMSH). *Terra Cognita*, **8**, 81.

WESTRICH, H.R. and HOLLOWAY, J.R. (1981): Experimental dehydration of pargasite and calculation of its entropy and Gibbs energy. *Am. J. Sci.*, **281**, 922-934.

WESTRICH, H.R. and NAVROTSKY, A. (1981): Some thermodynamic properties of fluorapatite, fluorpargasite, and fluorphlogopite. *Am. J. Sci.*, **281**, 1091-1103.

WITTE, P. (1975): Synthese und Stabilität von Amphibolphasen und wasserfreien Na-Mg-Silikaten im System Na_2O-MgO-SiO_2-H_2O, die Kompatibilitätsbeziehungen innerhalb des Si-reichen Teils des quaternären Systems oberhalb 600°C im Druckbereich 1 atm – 5 kb P(H_2O) und ihre petrologische Bedeutung. Doctoral dissertation. Ruhr-Universität Bochum. Bochum, F.R. Germany.

WOOD, B.J., HOLLAND, T.J.B., NEWTON, R.C., KLEPPA, O.J. (1980): Thermochemistry of jadeite-diopside pyroxenes. *Geochim. Cosmochim. Acta*, **44**, 1363-1371.

YIN, H.A. and GREENWOOD, H.J. (1983): Displacement of equilibria of OH-tremolite and F-tremolite solid solution. I. Determination of the equilibrium P-T curve of OH-tremolite. *Trans. Am. Geophys. Union*, **64**, 347.

CONTENTS